# IMPACT OF SOFC AND SOEC DEGRADATION ON SYSTEM OPERATION

# DEGRADATION OF SOFC AND SOEC AND ITS IMPACT ON SYSTEM OPERATION

By Mina Naeini, B.Sc., M.Sc.

A Thesis Submitted to the School of Graduate Studies in
Partial Fulfillment of the Requirement for the Degree
Doctor of Philosophy

| | |
|---|---|
| Ph.D. Candidate | McMaster University |
| Chemical Engineering | Hamilton, Ontario, Canada |

TITLE: Degradation of SOFC And SOEC and Its Impact on System Operation

AUTHOR: Mina Naeini

B.Sc. and M.Sc. of Materials Science and Engineering

SUPERVISOR: Dr. Thomas A. Adams II

COSUPERVISOR: Professor James S. Cotton

NUMBER OF PAGES: xxiii, 250

# LAY ABSTRACT

Solid oxide fuel cell (SOFC) and solid oxide electrolysis cell (SOEC) have been investigated for decades. Fuel flexibility, high efficiency, low levels of noise and environmental burdens are substantial advantages of these cells over the current power and hydrogen plants. The biggest limitation of previous studies is ignoring or underestimating degradation of SOFC and SOEC. Open literature lacks adequate research studies that address impacts of operating parameters on performance degradation of SOFC and SOEC. The inadequate understanding of degradation phenomena resulted in limited commercial development of this technology. This thesis focuses on developing models for prediction of SOFC and SOEC degradation with respect to their operating conditions. Moreover, this thesis addresses the impacts of degradation in economic and environmental feasibility of SOFC and SOEC.

# ABSTRACT

The key to a cleaner future is to alleviate reliance of energy sectors on non-renewable fossil fuel sources and reduce their environmental burdens. This can be achieved by using power generation units such as Solid Oxide Fuel Cell (SOFC) that use natural gas more efficiently compared to the existing fossil fuel-based technologies as well as energy storage units such as Solid Oxide Electrolysis Cell (SOEC) that enable increase in the amount of intermittent renewable power supply.

This thesis describes the models constructed for conventional SOFC and SOEC degradation to show how performance of these cells degrade over long periods of time under their operating conditions. The goal of this thesis is to evaluate the economic and environmental performance of SOFC and SOEC under degradation and compare them to the existing technologies.

In this thesis project, the economically optimal sizing, and trajectories of natural gas-SOFC and SOEC are found considering their degradation. Impacts of SOFC capital cost, price of natural gas, and $CO_2$ tax on economic performance of SOFC and impacts of SOEC capital cost and price of electricity on economic performance of SOEC are quantified to help decision makers evaluate economic feasibility of these cells in different locations. Economical operation of an SOFC plant requires lowering its current density slowly over time which results in power output reduction. This can limit the application of SOFC for communities that need constant load of power all the time. To combat this issue, this thesis also focuses on scheduling start-up of optimally operated SOFC modules such that SOFC system as a whole has a constant power output.

This thesis assesses environmental performances of SOFC and SOEC and compares them with the existing technologies. A detailed life cycle analysis of optimally operated natural gas-fueled SOFC

plant under degradation is performed using ReCiPe 2016 and TRACI 2.1 US-Canada 2008 methods. Then, it compares the major environmental impact categories of this plant with those of two mature technologies that use natural gas for power generation. Moreover, life cycle greenhouse gases (GHG) emitted from manufacturing SOEC and its power source are quantified to assess environmental performance of SOEC. This is performed for SOECs with various power sources from low GHG emission sources to high GHG emission ones. The levelized cost of hydrogen and life cycle GHG emissions of SOECs with different power sources are then compared to those of other hydrogen generation units.

SOFC can serve as an efficient, cost-effective, environmentally friendly option for power only or heat and power generation in many places even at high natural gas prices and carbon taxes. While SOEC, despite its high efficiency, might not be a very economical or environmentally responsible option for hydrogen production when the price of electricity is high and power supply has high GHG emissions.

# PREFACE

Chapters 2-4, and 6 involve multi-author articles published in peer-reviewed scientific journals.

Chapter 5 contains a work published in CSChE Systems and Control Transactions Vol 1. This article was not peer-reviewed.

Chapter 7 involves a manuscript submitted for publication in a peer-reviewed scientific journal.

My contribution to each chapter is as follows.

- Develop mathematical model for degradation of SOFC in MATLAB and validate it.
    - Haoxiang Lai helped with implementing some parts of this model in MATLAB.
- Develop data-driven model for degradation of SOEC in ALAMO and validate it.
- Formulate and solve the economic optimization problems in GAMS.
- Perform cradle-to-product LCA on SOFC in SimaPro.
- Schedule installation of SOFC modules for a constant power production.
- Analyze the findings and visualize the data.
- Write the original draft of each manuscript.

Contributions of Dr. Thomas Adams II in chapters 2-7 are as follows.

- Supervision.
- Conceptualize the research project and administer it.
- Provide resources and software.
- Provide insightful guidance and discussion on formulating the problems and analyzing the findings.
- Review and edit the manuscripts.

Contributions of Dr. James Cotton in chapters 2-7 involve:

- Provide funding.
- Supervision and project administration.
- Provide insightful feedback and advice on various stages of the project.
- Review and edit the manuscripts.

# ACKNOWLEDGEMENTS

I am thankful for many things and many people who helped me accomplish this journey. I would like to start by thanking my supervisor Dr. Thomas A. Adams II for his impeccable guidance and unwavering support over the past 4 years. He has been a wonderful mentor and an incredible supervisor whose guidance and expertise were invaluable for this project. His consistent encouragement throughout my doctorate gave me the confidence to accomplish this work.

I would also sincerely like to thank my co-supervisor Dr. James S. Cotton for all his insightful guidance, assistance, and support throughout my PhD. This project is stronger for his help and advice.

I would like to thank my committee member Dr. Drew Higgins for his insightful feedback and invaluable suggestions that helped me assess my work from a different perspective.

Thank you to the entire Cotton and Adams groups for their support during my time here. A special thanks to Dr. Ikenna Okeke, Dr. Pranav Madabhushi, Nina Monteiro, Haoxiang Lai, Daniela Dering and many more for always being there for me as amazing friends and great co-workers.

Last but not least, thank you to my parents Sedi and Davoud, and my sister Nazanin for a lifetime of love, support, and encouragement. Without them I would not be who I am today.

# Table of Contents

## CONTENTS

---

# List of Figures

# List of Tables

# List of Abbreviations

This is the list of abbreviations that are consistent throughout this thesis. Chapters 2 to 6 consists of published reprints that might have mathematical symbols and notations specific to their document. For the list of these symbols please refer to the Nomenclature tables of these publications.

| | |
|---|---|
| AP | Acidification potential |
| CHP | Combined heat and power |
| DOE | Design of experiments |
| FFD | Fossil fuel depletion |
| FS | Fossil resource scarcity |
| GHG | Greenhouse gas |
| GT | Gas turbine |
| GW | Global warming |
| HHV | Higher heating value |
| ICE | Internal combustion engine |
| LCA | Life cycle analysis |
| LCOE | Levelized cost of electricity |
| LCOEn | Levelized cost of energy |
| LCOH | Levelized cost of hydrogen |
| LHV | Lower heating value |

| | |
|---|---|
| NG | Natural gas |
| NLP | non-linear programs |
| OF | Ozone formation |
| PMF | Fine particulate matter formation |
| RE | Respiratory effects |
| TA | Terrestrial acidification |
| TEA | Techno-economic analysis |
| TPB | Triple phase boundary |
| SOFC | Solid oxide fuel cell |
| SOEC | Solid oxide electrolysis cell |
| VOC | Volatile organic compound |
| WD | Water depletion |

# Declaration of Academic Achievement

I, Mina Naeini, declare that the research presented in this thesis is my own work, I was the primary researcher under supervision of Dr. Thomas A. Adams II and Dr. James S. Cotton. I confirm that I am the sole researcher and author of this thesis with the exception of chapters 2 to 7 that consist of published reprints, or the article submitted for publication in a scientific journal in which case authorship and contributions are provided.

# CHAPTER 1: INTRODUCTION

## Preliminaries

This chapter contains a brief literature review, description of the conventional SOFC and SOEC technologies 1.2. The objective and the novelties of the thesis project are given in section 1.3. Finally, a description of the thesis outline is given in section 1.4.

## 1.1. Background

The worldwide energy demand is forecasted to grow 25% by 2050.[1] Governments have been trying to encourage energy sectors to switch to cleaner sources of energy and lower the $CO_2$ emissions by incentives such as $CO_2$ tax. Even though the share of renewable sources in the electricity generation industry is increasing, fossil fuels are still the dominant source of global electricity generation with ~63.3% of it.[2] There are several barriers to worldwide use of renewable energy sources such as high capital costs, geographic limitations, and unreliability. Thus, the share of natural gas in the electricity production sector has continued to grow on the global scale.[3] Currently in the electricity generation sector there is a compelling need for improving efficiency of the existing natural gas-fueled electricity generation technologies. Among the natural gas-fueled power generation technologies, solid oxide fuel cells (SOFCs) with promising features such as high energy (heat and power) efficiency, substantial amount of heat as a high-quality by-product, reduced noise, and low environmental burdens are a good replacement for the existing natural gas-based power-only and combined heat and power (CHP) technologies.[4] These cells can also be operated in electrolysis mode in which they consume power to electrolyze steam. Solid oxide electrolysis cells (SOECs) are an efficient technology for green hydrogen production. SOECs play a key role in deployment of clean and renewable power sources such as nuclear, wind, and solar, as SOECs enable storage of surplus power generated by these sources in the form of hydrogen.

### 1.1.1. Brief Description of Solid Oxide Fuel Cell and Solid Oxide Electrolysis Cell Technologies

SOFC is an efficient electrochemical unit that consumes fuel and oxidant (air) to generate electricity through exothermic reactions. Conventional SOFC consists of $La_{1-x}Sr_xMnO_3$ (LSM) cathode, Ni-Yttria stabilized Zirconia (Ni-YSZ) anode, and YSZ electrolyte. In SOFC fuel is delivered to the anode side, and oxidant (air) is supplied to the cathode side. Unlike other fuel cells, SOFCs are not limited to hydrogen gas as fuel and they can be operated with various fuel sources such as natural gas, coal, diesel, etc. When supplied with hydrocarbon fuels, fuel can be reformed internally inside anode or externally through a reformer. Ni in the anode works as a catalyst at the high operating temperature of SOFC and allows internal reforming of the carbonaceous fuel.[5,6] Figure 1 shows a schematic of operation of an SOFC supplied with a carbonaceous fuel.

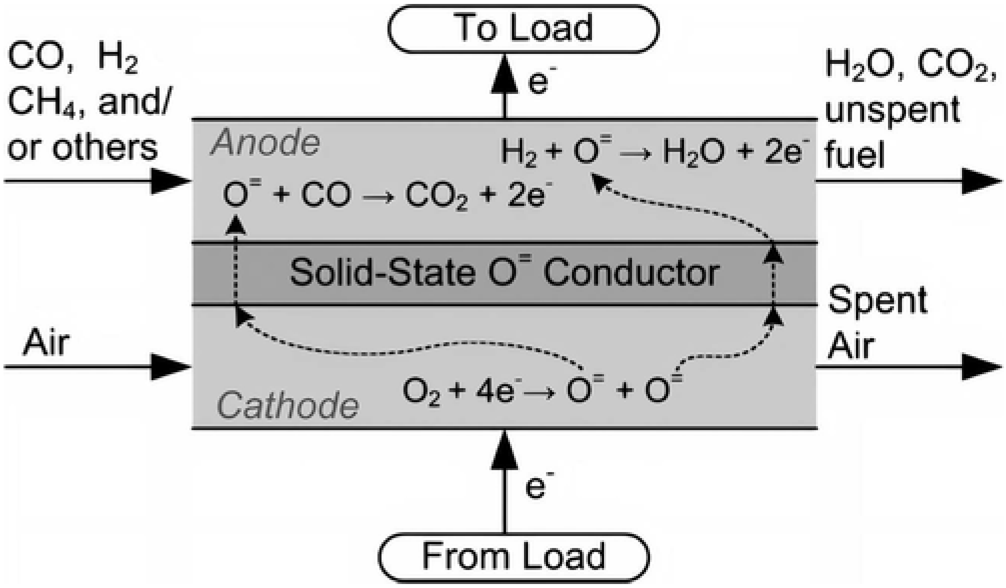

Figure 1. Schematic of an SOFC using carbonaceous fuel. Reprinted with permission from ref.[7] Copyright 2013 American Chemical Society.

The overall electrochemical reactions in hydrocarbon fuel-based SOFC are as follows,

$$H_2 + O^{2-} \rightarrow H_2O + 2e^- \qquad 1$$

$$CO + O^{2-} \rightarrow CO_2 + 2e^- \qquad 2$$

The solid oxide electrolyte of SOFC should have a low electrical conductivity in order to ensure that the released electrons flow from anode to cathode through the external circuit. Additionally, SOFC’s electrolyte has a dense structure with high ionic conductivity that conducts oxygen ions from cathode to anode, while it prevents the diffusion of gas molecules.[8] The electrochemical reactions take place at high temperatures. The anode exhaust contains some unspent fuel, steam, and carbon dioxide at high temperatures. The exhaust of pressurized SOFC can be delivered to gas turbines to generate more electricity and further improve the overall efficiency of the system.[9] Alternatively, the hot exhaust can be simply used for heat demands of the community through heat exchanger networks.

SOEC is a counterpart of SOFC that is operated in reverse. In SOEC, fuel gas which mostly consists of steam at high temperature is delivered to the fuel electrode. Electrolysis cells consume electricity to split molecules of water through following reaction,

$$H_2O + 2e^- \rightarrow H_2 + O^{2-} \qquad 3$$

The fuel electrode exhaust contains hydrogen and some unspent steam at high temperatures. Oxygen ions migrate from the fuel electrode to the air electrode where following reaction takes place and pure oxygen leaves air electrode at elevated temperatures.

$$2O^{2-} \rightarrow O_2 + 4e^- \qquad 4$$

SOEC feature higher efficiency compared to the low-temperature electrolysis cells such as alkaline or polymer electrolyte membrane (PEM) electrolysis cells. High-temperature SOECs consume less electrical energy because a part of required energy for the electrolysis of water is supplied as thermal energy.

### 1.1.2. Limitations of Solid Oxide Fuel Cell and Solid Oxide Electrolysis Cell

High operating temperatures of SOFC and SOEC, facilitate internal reforming of hydrocarbon-based fuels in SOFC, decrease the need for electrical energy in SOEC, and enable conduction of ions through solid oxide electrolyte. However, such high temperatures limit selection of materials for different parts of SOFC/SOEC. Number of unwanted reactions take place in different parts of SOFC/SOEC under their typical operating conditions that result in degradation of the cells. Performance degradation is the main barrier to commercialization of SOFC/SOEC. Several research studies have focused on developing new degradation-resistant materials.[10–14] However, none of the new SOFC/SOEC technologies had the economical feasibility, and chemical and thermal stability for widespread commercialization. Cells with Ni-YSZ anode, YSZ electrolyte, and LSM cathode are still the most common and mature SOFCs/SOECs. Degradation of SOFC can usually be classified in two different categories i.e., inevitable losses, and system degradation mechanisms. The overpotentials/polarizations caused by the cell's degradation decrease its voltage such that SOFCs supplied with a constant fuel flow deliver less voltage and power over time. Inevitable losses are usually caused by ohmic resistance in or between cell's components, gas concentration gradient in the electrodes, and activation barrier of electrochemical reactions. In the low current density region, the fuel cell is mainly affected by the activation polarization. The ohmic polarization occurs in the intermediate current density region and the concentration polarization is more dominant at high current densities (Figure 2).

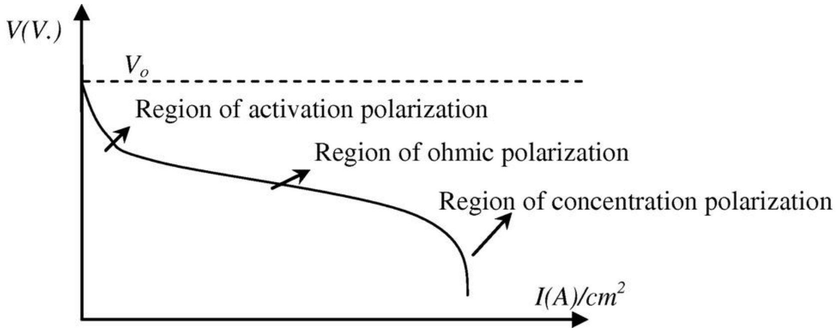

Figure 2. Polarization curve of a fuel cell. Reprinted with permission from ref.[15]

The governing system degradation reactions in anode-supported SOFC are mainly related to microstructural deterioration such as coarsening and oxidation of Ni in anode, changes in anode pore size. Decay of electrical conductivities of anode and electrolyte, and sulfur contamination of anode are other major system degradation phenomena in these cells. Even though the impacts of operating parameters on each degradation reaction have been studied previously, their influences on the system as a whole were not well understood until the recent past.[5,16–18] Moreover, there seemed to be a conflict between the findings of some of these studies, as some revealed a positive correlation between SOFC degradation and its operating temperature while others showed that degradation rate is lower at higher temperatures. As such, there was a paucity of comprehensive information about how degradation of a conventional SOFC system as a whole could be managed by adjusting the operating conditions.

Degradation reactions in SOEC and how they are affected by the operating parameters are not well investigated compared to that of SOFC. Sohal et al. conducted long-term experiments on SOEC followed by post-test analyses of the components of SOEC at Idaho National Laboratory (INL).[19] Post-mortem scanning electron microscopy (SEM) revealed changes in the Ni particle size distribution and changes in the microstructure of the fuel electrode-electrolyte interface. However, the nature of the degradation reactions and the influence of the operating conditions on them remained an enigma. Hoerlein et al. tested number of identical SOECs under various current densities, operating temperatures, and fuel gas humidities.[20] They measured time evolution of SOEC performance degradation without studying causes of degradation. Until recently, open literature was lacking a model for degradation of SOEC with conventional technology with respect to its operating parameters. This has led many researchers to attempt to improve the technology in order to lower the degradation issues. However, as discussed above the new SOEC technologies are not likely to be commercially available in near future.

## 1.2. Thesis Objectives

At present, there is an urgent need in the energy sectors for replacing the traditional power units and energy storage systems with more efficient and environmentally friendly options. SOFC and SOEC are promising options for this purpose. Even though these cells can benefit from advancement of technology in the future, the existing SOFC and SOEC with the traditional technology can be used to reduce fossil fuel consumption and lower the environmental impacts. The objective of this thesis is to find the optimal trajectories of SOFC and SOEC with the traditional technology for an economical power generation (by SOFC) and hydrogen production (by SOEC). The main novelty of this work is that SOFC and SOEC degradation is considered in their economic and environmental analyses unlike several other studies that ignored or underrated degradation of these cells. This is significant, because the findings will enable us to manage SOFC and SOEC degradation, increase their useful operational time, and use them in a cost-effective manner without the need for improving the technology.

## 1.3. Thesis Contribution

- I developed a first-principles model in MATLAB for SOFC degradation using the publicly available studies in the literature on SOFC degradation. This is the first-ever SOFC model that accounts for main system degradation reactions in SOFC as well as its inevitable losses. This is achieved by integrating mathematical models of six governing system degradation reactions into the thermodynamic models of SOFC inevitable losses. This model settled the contradiction in the literature about the impact of operating temperature on SOFC degradation. This model enables calculating instantaneous degradation rate at each point of time and resolves the issue of inconsistency in the calculation of this metric in the literature. This issue was a result of using different numerical finite difference methods and had led to a broad range of numbers found for SOFC degradation rate. The details of this model have been explained in a peer-reviewed paper published in Industrial and Engineering Chemistry Research (I&EC Research). This was the first peer-reviewed paper published from this thesis project. This paper is provided in Chapter 2.

- Next, I evaluated the economic of power generation in large-scale using SOFC fueled by natural gas. For this, I solved an economic optimization problem in GAMS (General Algebraic Modeling System). This is the first-ever economic study of SOFCs that considers the effects of degradation using a detailed degradation model. This work showed how one can manage degradation of conventional SOFC and operate them economically over extended periods of time only by varying the operating conditions. This work also compared degradation and economic performance of SOFC systems in different operating modes. Finally, the impact of heat recovery from the exhaust of SOFC by adding heat exchangers to heat water on the economics of the system was examined. Chapter 3 consists of the peer-reviewed paper published from findings of this economic analysis in I&EC Research.

- Then, I studied environmental performance of natural gas-fueled SOFC while accounting for its degradation. The cradle-to-product life cycle environmental impacts of power production by SOFC at mid-point level was evaluated in SimaPro. This life cycle analysis (LCA) was performed using ReCiPe 2016 and TRACI 2.1 US-Canada 2008 methodologies based on detailed life cycle inventory data from open literature. This work also compared the environmental impacts of electricity generation from three different CHP systems that use natural gas as fuel namely; SOFC, internal combustion engine, and gas turbine. The third peer-reviewed paper published in Energy Conversion and Management during this thesis explains the details of this work. Chapter 4 consists of this paper.
- In the next step, I focused on scheduling start-up sequence of SOFC modules such that each individual module is operated at the optimal conditions and in the optimal mode. With this staggering approach each module degrades smoothly over time, and gradually loses power but the entire SOFC system as a whole delivers constant power. Chapter 5 consists of the paper published from this work in non-peer reviewed CSChE Systems & Controls transactions. This is the fourth paper published during this thesis.
- Next, I developed a data-driven model for SOEC degradation in ALAMO (Automated Learning of Algebraic Models) based on publicly available data of

long-term examination of SOECs under different conditions. This is the first-ever model developed for SOEC degradation. This model provides good prediction of time variations of SOEC performance due to its degradation as a function of current density, operating temperature, and fuel gas humidity. The paper published from this work in peer-reviewed Computer Aided Chemical Engineering journal goes into details of this model. Chapter 6 consists of this paper.

- Finally, I addressed economic and environmental viability of using SOEC for hydrogen generation. The main novelty of this work is considering SOEC degradation in its economic and environmental assessment which is critical for design and operation of a reliable system. The optimal trajectories for the most economic hydrogen generation by SOEC were found. A sensitivity study was performed to address the impacts of SOEC capital cost and price of supplied electricity on the economics of SOEC system. The environmental performance of SOEC with various power sources was evaluated through computing its cradle-to-gate life cycle GHG emissions. To complete this study, the cradle-to-gate life cycle GHG emissions per kg of hydrogen and levelized cost of hydrogen of SOEC with those of the existing hydrogen generation processes were compared. The sixth paper submitted to the peer-reviewed journal of Frontiers in Energy Research consists of the findings of this work. This paper is provided in Chapter 7.

## 1.4. References

(1) van Ruijven, B. J.; De Cian, E.; Sue Wing, I. Amplification of Future Energy

Demand Growth Due to Climate Change. *Nature Communications* **2019**, *10* (1), 1–12. https://doi.org/10.1038/s41467-019-10399-3.

(2) https://ourworldindata.org/electricity-mix.

(3) Jackson, R. B.; Friedlingstein, P.; Andrew, R. M.; Canadell, J. G.; Le Quéré, C.; Peters, G. P. Persistent Fossil Fuel Growth Threatens the Paris Agreement and Planetary Health. *Environmental Research Letters* **2019**, *14* (12). https://doi.org/10.1088/1748-9326/ab57b3.

(4) Zaccaria, V.; Tucker, D.; Traverso, A. A Distributed Real-Time Model of Degradation in a Solid Oxide Fuel Cell, Part II: Analysis of Fuel Cell Performance and Potential Failures. *Journal of Power Sources* **2016**, *327*, 736–742. https://doi.org/10.1016/j.jpowsour.2016.01.027.

(5) Ryan, E. M.; Xu, W.; Sun, X.; Khaleel, M. A. A Damage Model for Degradation in the Electrodes of Solid Oxide Fuel Cells: Modeling the Effects of Sulfur and Antimony in the Anode. *Journal of Power Sources* **2012**, *210*, 233–242. https://doi.org/10.1016/j.jpowsour.2012.02.091.

(6) Hagen, A.; Johnson, G. B.; Hjalmarsson, P. Electrochemical Evaluation of Sulfur Poisoning in a Methane-Fuelled Solid Oxide Fuel Cell: Effect of Current Density and Sulfur Concentration. *Journal of Power Sources* **2014**, *272*, 776–785. https://doi.org/10.1016/j.jpowsour.2014.08.125.

(7) Adams II, T. A.; Nease, J.; Tucker, D.; Barton, P. I. Energy Conversion with Solid

Oxide Fuel Cell Systems: A Review of Concepts and Outlooks for the Short- and Long-Term. *Industrial and Engineering Chemistry Research* **2013**, *52* (9), 3089–3111. https://doi.org/10.1021/ie300996r.

(8) Williams, M. C.; Strakey, J. P.; Surdoval, W. A. U. S. DOE Solid Oxide Fuel Cells: Technical Advances. *Proceedings - Electrochemical Society* **2005**, *PV 2005-07* (2005), 20–31. https://doi.org/10.1149/200507.0020pv.

(9) Lai, H.; Harun, N. F.; Tucker, D.; Adams II, T. A. Design and Eco-Technoeconomic Analyses of SOFC/GT Hybrid Systems Accounting for Long-Term Degradation Effects. *International Journal of Hydrogen Energy* **2021**, *46* (7), 5612–5629. https://doi.org/10.1016/j.ijhydene.2020.11.032.

(10) Godoi, G. S.; de Souza, D. P. F. Electrical and Microstructural Characterization of La0.7Sr0.3MnO3 (LSM), Ce0.8Y0.2O2 (CY) and LSM-CY Composites. *Materials Science and Engineering B: Solid-State Materials for Advanced Technology* **2007**, *140* (1–2), 90–97. https://doi.org/10.1016/j.mseb.2007.04.006.

(11) Li, Q.; Zhao, H.; Huo, L.; Sun, L.; Cheng, X.; Grenier, J. C. Electrode Properties of Sr Doped La2CuO4 as New Cathode Material for Intermediate-Temperature SOFCs. *Electrochemistry Communications* **2007**, *9* (7), 1508–1512. https://doi.org/10.1016/j.elecom.2007.02.013.

(12) Ishihara, T.; Honda, M.; Shibayama, T.; Minami, H.; Nishiguchi, H.; Takita, Y. Intermediate Temperature Solid Oxide Fuel Cells Using a New LaGaO3 Based Oxide Ion Conductor: I. Doped as a New Cathode Material. *Journal of The*

*Electrochemical Society* **1998**, *145* (9), 3177–3183. https://doi.org/10.1149/1.1838783.

(13) Yang, J.; Cheng, J.; Jiang, Q.; Wang, Y.; Wang, R.; Gao, J. Preparation and Electrochemical Properties of Strontium Doped Pr 2NiO4 Cathode Materials for Intermediate-Temperature Solid Oxide Fuel Cells. *International Journal of Hydrogen Energy* **2012**, *37* (2), 1746–1751. https://doi.org/10.1016/j.ijhydene.2011.09.146.

(14) Patro, P. K.; Delahaye, T.; Bouyer, E. Development of Pr0.58Sr0.4Fe0.8Co0.2O3 − δ–GDC Composite Cathode for Solid Oxide Fuel Cell (SOFC) Application. *Solid State Ionics* **2010**, *181* (29–30), 1378–1386. https://doi.org/10.1016/J.SSI.2010.07.004.

(15) Atlam, O.; Kolhe, M. Performance Analysis of PEM Fuel Cell with Varying Oxidant Supply Rates. *Journal of Energy Engineering* **2013**, *139* (1), 60–63. https://doi.org/10.1061/(asce)ey.1943-7897.0000090.

(16) Nakajo, A.; Mueller, F.; Brouwer, J.; Van Herle, J.; Favrat, D. Progressive Activation of Degradation Processes in Solid Oxide Fuel Cells Stacks: Part I: Lifetime Extension by Optimisation of the Operating Conditions. *Journal of Power Sources* **2012**, *216*, 449–463. https://doi.org/10.1016/j.jpowsour.2012.05.078.

(17) Hansen, J. B. Correlating Sulfur Poisoning of SOFC Nickel Anodes by a Temkin Isotherm. *Electrochemical and Solid-State Letters* **2008**, *11* (10), 178–180. https://doi.org/10.1149/1.2960521.

(18) Parhizkar, T.; Roshandel, R. Long Term Performance Degradation Analysis and Optimization of Anode Supported Solid Oxide Fuel Cell Stacks. *Energy Conversion and Management* **2017**, *133*, 20–30. https://doi.org/10.1016/j.enconman.2016.11.045.

(19) Sohal, M. S.; O'Brien, J. E.; Stoots, C. M.; Sharma, V. I.; Yildiz, B.; Virkar, A. Degradation Issues in Solid Oxide Cells during High Temperature Electrolysis. *ASME 2010 8th International Conference on Fuel Cell Science, Engineering and Technology, FUELCELL 2010* **2010**, *1*, 377–387. https://doi.org/10.1115/FuelCell2010-33332.

(20) Hoerlein, M. P.; Riegraf, M.; Costa, R.; Schiller, G. A Parameter Study of Solid Oxide Electrolysis Cell Degradation: Microstructural Changes of the Fuel Electrode. *Electrochimica Acta journal* **2018**, *276*, 162–175. https://doi.org/10.1016/j.electacta.2018.04.170.

# CHAPTER 2: A MATHEMATICAL MODEL FOR PREDICTION OF LONG-TERM DEGRADATION EFFECTS IN SOLID OXIDE FUEL CELLS

The content of this chapter is a published reprint of the following peer-reviewed publication:

Naeini, M., Lai, H., Cotton, J.S. and Adams, T.A.. A Mathematical Model for Prediction of Long-Term Degradation Effects in Solid Oxide Fuel Cells. *Industrial & Engineering Chemistry Research* **2021**, *60(3)*, pp.1326-1340.

## Abstract

A mathematical model of long-term solid oxide fuel cell (SOFC) degradation is proposed, based on a cross-cutting meta-study of SOFC degradation research available in the open literature. This model is able to predict long-term SOFC performance under different operating conditions, and it accounts for the main degradation mechanisms, including: Ni coarsening and oxidation; anode pore size changes; degradation of anode and electrolyte conductivity; and sulfur poisoning. The results of the study indicate that SOFCs initially degrade quickly, but that the degradation rate diminishes significantly after approximately 1000 hours of operation. Consequently, the effects of different factors associated with degradation rate are investigated, including current density, temperature, and partial pressure of $H_2$ in fuel source. Sensitivity analyses show that current density and $H_2$ partial pressure have the highest and the lowest impact, respectively. In addition, the model has been developed to assess sulfur poisoning within pre-reformed hydrocarbon-fuel-based SOFCs, while previous models have mostly focused on performance loss in $H_2$-fueled SOFCs. $H_2S$ deactivates catalytic activity of the SOFCs by reducing electrochemical activity and hydrocarbon conversion. Therefore, sulfur affects SOFCs that use different fuel sources in different ways. As a result, the models developed for $H_2$-fueled SOFCs cannot be used for hydrocarbon-fueled ones.

## Nomenclature

| **Nomenclature** | **Greek Symbols** |
|---|---|

| | |
|---|---|
| $A$ | area, $m^2$ |
| $A_{opt}$ | area of active TPB region, $m^2$ |
| $A_j^V$ | volume-specific surface area of reaction j, $m^2\ m^{-3}$ |
| $c_i$ | stoichiometric coefficient of species i |
| $c'_j$ | stoichiometric coefficient of species in forward reaction |
| $c''_j$ | stoichiometric coefficient of species in backward reaction |
| $D_p$ | pore diameter, m |
| $D_w$ | width of a corrugation, m |
| $D_{\mathrm{YSZ}}$ | mean diameter of YSZ particles, m |
| $D_{\mathrm{Ni}}$ | mean diameter of Ni particles, m |
| $D_s$ | atomic surface diffusion coefficient, $m^2\ s^{-1}$ |
| $D_{\mathrm{eff}}$ | effective diffusivity, $m^2\ s^{-1}$ |
| $D_{i\text{-}j}$ | binary diffusivity, $m^2\ s^{-1}$ |
| $D_k$ | Knudsen diffusivity, $m^2\ s^{-1}$ |
| $E_{\mathrm{act}}$ | activation energy, KJ $mol^{-1}$ |
| F | Faraday’s constant, C $mol^{-1}$ |
| $I$ | current, A |
| $\eta$ | overpotential loss, V |
| $\sigma$ | electrical conductivity, $\Omega^{-1}\ m^{-1}$ |
| $\varphi$ | porosity |
| $\tau$ | relaxation time, s |
| $\tau_s$ | surface tortuosity |
| $\tau_l$ | electrode tortuosity |
| $\mathcal{E}$ | volume fraction |
| $\beta$ | fitting parameter |
| $\lambda$ | fitting parameter |
| $\gamma$ | surface energy, J $m^{-2}$ |
| $\gamma_l$ | pre-exponential factor in electrode, A $m^{-2}$ |
| $\Omega$ | volume element, $m^3$ |
| $\delta_s$ | thickness, m |
| $\alpha$ | fraction of the reaction heat produced in the anode |
| $\nu_i$ | diffusion volume of species i |
| $\theta$ | overlap angle, 15° |
| $\rho_i$ | density, kg $m^{-3}$ |

**Subscripts and Superscripts**

| | |
|---|---|
| $0$ | initial condition |
| ac | air channel |

| | |
|---|---|
| $i$ | current density, A cm$^{-2}$ |
| $i_0$ | exchange current density, A cm$^{-2}$ |
| $k_B$ | Boltzmann constant, J K$^{-1}$ |
| $L$ | length, m |
| $L'$ | reaction-region thickness, m |
| $M_i$ | mean molar mass, kg mol$^{-1}$ |
| $N_{Ni}$ | number of Ni particles |
| $n$ | equivalent electron per mole of reactant, equiv mol$^{-1}$ |
| $P$ | pressure, Pa |
| $Pr$ | site occupation probability |
| R | gas constant, J mol$^{-1}$ K$^{-1}$ |
| $R_i$ | net rate of phase i formation, mol m$^{-3}$ s$^{-1}$ |
| $r$ | average radius of particles, m |
| $rd$ | degradation rate, % / 1000 hours |
| $\dot{s}_{i,j}$ | rate of formation of phase i in reaction j mol m$^{-2}$ s$^{-1}$ (for two-phase reactions) mol m$^{-1}$ $s^{-1}$ (for three-phase reactions) |
| $T$ | temperature, K |
| $t$ | time, s |

| | |
|---|---|
| an | anode |
| ca | cathode |
| ch | channel |
| ele | electrolyte |
| fc | fuel channel |
| ic | interconnect |
| l | anode, cathode |
| ohm | ohmic |
| act | activation |
| con | concentration |
| $t$ | channel shoulder |
| el | electronic |
| io | ionic |
| ref | reference |
| $x$ | x direction |
| $y$ | y direction |
| $z$ | z direction |
| $pd$ | product |
| $re$ | reactant |

| | |
|---|---|
| $TPB$ | triple phase boundary |
| $\Delta V_s$ | voltage drop due to sulfur poisoning, V |
| $V$ | voltage, V |
| $V_{Ni}$ | volume of Ni phase, m$^3$ |
| $W$ | weighting factor |
| $\overline{Z_0}$ | average initial coordination number |

## 1. Introduction

A solid oxide fuel cell (SOFC) is a power-generation unit that enables direct conversion of chemical energy from a fuel source into electrical energy with high electrical efficiency (60 $\%_{LHV}$) [1]. SOFC systems can be used at a wide variety of scales, such as in integrated community energy systems (ICEs) to supply heat and power at scales on the order of ten thousand people. Unlike other fuel cells that require $H_2$, SOFCs can generate electricity using various types of hydrocarbon-based fuels, including natural gas. The large amount of useful waste heat generated at high operating temperatures means that the heat can be harvested to further increase the total system level energy efficiency to $85\%_{LHV}$ [1]. For instance, this captured heat can be distributed via hot water pipes to meet the community's heat demands [2]. This is a key feature of SOFCs when integrated in ICEs, as replacing typical gas boilers with SOFCs can significantly reduce a community's GHG emissions. However, the limited lifetime of SOFCs has prevented their large-scale commercialization. In addition, it is critical to determine the proper cell size when implementing SOFCs in an ICE, as this will ensure that the community's energy needs are met. Furthermore, the loss in performance over time makes it important to determine not only the SOFC's initial performance capabilities, but also what its power output will be after long-term operation, as this information is critical for sizing and operating decisions [3].

The key to increasing lifetime of the SOFCs is to understand the various physical, chemical, and electrochemical reactions that take place by contaminants in the gas feed and operating conditions of SOFCs [4,5]. Deterioration processes affect various characteristics of the cells, such as the number and size of nickel particles, anode pore size and conductivity, the density of the triple phase boundary (TPB), and electrolyte conductivity [5]. A good degradation model should enable the rate and magnitude of irreversible performance loss to be measured at particular operating conditions, and it should also enable the determination of the cell's optimal operating conditions, thus extending its lifetime. Once these specifications have been identified, it is then possible to calculate which size of SOFC is ideal for an ICE under the given conditions. Although several studies have explored SOFC degradation, a general model that accounts for degradation mechanisms in the literature is still lacking. Due to several assumptions, the previously proposed models underestimate the degradation rate, which leads to the unrealistic sizing of the system [4–8]. The following example clarifies the importance of accurate calculation of degradation rate on sizing of the cells. For example, suppose SOFCs are needed by a community to operate at a particular condition, and the system is designed expecting that after 1000 hours of operation, the SOFCs should be able to deliver a minimum power of 20 kW. One study predicted an average degradation rate of 5%/kh, and thus the designers purchased SOFCs with an initial capacity of 21 kW. However, a more accurate study predicted an average degradation rate of 10%/kh over the first 1000 operational hours at that particular condition. With this rate of deterioration, the 21 kW SOFCs cannot deliver more than 18.95 kW after 1000 hours. In fact, considering the accurate prediction of the degradation rate, SOFCs should have a minimum capacity of 22.2 kW in the beginning to be able to meet the power constraint after 1000 hours.

Operating conditions such as temperature and current density significantly impact the long-term performance of SOFCs [4]; hence, the development of a degradation model that can account for effect of these parameters would allow system designers to change the design or the way it is operated in order to increase the lifetime of the cells [4]. Although the SOFC's high operating temperature affects the electrochemical reactions and the chemical stability of its components, it is not clear whether the SOFC's lifespan would be enhanced if it were run at lower temperatures. While some studies have found a positive correlation between degradation rate and temperature [9–12], others have shown that the degradation rate actually increases at lower temperatures [10,13,14]. Degradation mechanisms that occur due to interdiffusion, decomposition, corrosion of materials, or agglomeration of particles are more severe at higher temperatures, while poisoning-based processes such as sulfur poisoning are more prominent at lower temperatures [12]. Although poisoning and contamination are highly deteriorative, they can usually be avoided or controlled by coating SOFC components or changing their microstructure, or by changing fuel composition or the stoichiometry ratio [15–21]. Experiments studying the poisoning of SOFC components are usually performed under accelerated contamination conditions or on symmetric cells rather than full cells. Moreover, these experiments often focus on the isolated effects of contaminants, which means that their results do not account for the complex interactions between deterioration reactions across a full SOFC [13,14]. Other studies have found that the effects of other degradation mechanisms can be decreased and controlled by varying operating parameters, though they cannot be completely avoided [5].

A summary of degradation models found in the literature can be found in Table 1. From this summary, it is clear that the effects of operating temperature on SOFC performance are not very straightforward. For example, Nakajo et al.'s data-driven model and Parhizkar's model show that SOFCs have longer lifetimes when operated at lower temperatures [5,11]. The model developed by Nakajo et al. accounts for deterioration processes such as Ni particle coarsening in the anode, reduced electrolyte conductivity, and the corrosion of interconnect material [11]. Parhizkar et al.'s model considers Ni coarsening and oxidation, and anode conductivity degradation [5]. In contrast, Yoshizumi et al. found sulfur poisoning to be the main SOFC degradation mechanism, and performance loss increased at lower temperatures due to sulfur contamination [22].

Table 1. Overview of different models for SOFC performance.

| **Ref.** | **Notes** | **Common system degradation mechanisms in conventional SOFCs** | **Other phenomena considered** | **Degradation correlation** |
|---|---|---|---|---|

| | | Ni coarsening | Ni oxidation | Changes in anode pore | Changes in anode | Changes in electrolyte | Sulfur poisoning | | **with temperature** |
|---|---|---|---|---|---|---|---|---|---|
| Zaccaria et al. [4] | An algebraic equation for degradation rate is found by fitting to the experimental data. | | | | | | | | Negative correlation |
| Parhizkar et al. [5] | | ✓ | ✓ | | ✓ | | | | Positive correlation |
| Larrain et al. [23] | | | | | | | | Interconnect degradation | Positive correlation |
| Nakajo et al. [24] | | ✓ | | | | ✓ | | Zirconate formation in the LSM/YSZ cathode and anode re-oxidation. Cr poisoning. | Positive correlation |
| Aguiar et al. [8] | Provides an electrochemical model for SOFC that only accounts for inevitable degradation processes. | | | | | | | | |

| | | | | | | | | | |
|---|---|---|---|---|---|---|---|---|---|
| Wen et al. [25] | Couples an electrochemical model with a thermodynamic model, but only accounts for inevitable degradation mechanisms. | | | | | | | | Negative correlation |
| Yang et al. [7] | Develops an electrochemical model for SOFC that only accounts for inevitable losses. | | | | | | | | |
| Ryan et al. [26] | Constructs a damage model for SOFC degradation using experimental plots and fitting methods. | | | | ✓ | | ✓ | Changes in TPB and anode electrical conductivity due to sulfur and antimony poisoning. | Negative correlation |
| Hansen [27] | | | | | | | ✓ | | Negative correlation |
| Tucker et al. [28] | An algebraic equation for degradation rate is found by fitting to the experimental data. | | | | | | | | |
| Nakajo et al. [11] | | ✓ | | | | ✓ | | Interconnect corrosion, | Negative correlation |

| | | | | | | | | | |
|---|---|---|---|---|---|---|---|---|---|
| | | | | | | | | and Chromium contamination of cathode | |
| Yoshizumi et al. [22] | | | | | | | ✓ | | Negative correlation |
| This Work | | ✓ | ✓ | ✓ | ✓ | ✓ | ✓ | | Positive correlation |

As it can be seen in Table 1, some of the models developed for SOFC performance prediction only consider inevitable performance drop, which is a part of overpotential caused by unavoidable physical, chemical, and electrochemical deteriorating processes. Conventional thermodynamic equations for ohmic, activation, and concentration overpotentials account for inevitable performance losses (Eqs. 7-9, 32, 36, and 37 in the next section). However, system degradation processes can increase overpotential. Overpotential caused by system degradation mechanisms can be avoided or controlled by system design and operation [5]. To yield a precise prediction of long-term performance degradation in SOFCs, system losses should be added to the inevitable overpotentials. In other words, a comprehensive degradation model should account for the overpotentials due to system degradation mechanisms (such as deterioration of anode microstructure, degradation of anode and electrolyte conductivities, and contamination of the cells) in addition to the inevitable overpotentials. Most of the system deterioration reactions that are common in the conventional SOFCs are listed in columns 3-8 of Table 1. All models for

SOFC performance degradation take inevitable overpotentials into account. But these models usually ignore most system losses for simplification.

## 1.1 System degradation mechanisms

Several models have been developed for system contamination and degradation mechanisms in SOFCs. Models employed in the proposed comprehensive SOFCs performance models in this work are discussed in the following subsections.

### *1.1.1 System degradation mechanisms in electrolyte*

As modeled by Coors et al., yttria-stabilized zirconia (YSZ), which is the conventional electrolyte material for SOFCs, shows deterioration in electrical conductivity with time [29]. This is a system degradation mechanism that increases ohmic overpotential, however SOFC performance models usually assume that the electrical conductivity of YSZ does not change with time [5,8,25].

### *1.1.2 System degradation mechanisms in anode*

Degradation of anode microstructure that occurs in the form of Ni coarsening and oxidation, and in the pore diameter is a common cause of performance loss in anode-supported SOFCs. The number of nickel particles in the Ni-cermet anode decreases due to coarsening and oxidation. Gao et al. have proposed a theoretical model for the coarsening of nickel particles under SOFC operating conditions [30], while Neidhardt et al. have developed a model for the oxidation of nickel particles due to the presence of oxygen and steam at high temperature [31].

In addition to these factors, it is also important for degradation models to consider other consequences of nickel coarsening and oxidization, such as changes in pore size, degradation of anode electrical conductivity, and changes in area of active regions. Hardjo et al. studied the degradation of anode electrical conductivity as a result of a decrease in the number of nickel particles and an increase in their size [32,33]. Although pore size is generally assumed to be constant in degradation models, changes in pore diameter over time can affect SOFC performance by altering the area of active regions, TPB density, and mass diffusivity at the anode [5,7,8,25]. The model by Divisek and Wilkenhoener was selected for calculation of anode pore size [34]. Then it was updated by the size of Ni particles after coarsening to measure the changes in the pore size.

Different methods have been proposed for avoiding or decreasing the effects of degradation mechanisms. For instance, it is possible to reduce or avoid some of the contaminating mechanisms in SOFCs by changing or modifying its microstructure. In addition, selecting the proper carbon-to-steam molar ratio makes it possible to largely avoid carbon deposits on Ni-based anodes in hydrocarbon-fueled SOFCs [21]. Chromium poisoning of the cathodes also can be reduced significantly by applying proper coatings on the interconnect and the cathode [17]. Conversely, other studies have shown that the best approach to reducing sulfur poisoning is by controlling operating conditions, such as temperature and current density [14,21,26,35,36]. SOFCs have a high degree of fuel flexibility, which makes them suitable for use in ICEs, as they can be easily operated using natural gas (NG). However, NG contains $H_2S$, which can contaminate the SOFC's anode. This is problematic, as Aguilar et al. found sulfur contamination of the anode to be the main cause of cell performance degradation, with overall cell resistance increasing alongside the $H_2S$ concentration [37].

Various researchers have also modeled sulfur poisoning of $H_2$-fueled SOFCs [26,27]. For instance, Ryan et al. developed a damage model to quantify SOFC performance loss due to sulfur contamination, with results showing that performance deterioration is more severe at lower temperatures and when the fuel contains higher concentrations of $H_2S$ [26]. Prior sulfur poisoning models account for the impact of temperature on sulfur contamination in SOFC anodes that are supplied with $H_2$. Other research has found that current density also affects sulfur poisoning in Ni-YSZ anodes, as oxygen ion concentration changes with current density [36].

Unfortunately, the developed sulfur-poisoning models for $H_2$-fueled anodes cannot be used for hydrocarbon-fueled SOFCs. This lack of transferability is due to the fact that $H_2S$ not only poisons electrochemical reactions in the presence of hydrocarbons, but it also reduces catalytic reactions such as internal methane reformation [26,36]. Studies have shown that sulfur contamination of the SOFC anode can mostly be avoided by removing $H_2S$ from the fuel stream [22,36,38]. For example, Yoshizumi et al. showed that injecting a desulfurized fuel into an anode that has previously been poisoned by sulfur will cause sulfur desorption from the anode surface, reversing the sulfur poisoning effects. [22]. However, recovering from the effects of sulfur contamination requires sulfur removal and gas sweetening operations upstream which, depending on the scale of the system and intended application, may not always be practical. This would come at additional balance-of-plant costs, and more research is needed to examine the economic and practicality trade-offs with the context of SOFC degradation for hydrocarbon systems.

The models listed in Table 1 and discussed above face two main issues: 1) they ignore some of the main deteriorating mechanisms, and 2) an algebraic expression of degradation or voltage is produced by fitting to experimental data points, making the expression case-specific rather than generalizable. The objective of the present study is to develop a comprehensive model that accounts for the dominant degradation processes that commonly happen in SOFCs, primarily via theoretical equations. The proposed model accounts for the following degradation mechanisms: a) Ni coarsening, b) Ni oxidation, c) changes in anode pore size, d) changes in anode electrical conductivity, e) changes in electrolyte ionic conductivity, and f) sulfur poisoning. These are most of the common deterioration processes in conventional SOFCs with Ni-YSZ anodes, YSZ electrolytes, and $La_{1-x}Sr_xMnO_3$ (LSM) cathodes. Although different models are developed for each of these mechanisms in the literature, to the best of authors' knowledge this is the first model that takes all of these into account holistically and can be used for a broad range of applications. In the previously proposed models, most of these mechanisms have been ignored for simplification which results in underestimation of SOFCs degradation over long period of time.

The proposed model considers the common degradation effects to simulate the impact of operating conditions on long-term performance of SOFCs, thus allowing it to provide realistic results requiring minimal assumptions. The model applies to both hydrogen and hydrocarbon fuels, because it is informed by data from current density impact studies by

Hagen et al [36]. The results of this research are important for the wide commercialization of SOFCs in ICEs, as the presented model will allow system designers to select the optimal ICE system design and operational parameters with the degradation rate integrated into the control and operation strategy. Not only will this increase the SOFC's lifetime, but it will also allow system designers to select the optimal cell size for their specific energy system.

## 2. Modeling approach

An SOFC consists of a porous anode and cathode, dense electrolytes, and a metallic interconnect. The cell works by reducing oxygen molecules at the cathode/electrolyte interface to form oxygen ions which then migrate through the electrolytes to the anode. Once at the anode, the ions oxidize the fuel source via an electrochemical reaction (Eq. 1), producing high-temperature steam and free electrons. In this work, we show a general form of the model that can be used for $H_2$ fuel. However, with minor changes in some of the equations, this model can be used for carbonaceous fuels.

$$H_2 + O^{2-} \rightarrow H_2O + 2\ e^- \tag{1}$$

Dense YSZ, which is the electrolyte conventionally used in SOFCs, prevents direct fuel combustion via the solid-state conduction of ions. YSZ has a selective diffusion property, which allows the conduction of oxygen ions, but prevents the transport of gases molecules [39]. Moreover, YSZ's low electrical conductivity ensures the transfer of free electrons through the external circuit connecting the anode and the cathode, resulting in the generation of electricity (Fig. 1). Electrochemical reactions occur at the triple phase boundary (TPB), which is the interface between gas, the electrode, and the electrolyte.

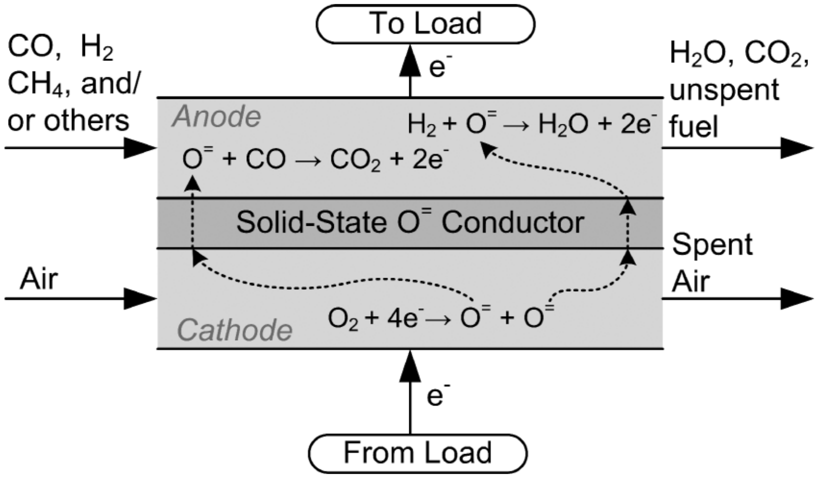

Fig. 1. Schematic of SOFC operation. Reprinted with permission from [40]. Copyright (2013) American Chemical Society.

The maximum voltage of an SOFC is achieved in an open circuit condition and is known as open circuit voltage (OCV). OCV can be calculated at different temperatures and partial gas pressures via the Nernst Equation (Eq. 4) and the Gibbs free energy change from the SOFC reaction, as shown in Eq. 2 [41].

$$\Delta G = \Delta G^{\circ} - \mathrm{R}T \ln\left(\frac{P_{\mathrm{H}_2} \cdot {P_{\mathrm{O}_2}}^{1/2}}{P_{\mathrm{H}_2\mathrm{O}}}\right) \qquad (2)$$

In Eq. 2, $\Delta G^{\circ}$ is the Gibbs free energy change of the water formation reaction (Eq. 1) at standard pressure (1 atm), and $P_i$ is the partial pressure of gas species $i$ in the fuel and air channels.

$$E = \frac{-\Delta G}{n\mathrm{F}} \tag{3}$$

Where $E$ is the OCV at the SOFC's operating condition, $n$ is the moles of electrons involved in the water formation reaction, (2 for Eq. 1), and F is the Faraday constant. The Nernst Equation is then obtained by substituting Eq. 2 into Eq. 3:

$$E = E^{\circ} + \frac{\mathrm{R}T}{n\mathrm{F}} \ln\left(\frac{P_{\mathrm{H_2}} \cdot {P_{\mathrm{O_2}}}^{1/2}}{P_{\mathrm{H_2O}}}\right) \tag{4}$$

In this equation, $E^{\circ}$ is the SOFC's OCV at standard pressure (1 atm).

In addition, the OCV for SOFCs that use other types of fuels can be calculated using the Nernst equation with the Gibbs free energy change of the fuel's oxidation reaction. Eq. 5 shows the general form of OCV for fuel's oxidation reaction:

$$E = E^{\circ} + \frac{\mathrm{R}T}{n\mathrm{F}} \ln\left(\frac{\prod_{re} P_{re}^{c_{re}}}{\prod_{pd} P_{pd}^{c_{pd}}}\right) \tag{5}$$

Where $re$ and $pd$ stand for reactants and products, respectively. $P_{re}$ and $P_{pd}$ are partial pressure of reactants and products. While, $c_{re}$ and $c_{pd}$ account for the stoichiometric coefficients of reactants and products in the fuel's oxidation reaction, respectively.

When current flows through the external circuit, voltage deviates from the OCV due to activation, ohmic, and concentration overpotentials/polarizations (Eq. 6) [8,41]. Overpotentials partially occur as a result of physical, chemical, and electrochemical reactions in the cell components; the rest of the potential loss is caused by degradation mechanisms, which can be reduced or controlled by varying the cell's operating parameters [5]:

$$V(t) = E - \left(\sum_k \eta_{\mathrm{ohm},k}(t) + \eta_{\mathrm{act,an}}(t) + \eta_{\mathrm{act,ca}}(t) + \eta_{\mathrm{con,an}}(t) + \eta_{\mathrm{con,ca}}(t)\right) \quad (6)$$

where $\eta_{\mathrm{ohm}}$ is the ohmic losses from electronic and ionic resistances in or between cell compartments ($k$ = anode, cathode, electrolyte, and interconnect), $\eta_{\mathrm{act,an}}$ and $\eta_{\mathrm{act,ca}}$ are the activation overpotentials that are needed to overcome energy barriers of electrochemical reactions in the anode and cathode respectively, and $\eta_{\mathrm{con,an}}$ and $\eta_{\mathrm{con,ca}}$ are concentration overpotentials due to the spatial gradient of gases concentration in the anode and cathode, respectively. Overpotentials are caused due to inevitable losses and system degradation mechanisms. Conventional thermodynamic equations for overpotentials only account for inevitable losses. To consider system losses, relative models of degradation mechanism should be implemented into/added to thermodynamic equations. Fig. 2 shows an outline of the prediction model for long-term performance of SOFCs in the current study.

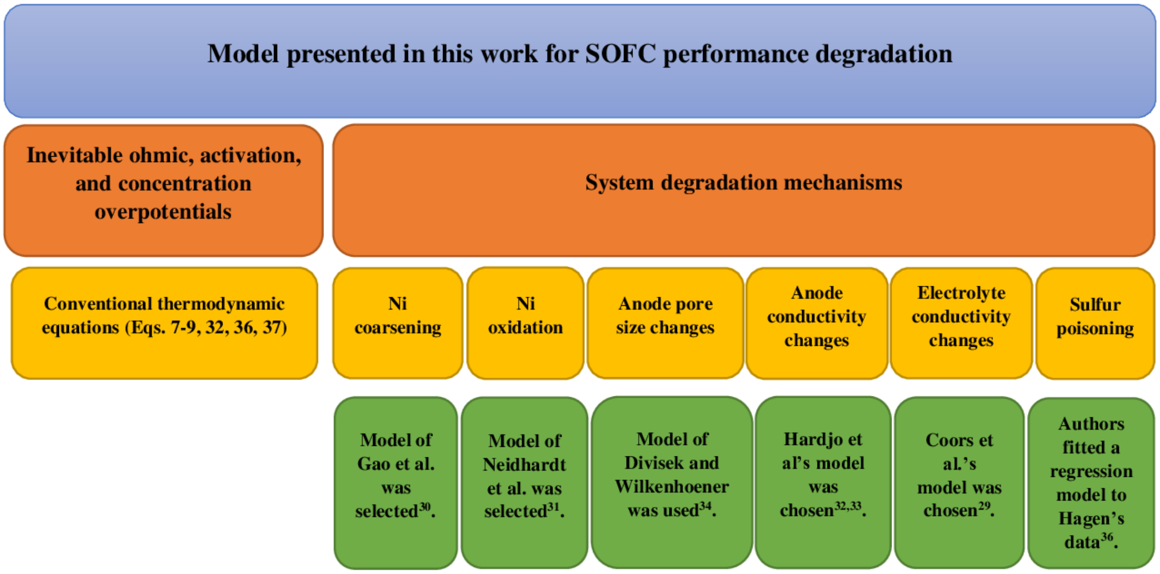

Fig. 2. Outline of the SOFC long-term performance model in the present study.

For some of the degradation mechanisms, different models have been presented in the literature. In this work, in order to find the best model for each phenomenon, the models were validated against experimental data. Those that showed the best agreement with experiments were used in the current model and reported in the following sections.

### 2.1. Ohmic polarization

Ohmic overpotential is the result of ionic and electronic resistances within or between components. Ohmic losses in different components can be calculated via Ohm's Law [8,25].

$$\eta_{\mathrm{ohm,ic}} = I\,\left(\frac{L_{\mathrm{ic}}}{L_y\,L_z\,\sigma_{\mathrm{ic}}} + \frac{L_{\mathrm{fc}}}{(1+n_{\mathrm{ch}})L_t\,L_y\,\sigma_{\mathrm{ic}}} + \frac{L_{\mathrm{ac}}}{(1+n_{\mathrm{ch}})L_t\,L_z\,\sigma_{\mathrm{ic}}}\right) \tag{7}$$

$$\eta_{\mathrm{ohm,ele}} = I\,\left(\frac{L_{\mathrm{ele}}}{L_y\,L_z\,\sigma_{\mathrm{ele}}\,(t)}\right) \tag{8}$$

$$\eta_{\mathrm{ohm,l}} = I\,\left(\frac{\left(A_{\mathrm{opt},l}(t)-L_y\,L_z\right)L'_{\mathrm{opt},l}}{2\,A_{\mathrm{opt},l}(t)\,L_y\,L_z\,(1-\varphi_l)\sigma_{\mathrm{ele}}\,(t)} + \frac{L_l-L'_{\mathrm{opt},l}}{L_y\,L_z\,(1-1.8\varphi_l)\,\sigma_l(t)}\right) \tag{9}$$

$l = \text{anode}, \text{cathode}$

Where $I$ is the working current (A), $L$ is the thickness (m), $n_{\mathrm{ch}}$ is the number of channels on electrode, $\sigma_l$ is the conductivity of component $l$ ($\Omega^{-1}$ $\mathrm{m}^{-1}$), and $A_{opt,l}$ is the area of active TPB regions, which can be expressed as:

$$A_{opt,l}\,(t) = \left(1 + 2\,\frac{L'_{\mathrm{opt},l}}{D_{p,l}}\right)\,L_y\,L_z \tag{10}$$

In Eq. 10 $L'_{\mathrm{opt}}$ is the active TPB region thickness (m), and $D_p$ is the average pore diameter (m). It can be assumed that cathode has parallel pores with average diameters that do not change over time, as cathodes are made from ceramic material that features high stability under oxidizing conditions (Eq. 11) [25].

$$D_{p,\mathrm{ca}} = D_{w,\mathrm{ca}}\, \varphi_{\mathrm{ca}}/(1 - \varphi_{\mathrm{ca}}) \tag{11}$$

$D_{w,\mathrm{ca}}$ is width of a corrugation in the cathode structure and $\varphi_{\mathrm{ca}}$ is the cathode porosity.

However, a more accurate model is required to capture the changes in the average diameter of anode pores that take place over time due to the oxidation and coarsening of Ni particles. Eq. 12 can be used to calculate anode pore size, as it accounts for the volume fraction and size of nickel particles that change over time [34].

$$D_{p,\mathrm{an}}(t) = D_{\mathrm{YSZ}}\, \varepsilon_{\mathrm{YSZ}}(t) + D_{\mathrm{Ni}}(t)\, \varepsilon_{\mathrm{Ni}}(t) \tag{12}$$

$D_j$ is the average diameter of phase $j$ particles (m), and $\varepsilon_j$ is the volume fraction of phase $j$ [7].

### *2.1.1. Nickel coarsening and Nickel oxidation*

The size and number of Ni particles, as well as the volume fraction of solid phases in the Ni-cermet anode, change due to the agglomeration and oxidation of the Ni particles. Gao et al. developed a theoretical model for Ni coarsening [30], which showed that Ni particles initially show a rapid growth rate, but that this growth rate slows with time. The presence of YSZ in the anode microstructure prevents the extreme growth of Ni particles; thus, Ni particles reach a maximum radius in the composite microstructure [42]. This theoretical model has a fitting parameter ($\beta$) for minor adjustments whose value has a small impact on the final results. The model was fitted to Tanasini et al's experimental data [43] and showed a good agreement with their data.

$$\frac{r_{\mathrm{Ni,max}}^5 - r_{\mathrm{Ni}}^5(t)}{r_{\mathrm{Ni,max}}^5 - r_{\mathrm{Ni,0}}^5} = \exp\left( \frac{-5\,C}{r_{\mathrm{Ni,max}}^5 - r_{\mathrm{Ni,0}}^5} t \right) \tag{13}$$

$r_{\mathrm{Ni,max}}$ and $C$ are given as follows,

$$r_{\mathrm{Ni,max}}\,(t) = \left( \frac{\varepsilon_{\mathrm{Ni}}\,(t)\,\overline{Z_0}\,(1+3\beta^2) + (1+\beta)^3}{(1+\beta)^3} \right)^{1/3} r_{\mathrm{Ni,0}} \tag{14}$$

$$C = D_s\,\frac{\gamma\,\Omega\,\delta_s}{2\,\mathrm{k_B}T}\,\frac{\beta}{(1-\beta^2)\,(1+\beta^2)^{0.5}\,(1+\beta)^3}\,\overline{Z_0}\,\frac{\varepsilon_{\mathrm{Ni}}(t)}{\frac{\varepsilon_{\mathrm{Ni}}(t)}{r_{\mathrm{Ni,0}}} + \frac{\varepsilon_{\mathrm{Ni}}(t)}{r_{\mathrm{YSZ}}}} \tag{15}$$

where $\mathrm{k_B}$ is the Boltzmann constant, $r_{\mathrm{Ni}}$ and $r_{\mathrm{YSZ}}$ are Ni particle size and radius of YSZ particles in the Ni-YSZ anode, $r_{\mathrm{Ni,0}}$ is the initial radius of Ni particle, $D_s$ is the atomic surface diffusion coefficient, $\Omega$ is the volume element, $\gamma$ is the surface energy , $\delta_s$ is the thickness, $\overline{Z_0}$ is the average initial coordination number, and $\beta$ is the fitting parameter which is adjusted such that model best fits the experimental data using a minimize sum of square errors approach. $\beta$ received the value 0.038 for the anode microstructure tested by Tanasini et al. [41].

The number of Ni particles after agglomeration ($N_{\mathrm{Ni,c}}$) can be calculated using the total volume of Ni phase [43]:

$$V_{\mathrm{Ni}}(t) = V_{\mathrm{Ni,0}} \tag{16}$$

$$N_{\mathrm{Ni}}(t)\,\frac{4}{3}\,\pi\,r_{\mathrm{Ni}}^3(t) = N_{\mathrm{Ni,0}}\,\frac{4}{3}\,\pi\,r_{\mathrm{Ni,0}}^3 \tag{17}$$

$$N_{\mathrm{Ni},c}\,(t) = \left(\frac{r_{\mathrm{Ni,0}}}{r_{\mathrm{Ni}}(t)}\right)^3 N_{\mathrm{Ni,0}} \tag{18}$$

$V_{\mathrm{Ni,0}}$ and $N_{\mathrm{Ni,0}}$ are initial volume of Ni phase (m$^3$) and initial number of Ni particles, respectively.

In addition, Ni can be oxidized with oxygen molecules (Eq. 19) or steam (Eq. 20) through a thermochemical reaction [31].

$$\mathrm{Ni} + \frac{1}{2}\,\mathrm{O_2} \leftrightarrow \mathrm{NiO} \tag{19}$$

$$\mathrm{Ni} + \mathrm{H_2O} \leftrightarrow \mathrm{NiO} + \mathrm{H_2} \tag{20}$$

In order to calculate number of remaining particles after oxidation, it is necessary to first calculate the rate of NiO formation. The model developed by Neidhardt et al. can be used to achieve this task [31,44].

$$N_{\mathrm{NiO}}(t) = \int R_{\mathrm{NiO}}\, dt \tag{21}$$

Where $R_{\mathrm{NiO}}$ is the rate of NiO formation (mol m$^{-3}$ s$^{-1}$) and $N_{\mathrm{NiO}}$ is the number of NiO particles formed during the oxidation of the anode. Eqs. 22-26 are used to calculate rate of NiO formation. The found Eq. for NiO formation then will substitute for $R_{\mathrm{NiO}}$ in Eq. 21 to quantify number of NiO particles formed in the anode.

$$\frac{\partial(\rho_i \varepsilon_i)}{\partial t} = R_i\, M_i \tag{22}$$

$\rho_i$ and $M_i$ are the density and molar mass of species $i$, respectively.

$$R_i = \sum_j \dot{s}_{i,j} A_j^V \tag{23}$$

$A_j^V$ is the volume-specific surface area of reaction $j$ ($m^2/m^3$).

$$A_j^V = f\, A_0^V \exp\left(-50\, \varepsilon_{\mathrm{NiO}}\right) \tag{24}$$

$$f = 1 - \left|\tanh(10^9 \varepsilon_{\mathrm{NiO}}) - \tanh(10^9\, \varepsilon_{\mathrm{Ni}})\right| \tag{25}$$

Where $\dot{s}_{\mathrm{i,j}}$ represents the rate of species $i$ production in reaction $j$ (mol $m^{-2}$ $s^{-1}$), which can be evaluated using Eq. 26.

$$\dot{s}_i = c_i \left(k_f \prod_{j \epsilon R_f} a_j^{c'_j} - k_r \prod_{j \epsilon R_r} a_j^{c''_j}\right) \tag{26}$$

In this equation, $k_f$ and $k_r$ represent the forward and backward rate constants, with $c_i$ as the stoichiometric coefficient of species $i$, and $c'_j$ and $c''_j$ as the stoichiometric coefficients of species *i* in forward and backward reactions, respectively.

Eq. 27 shows the number particles remaining after coarsening and oxidation.

$$N_{\mathrm{Ni}}(t) = N_{\mathrm{Ni},c}(t) - N_{\mathrm{NiO}}(t) \tag{27}$$

### 2.1.2. Electrical conductivity of anode

Microstructural changes in the anode due to Ni agglomeration and oxidation result in the degradation of TPB density and electrical conductivity. The anode has a percolated network that consists of YSZ and Ni phases. Percolation theory can be used to calculate the TPB density and electrical conductivity of the percolated network [9,33,45]:

$$A(t) = K_A N_{\mathrm{Ni}}(t) \times 4\pi\, r_{\mathrm{Ni}}^2(t) \tag{28}$$

$A(t)$ is the active surface area of the catalyst layer in the anode.

$$\frac{Pr(t)}{Pr_c} = \frac{A(t)}{A_0} \tag{29}$$

$Pr$ and $Pr_c$ are site occupation probability and site occupation at the percolation threshold, respectively.

The electrical conductivity of an anode drops rapidly during the first hours of operation, but levels off later. Deterioration in anode conductivity is correlated to the coarsening of Ni particles [33,46].

$$\sigma_{Ni}(t) = f_r\, \sigma_{0,\mathrm{an}} \left(\frac{Pr(t) - Pr_c}{1 - Pr_c}\right)^{1.3} \frac{\varepsilon_{\mathrm{Ni}}(t)}{\tau_s} \tag{30}$$

Where $\sigma_0$ represents bulk conductivity, with $\tau_s$ as surface tortuosity and $f_r$ as the ratio of the resistance of a continuous film to the resistance of a sintered film ($\frac{R_{\mathrm{film}}}{R_{\mathrm{eff}}}$), which is a function of the particles' overlap angle (almost 0.575 at angle 15°) [33]. Among the few models that were proposed for the anode electrical conductivity in the literature, we found this model to best agree with the experimental data by Klemenso et al. [47] with an $R^2$ of 0.947. In addition, the calculated site occupation probability in this work, showed an $R^2$ of 0.99 with the Klemenso et al.'s data [47]. The validation results are shown in the Supporting Information.

### *2.1.3. Electrolyte conductivity*

Research has shown an exponential drop in the ionic conductivity of the YSZ electrolytes, which has been modeled by Coors et al. as follows [29]:

$$\sigma(t) = (\sigma_i - \sigma_f) \exp(-t/\tau) + \sigma_i \tag{31}$$

In Eq. 31, $\sigma_i$ is the initial or maximum ionic conductivity of the electrolytes, while $\sigma_f$ represents their final conductivity and $\tau$ is the relaxation time.

## 2.2. Activation polarization

Activation polarization, which is defined as an overpotential above equilibrium, takes place in order to overcome the activation energy barrier that limits the electrochemical reaction in the fuel cell that generates current [48]. The following equation, which is obtained by solving the Butler-Volmer equation, is used to quantify the activation overpotential of an SOFC [25]. The length of the TPB regions plays an important role in activation overpotential, as less activation overpotential is required to produce a specific current when larger active regions are available [7]. In following equation, the effect of TPB density on activation polarization is embedded in the exchange current density, $i_0$.

$$\eta_{\mathrm{act},l} = \frac{\mathrm{R}T}{\alpha n\mathrm{F}} \sinh^{-1}\left(\frac{i_l(t)}{2i_{0,l}}\right) \tag{32}$$

Where α is the charge transfer coefficient and equals 0.5, and n is the number of electrons transferred in the reaction and takes the value of 2 for the anodic reaction and 4 for the cathodic reaction. The term $i_{0,l}$ represents the exchange current density (A m$^{-2}$), and can be calculated for the cathode and anode using Eqs. 33 and 34, respectively [49].

$$i_{0,\mathrm{ca}} = \gamma_{\mathrm{ca}}\left(\frac{P_{\mathrm{O_2}}}{P_{\mathrm{ref}}}\right)^{0.25} \exp\left(-\frac{E_{\mathrm{act,ca}}}{\mathrm{R}T}\right) \tag{33}$$

$$i_{0,\mathrm{an}} = \gamma_{\mathrm{an}}\left(\frac{P_{\mathrm{H_2}}}{P_{\mathrm{ref}}}\right)\left(\frac{P_{\mathrm{H_2O}}}{P_{\mathrm{ref}}}\right) \exp\left(-\frac{E_{\mathrm{act,an}}}{\mathrm{R}T}\right) \tag{34}$$

The working current density of the electrodes can be expressed as [25]:

$$i_l(t) = \frac{I}{A'_{opt,l}(t)} \tag{35}$$

Where $\gamma_l$ is the pre-exponential factor (A m$^{-2}$), $E_{\mathrm{act},l}$ is the activation energy of the electrode (kJ mol$^{-1}$), and $P_{\mathrm{ref}}$ is the reference pressure, which is set to the atmospheric pressure.

## 2.3. Concentration polarization

Concentration overpotential takes place when the concentration of the gaseous reactants at reaction sites is lower than the bulk concentration. In fact, a spatial concentration gradient is produced when the rate of consumption of a reactant is higher than the rate of diffusion, which leads to fuel cell voltage degradation. In open-circuit condition, the concentration of gaseous species in the pores of the electrodes is the same as bulk concentration; however, spatial variation in concentration evolves with current flow, with higher currents resulting in larger concentration gradients [8,50]. The following model is used to evaluate concentration overpotential in the electrodes of SOFCs. The TPB is considered as the electrochemical active region in which fuel cell reactions take place. $H_2$ and $H_2O$ are on the anode side, and $O_2$ and $N_2$ are on the cathode side [8].

$$\eta_{\mathrm{con,ca}} = \frac{\mathrm{R}T}{n\mathrm{F}} \ln\left(\frac{P_{\mathrm{O_2}}}{P_{\mathrm{O_2,TPB}}(t)}\right) \tag{36}$$

$$\eta_{\mathrm{con,an}} = \frac{\mathrm{R}T}{n\mathrm{F}} \ln\left(\frac{P_{\mathrm{H_2O,TPB}}(t)\, P_{\mathrm{H_2}}}{P_{\mathrm{H_2,TPB}}(t)\, P_{\mathrm{H_2O}}}\right) \tag{37}$$

The partial pressures of gaseous species at the TPB is a function of effective diffusivity at the electrode. Neglecting external diffusion, the partial pressures of gases at the TPB regions are given by [8,25]:

$$P_{\mathrm{H_2,TPB}}(T) = P_{\mathrm{H_2}} - \frac{\mathrm{R}T\, L_{\mathrm{an}}\, I}{n\, \mathrm{F}\, L_y\, L_z\, D_{\mathrm{eff,an}}(t)} \tag{38}$$

$$P_{\mathrm{H_2O,TPB}}(T) = P_{\mathrm{H_2O}} + \frac{\mathrm{R}T\, L_{\mathrm{an}}\, I}{n\, \mathrm{F}\, L_y\, L_z\, D_{\mathrm{eff,an}}(t)} \tag{39}$$

$$P_{\mathrm{O_2,TPB}}(t) = P_{\mathrm{air}} - \left(P_{\mathrm{air}} - P_{\mathrm{O_2}}\right) \exp\left(\frac{\mathrm{R}T\, L_{\mathrm{ca}}\, I}{n\, \mathrm{F}\, L_y\, L_z\, D_{\mathrm{eff,ca}}(t)\, P_{\mathrm{air}}}\right) \tag{40}$$

$$D_{\mathrm{eff,an}}(t) = \left(\frac{P_{\mathrm{H_2}}}{P_{\mathrm{f}}}\right) D_{\mathrm{H_2O,eff}}(t) + \left(\frac{P_{\mathrm{H_2O}}}{P_{\mathrm{f}}}\right) D_{\mathrm{H_2,eff}}(t) \tag{41}$$

$$D_{\mathrm{eff,ca}}(t) = D_{\mathrm{O_2,eff}}(t) \tag{42}$$

Where $D_{\mathrm{eff},l}$ is the effective diffusivity of the electrode ($\mathrm{m^2\ s^{-1}}$).

Depending on the mean size of the pores and the mean free path of the gas molecules, Knudsen or binary diffusion can take place in porous structures. Binary diffusion occurs when gas molecules diffuse through pores that are larger than the mean free path of gas particles, while Knudsen diffusion occurs when the pores are smaller than the mean free path of the molecules [50].

The effective diffusion of gases in the porous electrodes of SOFCs is generally considered as a combination of Knudsen ($D_{i,K}$) and binary diffusion ($D_{i-j}$) to account for different porous structures [7].

$$D_{\mathrm{H_2,eff}}(t) = \frac{\varphi_{\mathrm{an}}}{\tau_{\mathrm{an}}} \left(\frac{1}{D_{\mathrm{H_2-H_2O}}} + \frac{1}{D_{\mathrm{H_2},K}(t)}\right)^{-1} \tag{43}$$

$$D_{\mathrm{H_2O,eff}}(t) = \frac{\varphi_{\mathrm{an}}}{\tau_{\mathrm{an}}} \left(\frac{1}{D_{\mathrm{H_2-H_2O}}} + \frac{1}{D_{\mathrm{H_2O},K}(t)}\right)^{-1} \tag{44}$$

$$D_{\mathrm{O_2,eff}}(t) = \frac{\varphi_{\mathrm{ca}}}{\tau_{\mathrm{ca}}} \left(\frac{1}{D_{\mathrm{O_2-N_2}}} + \frac{1}{D_{\mathrm{O_2},K}(t)}\right)^{-1} \tag{45}$$

Chapman et al. [51], Arnold [52], Gilliland [53], and Fuller et al. [54] have all developed different empirical models for binary gas diffusion. However, Fuller et al.'s semi-empirical method provides the best agreement with experimental results. Their model is expressed as follows [54]:

$$D_{i-j} = \frac{0.00143\, T^{1.75}}{P\, M_{ij}^{0.5}\, [(\sum \nu)_i^{\frac{1}{3}} + (\sum \nu)_j^{\frac{1}{3}}]^2} \tag{46}$$

T and P are the temperature and total pressure of the gas stream, respectively, while $\nu_i$ is the diffusion volume of species $i$ ($\nu_{\mathrm{H_2}}$ = 6.12, $\nu_{\mathrm{H_2O}}$ = 13.1, $\nu_{\mathrm{O_2}}$ = 16.3 and $\nu_{\mathrm{N_2}}$ = 18.5). $M_{ij}$ is defined as,

$$M_{ij} = 2[\frac{1}{M_i} + \frac{1}{M_j}]^{-1} \tag{47}$$

Where $M_i$ is the molecular weight of species $i$ in kg/mol.

Knudsen diffusion can be calculated using following equation:

$$D_{i,K}(t) = 48.5\, D_{p,l}(t)(\frac{T}{M_i})^{0.5} \tag{48}$$

## 2.4. Sulfur Poisoning

Sulfur poisoning takes place when fuel containing $H_2S$ is supplied to the SOFC anode. This is commonly added as an odorant to hydrocarbon-based fuels, such as natural gas. The sulfur in the fuel is chemisorbed on the Ni-based anode at the SOFC's operating conditions, resulting in the deactivation of the anode's catalytic behavior [21,35]. A study by Matsuzaki and Yasuda showed that, at 750℃ and an $H_2S$ concentration as low as 0.05 ppm, anode electrochemical performance deteriorates dramatically [55].

The key to SOFCs' fuel flexibility is their ability to convert hydrocarbons at high operating temperatures. Sulfur poisoning affects hydrocarbon conversion and electrochemical reactions. Prior findings have shown that, when the fuel stream contains 50 ppm $H_2S$, a large amount of the $CH_4$ supplied to the anode leaves the cell without being converted [56]. Different empirical models have been developed using curve-fitting approaches in order to show how sulfur contamination affects the performance of SOFCs. Alstrup applied a Temkin-like isotherm to explain sulfur adsorption on the Ni catalyst [57]. While a model developed by Hansen et al. illustrates a linear relationship between sulfur surface coverage and a drop in SOFC performance. This model was obtained by fitting the experimental data obtained by Zha et al. and Cheng et al. for SOFC power loss with regards to surface coverage [27,58,59]. Ryan et al. used Zha et al.'s data to construct a damage model that shows the effects of sulfur poisoning on performance loss over a range of temperatures and $H_2S$ concentrations [26,58].

The complex nature of sulfur poisoning is not well understood, as it depends on several factors, such as temperature, $H_2S$ concentration, current density, and steam-to-carbon ratio [35,36,58]. Without considering these factors, models are confined to the operating conditions reported by Zha et al. for $H_2$-fueled SOFCs.

Studies have illustrated that impact of sulfur compounds on the catalytic activity of the Ni-based anodes occurs very rapidly that the time dependency of it can be neglected comparing to the long lifetime of the SOFCs [27]. In the present work, Hagen et al.'s experimental data is adapted to enable the model to be capable of simulating changes in SOFC performance with respect to current density at different $H_2S$ concentrations [36]. The experimental data used in this model was obtained from a cell supplied with a fuel stream of 29% $CH_4$, 58% $H_2O$, and 13% $H_2$ mixed with various amounts of $H_2S$. This fuel mixture is a good representative of pre-reformed $CH_4$-containing fuel. Accumulated voltage drop versus $H_2S$ concentration plots were given at 4 different current densities (0, 0.25, 0.5 and 1 A/cm$^2$). Using the given information at 0, 0.5 and, 1 A/cm$^2$, performance loss was modeled as a function of $H_2S$ concentration and current density.

Thus, the following equations are suggested based on the cell's behaviour over the studied range of $H_2S$ concentrations and current densities:

$$\Delta V_{\mathrm{s}} = W_1 \, f_1\left(i, C_{\mathrm{H_2S}}\right) + W_2 \, f_2\left(i, C_{\mathrm{H_2S}}\right) \tag{49}$$

where $\Delta V_{\mathrm{s}}$ is the voltage drop due to sulfur poisoning (V), with $i$ as the current density (A/cm$^2$) and $C_{\mathrm{H_2S}}$ as the $H_2S$ concentration in the fuel source (ppm).

When the model was fitted to Zha et al.'s experimental data, the functions of coefficients A and B were found to be;

$$f_1\left(i, C_{\mathrm{H_2S}}\right) = \ln(C_{\mathrm{H_2S}}) \tag{50}$$

$$f_2\left(i, C_{\mathrm{H_2S}}\right) = Y_{\max}(i)(1 - A_1(i) \, \exp\left(-A_2(i) \times C_{\mathrm{H_2S}}\right)) \tag{51}$$

As shown in Figure 3, model replicates the shape of the experimental data by considering the weighted sum of two different functions with logarithmic or asymptotic behaviour. Each function has a different weighting at different current densities. The weighting factors, $W_1$ and $W_2$, and other coefficients are given as follows:

$$W_1 = -0.039\, i^2 + 0.009\, i + 0.030 \tag{52}$$

$$W_2 = 1 - W_1 \tag{53}$$

$$A_1 = 0.827 \exp(0.411\, i) \tag{54}$$

$$A_2 = 0.064 \exp(0.995\, i) \tag{55}$$

SOFC performance declines as $H_2S$ concentration increases until a monolayer of sulfur forms on the Ni-cermet anode. At this point, the anode reaches a saturation point after which the addition of more $H_2S$ no longer significantly inhibits SOFC performance [27]. The saturation point depends on the current density, with higher current densities resulting in a greater loss in performance prior to reaching it. $Y_{\max}$ in Eq. 51 corresponds to the maximum performance loss (V), which is obtained under saturation conditions. Comparing the plots reported by Hagen et al. [36], it can be concluded that saturated performance loss is exponentially correlated with current density. Eq. 55 had the best agreement with the experimental data.

$$Y_{\max} = 6.749 \exp\,(1.559\, i) \tag{56}$$

The values of the coefficients were then calculated at 0.25 A/cm$^2$ to predict the accumulated voltage loss of the same cell obtained by the model (Fig. 3). An $R^2$ of 0.976 demonstrates the model's ability to predict the decline in SOFC performance due to the sulfur contamination when $H_2S$ enters the cell with a pre-reformed hydrocarbon-based fuel mixture.

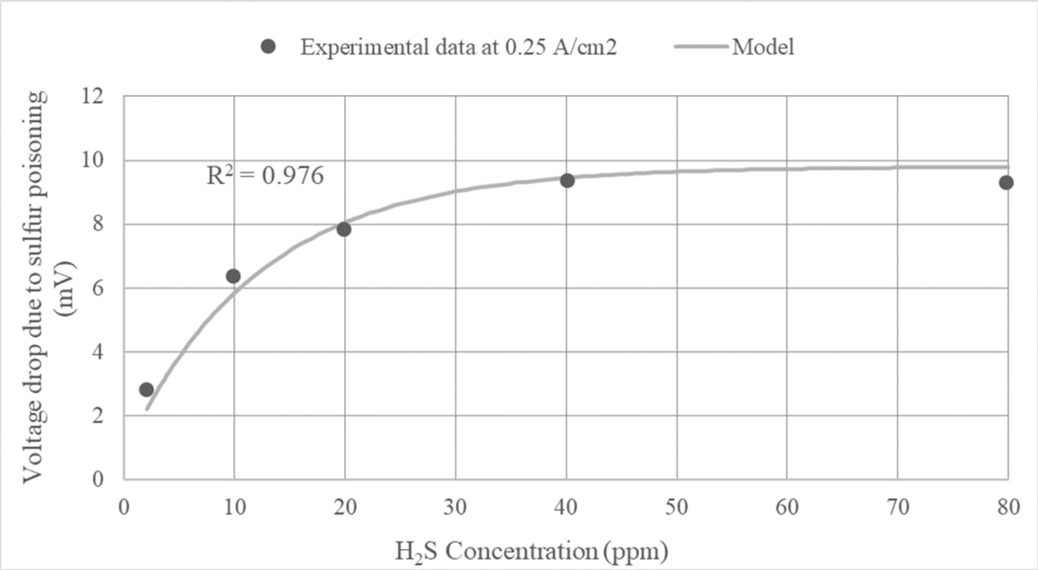

Fig. 3. Voltage drop due to sulfur poisoning versus $H_2S$ concentration at 0.25 A/cm$^2$. The solid line shows the results of the proposed empirical model, while the circles represent Hagen et al.'s experimental data [36].

## 2.5. Degradation rate evaluation

Very different values have been reported for the degradation rate of conventional SOFCs in the literature [4,9,60,61]. There are several causes as to why the values reported for SOFC degradation rates are very different. Some possible reasons are that the components have microstructural differences from study to study which could be due to component composition or structure, cell design, testing condition, or fuel composition. However, one important cause of these differences is inconsistent definitions of the degradation rate itself. Eqs. 57 and 58 that have been used by Hagen et al. [60] and Gemmen et al. [61], respectively are two examples of degradation rate models in the literature.

$$rd(t) = \frac{OCV - V_t}{t} \times 1000 \tag{57}$$

$$rd(t) = \frac{V_i - V_t}{V_i \times (t - t_i)} \times 100 \tag{58}$$

where $rd$ is the degradation rate, with $V_i$ as initial voltage in the testing range and $V_t$ as voltage at time $t$. These equations calculate $rd$ over a long time period using backward finite differences with large timesteps (at least several hundred hours). The timesteps used in these equations are inconsistent. Eq. 58 defines degradation rate as voltage percentage change that happens over a specific time range with respect to the initial voltage of that range, while Eq. 57 measures degradation rate as absolute change in voltage from OCV and then normalized to 1000 hours. The unit of $rd$ in Eq. 57 is V/1000h whereas that of Eq. 58 is %/h. Therefore, not only the differences in cell microstructure and experiment methodologies but inconsistent definitions make degradation rate values incomparable. To solve this problem, instantaneous $rd$ should be computed (Eq. 59) instead of using different approximations of finite differences with inconsistent, large timesteps.

$$rd(t) = \frac{1}{V_i} \times \frac{dV_t}{dt} \tag{59}$$

The instantaneous $rd$ is preferable for modeling because models are smooth and noiseless, and it can be consistently and unambiguously applied everywhere. We note that this definition cannot be applied directly to experimental data due to the noise involved, but it can be approximated numerically through a centred finite differences approach with a relatively short timestep (a few hours), or though a local line fitting approach, depending on the noise.

## 2.6. Model Implementation

The model was implemented in MATLB. In order to calculate cell voltage at specific operating conditions, ohmic, activation and concentration polarizations should be calculated and implemented in Eq. 6. Eqs. 10-31 were utilized to find the impacts of various phenomena on ohmic losses in the cell components. These equations were then incorporated into Eqs. 7-9 to quantify ohmic polarization. In this section, ODE45 was used to compute the rate of nickel oxidation reaction (Eq. 25). Then, Eqs. 33-35 were substituted in Eq. 32 to calculated activation polarization in the electrodes. In addition, Eqs. 38-48 were implemented in Eqs. 36 and 37 to evaluate anode and cathode concentration polarization.

If the fuel contains $H_2S$, voltage drop as a result of sulfur poisoning needs to be added to the losses in Eq. 6.

## 3. Results and discussion

### 3.1. Validation

The model has been validated against some experimental data, which were not used in the development of the model. Details and results of the model validation are given in the Supporting Information.

### 3.2. Sensitivity analysis

A sensitivity analysis was conducted in order to investigate how the degradation rate is affected by the main control parameters, namely, temperature, current, and partial pressure of gases. For the sensitivity study, we calculated the average of the instantaneous degradation rates over the first 1000 hours of operation, over the second 1000 hours, and over the third 1000 hours of operation.

It should be noted that sulfur poisoning was not included in the scope of the sensitivity analysis because sulfur poisoning has a limited impact which is reached very rapidly. As it was mentioned in section 2.4, sulfur adsorbs on the surface of the anode in a short period of time. In the presence of $H_2S$, anode reaches a saturation point in almost ten hours and thus it only affects degradation rates in the beginning of the operation. For this reason, we performed sensitivity analysis for a sulfur free fuel. This allows us to compare average degradation rates over the first, the second, and the third 1000 hours of operation.

A conventional SOFC can operate within a temperature range of 600-900°C [62]. High operating temperatures enable SOFCs to be electrochemically active when using hydrocarbons as fuel, which eliminates the need for expensive platinum-based catalysts [63]. However, running SOFCs at temperatures above 900°C requires the use of expensive sealants that have high mechanical and chemical stability, as well as compatibility with the electrode materials. On the other hand, traditional component materials lack sufficient electrochemical activity at temperatures lower than 600°C.

In this study, current density is changed in the range of 0.2 to 1 $A/cm^2$ [64]. Although increasing the current density enables the use of a smaller SOFC at start of operation, which lowers capital costs, these smaller cells degrade faster, which increases maintenance costs and results in system instability.

Moreover, in the present work, it is assumed that fuel is composed of hydrogen and steam. Partial pressure of hydrogen in the fuel feed is varied from 70% to 90% of the fuel pressure.

The contour plots in Fig. 4-a, 4-d and 4-g show the sensitivity analysis results for the average degradation rate in the first 1000 hours of operation at 70, 80 and 90 kPa $P_{\mathrm{H}_2}$, respectively. As can be seen, current density has the highest impact on the degradation rate, followed by temperature and hydrogen partial pressure, respectively.

The results over the second 1000 hours of operation (Fig. 4-b, 4-e and 4-h) show that the effects of the parameters were similar to the first 1000 hours. In other words, the degradation rate is the most sensitive to current density, with the sensitivity increasing at higher temperatures. However, degradation rate values are smaller over the second 1000 hours than the first 1000 hours, which is due to the trend of reduced degradation over time. However, the changes in degradation rate between the second and third 1000s hours of operation are not very significant. These results demonstrate that the behavior of cells changes over time, and that cells generally become more stable after approximately 1000 hours of operation.

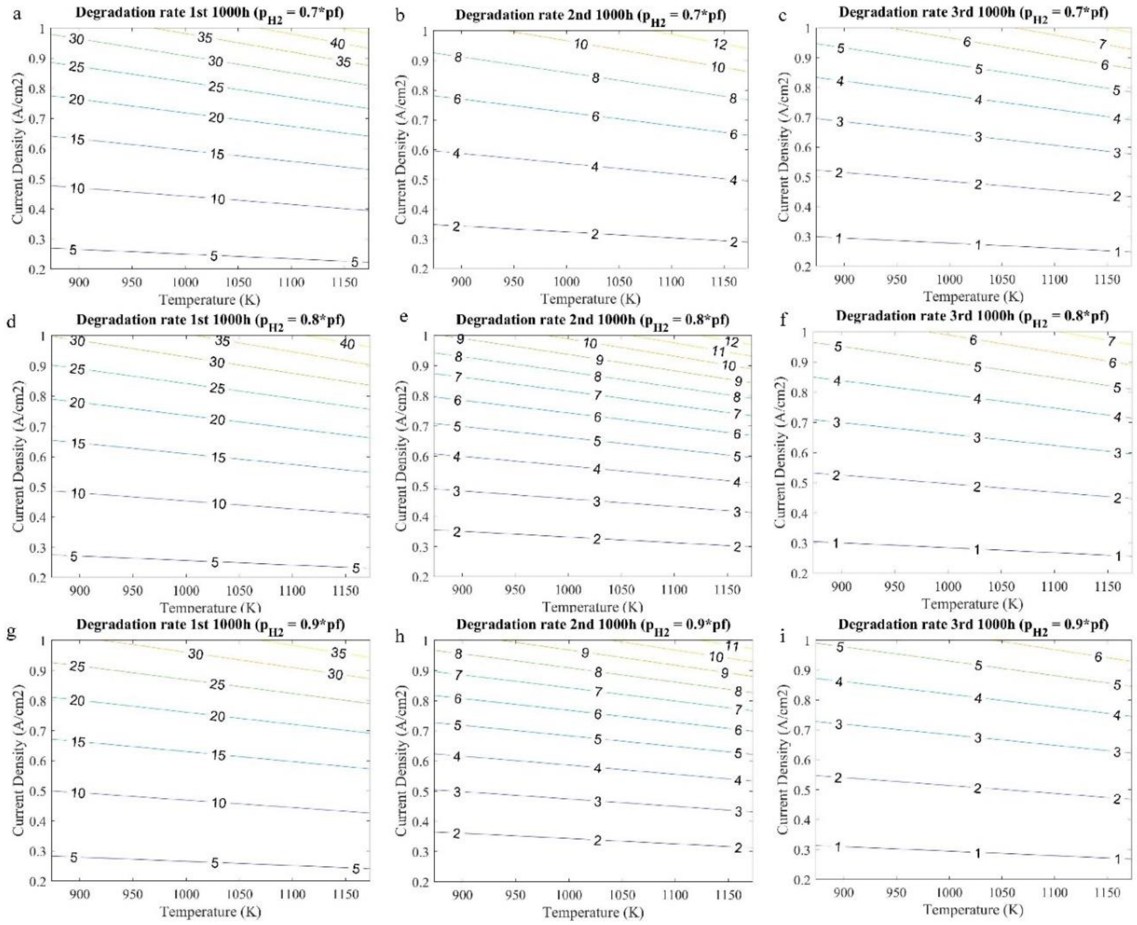

Fig. 4. Contour plots—Sensitivity analysis for the average degradation rate: a-c) at 70 kPa $P_{H_2}$ for the first, second and third 1000 hours of operation, respectively; d-f) at 80 kPa $P_{H_2}$ for the first, second and third 1000 hours of operation; and g-i) at 90 kPa $P_{H_2}$ for the first, second and third 1000 hours of operation, respectively.

A histogram plot of the degradation rate for 6000 random samples (using Monte Carlo random combinations of temperature, hydrogen partial pressure, and current density using the same ranges shown in Fig. 4) in different time ranges is shown in Fig. 5. As can be seen, the histograms for all three time ranges exhibit right-skewed behaviour. This asymmetric distribution shows the lower bound of the degradation rate, which is represented by the highest peak at the far left side of the histogram. However, the histogram maintains its skewed behaviour as it moves to the right, as the peaks and the entire range of degradation rates gradually become smaller with the passage of time. In addition, the height of the peak increases significantly with time as the highest peak belongs to the third 1000 hours of operation and the smallest one belongs to the first 1000 hours of operation, while the height of the tail decreases with time.

This trend is the result of the high degradation rates that occur at the beginning of SOFC operation; the exception to this trend occurs when the SOFC is operated at a very low temperature and current density using fuel that is high in $H_2$. This trend of decreased deterioration over time means that the highest degradation rate also becomes less frequent after approximately 1000 hours of operation. Moreover, the value of the lowest rate, also becomes smaller over longer periods of time. As can be seen in the histogram plot, during the first 1000 hours cells might degrade up to 40 % / 1000 h when they perform at very severe conditions, while after 1000 hours of operation, degradation rates are always less than 20 % / 1000 h.

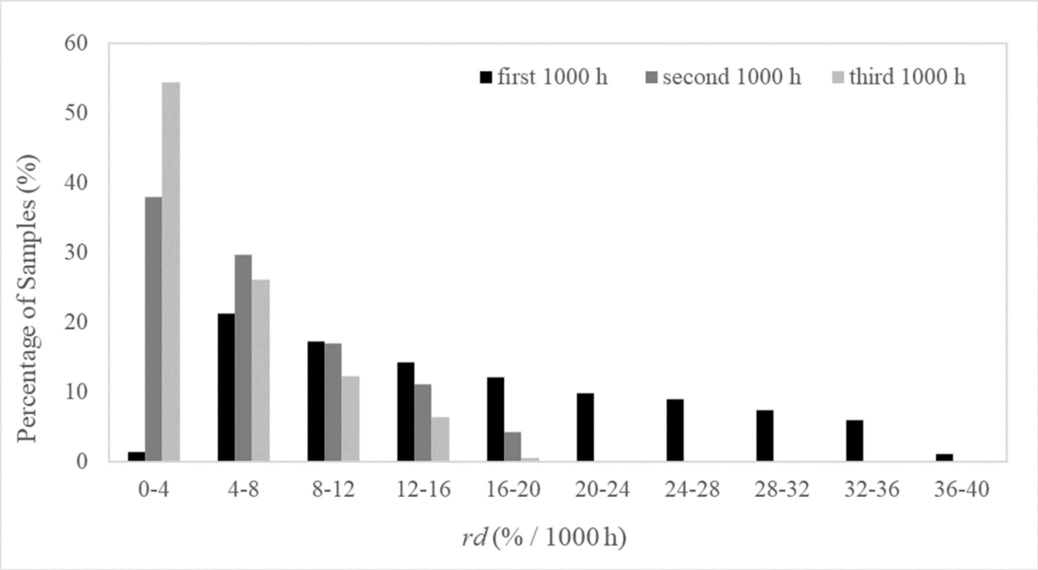

Fig. 5. Histogram plots of degradation rate percentage per 1000 hours for the first 1000 hours of operation; the second 1000 hours of operation; and the third 1000 hours of operation.

Since the focus of this work was to determine how an SOFC's operating parameters affect its performance, the sensitivity analysis is critical because it can provide specific information necessary to determine optimal operating conditions.

### 3.3. Application of the model to predict long-term SOFC performance

One key goal of this study was to predict the degradation rate of an SOFC over a long period of operation under different operating conditions. In order to show the variation in cell voltage over time, a simulation was run at 0.5 A/cm$^2$ and 750°C. The model input parameters, including physical and chemical properties of the modeled SOFCs, are given in Supporting Information; table S1.

Fig. 6 shows that voltage degradation occurs quickly during the early hours of operation, but slows after about 1500 hours. Degradation behaviour can be explained by changes in the microstructure and properties of the cell components. As discussed in the previous section, the anode's microstructure and performance changes rapidly at first, but levels off later [46]. For instance, it was noted that Ni particles show initial rapid growth upon being exposed to gases under the SOFC's operating conditions. However, after a while, the YSZ particles slow this growth. This trend is also observed in TPB length and anode electrical conductivity, as they too are affected by number and size of Ni particles.

Fig. 6 also illustrates corresponding degradation rate of the cell. The degradation rate of the SOFC is higher in the beginning of operation and levels off as time passes. This trend indicates that, while the cells are prone to changes initially, they "mature" after about 1000 hours of operation.

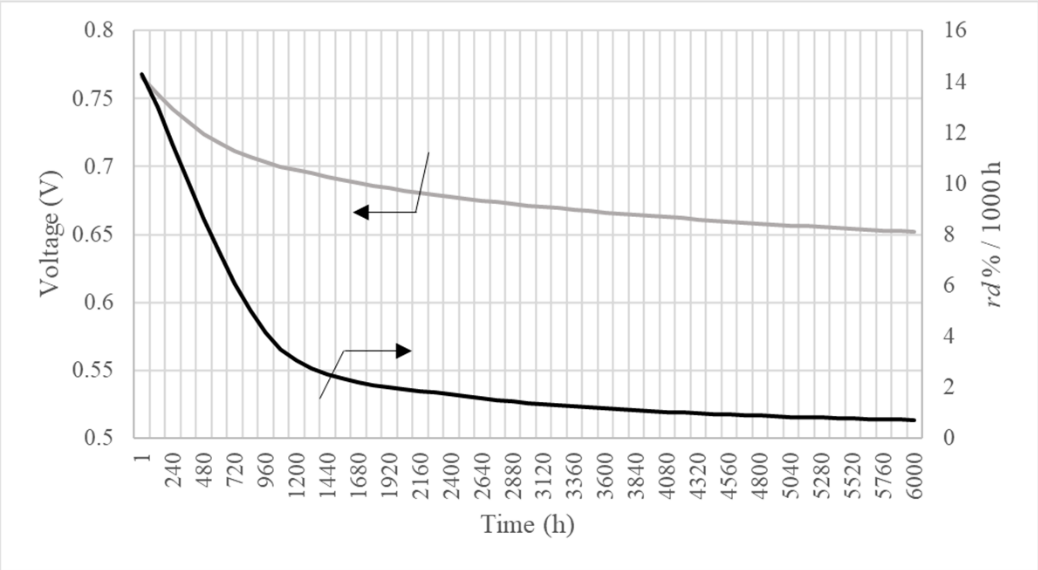

Fig. 6. Voltage profile over time, and Degradation rate percentage per 1000 hours versus time for the SOFC running at 750℃ and 0.5 A/cm$^2$.

## 3.4. Effect of system operation parameters on lifetime power production

Operating parameters highly affect long-term performance of SOFCs. Depending on the operating conditions, SOFCs that perform better initially might produce less energy cumulatively over their lifetime. Fig. 7-a shows the lifetime power curves of two SOFCs that operate at different current densities but using the same fuel composition and temperature. As can be seen, the SOFC with the larger current density initially generates more power under the same conditions. However, due to the faster degradation rate associated with high current densities, the cell with the lower current density ends up providing superior power generation after about 2000 hours of operation. Comparing the cumulative energy delivered by the cells shows that after 5760 hours, cell 1 produces more energy over its lifetime.

Fig. 7-b illustrates how different the lifetime power production plots can be depending on the operating parameters. Cell 1, which runs at a higher current density and lower temperature, produces more power initially. However, after about 3000 hours, cell 1's power generation falls below that of cell 2, which is run at a lower current density and higher temperature. In fact, despite its lower operating temperature, cell 1 degrades faster due to current density's dominant effect on performance loss. The cumulative energy delivered over operation time by cell 1 exceeds that of cell 2 after 7918 hours (at 227 kWh). The difference becomes more significant in longer periods of time as the energy generated by cell 1 over 12000 hours of operation is 335 kWh whereas, cell 2 delivers 309 kWh over the same period of time.

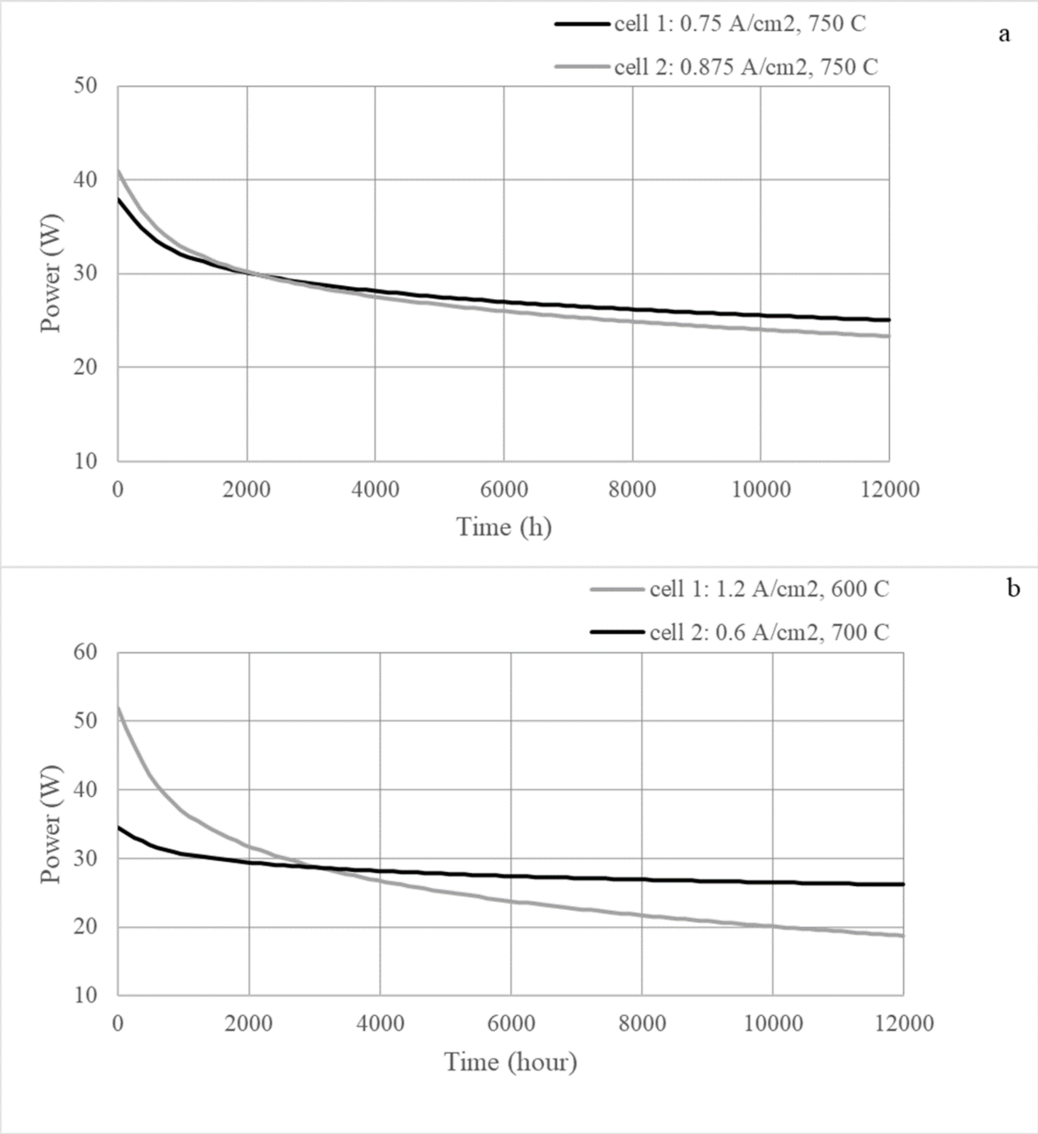

Fig. 7. a) Power profile over time for SOFCs operating at: a) 0.75 A/cm$^2$ and 750°C, and 0.875 A/cm$^2$ and 750°C; b) 1.2 A/cm$^2$ and 600°C, and 0.6 A/cm$^2$ and 700°C.

## 4. Future work

A detailed degradation-based system-level optimization is required to determine the optimal operating conditions for an SOFC in an ICE system. The optimal values will be highly dependent on the objective function, system level design, goals, constraints, and expected usage. If system cost is taken as the most important factor in making decisions, an optimal point will be achieved when the SOFC is able to provide a long lifespan, while still being limited in size. Applying the proposed model into an optimization framework will enable the design of a reliable system.

In addition, although the proposed degradation model was validated for 1400 hours of operation using Hagen et al.'s experimental data, some of the data-driven equations used in this research were obtained using short-term experiments [60]. Thus, these equations may not adequately represent the long-term behaviour of SOFCs. As such, more experiments are required to validate the proposed model's reliability over longer periods of time.

## 5. Conclusion

This paper presented a unique, cross-cutting model for long-term performance of conventional SOFCs that considers most of the common degradation phenomena in conventional SOFCs, including: coarsening and oxidation of Ni particles in the Ni-cermet anode; changes in anode pore size; deterioration in anode and electrolyte conductivity; and sulfur poisoning. By providing realistic results, this model is capable of being used to answer some important questions regarding the optimal sizing and operation of the cells for an efficient, stable performance, that previously developed models are not able to answer due to too many assumptions made for simplification. The proposed model was validated against the experimental data that was not considered in developing the model. As a result, this model can be used to predict performance of SOFCs at various operating conditions over a long period of time. This allows system designers to find the proper sizing and operation setting for SOFCs in specific ICEs. This is a critical piece of information that helps widespread commercialization of conventional SOFCs for ICEs.

The results of the sensitivity analysis can help decision makers to take control actions by showing how each key parameter impacts SOFCs long-term operation. The results illustrated that current density affects SOFCs performance significantly, while hydrogen partial pressure does not have a high impact.

This study resolved the apparent conflict in the literature about whether temperature positively or negatively affects SOFCs performance degradation. Our investigations illustrated that all these studies are correct and not actually in contradiction with each other. Instead, each study examined only specific subsets of possible degradation mechanisms and looked only at small regions of the parameter space. For example, where high temperature might cause increasing degradation of one form on one case, high temperature might actually result in lower degradation of another form in different cases. However, taking all common degradation phenomena into account holistically as a single model in the current research gave a sense of the big picture and exhibited that temperature positively correlates to degradation. In other words, the degradation rate overall increases with increasing the operating temperature.

In addition, this work highlighted the inconsistency in the literature with regard to how degradation is calculated. Instead of using the instantaneous concept of degradation rate, differing definitions of this metric are utilized across the literature which are essentially differences in the numerical finite difference approximations used with very long step sizes due to the noise in the data. This makes very different and incongruous computations of degradation rate and results in a wide range of values reported for this metric across the literature. But, with the developed model that starts from the data and utilizes an instantaneous definition, this problem is resolved and can be applied and interpreted meaningfully across all studies.

# Acknowledgement

We thank Dr. Valentina Zaccaria for providing insights for this article and her useful suggestions. This work was supported by the Natural Sciences and Engineering Research Council of Canada [NSERC CRDPJ 509219-2017] and the Ontario Centre of Excellence [OCE 27851-2018].

## 6. References

(1) Baldi, F.; Wang, L.; Pérez-Fortes, M.; Maréchal, F. A Cogeneration System Based on Solid Oxide and Proton Exchange Membrane Fuel Cells with Hybrid Storage for Off-Grid Applications. *Frontiers in Energy Research* **2019**, *6* (January).

https://doi.org/10.3389/fenrg.2018.00139.

(2) Vialetto, G.; Rokni, M. Innovative Household Systems Based on Solid Oxide Fuel Cells for a Northern European Climate. *Renewable Energy* **2015**, *78*, 146–156. https://doi.org/10.1016/j.renene.2015.01.012.

(3) Barelli, L.; Bidini, G.; Cinti, G.; Ottaviano, A. SOFC Regulation at Constant Temperature: Experimental Test and Data Regression Study. *Energy Conversion and Management* **2016**, *117*, 289–296. https://doi.org/10.1016/j.enconman.2016.03.028.

(4) Zaccaria, V.; Tucker, D.; Traverso, A. A Distributed Real-Time Model of Degradation in a Solid Oxide Fuel Cell, Part II: Analysis of Fuel Cell Performance and Potential Failures. *Journal of Power Sources* **2016**, *327*, 736–742. https://doi.org/10.1016/j.jpowsour.2016.01.027.

(5) Parhizkar, T.; Roshandel, R. Long Term Performance Degradation Analysis and Optimization of Anode Supported Solid Oxide Fuel Cell Stacks. *Energy Conversion and Management* **2017**, *133*, 20–30. https://doi.org/10.1016/j.enconman.2016.11.045.

(6) Wen, H.; Ordonez, J. C.; Vargas, J. V. C. Single Solid Oxide Fuel Cell Modeling and Optimization. *Journal of Power Sources* **2011**, *196* (18), 7519–7532. https://doi.org/10.1016/j.jpowsour.2010.10.113.

(7) Yang, S.; Chen, T.; Wang, Y.; Peng, Z.; Wang, W. G. Electrochemical Analysis of

an Anode-Supported SOFC. *International Journal of Electrochemical Science* **2013**, *8* (2), 2330–2344.

(8) Aguiar, P.; Adjiman, C. S.; Brandon, N. P. Anode-Supported Intermediate Temperature Direct Internal Reforming Solid Oxide Fuel Cell. I: Model-Based Steady-State Performance. *Journal of Power Sources* **2004**, *138* (1–2), 120–136. https://doi.org/10.1016/j.jpowsour.2004.06.040.

(9) Parhizkar, T.; Hafeznezami, S. Degradation Based Operational Optimization Model to Improve the Productivity of Energy Systems, Case Study: Solid Oxide Fuel Cell Stacks. *Energy Conversion and Management* **2018**, *158* (August 2017), 81–91. https://doi.org/10.1016/j.enconman.2017.12.045.

(10) Liu, Y. L.; Hagen, A.; Barfod, R.; Chen, M.; Wang, H. J.; Poulsen, F. W.; Hendriksen, P. V. Microstructural Studies on Degradation of Interface between LSM-YSZ Cathode and YSZ Electrolyte in SOFCs. *Solid State Ionics* **2009**, *180* (23–25), 1298–1304. https://doi.org/10.1016/j.ssi.2009.07.011.

(11) Nakajo, A.; Mueller, F.; Brouwer, J.; Van Herle, J.; Favrat, D. Progressive Activation of Degradation Processes in Solid Oxide Fuel Cells Stacks: Part I: Lifetime Extension by Optimisation of the Operating Conditions. *Journal of Power Sources* **2012**, *216*, 449–463. https://doi.org/10.1016/j.jpowsour.2012.05.078.

(12) Weber, A.; Szász, J.; Dierickx, S.; Endler-Schuck, C.; Ellen, I.-T. Accelerated Lifetime Tests for SOFCs. *ECS Transactions* **2015**, *68* (1), 1953–1960. https://doi.org/10.1149/06801.1953ecst.

(13) Taniguchi, S.; Kadowaki, M.; Kawamura, H.; Yasuo, T.; Akiyama, Y.; Miyake, Y.; Saitoh, T. Degradation Phenomena in the Cathode of a Solid Oxide Fuel Cell with an Alloy Separator. *Journal of Power Sources* **1995**, *55* (1), 73–79. https://doi.org/10.1016/0378-7753(94)02172-Y.

(14) Abreu-Sepulveda, M. A.; Harun, N. F.; Hackett, G.; Hagen, A.; Tucker, D. Accelerated Degradation for Hardware in the Loop Simulation of Fuel Cell-Gas Turbine Hybrid System. *Journal of Fuel Cell Science and Technology* **2015**, *12* (2), 1–7. https://doi.org/10.1115/1.4028953.

(15) Kim, T.; Liu, G.; Boaro, M.; Lee, S. I.; Vohs, J. M.; Gorte, R. J.; Al-Madhi, O. H.; Dabbousi, B. O. A Study of Carbon Formation and Prevention in Hydrocarbon-Fueled SOFC. *Journal of Power Sources* **2006**, *155* (2), 231–238. https://doi.org/10.1016/j.jpowsour.2005.05.001.

(16) Chen, D.; Lødeng, R.; Anundskås, A.; Olsvik, O.; Holmen, A. Deactivation during Carbon Dioxide Reforming of Methane over Ni Catalyst: Microkinetic Analysis. *Chemical Engineering Science* **2001**, *56* (4), 1371–1379. https://doi.org/10.1016/S0009-2509(00)00360-2.

(17) Chen, X.; Zhang, L.; Liu, E.; Jiang, S. P. A Fundamental Study of Chromium Deposition and Poisoning at (La 0.8Sr0.2)0.95(Mn1-XCo x)O3 ± δ (0.0≤ x ≤1.0) Cathodes of Solid Oxide Fuel Cells. *International Journal of Hydrogen Energy* **2011**, *36* (1), 805–821. https://doi.org/10.1016/j.ijhydene.2010.09.087.

(18) Chen, X.; Zhen, Y.; Li, J.; Jiang, S. P. Chromium Deposition and Poisoning in Dry

and Humidified Air at (La0.8Sr0.2)0.9MnO3+δ Cathodes of Solid Oxide Fuel Cells. *International Journal of Hydrogen Energy* **2010**, *35* (6), 2477–2485. https://doi.org/10.1016/j.ijhydene.2009.12.185.

(19) Jiang, S. P.; Zhang, J. P.; Zheng, X. G. A Comparative Investigation of Chromium Deposition at Air Electrodes of Solid Oxide Fuel Cells. *Journal of the European Ceramic Society* **2002**, *22* (3), 361–373. https://doi.org/10.1016/S0955-2219(01)00280-1.

(20) Cheng, Z.; Wang, J. H.; Choi, Y.; Yang, L.; Lin, M. C.; Liu, M. From Ni-YSZ to Sulfur-Tolerant Anode Materials for SOFCs: Electrochemical Behavior, in Situ Characterization, Modeling, and Future Perspectives. *Energy and Environmental Science* **2011**, *4* (11), 4380–4409. https://doi.org/10.1039/c1ee01758f.

(21) Wang, W.; Su, C.; Wu, Y.; Ran, R.; Shao, Z. Progress in Solid Oxide Fuel Cells with Nickel-Based Anodes Operating on Methane and Related Fuels. *Chemical Reviews* **2013**, *113* (10), 8104–8151. https://doi.org/10.1021/cr300491e.

(22) Yoshizumi, T.; Taniguchi, S.; Shiratori, Y.; Sasaki, K. Sulfur Poisoning of Sofcs: Voltage Oscillation and Ni Oxidation. *Journal of the Electrochemical Society* **2012**, *159* (11). https://doi.org/10.1149/2.032211jes.

(23) Larrain, D.; Van herle, J.; Favrat, D. Simulation of SOFC Stack and Repeat Elements Including Interconnect Degradation and Anode Reoxidation Risk. *Journal of Power Sources* **2006**, *161* (1), 392–403. https://doi.org/10.1016/j.jpowsour.2006.04.151.

(24) Nakajo, A.; Mueller, F.; Brouwer, J.; Van Herle, J.; Favrat, D. Progressive Activation of Degradation Processes in Solid Oxide Fuel Cell Stacks: Part II: Spatial Distribution of the Degradation. *Journal of Power Sources* **2012**, *216*, 434–448. https://doi.org/10.1016/j.jpowsour.2012.05.077.

(25) Wen, H.; Ordonez, J. C.; Vargas, J. V. C. Single Solid Oxide Fuel Cell Modeling and Optimization. *Journal of Power Sources* **2011**, *196* (18), 7519–7532. https://doi.org/10.1016/j.jpowsour.2010.10.113.

(26) Ryan, E. M.; Xu, W.; Sun, X.; Khaleel, M. A. A Damage Model for Degradation in the Electrodes of Solid Oxide Fuel Cells: Modeling the Effects of Sulfur and Antimony in the Anode. *Journal of Power Sources* **2012**, *210*, 233–242. https://doi.org/10.1016/j.jpowsour.2012.02.091.

(27) Hansen, J. B. Correlating Sulfur Poisoning of SOFC Nickel Anodes by a Temkin Isotherm. *Electrochemical and Solid-State Letters* **2008**, *11* (10), 178–180. https://doi.org/10.1149/1.2960521.

(28) Tucker, D.; Abreu-Sepulveda, M.; Harun, N. F. SOFC Lifetime Assessment in Gas Turbine Hybrid Power Systems. *Journal of Fuel Cell Science and Technology* **2014**, *11* (5), 1–7. https://doi.org/10.1115/1.4028158.

(29) Coors, W. G.; O’Brien, J. R.; White, J. T. Conductivity Degradation of NiO-Containing 8YSZ and 10YSZ Electrolyte during Reduction. *Solid State Ionics* **2009**, *180* (2–3), 246–251. https://doi.org/10.1016/j.ssi.2008.12.004.

(30) Gao, S.; Li, J.; Lin, Z. Theoretical Model for Surface Diffusion Driven Ni-Particle Agglomeration in Anode of Solid Oxide Fuel Cell. *Journal of Power Sources* **2014**, *255*, 144–150. https://doi.org/10.1016/j.jpowsour.2014.01.033.

(31) Neidhardt, J. P.; Fronczek, D. N.; Jahnke, T.; Danner, T.; Horstmann, B.; Bessler, W. G. A Flexible Framework for Modeling Multiple Solid, Liquid and Gaseous Phases in Batteries and Fuel Cells. *Journal of the Electrochemical Society* **2012**, *159* (9), 1528–1542. https://doi.org/10.1149/2.023209jes.

(32) Hardjo, E.; Monder, D.; Karan, K. Numerical Modeling of Nickel-Impregnated Porous YSZ-Supported Anodes and Comparison to Conventional Composite Ni-YSZ Electrodes. *ECS Transactions* **2011**, *35* (2 PART 2), 1823–1832. https://doi.org/10.1149/1.3570171.

(33) Hardjo, E. F.; Monder, D. S.; Karan, K. An Effective Property Model for Infiltrated Electrodes in Solid Oxide Fuel Cells. *Journal of the Electrochemical Society* **2014**, *161* (1), 83–93. https://doi.org/10.1149/2.036401jes.

(34) Divisek, J.; Wilkenhöner, R.; Volfkovich, Y. Structure Investigations of SOFC Anode Cermets Part I: Porosity Investigations. *Journal of Applied Electrochemistry* **1999**, *29* (2), 153–163. https://doi.org/10.1023/A:1003420815623.

(35) Yoshizumi, T.; Uryu, C.; Oshima, T.; Shiratori, Y.; Ito, K.; Sasaki, K. Sulfur Poisoning of SOFCs: Dependence on Operational Parameters. *ECS Transactions* **2011**, *35* (2 PART 2), 1717–1725. https://doi.org/10.1149/1.3570159.

(36) Hagen, A.; Johnson, G. B.; Hjalmarsson, P. Electrochemical Evaluation of Sulfur Poisoning in a Methane-Fuelled Solid Oxide Fuel Cell: Effect of Current Density and Sulfur Concentration. *Journal of Power Sources* **2014**, *272*, 776–785. https://doi.org/10.1016/j.jpowsour.2014.08.125.

(37) Aguilar, L.; Zha, S.; Cheng, Z.; Winnick, J.; Liu, M. A Solid Oxide Fuel Cell Operating on Hydrogen Sulfide (H2S) and Sulfur-Containing Fuels. *Journal of Power Sources* **2004**, *135* (1–2), 17–24. https://doi.org/10.1016/j.jpowsour.2004.03.061.

(38) Langnickel, H.; Hagen, A. New Methodology of Studying H2S Poisoning Effects on SOFC's Fueled by Carbon Containing Fuels like Biogas. *ECS Transactions* **2019**, *91* (1), 511–521. https://doi.org/10.1149/09101.0511ecst.

(39) Williams, M. C.; Strakey, J. P.; Surdoval, W. A. U. S. DOE Solid Oxide Fuel Cells: Technical Advances. *Proceedings - Electrochemical Society* **2005**, *PV 2005-07* (2005), 20–31. https://doi.org/10.1149/200507.0020pv.

(40) Adams II, T. A.; Nease, J.; Tucker, D.; Barton, P. I. Energy Conversion with Solid Oxide Fuel Cell Systems: A Review of Concepts and Outlooks for the Short- and Long-Term. *Industrial and Engineering Chemistry Research* **2013**, *52* (9), 3089–3111. https://doi.org/10.1021/ie300996r.

(41) Chiodelli, G.; Malavasi, L. Electrochemical Open Circuit Voltage (OCV) Characterization of SOFC Materials. *Ionics* **2013**, *19* (8), 1135–1144. https://doi.org/10.1007/s11581-013-0843-z.

(42) Faes, A.; Hessler-Wyser, A.; Presvytes, D.; Vayenas, C. G.; Vanherle, J. Nickel-Zirconia Anode Degradation and Triple Phase Boundary Quantification from Microstructural Analysis. *Fuel Cells* **2009**, *9* (6), 841–851. https://doi.org/10.1002/fuce.200800147.

(43) Tanasini, P.; Cannarozzo, M.; Costamagna, P.; Faes, A.; Van Herle, J.; Hessler-Wyser, A.; Comninellis, C. Experimental and Theoretical Investigation of Degradation Mechanisms by Particle Coarsening in Sofc Electrodes. *Fuel Cells* **2009**, *9* (5), 740–752. https://doi.org/10.1002/fuce.200800192.

(44) Laosiripojana, N.; Wiyaratn, W.; Kiatkittipong, W.; Arpornwichanop, A.; Soottitantawat, A.; Assabumrungrat, S. R Eviews on S Olid O Xide. **2009**, *13* (1), 65–83. https://doi.org/10.4186/ej.2009.13.1.65.

(45) Zhu, W.; Ding, D.; Xia, C. Enhancement in Three-Phase Boundary of SOFC Electrodes by an Ion Impregnation Method: A Modeling Comparison. *Electrochemical and Solid-State Letters* **2008**, *11* (6), 83–86. https://doi.org/10.1149/1.2895009.

(46) Chen, J.; Bertei, A.; Ruiz-Trejo, E.; Atkinson, A.; Brandon, N. P. Characterization of Degradation in Nickel Impregnated Scandia-Stabilize Zirconia Electrodes during Isothermal Annealing. *Journal of the Electrochemical Society* **2017**, *164* (9), F935–F943. https://doi.org/10.1149/2.0821709jes.

(47) Klemensø, T.; Thydén, K.; Chen, M.; Wang, H. J. Stability of Ni-Yttria Stabilized Zirconia Anodes Based on Ni-Impregnation. *Journal of Power Sources* **2010**, *195*

(21), 7295–7301. https://doi.org/10.1016/j.jpowsour.2010.05.047.

(48) T, M. Cs.-K. Ml. *No Title*. https://doi.org/https://doi.org/10.1016/C2013-0-16429-X.

(49) Costamagna, P.; Honegger, K. Modeling of Solid Oxide Heat Exchanger Integrated Stacks and Simulation at High Fuel Utilization. *Journal of the Electrochemical Society* **1998**, *145* (11), 3995–4007. https://doi.org/10.1149/1.1838904.

(50) Chan, S. H.; Khor, K. A.; Xia, Z. T. Complete Polarization Model of a Solid Oxide Fuel Cell and Its Sensitivity to the Change of Cell Component Thickness. *Journal of Power Sources* **2001**, *93* (1–2), 130–140. https://doi.org/10.1016/S0378-7753(00)00556-5.

(51) Chapman, S.; Cowling, T. G.; Park, D. The Mathematical Theory of Non-Uniform Gases. *American Journal of Physics* **1962**, *30* (5), 389–389. https://doi.org/10.1119/1.1942035.

(52) Arnold, J. H. Studies in Diffusion: I—Estimation of Diffusivities in Gaseous Systems. *Industrial and Engineering Chemistry* **1930**, *22* (10), 1091–1095. https://doi.org/10.1021/ie50250a023.

(53) Gilliland, E. R. Diffusion Coefficients in Gaseous Systems. *Industrial and Engineering Chemistry* **1934**, *26* (6), 681–685. https://doi.org/10.1021/ie50294a020.

(54) Fuller, E. N.; Ensley, K.; Giddings, J. C. Diffusion of Halogenated Hydrocarbons

in Helium. The Effect of Structure on Collision Cross Sections. *Journal of Physical Chemistry* **1969**, *73* (11), 3679–3685. https://doi.org/10.1021/j100845a020.

(55) Matsuzaki, Y.; Yasuda, I. Poisoning Effect of Sulfur-Containing Impurity Gas on a SOFC Anode: Part I. Dependence on Temperature, Time, and Impurity Concentration. *Solid State Ionics* **2000**, *132* (3), 261–269. https://doi.org/10.1016/s0167-2738(00)00653-6.

(56) Rasmussen, J. F. B.; Hagen, A. The Effect of H2S on the Performance of Ni-YSZ Anodes in Solid Oxide Fuel Cells. *Journal of Power Sources* **2009**, *191* (2), 534–541. https://doi.org/10.1016/j.jpowsour.2009.02.001.

(57) Ib Alstrup, J. R. R.-N. and S. R. High Temperature Hydrogen Sulfide Chemisorption on Nickel Catalysts. *Applied Catalysis* **1981**, *1*, 303–314.

(58) Zha, S.; Cheng, Z.; Liu, M. Sulfur Poisoning and Regeneration of Ni-Based Anodes in Solid Oxide Fuel Cells. *Journal of the Electrochemical Society* **2007**, *154* (2), 201–206. https://doi.org/10.1149/1.2404779.

(59) Cheng, Z.; Zha, S.; Liu, M. Influence of Cell Voltage and Current on Sulfur Poisoning Behavior of Solid Oxide Fuel Cells. *Journal of Power Sources* **2007**, *172* (2), 688–693. https://doi.org/10.1016/j.jpowsour.2007.07.052.

(60) Hagen, A.; Barfod, R.; Hendriksen, P. V.; Liu, Y. L.; Ramousse, S. Degradation of Anode Supported SOFCs as a Function of Temperature and Current Load. *Journal of the Electrochemical Society* **2006**, *153* (6), 1165–1171.

https://doi.org/10.1149/1.2193400.

(61) Gemmen, R. S.; Williams, M. C.; Gerdes, K. Degradation Measurement and Analysis for Cells and Stacks. *Journal of Power Sources* **2008**, *184* (1), 251–259. https://doi.org/10.1016/j.jpowsour.2008.06.047.

(62) Kulikovsky, A. A. Analytical Modeling of Fuel Cells; 2010; pp 1–33.

(63) Uttamchandani, D. Wireless MEMS Networks and Apllications; 2016; p 40.

(64) Lang, M.; Bohn, C.; Henke, M.; Schiller, G.; Willich, C.; Hauler, F. Understanding the Current-Voltage Behavior of High Temperature Solid Oxide Fuel Cell Stacks. *Journal of the Electrochemical Society* **2017**, *164* (13), F1460–F1470. https://doi.org/10.1149/2.1541713jes.

## 7. Supporting information

The supporting information can be found at https://pubs.acs.org/doi/10.1021/acs.iecr.0c05302

# CHAPTER 3: ECONOMICALLY OPTIMAL SIZING AND OPERATION STRATEGY FOR SOLID OXIDE FUEL CELLS TO EFFECTIVELY MANAGE LONG-TERM DEGRADATION

The content of this chapter is a published reprint of the following peer-reviewed publication:

Naeini, M., Cotton, J.S. and Adams, T.A. Economically Optimal Sizing and Operation Strategy for Solid Oxide Fuel Cells to Effectively Manage Long-Term Degradation. *Industrial & Engineering Chemistry Research* **2021**, *60(47)*, pp.17128-17142.

## Abstract

In this paper, an economic analysis is conducted on standalone conventional solid oxide fuel cells (SOFCs) to determine their optimal economic operating conditions, and to contribute to the commercialization of this technology. To this end, a mathematical model that accounts for dominant degradation phenomena is used to predict the long-term performance of SOFCs. The results of this analysis revealed that, although SOFCs carry high capital costs, they are able to generate electricity at a similar cost to that of traditional power generators under optimal operational conditions. Moreover, it is possible to lower degradation rate of the cells and run SOFCs under these conditions for several years. Sensitivity analysis showed that capital and fuel costs have the highest impacts on the levelized cost of electricity (LCOE) of SOFCs, while $CO_2$ tax has the smallest. The findings of this analysis illustrate that performance and operational economics of an SOFC are dependent on its mode of operation: SOFCs operating in constant-power-generation mode had the highest LCOE (ranging from 0.131 to 0.409 \$/kWh for different lifespans), while those with varying current densities, voltages, and power output during operation were able to generate electricity with a very low LCOE (0.12 to 0.357 \$/kWh for different lifespans).

### Keywords

Solid oxide fuel cell, Performance degradation, Levelized cost of electricity, Levelized cost of energy, Operating conditions, Operational modes.

## 1. Introduction

Solid oxide fuel cells (SOFCs) have emerged as a potential replacement technology for conventional power generation units due to their high efficiency, low levels of direct greenhouse gas (GHG) emissions, and fuel flexibility.[1] However, SOFCs are relatively expensive and have yet to be commercialized on a large scale. Furthermore, the application of SOFCs has been limited due to issues with degradation, and, until recently the lack of an accurate, inclusive model for predicting long-term performance deterioration under various operating conditions.[2,3] This latter limitation is significant, as understanding how SOFCs degrade under different conditions can ensure that operators do not operate them under conditions that are destructive, which can severely diminish their lifespan.[4]

To overcome the issue of SOFC degradation, there are two main approaches. The first and most actively studied approach is to improve the performance of the cell compartments by either developing new materials[5,6] or modifying the structure of the SOFCs components.[7–9] This can lead to fundamental improvements in the cells and stack designs, but the disadvantage is that it requires expensive materials that may only addresses part of the degradation problem, and it can take time to commercialize. The second approach is to alter the operation of the cells. By carefully choosing and varying the current, voltage, and/or power output over time, the long-term degradation rate can dramatically reduce. One advantage of this is that by changing operational strategies in an optimal fashion, one can drastically improve the lifetime and economics of existing materials and SOFCs. This paper focuses on this second approach.

It has been shown repeatedly in the literature that SOFCs degrade very rapidly when operated with the goal of producing a nearly constant supply of power. [4,10] Rather, it is preferable to vary the operation of the cells such that the power output decreases gradually, which significantly increases its usable lifetime. From a systems perspective, standalone SOFCs are therefore not well suited for constant-power applications. Instead, many studies suggest combining conventional SOFCs with other energy devices such as compressed air energy storage (CAES), steam turbine, gas turbines (GT), and solid oxide electrolysis cells (SOECs), as these devices can improve overall performance of the system by harvesting waste heat from the cells. This harvested heat can be utilized for a variety of purposes. For instance, in an integrated SOFC-GT system, the GT uses captured exhaust heat to produce extra power. As the SOFC degrades and produces less power over its lifetime, the GT power increases to compensate, such that the net system power remains essentially constant over the lifetime of the system. [1,11,12] Al-Khori et al. also studied economical feasibility of a combined SOFC-photovoltaic (PV) solar panels system for a reliable 24/7 power generation with low environmental impacts.[13]

Most economic studies have focused on determining the optimal conditions for these SOFC-based plants in which SOFCs are integrated with other energy devices as a part of a larger system.[1,11–16] However, these studies have tended to use SOFC models that ignore or underrate long-term declines in performance of fuel cells, which can produce unrealistic results. Therefore, while running SOFCs under the operational conditions suggested in previous research may technically function in practice, it can also produce unexpected high costs in real systems and lead to premature cell breakdown. For example, Lai et al. recently performed an eco-techno-economic analysis of an SOFC/GT hybrid system using a regression model developed by Abreu Sepulveda et al.[17] based on experimental data collected over 1500 hours of operation. Abreu Sepulveda et al.'s model is based on an algebraic equation that correlates the degradation rate of the stack to current density, operating temperature, and fuel utilization. The accuracy of a regression model is limited to the range of operating conditions under which experimental data was collected. Abreu Sepulveda et al. used the following experimental data to develop their model: a current density range of 0.25 to 0.75 mA/cm$^2$; a temperature range of 750 to 850°C; and a fuel utilization range of 75% to 85%.[17] Outside of these specific ranges, Abreu Sepulveda et al.'s regression model is unable to predict the degradation rate of SOFCs with much accuracy. Although this work is a good first step, this is an empirical model that does not capture much of the degradation phenomena, since it simulates degradation of the whole system as a function of a few parameters without considering details of the various degradation phenomena.

Our research focuses on the commercialization of conventional SOFCs without the need for modifying any of the materials or structure of the components. Conventional SOFCs are composed of dense yttria-stabilized zirconia (YSZ) electrolytes, porous Ni-YSZ cermet anodes, and porous LaSrMn-oxide (LSM) cathodes. An optimization study that accurately identifies the optimal sizing and conditions for economical operation of SOFCs is necessary if this technology is to be commercialized. As such, the present study aims to find the optimal operating conditions under which conventional standalone SOFCs become economical power-generation devices, despite their high capital costs. To this end, we utilize a detailed degradation model, developed in our prior work [3], that accounts for the major degradation mechanisms in the cells, as this will help ensure that the results of this economic analysis are more realistic compared to previous studies. The model developed in our prior work accounts for following deterioration mechanisms in conventional anode-supported SOFCs, namely: oxidation and the agglomeration of nickel particles in the anode; changes in anode pore size; deterioration of electrical conductivity in the anode and YSZ electrolytes; and sulfur contamination of the anode. [3] The following section provides a summary of the major parts of this model.

## 2. Mathematical model for the long-term performance of conventional anode-supported SOFCs

The mathematical model used in this work was developed and validated in the prior work.[3] It is a dynamic model that considers the six largest contributors to long-term degradation: nickel coarsening, nickel oxidation, anode pore size changes, anode conductivity changes, electrolyte conductivity changes, and sulfur poisoning. These degradation mechanisms are related to the operating conditions such as current density, operating temperature, and fuel pressure, and affect voltage and power output. This model was developed in general form for natural gas fuels. The model is summarized here for the convenience of the reader. [3]

Electrochemical behaviour of SOFCs can be modeled through thermodynamic equations, a summary of which is given in this section. For more detail, please refer to our previous work.[3] SOFCs show the highest voltage, known as the open circuit voltage (OCV), when there is zero current in the external circuit. However, voltage declines when current is drawn from the cells. The level of voltage drop depends on several parameters and can vary over time. Potential losses in SOFCs are known as overpotentials or polarizations, and can be divided into three main types, known as: ohmic, activation, and concentration overpotentials.[18]

$$V(t) = E - \left(\sum_k \eta_{\mathrm{ohm,k}}(t) + \eta_{\mathrm{act,an}}(t) + \eta_{\mathrm{act,ca}}(t) + \eta_{\mathrm{con,an}}(t) + \eta_{\mathrm{con,ca}}(t)\right) \qquad (1)$$

In Eq. 1, $\eta_{\mathrm{ohm}}$, $\eta_{\mathrm{act}}$, and $\eta_{\mathrm{con}}$ are the ohmic, activation, and concentration overpotentials, respectively, and $E$ is the OCV, which is obtained via the Nernst equation (Eq. 2) as follows,

$$E = E^{\circ} + \frac{\mathrm{R}T}{n\mathrm{F}} \ln\left(\frac{P_{\mathrm{H_2}} \cdot {P_{\mathrm{O_2}}}^{1/2}}{P_{\mathrm{H_2O}}}\right) \qquad (2)$$

Where $E^{\circ}$ is the OCV of the fuel cell at standard condition, $n$ is the number of moles equivalent to the electrons transferred during the electrochemical reaction per one mole of reactants, and F represents the Faraday constant.

Thermodynamic equations (Eq. 3-5, 11, 15, and 16) can be used to explain the aspects of the polarizations that are known as inevitable voltage drops, and caused by some chemical, physical, and electrochemical reactions in the fuel cell; the remaining losses occur due to phenomena related to system degradation. The model, developed in the prior work, integrates models of system degradation phenomena into the conventional thermodynamic equations in order to account for both inevitable overpotentials and system degradation processes. The general form of thermodynamic equations and models of system degradation mechanisms are given in the following. The reader is referred to our previous paper for more details and discussion. [3] Voltage losses due to ohmic polarization were computed using Eqs. 3-5, losses due to activation polarization were calculated using Eq. 11, and losses due to concentration polarization were determined via Eqs. 15 and 16.

## 2.1. Ohmic polarization

The ohmic polarization of the SOFC compartments is computed using Ohm's law.[19,20]

$$\eta_{\mathrm{ohm,ic}} = I\,\left(\frac{L_{\mathrm{ic}}}{L_y\,L_z\,\sigma_{\mathrm{ic}}} + \frac{L_{\mathrm{fc}}}{(1+n_{\mathrm{ch}})L_t\,L_y\,\sigma_{\mathrm{ic}}} + \frac{L_{\mathrm{ac}}}{(1+n_{\mathrm{ch}})L_t\,L_z\,\sigma_{\mathrm{ic}}}\right) \tag{3}$$

$$\eta_{\mathrm{ohm,ele}} = I\,\left(\frac{L_{\mathrm{ele}}}{L_y\,L_z\,\sigma_{\mathrm{ele}}\,(t)}\right) \tag{4}$$

$$\eta_{\mathrm{ohm,l}} = I\,\left(\frac{(\,A_{\mathrm{opt},l}(t)-L_y\,L_z\,)\,L'_{\mathrm{opt},l}}{2\,A_{\mathrm{opt},l}(t)\,L_y\,L_z\,(1-\varphi_l)\sigma_{\mathrm{ele}}\,(t)} + \frac{L_l-L'_{\mathrm{opt},l}}{L_y\,L_z\,(1-1.8\varphi_l)\,\sigma_l(t)}\right) \tag{5}$$

where $I$ represents the operating current measured, $L$ is the length or thickness, $n_{\mathrm{ch}}$ represents the number of channels, $\sigma$ is the electrical conductivity, $A_{\mathrm{opt},l}$ denotes the area of the regions where electrochemical reactions take place. Additionally, subscript $l$ denotes the electrode (anode, cathode), ele is the electrolyte, and ic, fc, and ac denote interconnect, fuel channel, and air channel, respectively.

$A_{\mathrm{opt},l}$ is a function of the electrode pore size, and it changes during the operation of the SOFC.

$$A_{\mathrm{opt},l}\,(t) = \left(1 + 2\,\frac{L'_{\mathrm{opt},l}}{D_{p,l}(t)}\right)\,L_y\,L_z \tag{6}$$

$L'_{\mathrm{opt}}$ is the thickness of the triple phase boundary (TPB). Knowing the size and number of particles, this parameter can be calculated using percolation theory.[18] Wen et al. found its optimal values by some trade-offs between all the polarizations of SOFC.[20,21] $D_p$ is the average size of the electrode pores, which can be calculated using the following equation for the anode.[22]

$$D_{p,\mathrm{an}}(t) = D_{\mathrm{YSZ}}\,\varepsilon_{\mathrm{YSZ}}(t) + D_{\mathrm{Ni}}(t)\,\varepsilon_{\mathrm{Ni}}(t) \tag{7}$$

During the operation of an SOFC, the average size ($D_{\mathrm{Ni}}$) and hence volume fraction ($\varepsilon_{\mathrm{Ni}}$) of Ni particles vary as a result of agglomeration and oxidation. We used the model developed by Gao et al. [23] and Neidhardt et al.'s model[24] to account for the agglomeration and oxidation of Ni particles, respectively. The reader is referred to the literature for more details. [3]

Degradation of anode conductivity can be quantified by the percolation theory. [25,26]

$$\sigma_{\mathrm{Ni}}(t) = f_r\,\sigma_{0,\mathrm{an}}\left(\frac{Pr(t) - Pr_{\mathrm{c}}}{1 - Pr_{\mathrm{c}}}\right)^{1.3} \frac{\varepsilon_{\mathrm{Ni}}(t)}{\tau_s} \tag{8}$$

$$f_r = \frac{R_{\mathrm{film}}}{R_{\mathrm{eff}}} \tag{9}$$

where $\sigma_{0,\mathrm{an}}$ is the electrical conductivity of the bulk material, $\tau_s$ represents the tortuosity of the porous anode, $Pr$ is the probability of site occupancy, and $Pr_c$ is the occupancy at the threshold of site percolation while $f_r$ has a value of 0.575 for the anode of an SOFC with a 15° overlap angle between particles. In Eq. 9, $R_{\mathrm{film}}$ is the ohmic resistance of a thin layer with continuous structure and $R_{\mathrm{eff}}$ is the ohmic resistance of a sintered layer, For more details of these equations, please refer to the literature. [3]

Eq. 10 was presented by Coors et al. to calculate degradation of the electrolyte conductivity.[27]

$$\sigma(t) = (\sigma_i - \sigma_f)\exp(-t/\tau) + \sigma_i \tag{10}$$

Where $\sigma_i$ and $\sigma_f$ represent the conductivity of the YSZ electrolyte before and after deterioration, respectively, and $\tau$ represents the time of relaxation of electrons (s).

### 2.2. Activation polarization

Activation polarization is quantified by the Butler-Volmer equation,[20]

$$\eta_{\mathrm{act},l} = \frac{\mathrm{R}T}{\alpha n\mathrm{F}}\sinh^{-1}\left(\frac{i_l(t)}{2i_{0,l}}\right) \tag{11}$$

In the activation polarization calculation α is a coefficient for electron transfer in the electrochemical reactions, and $i_l$ and $i_{0,l}$ are the working and exchange current densities of the electrode, $l$, respectively.

$$i_l(t) = \frac{I}{A'_{\mathrm{opt},l}(t)} \tag{12}$$

$$i_{0,\mathrm{ca}} = \gamma_{\mathrm{ca}}\left(\frac{P_{\mathrm{O_2}}}{P_{\mathrm{ref}}}\right)^{0.25}\exp\left(-\frac{E_{\mathrm{act,ca}}}{\mathrm{R}T}\right) \tag{13}$$

$$i_{0,\mathrm{an}} = \gamma_{\mathrm{an}}\left(\frac{P_{\mathrm{H_2}}}{P_{\mathrm{ref}}}\right)\left(\frac{P_{\mathrm{H_2O}}}{P_{\mathrm{ref}}}\right)\exp\left(-\frac{E_{\mathrm{act,an}}}{\mathrm{R}T}\right) \tag{14}$$

$\gamma_{an}$ and $\gamma_{ca}$ are the pre-exponential constants for the anode and cathode, respectively, the activation energy is denoted as $E_{\mathrm{act}}$, $P_{\mathrm{ref}}$ and $P_i$ represent the reference pressure and partial pressure of the species, $i$, respectively.[28,29]

### 2.3. Concentration polarization

The following equations are used to quantify the concentration overpotentials of the cathode and anode.[19]

$$\eta_{\mathrm{con,ca}} = \frac{\mathrm{R}T}{n\mathrm{F}} \ln \left(\frac{P_{\mathrm{O_2}}}{P_{\mathrm{O_2,TPB}}(t)}\right) \tag{15}$$

$$\eta_{\mathrm{con,an}} = \frac{\mathrm{R}T}{n\mathrm{F}} \ln\left(\frac{P_{\mathrm{H_2O,TPB}}(t)\, P_{\mathrm{H_2}}}{P_{\mathrm{H_2,TPB}}(t)\, P_{\mathrm{H_2O}}}\right) \tag{16}$$

In the concentration polarization calculation, $P_{i,\mathrm{TPB}}$ is the partial pressure of molecules, $i$ at TPB region. This can be expressed as follows:[19,20]

$$P_{\mathrm{H_2,TPB}}(t) = P_{\mathrm{H_2}} - \frac{\mathrm{R}T\, L_{\mathrm{an}}\, I}{n\,\mathrm{F}\, L_y\, L_z\, D_{\mathrm{eff,an}}(t)} \tag{17}$$

$$P_{\mathrm{H_2O,TPB}}(t) = P_{\mathrm{H_2O}} + \frac{\mathrm{R}T\, L_{\mathrm{an}}\, I}{n\,\mathrm{F}\, L_y\, L_z\, D_{\mathrm{eff,an}}(t)} \tag{18}$$

$$P_{\mathrm{O_2,TPB}}(t) = P_{\mathrm{air}} - \left(P_{\mathrm{air}} - P_{\mathrm{O_2}}\right) \exp\left(\frac{\mathrm{R}T\, L_{\mathrm{ca}}\, I}{n\,\mathrm{F}\, L_y\, L_z\, D_{\mathrm{eff,ca}}(t)\, P_{\mathrm{air}}}\right) \tag{19}$$

$D_{\mathrm{eff},l}$ which is known as the effective gas-phase diffusivity or diffusion coefficient; is obtained via,

$$D_{\mathrm{eff,an}}(t) = \left(\frac{P_{\mathrm{H_2}}}{P_{\mathrm{f}}}\right) D_{\mathrm{H_2O,eff}}(t) + \left(\frac{P_{\mathrm{H_2O}}}{P_{\mathrm{f}}}\right) D_{\mathrm{H_2,eff}}(t) \tag{20}$$

$$D_{\mathrm{eff,ca}}(t) = D_{\mathrm{O_2,eff}}(t) \tag{21}$$

$D_{i,\mathrm{eff}}$ denotes the effective diffusion of the gaseous molecules, $i$, through the pores of the electrodes structure, and can be expressed as follows,

$$D_{\mathrm{H_2,eff}}(t) = \frac{\varphi_{\mathrm{an}}}{\tau_{\mathrm{an}}} \left(\frac{1}{D_{\mathrm{H_2-H_2O}}} + \frac{1}{D_{\mathrm{H_2,K}}(t)}\right)^{-1} \tag{22}$$

$$D_{\mathrm{H_2O,eff}}(t) = \frac{\varphi_{\mathrm{an}}}{\tau_{\mathrm{an}}} \left(\frac{1}{D_{\mathrm{H_2-H_2O}}} + \frac{1}{D_{\mathrm{H_2O,K}}(t)}\right)^{-1} \tag{23}$$

$$D_{\mathrm{O_2,eff}}(t) = \frac{\varphi_{\mathrm{ca}}}{\tau_{\mathrm{ca}}} \left(\frac{1}{D_{\mathrm{O_2-N_2}}} + \frac{1}{D_{\mathrm{O_2,K}}(t)}\right)^{-1} \tag{24}$$

where $D_{i,\mathrm{K}}$ and $D_{i-j}$ are Knudsen and binary diffusion, respectively. [30] [31]

## 2.4. Sulfur poisoning

Hydrogen sulfide ($H_2S$) is commonly used in odorless hydrocarbon fuel sources as an odorant for safety reasons. However, the interaction between the anode and this compound results in the adsorption of sulfur to the surface of anode, which in turn deteriorates an Ni-YSZ anode's ability to enable electrochemical reactions and the internal reformation of hydrocarbons.[32,33] We utilized Hagen et al.'s experimental data to construct a regression model for sulfur contamination of a SOFC supplied with hydrocarbon fuel.[33] Voltage loss was used as an indication of sulfur poisoning. Voltage drops are a function of $H_2S$ concentrations in the fuel stream and current density. Final equations are listed below. For the details of deriving these equations please refer to the prior work.[3]

$$\Delta V_{\mathrm{s}} = W_1 \ln(C_{\mathrm{H_2S}}) + W_2\, Y_{\max}(i)(1 - A_1(i) \exp\left(-A_2(i) \times C_{\mathrm{H_2S}}\right)) \tag{25}$$

In Eq. 25, $\Delta V_{\mathrm{s}}$ is the potential loss due to sulfur adsorption on the anode surface, $i$ is the cell's current density, and $C_{\mathrm{H_2S}}$ is the concentration of hydrogen sulfide in the fuel stream. $W_1$, $W_2$, $Y_{\max}$, $A_1$, and $A_2$ are computed via Eqs. 26-30 as follows:

$$W_1 = -0.039\, i^2 + 0.009\, i + 0.030 \tag{26}$$

$$W_2 = 1 - W_1 \tag{27}$$

$$A_1 = 0.827\,\exp(0.411\,i) \tag{28}$$

$$A_2 = 0.064\,\exp(0.995\,i) \tag{29}$$

$$Y_{\max} = 6.749\,\exp\,(1.559\,i) \tag{30}$$

This model was not only tested using Hagen et al.'s experimental data, but it was also validated against third-party experimental data obtained by Papurello et al.[33,34] Using these data sets, the model predicted potential drop due to sulfur contamination with an $R^2$ of 0.85. This result indicates that the constructed model is capable of accurately projecting potential loss in sulfur-contaminated SOFCs supplied with hydrocarbon fuels.[3]

### 2.5. Validation

The reliability of the simulation outputs was validated in our previous study, using data from Hagen et al. that was not utilized in construction of the SOFC model.[3,10] The proposed model predicted performance deterioration of SOFCs with a high level of precision (with an $R^2$ of 0.934 over 1400 hours of cell operation).

### 2.6. Catastrophic failure

It should be noted that the model does not account for catastrophic mechanical failures, such as delamination and cracking. Catastrophic failure of solid oxide cells depends on their operating conditions. There is still lack of adequate knowledge of how long SOFCs can be run under various operating conditions until a catastrophic failure occur. Models that can predict catastrophic failure would be an important subject for future work but are difficult to obtain experimentally.

## 3. Power Plant Simulations

The above-described degradation-based model was used to perform an economic analysis of standalone SOFCs. To the best of the authors' knowledge, this is the first economic analysis of SOFCs to use such a detailed degradation-based model.

In this economic assessment, LCOE was selected as the measure of the cost of electricity produced by an SOFC over its lifetime. As noted above, the SOFC model used in this study accounts for the dominant deterioration phenomena in SOFCs and is highly accurate in predicting performance of SOFCs under various operating conditions. This is the key difference between this research and previous economic studies, as degradation rate greatly affects cost and performance of the cells. Since previous economic studies have routinely ignored or underestimated the degradation rate, the calculated costs and lifetime under the operating conditions reported in these works will likely be inaccurate and of little help in commercializing real SOFCs.

In this study, the plant is assumed to have a lifetime of 20 years, while the SOFCs are assumed to have a lifetime of less than 20 years, as described in the next paragraph.

SOFC lifetime is arbitrary, as there is not a unique definition for the end of life of SOFCs in the literature. In general, as long as there has not been a catastrophic failure, one can decide the SOFC is at its end of life based on case-specific criteria. In this work, SOFC lifespan is an independent variable, taken as a parameter in the optimization, rather than a decision variable. So-called SOFC lifetime in this problem is our intended cell replacement schedule. SOFCs should meet an average power-generation constraint over this operational lifetime. For example, a 5-year SOFC lifetime means that over the 20 years lifetime of the power plant, SOFCs should be replaced with identical cells every 5 years. The brand-new cells have the same size as the previous cells and should deliver the same initial performance. Recent studies aim to assess performance of SOFCs over 15 years of operation under fuel cell, electrolysis, or reversible mode.[35,36] A recent study on long-term performance of conventional solid oxide cells, reported a catastrophic failure in the 15th years of cells operation in the electrolysis mode with similar operating current density and temperature as the fuel cell mode.[36] As such, we estimate that maximum lifetime of cells cannot exceed 14 years and decided to solve the problem for various replacement schedules (lifetimes) from 1 to 14 years. Catastrophic breaks of solid oxide cells depend on operating conditions. Even though one study showed that cells can operate 15 years before they are catastrophically broken, there is still a lack of adequate knowledge of how long SOFCs can be run under various operating conditions until a catastrophic failure occurs.

We employ the General Algebraic Modeling System (GAMS) to formulate and solve an optimization problem, namely, to find the conditions best suited to minimizing LCOE (Eq. 32) and the effects of various parameters on the cost of electricity. To this end, we utilized BARON, which is a solver for the global solution of non-linear programs (NLP) in GAMS.

A mathematical description of the base case optimization problem is provided as follows. The problem definition is given for a 6-year replacement schedule as an example, where SOFCs are replaced with same size, brand-new cells, every six years. Instead of solving the problem over the entire 20-year life of the plant, we find the size and performance of the cells, and system's expenses for the first six years of operation, then we use some additional constraints to calculate the total expenses over 20 years of plant's life.

The LCOE calculations used in this work are detailed below.

$$\min_{T, i_j, A_m} LCOE \tag{31}$$

The LCOE of the standalone SOFCs was calculated using Eq.32.

$$LCOE = \sum_{y=1}^{N} \left( \frac{\frac{CC_y + NO_y + FC_y}{(1+r)^y}}{\sum_{y=1}^{N} \frac{P_y}{(1+r)^y}} \right) \tag{32}$$

where $CC_y$, $NO_y$, and $FC_y$ are the capital costs, non-fuel operating and maintenance costs, and fuel costs, respectively; $P_y$ is the total power produced in year $y$; $r$ is the discount interest rate (10%),[37] which indicates the time value of money; and $N$ is the lifetime of the plant (20 years).

Eqs. 33-42 are used for $1 \leq y \leq 6$; As shown in Eq. 31, current density as a function of time (taken in constant increments lasting 5 days each), spatially-averaged SOFC operating temperature, and membrane area are decision variables.

$$973 \leq T \leq 1073 \text{ (K)} \tag{33}$$

$$0 \leq i_j \leq 2 \left(\frac{\text{A}}{\text{cm}^2}\right) \tag{34}$$

where $j$ represents the timestep index (each timestep lasts for 120 hours, with 73 timesteps per year), and $i_j$ is the current density in the $j$th timestep. Eqs. 33 and 34 show the normally accepted ranges of current density and temperature.[38–41]

$$0.9 \times i_{j-1} \leq i_j \leq 1.1 \times i_{j-1} \quad (35)$$

As noted earlier, current density has significant impact on degradation of the cells. In addition, changes to current density require very accurate monitoring of the fuel flow. Therefore, abrupt or high-scale changes to the current density might not be practical or safe for the long-term operation of SOFCs. As such, we decided to keep the current constant for each time period (5 days), and then constrained it to change no more than $\pm$10% of that figure for the next 5-day period (Eq. 35).

$$V_j = E - f(T, i_j) \quad (36)$$

where $V_j$ is cell voltage in the $j$th timestep, $E$ is the OCV, and $f(T,\ i_j)$ is the total polarization computed as sum of equations 3-5, 11, 15, and 16 in the previous section.

$$P_j = V_j \times i_j \times A_m \quad (37)$$

where $P_j$ is the power output in the $j$th timestep, and $A_m$ is the membrane area.

$$\frac{\sum_{y=1}^{y=6} P_y \times 96.5\%\ (\text{DC to AC inversion efficiency})}{6 \times 8760} = 550\ \text{MW (AC)} \quad (38)$$

The SOFCs in the base case are constrained to generate an average of 550 MW of electricity (AC) over their lifespan; it is assumed that the 96.5% of the DC power output from the SOFCs will be converted to AC power. This constraint (Eq. 38) allows us to have a consistent basis of comparison, such that all plants provide essentially the same service.

Capital expenses and Non-fuel operating cost are computed as follows.

$$CC_y = A_m \times \text{SOFC capital cost} \times (1+d)^{y-1} \quad (39)$$

$$NO_y = A_m \times \text{non} - \text{fuel operating cost} \times (1+d)^{y-1} \tag{40}$$

where the value of $\text{SOFC capital cost}$ and $\text{non} - \text{fuel operating cost}$ are given in $/cm$^2$, $d$ is the annual inflation rate and it is assumed that the costs inflate at an annual rate of 2.8% (0.038% per 120-hour). The capital costs are paid in the first year of a cell's operation.

$$FC_y = \sum_{j=(y-1)\times 73+1}^{j=y\times 73} n_{\text{fuel},j} \times \text{HHV}_{\text{fuel}} \times \text{cost of Fuel} \times (1+\frac{d}{73})^{(j)} \tag{41}$$

$$n_{\text{fuel},j} = f(A_m, i_j) \tag{42}$$

The value of $\text{cost of Fuel}$ is in $/GJ$_{\text{HHV}}$, $n_{fuel,j}$ is the fuel consumed over the $j$th time interval. Fuel consumption changes with the current density (please see Aguiar et al.'s work[19] for details of Eq. 42) and thus its value varies for each timestep. The fuel expenses use an equivalent 0.038 % inflation rate per timestep in order to model gradual cost increases over time, rather than discrete annual increases. The values of $\text{SOFC capital cost}$, $\text{non} - \text{fuel operating cost}$, and $\text{cost of Fuel}$ are provided in the last paragraph of this section.

The following are additional constraints for replacement cells (for $y > 6$);

$$P_y = P_{y-6} \tag{43}$$

This constraint is used to ensure that the replacement cells provide the same service as the previous cells. In other words, this equation ensures that the total power produced by replacement cells in year $y$ is equal to the total power produced by the previous cells in year $y - 6$.

$$CC_y = CC_{y-6} \times (1+d)^6 \tag{44}$$

$$NO_y = NO_{y-6} \times (1+d)^6 \tag{45}$$

$$FC_y = FC_{y-6} \times (1+\frac{d}{73})^{(6\times73)} \tag{46}$$

When lifespan of the cells is not an integer multiple of 20-year life of plant, the capital cost for the last operating interval is a fraction of the capital cost for a full operating interval. This fraction is calculated as the length of the last operating interval to the lifetime of the cells. For 6-year SOFCs, the last operating interval is 2 years ($19 \leq y \leq 20$), and thus the capital expenses are computed as follows.

$$CC_y = \frac{2}{6} \times CC_{y-6} \times (1+d)^6 \tag{47}$$

The power delivered and fuel costs in $19 \leq y \leq 20$ are obtained from Eqs. 43 and 46, respectively. Meaning that they are calculated as the power delivered and cost of fuel consumed in the initial years of operating the cells. Unlike capital and non-fuel operating costs that only depend on the size of the cells, fuel cost and power output depend on the performance of the cells, and thus they should be calculated over the same operating years. The figure provided by the U.S. Department of Energy (U.S. DOE) were used as the standard costs in this study,[42] with capital and $\mathrm{non-fuel}$ operating costs being expressed in \$/kW. Based on the size of the SOFCs in DOE report, we converted the capital cost into \$/cm$^2$. The capital cost of the SOFCs was determined to be \$0.58/cm$^2$ when waste heat is not recovered from the cells, while the non-fuel operating costs were calculated as 0.011 \$/cm$^2$. In fact, a price of almost 2000 \$/kW-installed for conventional SOFCs with a nominal power density of 0.28 W/cm$^2$ was reported by U.S. DOE. The \$/kW metric is based on the assumption that SOFCs will be operated in a particular mode, where they generate a constant amount of power over their operational time. However, we are conducting a more general study, trying to assess economics of SOFCs in various power generation modes. As such, we need to express costs in more tangible terms without these assumptions. Furthermore, using the \$/cm$^2$ metric will allow decision makers to find the operational modes, operating parameters, and sizing of the cells such that they best suit the limitations on availability and cost of the land in their regions. It is noteworthy that the abovementioned costs account for all the stack manufacturing and assembly, fuel and air supply components (sulfur sorption reactor, preheater, filter, and blower), power electronic, control, and instrumentation components such as sensors, DC/AC inverter, etc. (Figure 1). The costs of heat recovery system are not included in the base case costs. We assumed that the SOFCs were fueled with natural gas (NG) at a cost of 7.78 \$/GJ$_{HHV}$, which is the price of NG in California, 2016. Even though, NG price in California is higher than the average price in the U.S., it was selected for more conservative cost assessment[42], and because SOFCs are more likely to be implemented in regions with high fuel costs. All costs are expressed in 2016 U.S. dollars. While the U.S. DOE has computed the capital and operating costs for 100-kW and 250-kW SOFC stacks, this study uses the values for the 100-kW stack. Although the 100-kW stack has slightly higher capital costs due to its smaller size, it was selected because it would enable cells to be monitored, maintained, repaired, or replaced much more easily, and also serves as the more conservative estimate.

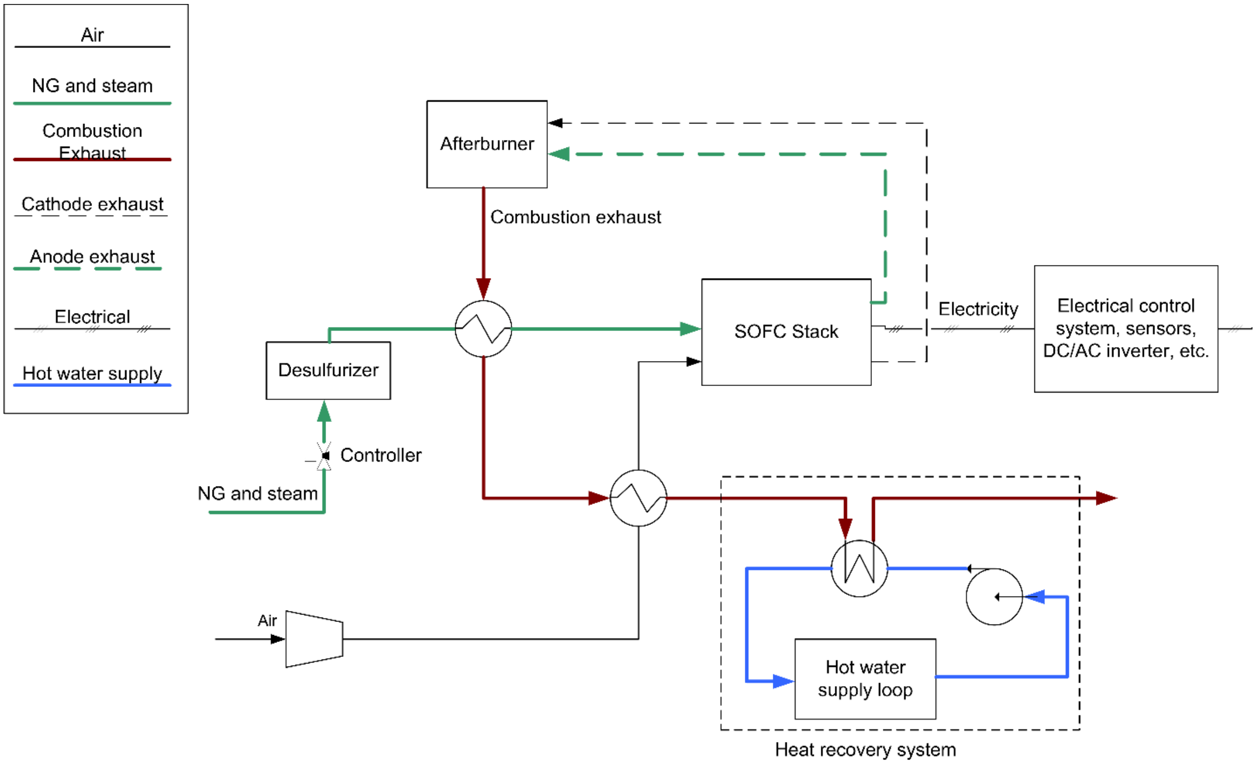

Figure 1. An outline of SOFC system.

The base case uses the costs reported by the U.S. DOE and ignores the $CO_2$ tax. NG fed to the SOFC contains 95% $CH_4$. [43]

Table 1. shows the costs used in the base case.

**Table 1.** system's unit costs in the base case

| | **Value** | **Unit** |
|---|---|---|
| Capital cost | 0.58 | $\$/cm^2$ |

| | | |
|---|---|---|
| Non-fuel operating cost | 0.011 | $\$/cm^2$ |
| Fuel cost | 7.78 | $\$/GJ_{HHV}$ |
| $CO_2$ tax | 0 | $\$/tonne CO_2$ |

# 4. Results and Discussion

## 4.1. Base case optimization

As noted in previous section, the base case was optimized for various SOFC lifespans (1 to 14 years). Figure 2 illustrates the minimum LCOEs of SOFCs with various lifespans. Due to their relatively high capital costs, the cost of generating electricity decreases as the lifespan of SOFCs increases. For example, the LCOE drops markedly (55%) when the lifespan of the SOFC is extended from 1 year to 5 years, and by an additional 25% when it is extended from 5 to 14 years.

One important result of this analysis is that it helps system designers to select a target replacement rate based on experiential knowledge of the catastrophic failure of the cells with respect to operating time; and to run the cells accordingly.

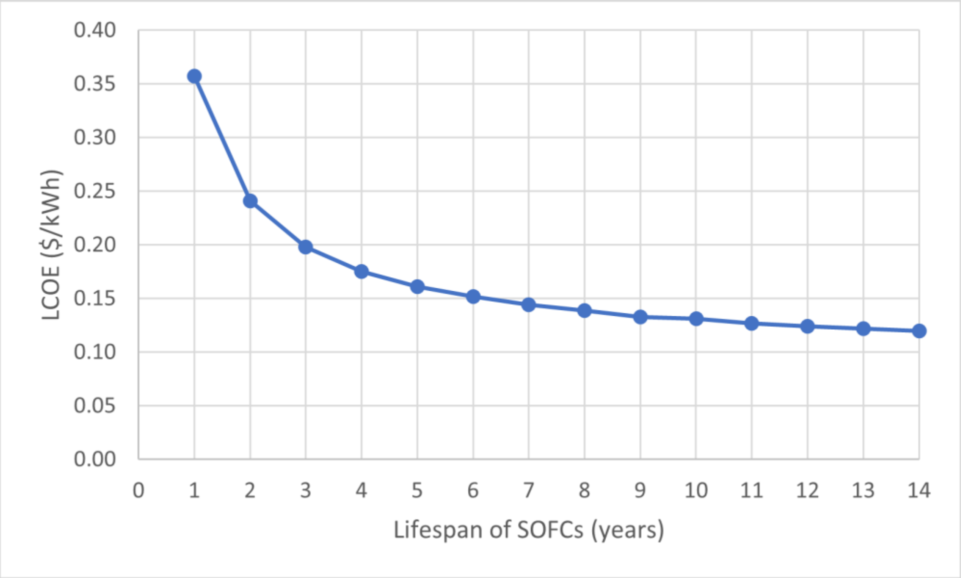

Figure 2. Minimum LCOEs of base case SOFCs at various lifespans

The results showed that it is always best for SOFCs to be operated at the lower bound (750°C). The reason is that degradation rate increases with increasing the temperature. The optimal average current densities, average voltages, and membrane areas used in the base case SOFCs are shown in Figs. 3a-c. In our previous work, we showed that current density has the highest impact on long-term performance of the cells and that SOFCs tended to degrade faster when they were operated at higher current densities. Therefore, SOFCs should be operated at lower current densities, as doing so will extend their lifespan. However, in order to meet the power constraint, cells with lower average current densities require higher voltages and larger membrane areas which leads to higher capital costs.

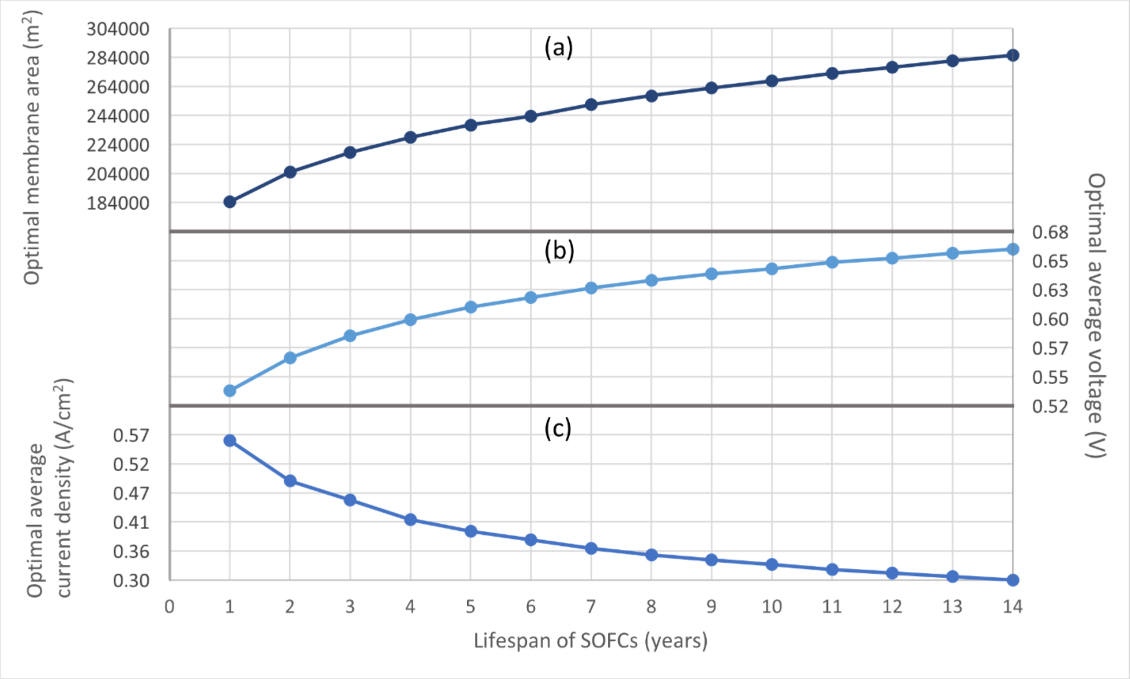

Figure 3. Optimal values of (a) membrane area, (b) average voltage, and (c) average current density of the base case for different operational times.

Figure 4a, b illustrates trajectories of optimal current density and voltage for different replacement schedules of 1, 2, 5, and 10 years. In the optimal operation of the base case SOFC, current density decreases rapidly within the first months of operation, but it shows small changes after the first year. Moreover, even though current density has an upper bound of 2 A/cm$^2$, it can be seen from the optimal trajectories that the highest current density reaches is 0.828 A/cm$^2$ for SOFCs with 1-year lifetime. This is only for a brief period of time, and then it decreases substantially.

Activation polarization is the major source of voltage loss at lower current densities, while ohmic and concentration polarizations are dominant at higher current densities. Therefore, optimal trajectories in this study suggest that concentration and ohmic polarizations are dominating initially, however later with decreasing the current density activation polarization becomes more important. Additionally, it should be noted that system degradation mechanisms such as Ni coarsening and oxidation, and anode and electrolyte electrical conductivity degradation occur at higher rates initially, but their rates diminish over time. Moreover, comparing optimal trajectories of SOFCs with different lifetimes show that the key to lower degradation rate of SOFCs and extend their lifetime is operating them at lower current densities.

For more base case results please see the supporting information.

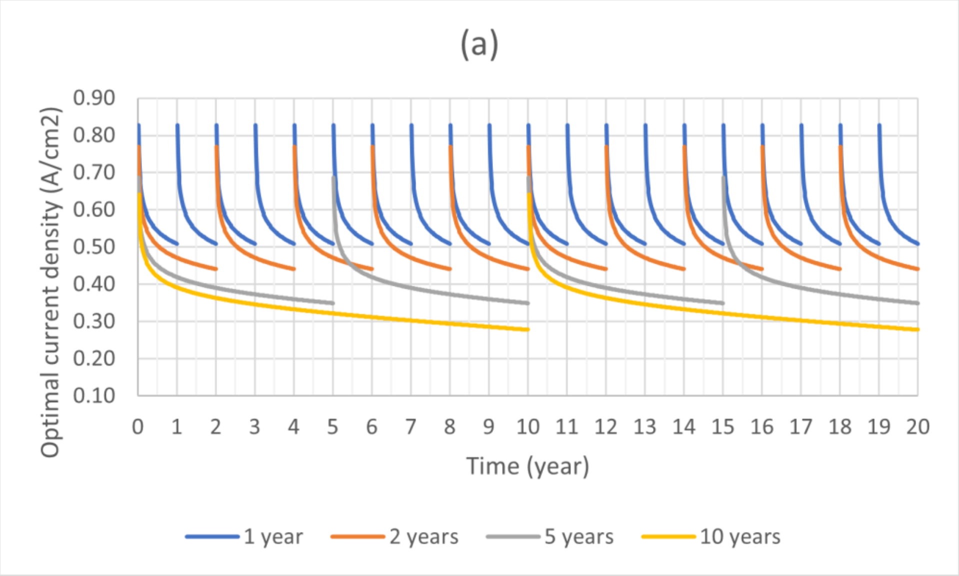

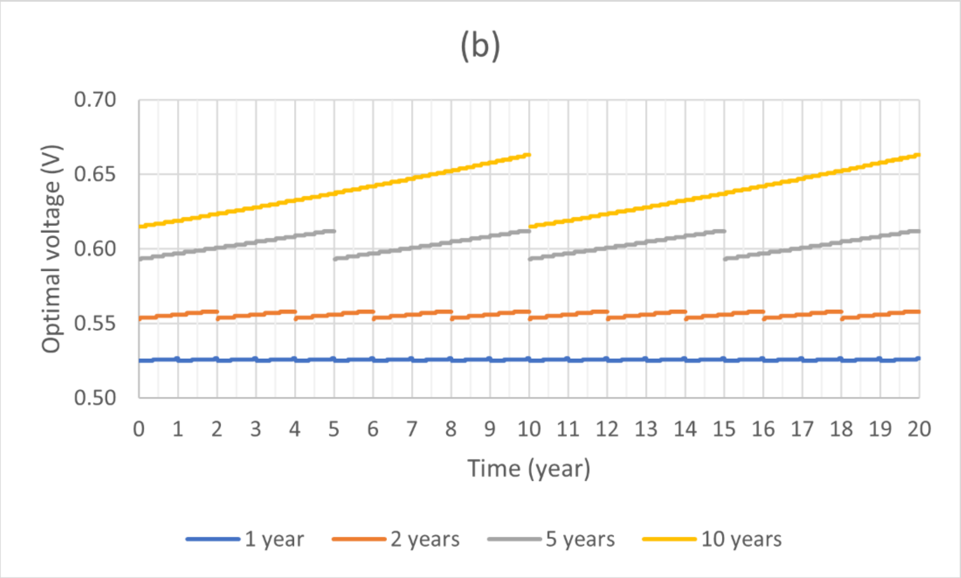

Figure 4. Profile of a) optimal current density and b) optimal voltage for SOFCs with replacement schedules of 1, 2, 5, and 10 years, over the lifetime of the plant.

## 4.2. Sensitivity analysis

Figure 5 shows the effect of various capital cost values on LCOE under similar conditions as the base case. A wide range of costs have been suggested for the SOFCs equipment by different manufacturers depending on the size and application of the cells. We studied the effects of capital cost on the LCOE of SOFCs by varying the capital costs from a low value to very high values. This was done by solving the optimization problem for a lower capital cost of 0.29 $/cm$^2$, and two higher capital costs of 1.16 and 3.25 $/cm$^2$, while other parameters and costs were the same as those of the base case (Table 1). The findings provide system designers with a rough estimate of their system's LCOE based on the price and expected time to catastrophic failure of their SOFCs. As can be seen, capital costs significantly influence the LCOE, especially at shorter SOFC lifespans where SOFCs should be replaced more frequently. For example, reducing the capital costs from \$0.58 to \$0.29/cm$^2$ and using an SOFC lifespan of 1-year results in a 38% decrease in LCOE; in contrast, reducing capital costs from \$0.58 to \$0.29/cm$^2$ and using an SOFC lifetime of 5 years will reduce LCOE by 26%. The capital costs associated with SOFCs can be lowered via mass production, which can in turn significantly reduce the costs of generating electricity, thus making SOFCs an economical alternative to traditional power generation units. However, operational lifetime increases resulting from the use of the optimal operational profiles determined through this study can have just as large an impact.

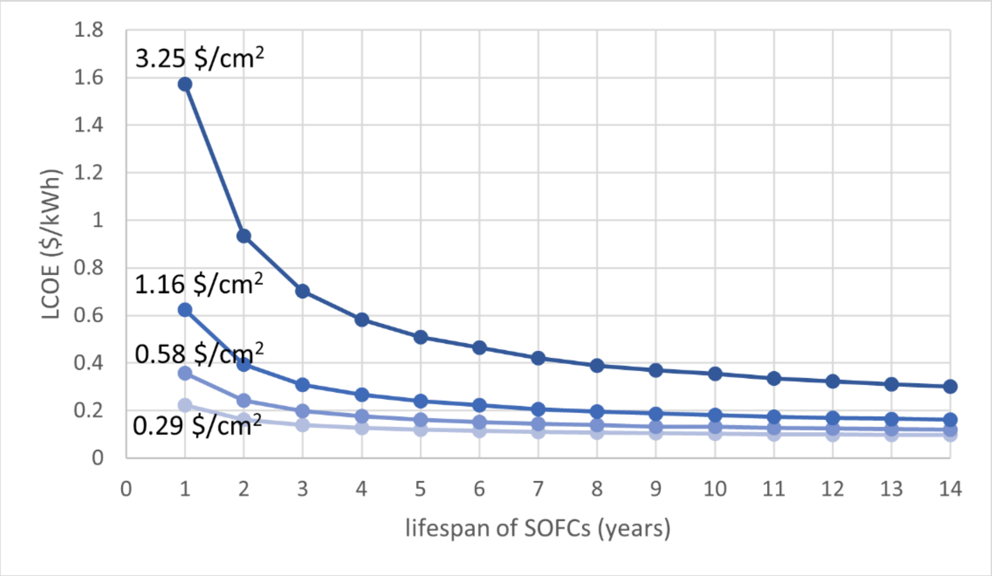

Figure 5. Effect of SOFC capital cost on LCOE with an NG price of 7.78 \$/GJ$_{HHV}$ and without $CO_2$ tax. Base case capital cost is 0.58/cm$^2$ of membrane area. The NG price for all cases was 7.78 \$/GJ$_{HHV}$, and the $CO_2$ tax was 0 \$/tonne.

### 4.3. Effects of $CO_2$ tax and NG price on the LCOE of SOFCs

We re-solve the optimization problem for different $CO_2$ taxes ($0; the base case, $25, $50, $100, $150/tonne of $CO_2$ emitted). All other costs and conditions used in these analyses are the same as the base case (Table 1). As discussed in the introduction, SOFCs offer highly efficient electricity production with very little $CO_2$ emissions. Given these low levels of GHG emissions, the LCOE of SOFC-generated electricity is largely unaffected by $CO_2$ taxes. As shown in Figures 5 and 6, $CO_2$ tax has a much smaller impact on the LCOE of SOFCs than does capital costs.

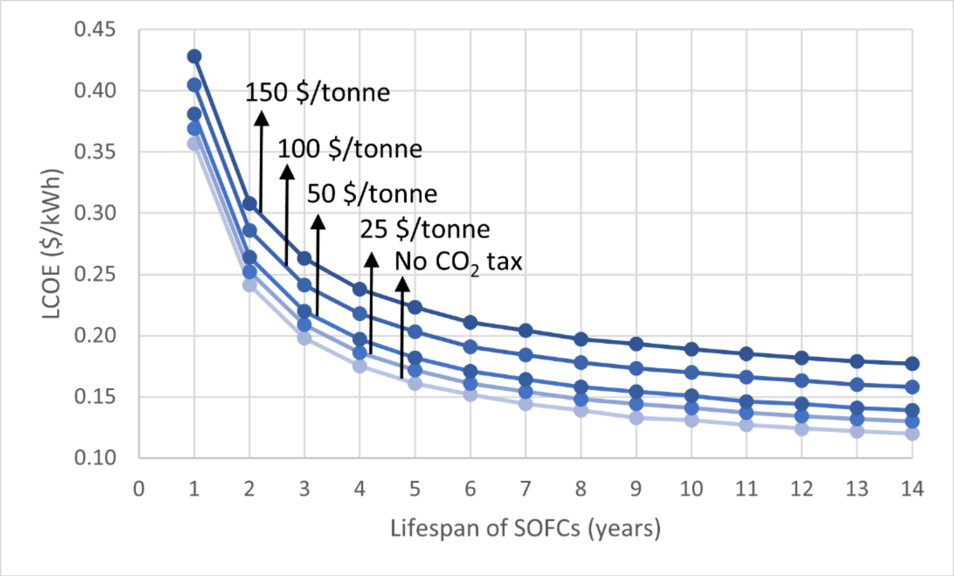

Figure 6. Effect of $CO_2$ tax on LCOE where capital cost = 0.58$/cm$^2$ of membrane area and NG price = 7.78 $/GJ$_{HHV}$.

The following surface plots (Figure 7) demonstrate how the LCOE varies in response to changes in the NG price and $CO_2$ tax. These plots were obtained by changing the NG price from $2 to $10/GJ$_{HHV}$ and the $CO_2$ tax from $0 to $100/tonne, and re-solving the optimization problem for each case. Considering wide ranges of NG price and $CO_2$ tax in this analysis, these are useful for estimating the electricity costs of SOFC systems in various regions. All other costs and conditions are the same as those used in the base case (Table 1). The minimum costs of electricity produced by SOFCs with lifespans of 5, 10, and 14 years were found for various NG prices and $CO_2$ taxes within the above-noted ranges. As can be seen in this figure, LCOE increases with the rise of NG price and $CO_2$ tax. Also, a comparison of three surface plots indicates that with the same NG price and $CO_2$ tax, SOFCs with longer lifetime generate electricity at lower LCOE.

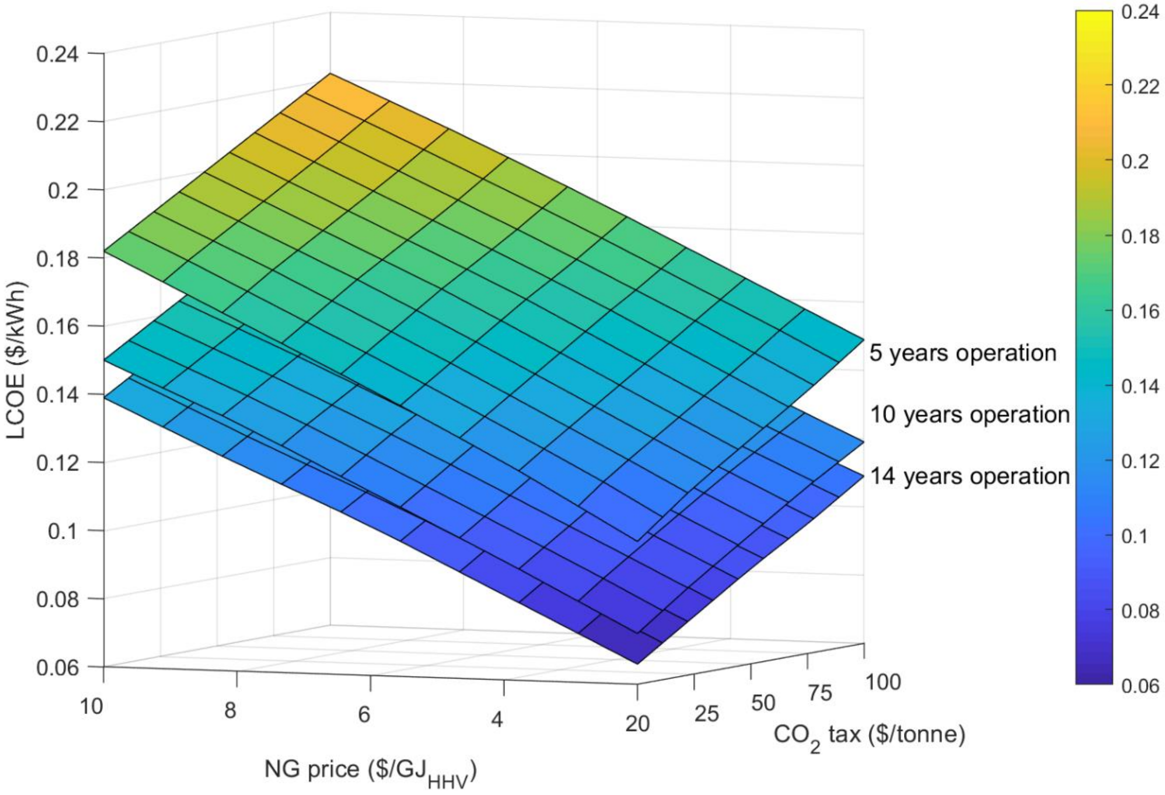

Figure 7. Surface plot: LCOE for different NG prices and $CO_2$ tax values for 5 years operation, 10 years operation, and 14 years operation.

## 4.4. Effect of waste heat recovery on levelized cost of energy

SOFCs operate at high temperatures and generate a considerable amount of high-quality heat. Thermal energy can be recovered from the exhaust gases of SOFCs and utilized to satisfy community heating demands. This feature enhances the economic attractiveness of SOFCs, as they can still be efficient even after they begin to degrade and produce less power.

The levelized cost of energy (LCOEn) is a measure of the cost of electricity and useful heat produced over a plant's lifetime. When waste heat is not recovered from the cells, LCOEn is equal to LCOE. Since thermal energy and electricity have different energy grades, we used an approach in which we calculate the exergy content of thermal energy and electricity. For this purpose, a conversion factor of 1 is used for electricity, while Carnot method is used to calculate conversion factor for thermal energy; as suggested by Rillo et al [44] (Eq. 48).

$$b = 1 - \frac{T_0}{T} \tag{48}$$

Where $T_0$ is the ambient temperature (293 K), and $T$ is the temperature of the recovered heat. The heat recovered from SOFCs is multiplied by a conversion factor of 0.19 to compute the electricity-equivalent energy of the heat recovered at 90°C for hot water supply.

$$LCOEn = \sum_{y=1}^{N} \left( \frac{\frac{CC_y + NO_y + F_y}{(1+r)^y}}{\sum_{y=1}^{N} \frac{P_y + b * Q_y}{(1+r)^y}} \right) \tag{49}$$

Using the costs provided by U.S. DOE for the heat recovery components, such as heaters and bypass valves (heat recovery system in Figure 1), we computed the capital cost of SOFCs when combined with waste heat recovery facilities to be 0.64 \$/cm$^2$. In order to evaluate the energy costs of SOFCs, we ran an optimization problem with the objective of minimizing the LCOEn for SOFCs with different lifespans. All costs, conditions, and variables used in this problem were the same as those in Table 1, except for the higher capital cost accounting for heat recovery. Figure 8 compares the LCOEn of SOFCs with and without heat recovery. As can be seen, harvesting waste heat from SOFCs, and utilizing it to meet the thermal needs of community can reduce energy costs by up to 13%. As it was shown in Figs. 3, SOFCs with shorter lifespans have higher current densities and lower voltages, which result in generating larger amounts of heat. As such, harvesting thermal energy from the SOFCs operating for 1 year, reduces cost of energy by 13%; in contrast, capturing the waste heat when using SOFCs for 14 years, decreases cost of energy by 10%. These findings indicate that the optimal use for SOFCs is when combined with a waste heat recovery system rather than on their own for power generation. This is especially important when using SOFCs for shorter periods of time. This information is invaluable to efforts to commercialize SOCFs, as it offers an easy way of reducing energy costs. Moreover, the ability of CHP systems to efficiently capture and utilize excess heat from the SOFC minimizes concerns about the large amount of exhaust heat from the cells.

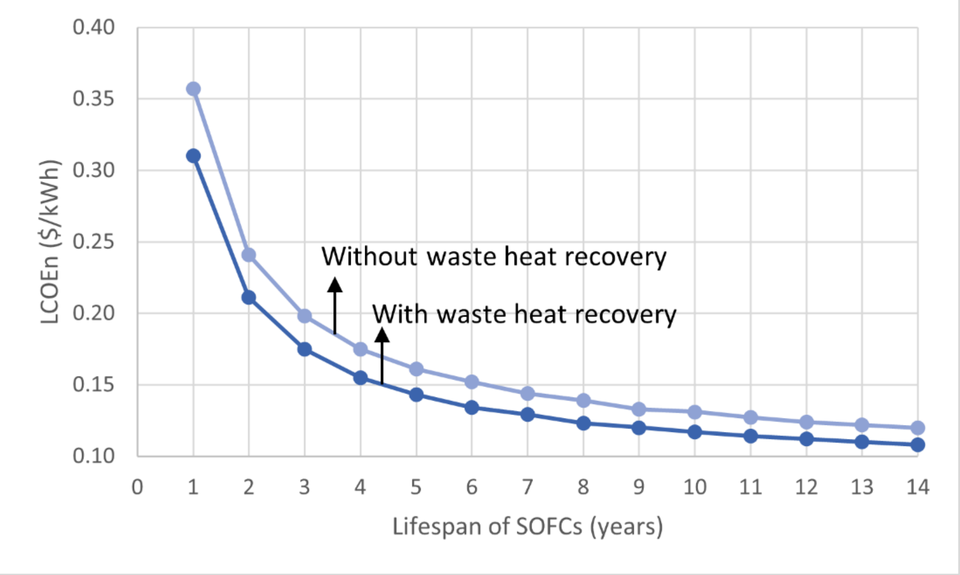

Figure 8. Levelized cost of energy where NG price = 7.78 $/GJ$_{HHV}$, $CO_2$ tax = 0 $/tonne, capital cost = 0.58/cm$^2$ of membrane area without waste heat recovery, and capital cost = 0.64/cm$^2$ of membrane area with waste heat recovery.

## 4.5. Effects of operational modes of SOFCs on the LCOE

SOFCs can be operated in various modes depending on the needs and constraints of the system. In this study we compared the economics of four different modes of operation. The details relating to these operational modes are provided in Table 2.

**Table 2.** Operational modes

| | **Current density** | **Voltage** | **Power** |
|---|---|---|---|
| Mode 1 | Variable | Variable | Variable |
| Mode 2 | Constant | Variable | Variable |
| Mode 3 | Variable | Constant | Variable |
| Mode 4 | Variable | Variable | Constant |

All the results presented in this report so far were obtained from SOFCs operating in Mode 1, wherein current density, voltage, and power are variable (with trajectories chosen by optimization) and are repeated here for comparison. In Mode 2, the optimization problem was modified such that the current density is a single decision variable for the entire operational lifetime of SOFCs, with the remainder of the problem formulation the same. Mode 3 modifies the original optimization problem is modified such that the voltage is a single decision variable for the entire operational lifetime of the SOFCs, with the remainder of the original problem formulation the same. In Mode 4, the original optimization problem is modified by removing the constraint specifying the average power output to be 550 MW (AC) over the specified lifetime (Eq. 38) and replacing with a constraint that the power output must be 550 MW (AC) at all points in time (Eq. 50).

$$P_j = 550\ \mathrm{MW(AC)} \tag{50}$$

This is because SOFCs used in industrial, residential, and research applications are most commonly run at constant power mode (Mode 4).[45–48]

The results are shown in Figure 9. Modes 1, 2, and 3 are very similar, because in Mode 1 and 3, the optimal operation strategies are very similar and after the first few months of operation, require only small changes in the current density over the cell lifetime (see Fig 10), and so fixing the current density at about the same value has little impact on the overall performance. The optimization results illustrate that the average current densities drawn from the cells running in baseload power mode (Mode 4) are lower than in Modes 1, 2 and 3. In this case, larger membrane areas are required to meet the power constraint (Figure 11). The larger membrane areas result in higher capital costs in the baseload mode comparing to other operational modes. Current density profiles of 5-year SOFCs for the four operational modes are shown in Figure 10. In Modes 1, 2, and 3, power production declines over time. Therefore, SOFCs operating in Modes 1, 2, and 3 are unable to function as standalone power-generation units when a constant production is required or expected. However, they can still be used within a larger system that delivers constant (or near-constant) power by being combined with other power-generation technologies such as gas turbines or engines that combust anode off-gases, or energy storage options, or by being connected to the electrical grid. On the other hand, operating SOFCs in baseload power-generation mode (Mode 4) can provide a constant baseload production where it is demanded without additional system components. However, when constant baseload is not required, it is not economically preferable to run SOFCs in constant power mode (Figure 9).

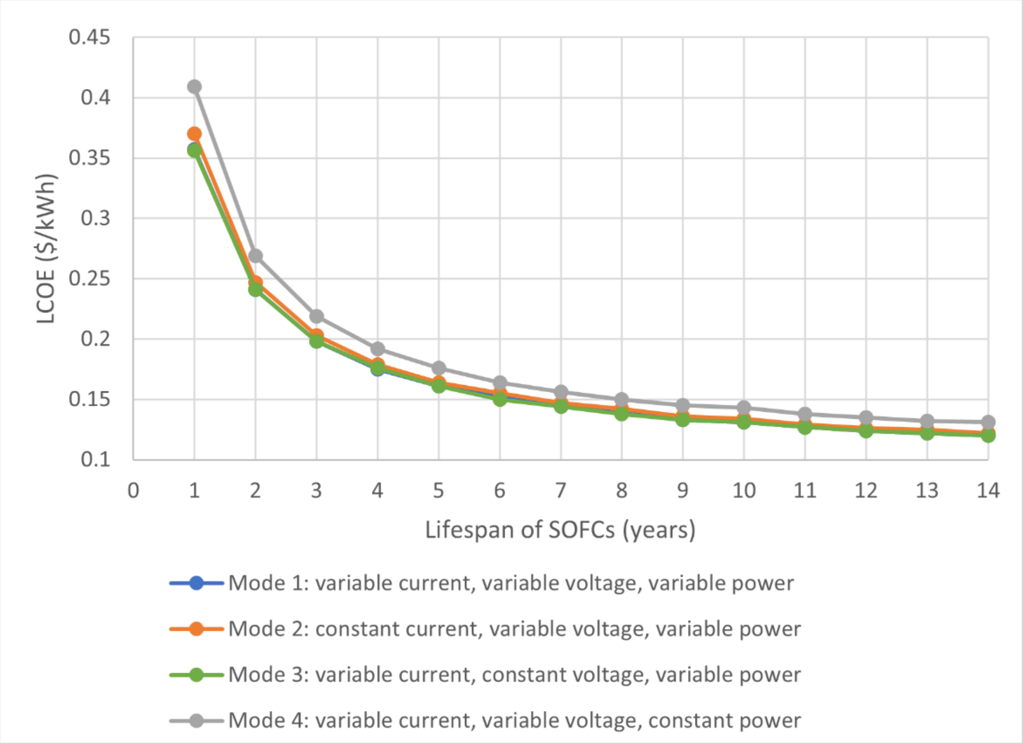

Figure 9. LCOE for different modes of operation where SOFCs capital cost = 0.58/cm$^2$ of membrane area, NG price = 7.78 \$/GJ$_{HHV}$, and CO2 tax = 0 \$/tonne. Note that the LCOEs for Modes 1 and 3 are virtually indistinguishable. Also, it should be noted that SOFCs in Modes 1, 2, and 3 generate an average of 550 MW during their lifetime, and SOFCs in Mode 4 run at constant power output of 550 MW throughout their lifetime.

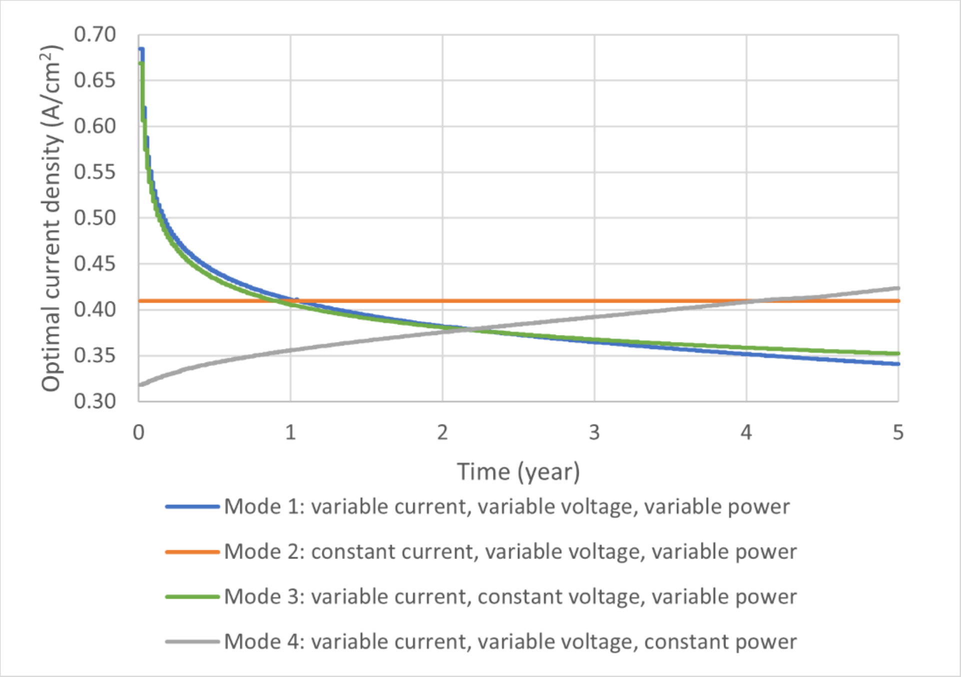

Figure 10. Time variation of current density for 5-years SOFCs in different operational modes.

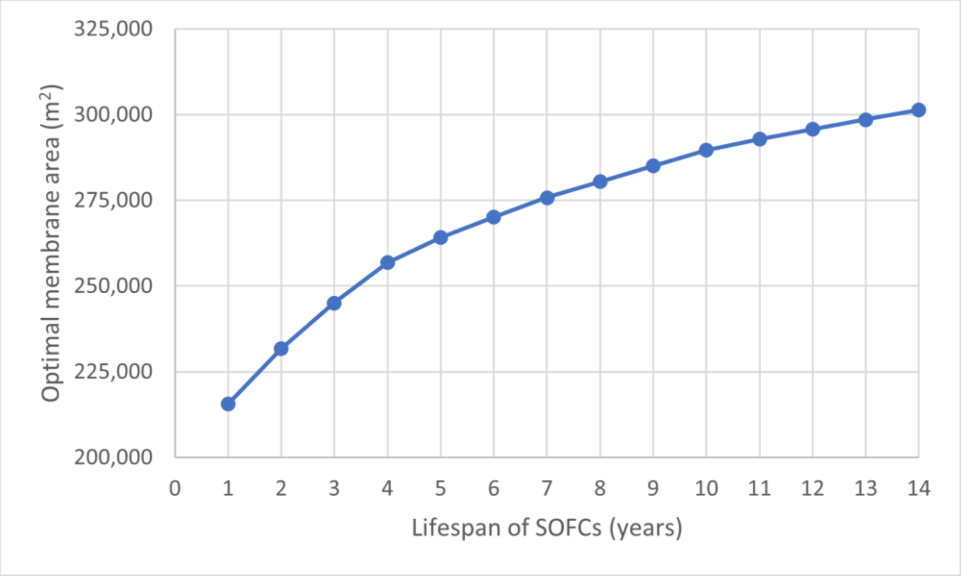

Figure 11. Optimal membrane area for SOFCs operated in Mode 4.

This work does not address the question of whether a standalone SOFC operating in Mode 4 (constant power) is more economical than an SOFC operating in Mode 1 combined with other system elements, such as a GT or combustion engine, such that the system as a whole produces constant or near-constant power. However, our prior work [49] did address this issue specifically, and found that SOFC/GT hybrids with SOFCs operating in Mode 3 were significantly better economically than standalone SOFC systems operating in Mode 4. However, that work used a less robust degradation model that does not capture most of the phenomena considered in the present study, it did not use optimization to determine optimal operating trajectories for any of its cases, and it used a coal-based syngas fuel. Therefore, it would be an interesting subject of future work to revisit the economics of SOFC/GT systems by considering these robust degradation model used in the present work, by using optimization to determine the best operating trajectories for all cases, and especially by allowing the SOFCs in the SOFC/GT system to operate in Mode 1, since the present work has shown superior performance to Mode 4.

# Nomenclature

| | |
|---|---|
| $\boldsymbol{A_{opt}}$ | area of the active<br>TPB region, m2 |

| | |
|---|---|
| $\boldsymbol{A_m}$ | membrane area, $cm^2$ |
| $\boldsymbol{b}$ | Carnot factor |
| $\boldsymbol{C_{H_2S}}$ | concentration of $H_2S$ in the fuel stream, ppm |
| $\boldsymbol{CC_y}$ | capital costs in year $y$, \$ |
| $\boldsymbol{d}$ | annual inflation rate |
| $\boldsymbol{D_{YSZ}}$ | mean diameter of YSZ particles, m |
| $\boldsymbol{D_{Ni}}$ | mean diameter of Ni particles, m |
| $\boldsymbol{D_{eff}}$ | effective diffusivity, $m^2$ $s^{-1}$ |
| $\boldsymbol{D_{i-j}}$ | binary diffusivity, $m^2$ $s^{-1}$ |
| $\boldsymbol{D_K}$ | Knudsen diffusivity, $m^2$ $s^{-1}$ |
| $\boldsymbol{D_p}$ | pore diameter, m |
| $\boldsymbol{E}$ | open circuit voltage, V |

| | |
|---|---|
| $\boldsymbol{E_{act}}$ | activation energy, kJ mol$^{-1}$ |
| $\boldsymbol{FC_{\mathrm{y}}}$ | fuel costs in year $y$, $ |
| **F** | Faraday's constant, C mol$^{-1}$ |
| $\boldsymbol{I}$ | current, A |
| $\boldsymbol{i}$ | current density, A cm$^{-2}$ |
| $\boldsymbol{i_0}$ | exchange current density, A cm$^{-2}$ |
| $\boldsymbol{i_j}$ | current density in the $j$th time step, A cm$^{-2}$ |
| $\boldsymbol{L}$ | length, m |
| $\boldsymbol{L'}$ | reaction region thickness, m |
| $\boldsymbol{LCOE}$ | Levelized cost of electricity, $ kWh$^{-1}$ |
| $\boldsymbol{LCOEn}$ | Levelized cost of energy, $ kWh$^{-1}$ |

| | |
|---|---|
| $\boldsymbol{n}$ | equivalent electron per mole of reactant, eqiv. mol$^{-1}$ |
| $\boldsymbol{n_{fuel,j}}$ | Fuel consumed in the $j$th time step, mol |
| $\boldsymbol{N}$ | lifetime of the plant, year |
| $\boldsymbol{NO}_{\mathbf{y}}$ | non-fuel operating costs in year $y$, $ |
| $\boldsymbol{P}$ | pressure, Pa |
| $\boldsymbol{P}_{\mathbf{j}}$ | power produced in the $j$th time step, W |
| $\boldsymbol{P}_{\mathbf{y}}$ | total power produced in year $y$, kWh |
| $\boldsymbol{Pr}$ | site occupation probability |
| $\boldsymbol{Q}_{\mathbf{y}}$ | total heat produced in year $y$, kWh |
| $\boldsymbol{r}$ | interest rate |
| **R** | gas constant, J mol$^{-1}$ K$^{-1}$ |

| | |
|---|---|
| $\boldsymbol{T}$ | temperature, K |
| $\boldsymbol{T_0}$ | ambient temperature, K |
| $\boldsymbol{T}$ | temperature, K |
| **TPB** | triple phase boundary |
| $\boldsymbol{V}$ | voltage, V |
| $\boldsymbol{V_j}$ | voltage in the $j$th time step, V |
| $\boldsymbol{\Delta V_s}$ | potential loss due to sulfur poisoning, V |
| $\boldsymbol{W}$ | weighting factor |

**Greek Symbols**

| | |
|---|---|
| $\eta$ | overpotential loss, V |
| $\sigma$ | electrical conductivity, $\Omega^{-1}$ $m^{-1}$ |
| $\varphi$ | porosity |
| $\boldsymbol{\tau}$ | relaxation time |
| $\boldsymbol{\tau_s}$ | surface tortuosity |
| $\Sigma$ | electrical conductivity, $\Omega^{-1}$ $m^{-1}$ |

| | |
|---|---|
| $\gamma_l$ | pre-exponential factor in the electrode, A m$^{-2}$ |
| $\alpha$ | fraction of the reaction heat produced in the anode |

**Subscripts and Superscripts**

| | |
|---|---|
| **ac** | air channel |
| **an** | anode |
| **ca** | cathode |
| **ch** | channel |
| **ele** | electronic |
| fc | fuel channel |
| **ic** | interconnect |
| **j** | time step |
| **k** | anode, cathode, electrolyte |
| **l** | anode, cathode |
| **ohm** | ohmic |
| **act** | activation |
| **con** | concentration |

| | |
|---|---|
| **t** | channel shoulder |
| **x** | x direction |
| **y** | y direction |
| z | z direction |

# Supporting Information

Trajectories of optimal power output, fuel flow rate, and efficiency of SOFCs in base case (Mode 1) are provided in the supporting information.

## 5. Conclusion

In this paper, a detailed degradation-based optimization of a standalone conventional SOFC was performed with the aim of minimizing its levelized cost of electricity by varying the operational conditions, and without modifying the materials or structure of the SOFCs. While the literature contains several economic studies of SOFCs, these studies use simplified models for SOFCs that ignore or underestimate long-term degradation of the cells. To the best of the authors' knowledge, the present study is the first economic optimization to utilize an accurate, detailed prediction model of SOFC performance that accounts for the dominant degradation phenomena in the cells.

The results showed that by altering the operational conditions and modes, the cost of electricity/energy generated by SOFCs varies from very high values to lower costs that are comparable with the LCOEs of traditional power generators. The very high capital costs of noncommercial SOFCs have cast SOFCs as an economically untenable option in the near future. However, the knowledge of long-term performance of SOFCs and effects of operating conditions on their performance degradation obtained through the detailed mathematical model for SOFCs enabled us to identify the optimal sizing and operating conditions at which the use of SOFCs made from existing technology becomes economically comparable to conventional power generators. In fact, this economic investigation allowed us to find the optimal conditions at which conventional SOFCs can be operated economically over a particular period of time, without the need for improving the design or materials of the cells. The results of optimization study revealed that with small reductions in the current densities we can expand the lifetime of SOFCs and lower their LCOE accordingly.

The findings of the sensitivity analysis can be of use to decision makers in different regions, as they can help them determine whether the use of SOFCs is economically viable based on the current NG price and $CO_2$ tax. This study demonstrated that, under optimal conditions, using conventional SOFCs in variable output power-generation mode, can be very economical in regions with low NG prices and low or no $CO_2$ tax.

Finally, this study examined the impact of operational modes on the cost of electricity generated by SOFCs. Although previous studies have mostly run SOFCs in baseload mode, our research shows that the electricity produced in this mode is the most expensive. This is a critical finding, as it indicates that is more economical to avoid operating in constant power mode and to capture the high-quality exhaust heat from the cells and utilize it for the heat demands of the community.

# Acknowledgement

We thank the Natural Sciences and Engineering Research Council of Canada [NSERC CRDPJ 509219-2017] and the Ontario Centre of Excellence [OCE 27851-2018] for the financial support that enabled this research.

## 6. References

(1) Adams II, T. A.; Nease, J.; Tucker, D.; Barton, P. I. Energy Conversion with Solid Oxide Fuel Cell Systems: A Review of Concepts and Outlooks for the Short- and Long-Term. *Industrial and Engineering Chemistry Research* **2013**, *52* (9), 3089–3111. https://doi.org/10.1021/ie300996r.

(2) Zaccaria, V.; Traverso, A.; Tucker, D. A Real-Time Degradation Model for Hardware in the Loop. In *Proceedings of ASME Turbo Expo 2015: Turbine Technical Conference and Exposition GT2015*; 2015; pp 1–8.

(3) Naeini, M.; Lai, H.; Cotton, J. S.; Adams II, T. A. A Mathematical Model for Prediction of Long-Term Degradation Effects in Solid Oxide Fuel Cells. *Industrial and Engineering Chemistry Research* **2021**, *60* (3), 1326–1340.

https://doi.org/10.1021/acs.iecr.0c05302.

(4) Tucker, D.; Abreu-Sepulveda, M.; Harun, N. F. SOFC Lifetime Assessment in Gas Turbine Hybrid Power Systems. *Journal of Fuel Cell Science and Technology* **2014**, *11* (5), 1–7. https://doi.org/10.1115/1.4028158.

(5) Wei, B.; Lü, Z.; Li, S.; Liu, Y.; Liu, K.; Su, W. Thermal and Electrical Properties of New Cathode Material Ba 0.5Sr0.5Co0.8Fe0.2O 3-δ for Solid Oxide Fuel Cells. *Electrochemical and Solid-State Letters* **2005**, *8* (8), 17–21. https://doi.org/10.1149/1.1951232.

(6) Rieu, M.; Sayers, R.; Laguna-Bercero, M. A.; Skinner, S. J.; Lenormand, P.; Ansart, F. Investigation of Graded La2NiO4+δ Cathodes to Improve SOFC Electrochemical Performance. *Journal of The Electrochemical Society* **2010**, *157* (4), B477. https://doi.org/10.1149/1.3298439.

(7) Lee, H. W.; Kim, S. M.; Kim, H.; Jung, H. Y.; Jung, H. G.; Lee, J. H.; Song, H.; Kim, H. R.; Son, J. W. Advanced Planar SOFC Stack with Improved Thermo-Mechanical Reliability and Electrochemical Performance. *Solid State Ionics* **2008**, *179* (27–32), 1454–1458. https://doi.org/10.1016/j.ssi.2008.01.093.

(8) Xu, Y.; Tsumori, F.; Osada, T.; Miura, H. Improvement of Solid Oxide Fuel Cell by Imprinted Micropatterns on Electrolyte. *Micro and Nano Letters* **2013**, *8* (10), 571–574. https://doi.org/10.1049/mnl.2013.0310.

(9) Ding, D.; Li, X.; Lai, S. Y.; Gerdes, K.; Liu, M. Enhancing SOFC Cathode

Performance by Surface Modification through Infiltration. *Energy and Environmental Science* **2014**, *7* (2), 552–575. https://doi.org/10.1039/c3ee42926a.

(10) Hagen, A.; Barfod, R.; Hendriksen, P. V.; Liu, Y. L.; Ramousse, S. Degradation of Anode Supported SOFCs as a Function of Temperature and Current Load. *Journal of the Electrochemical Society* **2006**, *153* (6), 1165–1171. https://doi.org/10.1149/1.2193400.

(11) Gandiglio, M.; Lanzini, A.; Leone, P.; Santarelli, M.; Borchiellini, R. Thermoeconomic Analysis of Large Solid Oxide Fuel Cell Plants : Atmospheric vs . Pressurized Performance. *Energy* **2013**, *55*, 142–155. https://doi.org/10.1016/j.energy.2013.03.059.

(12) Al-Khori, K.; Bicer, Y.; Boulfrad, S.; Koç, M. Techno-Economic and Environmental Assessment of Integrating SOFC with a Conventional Steam and Power System in a Natural Gas Processing Plant. *International Journal of Hydrogen Energy* **2019**, *44* (56), 29604–29617. https://doi.org/10.1016/J.IJHYDENE.2019.07.016.

(13) Al-Khori, K.; Bicer, Y.; Koç, M. Comparative Techno-Economic Assessment of Integrated PV-SOFC and PV-Battery Hybrid System for Natural Gas Processing Plants. *Energy* **2021**, *222*, 119923. https://doi.org/10.1016/J.ENERGY.2021.119923.

(14) Nease, J.; Adams II, T. A. Application of Rolling Horizon Optimization to an Integrated Solid-Oxide Fuel Cell and Compressed Air Energy Storage Plant for

Zero-Emissions Peaking Power under Uncertainty. *Computers and Chemical Engineering* **2014**, *68*, 203–219. https://doi.org/10.1016/j.compchemeng.2014.06.001.

(15) Habibollahzade, A.; Gholamian, E.; Behzadi, A. Multi-Objective Optimization and Comparative Performance Analysis of Hybrid Biomass-Based Solid Oxide Fuel Cell/Solid Oxide Electrolyzer Cell/Gas Turbine Using Different Gasification Agents. *Applied Energy* **2019**, *233–234* (September 2018), 985–1002. https://doi.org/10.1016/j.apenergy.2018.10.075.

(16) Cuneo, A.; Zaccaria, V.; Tucker, D.; Sorce, A. Gas Turbine Size Optimization in a Hybrid System Considering SOFC Degradation. *Applied Energy* **2018**, *230*, 855–864. https://doi.org/10.1016/J.APENERGY.2018.09.027.

(17) Abreu-Sepulveda, M. A.; Harun, N. F.; Hackett, G.; Hagen, A.; Tucker, D. Accelerated Degradation for Hardware in the Loop Simulation of Fuel Cell-Gas Turbine Hybrid System. *Journal of Fuel Cell Science and Technology* **2015**, *12* (2), 1–7. https://doi.org/10.1115/1.4028953.

(18) Parhizkar, T.; Roshandel, R. Long Term Performance Degradation Analysis and Optimization of Anode Supported Solid Oxide Fuel Cell Stacks. *Energy Conversion and Management* **2017**, *133*, 20–30. https://doi.org/10.1016/j.enconman.2016.11.045.

(19) Aguiar, P.; Adjiman, C. S.; Brandon, N. P. Anode-Supported Intermediate Temperature Direct Internal Reforming Solid Oxide Fuel Cell. I: Model-Based

Steady-State Performance. *Journal of Power Sources* **2004**, *138* (1–2), 120–136. https://doi.org/10.1016/j.jpowsour.2004.06.040.

(20) Wen, H.; Ordonez, J. C.; Vargas, J. V. C. Single Solid Oxide Fuel Cell Modeling and Optimization. *Journal of Power Sources* **2011**, *196* (18), 7519–7532. https://doi.org/10.1016/j.jpowsour.2010.10.113.

(21) Parhizkar, T.; Hafeznezami, S. Degradation Based Operational Optimization Model to Improve the Productivity of Energy Systems, Case Study: Solid Oxide Fuel Cell Stacks. *Energy Conversion and Management* **2018**, *158* (August 2017), 81–91. https://doi.org/10.1016/j.enconman.2017.12.045.

(22) Divisek, J.; Wilkenhöner, R.; Volfkovich, Y. Structure Investigations of SOFC Anode Cermets Part I: Porosity Investigations. *Journal of Applied Electrochemistry* **1999**, *29* (2), 153–163. https://doi.org/10.1023/A:1003420815623.

(23) Gao, S.; Li, J.; Lin, Z. Theoretical Model for Surface Diffusion Driven Ni-Particle Agglomeration in Anode of Solid Oxide Fuel Cell. *Journal of Power Sources* **2014**, *255*, 144–150. https://doi.org/10.1016/j.jpowsour.2014.01.033.

(24) Neidhardt, J. P.; Fronczek, D. N.; Jahnke, T.; Danner, T.; Horstmann, B.; Bessler, W. G. A Flexible Framework for Modeling Multiple Solid, Liquid and Gaseous Phases in Batteries and Fuel Cells. *Journal of the Electrochemical Society* **2012**, *159* (9), 1528–1542. https://doi.org/10.1149/2.023209jes.

(25) Hardjo, E. F.; Monder, D. S.; Karan, K. An Effective Property Model for Infiltrated Electrodes in Solid Oxide Fuel Cells. *Journal of the Electrochemical Society* **2014**, *161* (1), 83–93. https://doi.org/10.1149/2.036401jes.

(26) Chen, J.; Bertei, A.; Ruiz-Trejo, E.; Atkinson, A.; Brandon, N. P. Characterization of Degradation in Nickel Impregnated Scandia-Stabilize Zirconia Electrodes during Isothermal Annealing. *Journal of the Electrochemical Society* **2017**, *164* (9), F935–F943. https://doi.org/10.1149/2.0821709jes.

(27) Coors, W. G.; O’Brien, J. R.; White, J. T. Conductivity Degradation of NiO-Containing 8YSZ and 10YSZ Electrolyte during Reduction. *Solid State Ionics* **2009**, *180* (2–3), 246–251. https://doi.org/10.1016/j.ssi.2008.12.004.

(28) Wen, H.; Ordonez, J. C.; Vargas, J. V. C. Single Solid Oxide Fuel Cell Modeling and Optimization. *Journal of Power Sources* **2011**, *196* (18), 7519–7532. https://doi.org/10.1016/j.jpowsour.2010.10.113.

(29) Costamagna, P.; Honegger, K. Modeling of Solid Oxide Heat Exchanger Integrated Stacks and Simulation at High Fuel Utilization. *Journal of the Electrochemical Society* **1998**, *145* (11), 3995–4007. https://doi.org/10.1149/1.1838904.

(30) Yang, S.; Chen, T.; Wang, Y.; Peng, Z.; Wang, W. G. Electrochemical Analysis of an Anode-Supported SOFC. *International Journal of Electrochemical Science* **2013**, *8* (2), 2330–2344.

(31) Fuller, E. N.; Ensley, K.; Giddings, J. C. Diffusion of Halogenated Hydrocarbons

in Helium. The Effect of Structure on Collision Cross Sections. *Journal of Physical Chemistry* **1969**, *73* (11), 3679–3685. https://doi.org/10.1021/j100845a020.

(32) Ryan, E. M.; Xu, W.; Sun, X.; Khaleel, M. A. A Damage Model for Degradation in the Electrodes of Solid Oxide Fuel Cells: Modeling the Effects of Sulfur and Antimony in the Anode. *Journal of Power Sources* **2012**, *210*, 233–242. https://doi.org/10.1016/j.jpowsour.2012.02.091.

(33) Hagen, A.; Johnson, G. B.; Hjalmarsson, P. Electrochemical Evaluation of Sulfur Poisoning in a Methane-Fuelled Solid Oxide Fuel Cell: Effect of Current Density and Sulfur Concentration. *Journal of Power Sources* **2014**, *272,* 776–785. https://doi.org/10.1016/j.jpowsour.2014.08.125.

(34) Papurello, D.; Lanzini, A.; Fiorilli, S.; Smeacetto, F.; Singh, R.; Santarelli, M. Sulfur Poisoning in Ni-Anode Solid Oxide Fuel Cells (SOFCs): Deactivation in Single Cells and a Stack. *Chemical Engineering Journal* **2016**, *283*, 1224–1233. https://doi.org/10.1016/j.cej.2015.08.091.

(35) Wang, Q.; Wei, H. H.; Xu, Q. A Solid Oxide Fuel Cell (SOFC)-Based Biogas-from-Waste Generation System for Residential Buildings in China: A Feasibility Study. *Sustainability (Switzerland)* **2018**, *10* (7), 1–9. https://doi.org/10.3390/su10072395.

(36) Hauch, A.; Küngas, R.; Blennow, P.; Hansen, A. B.; Hansen, J. B.; Mathiesen, B. V.; Mogensen, M. B. Recent Advances in Solid Oxide Cell Technology for Electrolysis. *Science* **2020**, *370* (6513). https://doi.org/10.1126/science.aba6118.

(37) Adams II, T. A.; Barton, P. I. High-Efficiency Power Production from Natural Gas with Carbon Capture. *Journal of Power Sources* **2010**, *195* (7), 1971–1983. https://doi.org/10.1016/J.JPOWSOUR.2009.10.046.

(38) Stamatis, A.; Vinni, C.; Bakalis, D.; Tzorbatzoglou, F.; Tsiakaras, P. Exergy Analysis of an Intermediate Temperature Solid Oxide Fuel Cell-Gas Turbine Hybrid System Fed with Ethanol. *Energies* **2012**, *5* (11), 4268–4287. https://doi.org/10.3390/en5114268.

(39) Udomsilp, D.; Rechberger, J.; Neubauer, R.; Bischof, C.; Thaler, F.; Schafbauer, W.; Menzler, N. H.; de Haart, L. G. J.; Nenning, A.; Opitz, A. K.; Guillon, O.; Bram, M. Metal-Supported Solid Oxide Fuel Cells with Exceptionally High Power Density for Range Extender Systems. *Cell Reports Physical Science* **2020**, *1* (6), 100072. https://doi.org/10.1016/J.XCRP.2020.100072.

(40) D. Nishijima, H. Ishikawa, M. Shibata, H. Uematsu, H. Sumi Y. Okuyama, Y. Todo, D. Komatsu, S. I. and K. F. R. Development of SOFC Stack at NGK Spark Plug Co., Ltd. *The Electrochemical Society* **2009**, *25* (2), 91–96. https://doi.org/10.1149/1.3205513.

(41) Shakouri, O.; Ahmadi, M. H.; Gord, M. F. Thermodynamic Assessment and Performance Optimization of Solid Oxide Fuel Cell-Stirling Heat Engine-Reverse Osmosis Desalination. *International Journal of Low-Carbon Technologies* **2021**, *16* (2), 417–428. https://doi.org/10.1093/ijlct/ctaa073.

(42) U.S. Department of Energy. Manufacturing Cost Analysis of 100 and 250 KW

Fuel Cell Systems for Primary Power and Combined Heat and Power Applications. **2016**.

(43) Mehr, A. S.; Mahmoudi, S. M. S.; Yari, M.; Chitsaz, A. Thermodynamic and Exergoeconomic Analysis of Biogas Fed Solid Oxide Fuel Cell Power Plants Emphasizing on Anode and Cathode Recycling : A Comparative Study. *Energy Conversion and Management* **2015**, *105*, 596–606. https://doi.org/10.1016/j.enconman.2015.07.085.

(44) Rillo, E.; Gandiglio, M.; Lanzini, A.; Bobba, S.; Santarelli, M.; Blengini, G. Life Cycle Assessment (LCA) of Biogas-Fed Solid Oxide Fuel Cell (SOFC) Plant. *Energy* **2017**, *126* (2017), 585–602. https://doi.org/10.1016/j.energy.2017.03.041.

(45) Kim, K.; Von Spakovsky, M. R.; Wang, M.; Nelson, D. J. Dynamic Optimization under Uncertainty of the Synthesis/Design and Operation/Control of a Proton Exchange Membrane Fuel Cell System. *Journal of Power Sources* **2012**, *205*, 252–263. https://doi.org/10.1016/j.jpowsour.2011.11.014.

(46) Zaccaria, V.; Tucker, D.; Traverso, A. Gas Turbine Advanced Power Systems to Improve Solid Oxide Fuel Cell Economic Viability. *Journal of the Global Power and Propulsion Society* **2017**, *1*, U96IED. https://doi.org/10.22261/u96ied.

(47) Nease, J.; Adams II, T. A. Life Cycle Analyses of Bulk-Scale Solid Oxide Fuel Cell Power Plants and Comparisons to the Natural Gas Combined Cycle. *Canadian Journal of Chemical Engineering* **2015**, *93* (8), 1349–1363. https://doi.org/10.1002/cjce.22207.

(48) Provenzano, M. Analysis of the Energy Consumption in the Hotel Sector and Feasibility Study for the Installation of SOFC-Based Cogeneration Systems, Politecnico di Torino, 2021.

(49) Lai, H.; Harun, N. F.; Tucker, D.; Adams II, T. A. Design and Eco-Technoeconomic Analyses of SOFC/GT Hybrid Systems Accounting for Long-Term Degradation Effects. *International Journal of Hydrogen Energy* **2021**, *46* (7), 5612–5629. https://doi.org/10.1016/j.ijhydene.2020.11.032.

## 7. Supporting information

Supporting information can be found at https://pubs.acs.org/doi/10.1021/acs.iecr.1c03146.

# CHAPTER 4: DYNAMIC LIFE CYCLE ASSESSMENT OF SOLID OXIDE FUEL CELL SYSTEM CONSIDERING LONG-TERM DEGRADATION EFFECTS

The content of this chapter is a published reprint of the following peer-reviewed publication:

Naeini, M., Cotton, J.S. and Adams II, T.A.. Dynamic life cycle assessment of solid oxide fuel cell system considering long-term degradation effects. *Energy Conversion and Management* **2022**, *255*, p.115336.

## Abstract

In this work, we conduct a detailed cradle-to-product lifecycle analysis in order to quantify the environmental impact of generating electricity using a conventional natural gas-fueled solid oxide fuel cell (SOFC). In contrast to previous studies, we account for SOFC degradation using a model previously developed by the authors to simulate deterioration in performance of SOFC over operating time. Midpoint environmental impacts were quantified using the ReCiPe 2016 and TRACI 2.1 US-Canada 2008 characterization methodologies in SimaPro. The resulting global warming potential was higher than those reported for SOFCs, which are underestimated because they neglect degradation. The results were compared with the environmental burdens associated with power generation using two conventional combined heat and power systems (i.e., gas turbines and internal combustion engines of various capacities), showing that even when accounting for long-term SOFC degradation impacts, the environmental performance of SOFCs is superior. This is true even though the analysis used a conservative approach in which SOFC system waste heat was not utilized. This means that if waste heat was utilized, the next environmental impact per unit energy produced would be even lower.

## Keywords

Lifecycle assessment, Environmental impacts, SOFC, Performance degradation

## 1. Introduction

The global demand for energy is anticipated to increase by as much as 25% by 2050.[1] This poses a major challenge, as our ever-increasing need for energy has accelerated global warming and led to numerous other harmful environmental outcomes. Indeed, the consumption of fossil fuels for energy generation is the single greatest contributor to global greenhouse gas (GHG) emissions and is responsible for a variety of other harmful environmental outcomes such as smog and acid rain formation. Concerns about global warming and its consequences have led many countries to adopt economic incentive policies to reduce GHG emissions, such as carbon taxes.[2] However, despite the motivation of these countries to reduce fossil fuel consumption and to switch to sustainable sources of energy, global natural gas (NG) use has continued to rise, increasing at an annual rate of 2.6% from 2013 to 2018.[3]

Thus, there is an urgent need to improve the efficiency of NG-based electricity generation, and to work towards replacing conventional NG power generation systems with more environmentally friendly technologies. Among the many NG-based power generation units, solid oxide fuel cells (SOFCs) are a promising technology for power-only and a particularly promising technology for combined heat and power (CHP) generation (e.g., gas turbines and internal combustion engines), as they offer high efficiency, lower noise levels, reduced environmental impact, and a large amount of exhaust heat generated via exothermic electrochemical reactions.[4,5] Unlike internal combustion engines and gas turbines, SOFC performance is not size dependent; therefore, small- and large-scale SOFCs can provide the same performance with an equally low environmental burden.[6] This is one of the key strengths that makes SOFCs suitable for various applications ranging from residential-scale power generators to large-scale ones.[7] However, the environmental performance of SOFCs can be affected by cell degradation, which occurs as a result of the cell's operating conditions over long periods of time.

The literature contains a number of research studies focusing on the lifecycle environmental impacts of using different materials and configurations in manufacturing SOFCs and their corresponding balance of plant (BoP) items, as well as analyses of the SOFC system's operation phase. For instance, Bicer and Khalid quantified the lifecycle impacts of supplying SOFCs with various fuel sources, including hydrogen, natural gas, ammonia, and methanol.[8] In addition, they also investigated how different fuel production methodologies affect life-cycle environmental impacts of the system. In their study, Bicer and Khalid assumed that the SOFC would be operated for 5 years, and that it would generate a constant power density of 0.4 $W/cm^2$ during this time.[8] In a separate study, Gandiglio et al. examined the environmental impact of operation of a 174 $KW_e$ SOFC module fed with biogas from a wastewater treatment plant, as well as the impacts associated with its construction and its BoP equipment.[9,10] The examined module was fabricated using three 58 $KW_e$ SOFCs, and was run for more than 5600 hours. Strazza et al. performed a full lifecycle assessment on the use of a small-scale (20 $KW_e$) methanol-powered SOFC as an auxiliary power unit for marine applications, and compared their results to those for existing ship engines.[11] Nease and Adams conducted a cradle-to-grave lifecycle study on the use of a NG-powered SOFC for electricity generation at community scale (~10,000 residents), and compared their results to those obtained for conventional natural gas combined cycle (NGCC) power plants.[12] In their study, Nease and Adams assumed that the SOFC would have a lifetime of 10 years at full load operation.[12] Their results also showed that the addition of carbon capture and sequestration technology can decrease the direct $CO_2$ emissions from SOFCs by 100%, compared to a 90% reduction in NGCC emissions. Total lifecycle emissions (direct plus indirect) were reduced by about 82% for SOFCs and 68% for NGCC. However, these did not consider the negative impacts of degradation.

Degradation is one of the major drawbacks to using SOFCs, as it can negatively impact performance and environmental sustainability over long periods of time. Degradation of the fuel cells makes it challenging to simulate performance of SOFC over long operational times, or to find the required capacity of an SOFC for a specific application/community. To the best of the authors' knowledge, this issue has not been properly addressed in any previous SOFC system economic and lifecycle assessments.[5,8,12,13] Moreover, prior lifecycle assessments of SOFCs have commonly quantified their environmental impacts in baseload power generation mode, where the fuel cells are expected to generate a constant power load during their operational lifetime. Although it is technically viable to operate SOFCs as baseload power generation units, the findings of our previous research study indicate that it is not economically advantageous because operating in constant power significantly increases degradation rates.[14]

In this work, we conduct a detailed cradle-to-product lifecycle analysis (LCA) on planar anode-supported SOFCs fueled with NG and fabricated using conventional materials and configurations in order to quantify the impacts associated with manufacturing SOFC and BoP items, upstream of the NG supply chain, and system maintenance and operation. We then compare our results—particularly impacts related to operation of SOFC, and upstream of the NG supply chain—to those of two commercially available CHP systems that do not suffer from significant short-term materials degradation: NG-supplied internal combustion engines and gas turbines. SOFC degradation and its effect on the environmental performance of the system was assessed using a mathematical prediction model that we developed in a previous work for the SOFC performance loss that occurs due to six dominant degradation reactions during long-term operation. The mathematical model used in this work was described in greater detail in [15], and used to determine the economically optimal operating trajectories in [14], and so are described only briefly here. The mathematical model describes how six different individual degradation mechanisms namely Ni coarsening, Ni oxidation, changes in anode pore size, degradation of electrical conductivities of anode and electrolyte, and sulfur poisoning, impact overall system degradation. The impact of each individual mechanism was either a model previously published in the literature or developed in the prior work from openly available experimental data. These degradation mechanisms are incorporated into a larger model that includes thermodynamic equations to describe the system as a whole. The system degradation models are influenced by factors such as instantaneous current density, temperature, fuel pressure, and other factors. Thus, the model as a whole can be used to simulate the degradation of a system over many years as these factors are allowed to change slowly over time.

This model has been described in greater detail in our previous work.[15] Moreover, instead of operating the SOFCs in this study in baseload power generation mode, we utilize a general operational mode where voltage, current density, and power output can vary over time. This approach was selected, as the results of our prior work indicate that it is more economical than running fuel cells in constant power output mode. This work can be considered to be a dynamic LCA (DLCA) according to the definitions of Beloin-Saint-Pierre at al. and Sohn et al.[16,17] In the following sections, we present the LCA methodology, the boundary regions of the lifecycle stages, the functional units, and the calculation strategies that were used in this DLCA.

## 2. Methodology

### 2.1.Goal, scope, and functional unit

The goal of this analysis was to assess and evaluate the environmental impacts of electricity generation using NG-fueled SOFCs, and to compare the results with those of existing NG-fueled internal combustion engines and gas turbines. All input and output flows, including materials, energy, and lifecycle emissions, were considered in the scope of this study.

The functional unit for the product system was chosen to be 1 kWh of the produced electricity (alternating current (AC), grid quality, at plant). This means that an AC/DC inverter is included in the analysis.

Inventory data related to the fabrication of the SOFC and its BoP items and annual system maintenance data were collected from various sources.[13,18–20] In a previous study, Rio et al. collected data relating to the construction of a conventional, planar SOFC with an 81 $cm^2$

active membrane area from the manufacturer.[13] Notably, they ignored degradation of SOFCs and assumed that the SOFC can be operated at a constant voltage and current density of 0.8 V and 0.5 A/cm$^2$, respectively; thus, such an SOFC would be able to deliver a constant power density of 0.4 W/cm$^2$ during its lifetime. Using these assumptions, Rio et al. converted the units from per cm$^2$ of active cellular membrane area to per kW installed capacity, and then scaled the inventory data for a 250-kW SOFC. However, this unit basis is both very case specific and optimistic, as SOFCs in real functional systems generate different power densities depending on their operating conditions and needs of the system. Moreover, due to cellular degradation, it is not very practical to maintain constant voltage, current density, and power density in full load operation. As noted above, we account for SOFC degradation, and we study a general SOFC operational mode wherein fuel cell operation (i.e. current density, voltage, and power output) can vary over time. To this end, we used Rillo et al.'s assumptions to calculate the inventory data per cm$^2$ of active cellular membrane area, with the results leading to the selection of 1 cm$^2$ of membrane area as the unit basis for the equipment manufacturing and maintenance data. This unit basis is more general and allows investigators to perform LCA studies on SOFCs with different power densities, operating in partial or full load and at various operational modes.

1 $MJ_{HHV}$[1] was selected as the functional unit for the processed NG, which was supplied to the SOFCs, internal combustion engines, and gas turbines.

---

[1] Higher Heating Value

### 2.2.Boundaries

The system boundaries for the current LCA include: NG production and processing; the construction and assembly of the SOFC and its associated BoP equipment; system maintenance; and SOFC operation. As this is a cradle-to-product analysis, it does not consider the "end of life" of the system. Fig. 1 illustrates the lifecycle boundary of the entire system with final product of 1 kWh electricity.

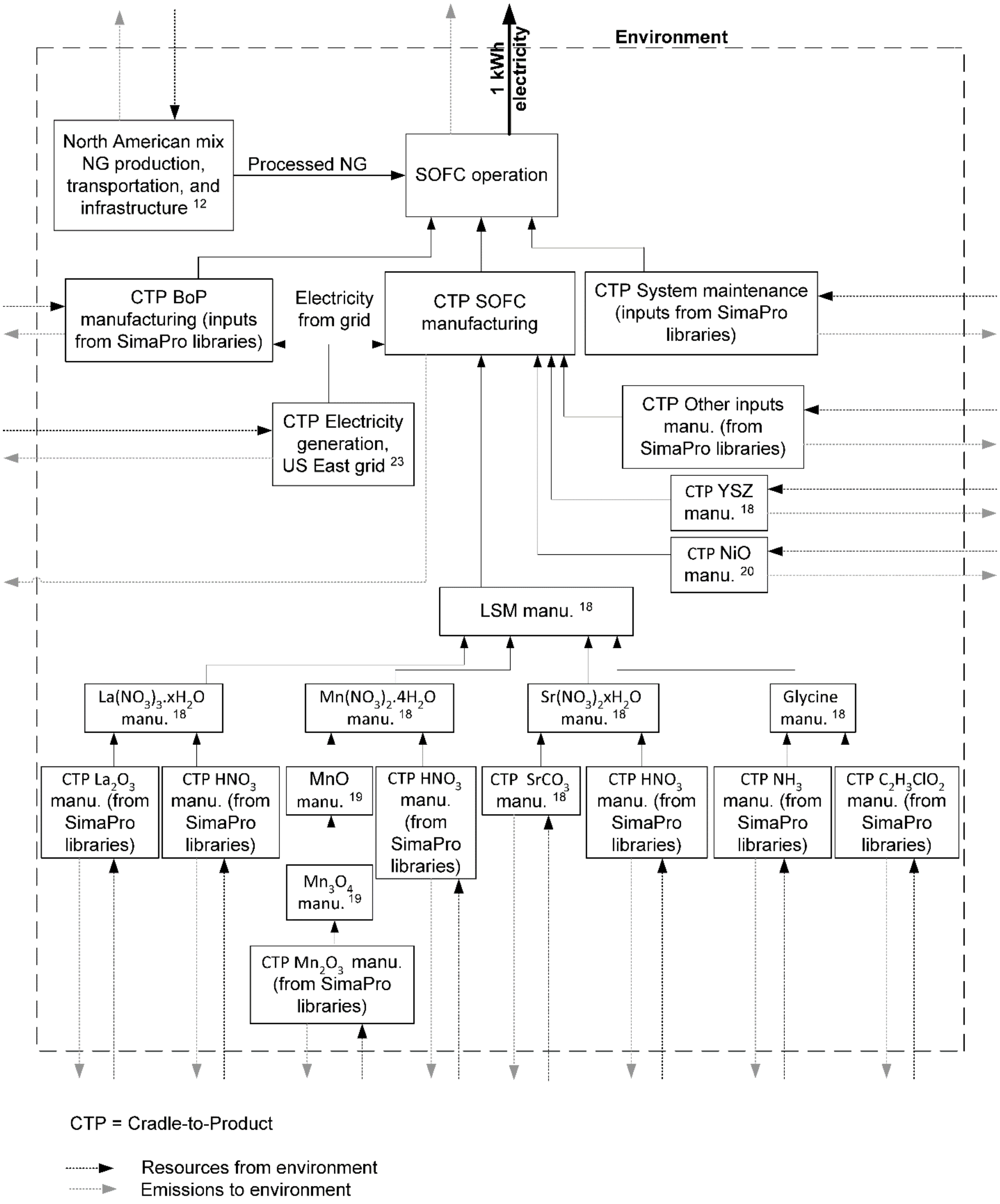

Fig. 1. System boundary for electricity generation using an NG-fueled SOFC.

Fig. 2 depicts the boundary region of the NG supply chain, which starts with the extraction of NG from the wells and ends with delivery of 1 $MJ_{HHV}$ processed NG to the power generation system. All resource inflows and emissions related to the extraction, processing, and distribution of NG are taken into account. More detail regarding the composition and characteristics of NG are provided in the following section.

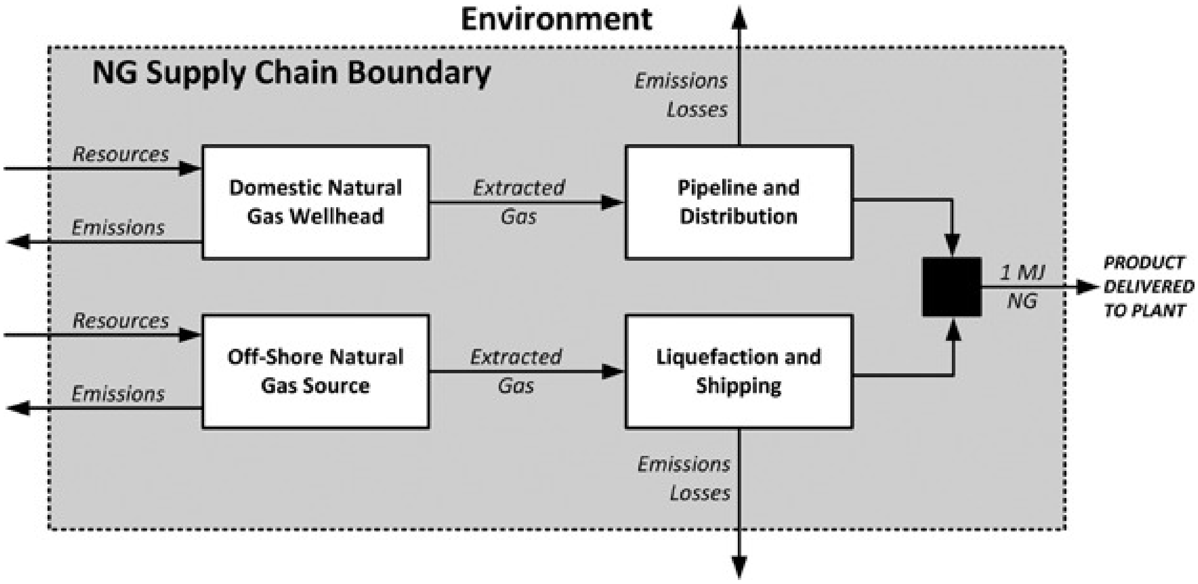

Fig. 2. NG supply chain boundary region. Published with permission from [12].

Processed NG is sent to the SOFC for the purpose of electricity generation. Fig. 3 shows the operation stage boundary of an SOFC using NG for power production, along with all of the input and output flows.

In the SOFC operation section, cleaned, preheated NG and preheated air are fed into the anode and cathode, respectively, with electrical energy being produced as a result of an exothermic electrochemical reaction between the fuel and the oxygen in the air. The anode exhaust is then sent to the afterburner, where the remaining fuel is combusted with air to avoid emitting unspent fuel to the atmosphere, which generates more waste heat.

### 2.3.Allocations

Although the waste heat generated by SOFC systems is in large measure and of high quality, its value depends on how it is used in a larger system on a case-by-case basis. To preserve generality, we do not consider heat to be a by-product in this study. Thus, the heat in the combustion exhaust is assumed to be a waste product; emitted into the atmosphere after leaving the preheaters. In other words, in order to provide general results that can be compared to the impacts of electricity production from other power generation technologies, we take a conservative approach in this study and assign all of the environmental impacts to electrical energy.

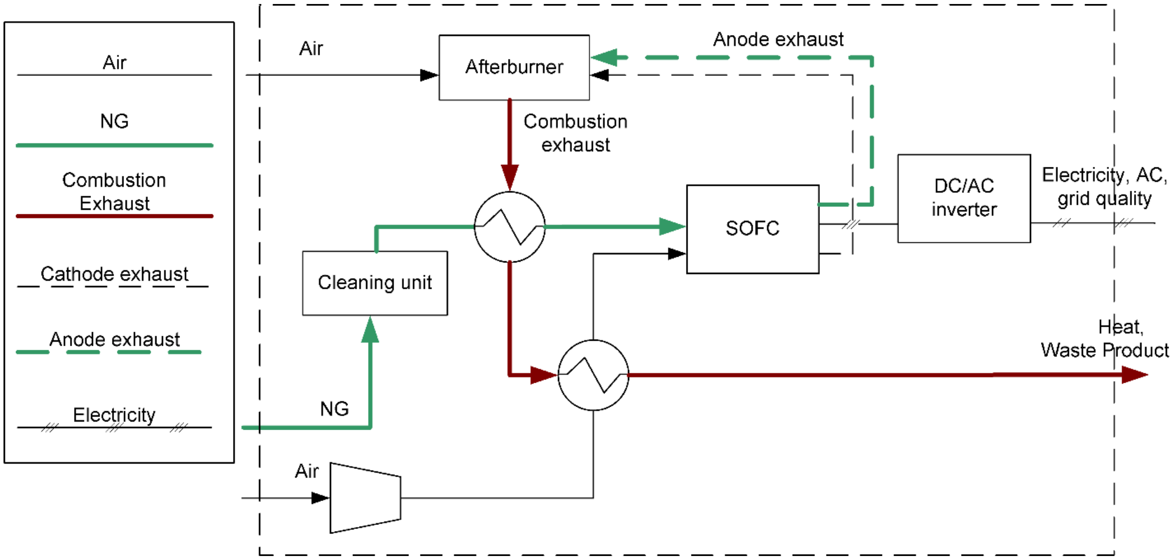

Fig. 3. The boundary of operation stage of SOFC.

### 2.4.Lifecycle inventories and assumptions

The lifecycle inventory data for the sub-processes and necessary assumptions are given below.

#### *2.4.1. SOFC and BoP fabrication*

- The SOFC and BoP manufacturing and maintenance inventory data are given in Tables 1-3.
- The inventories are for an anode-supported SOFC fabricated using conventional materials and conventional structure for all the components. The SOFC in question has a rectangular, planar design.[13]
- As noted earlier, the lifecycle inventory data for the fabrication and assembly of the SOFCs and BoP items, as well as annual system maintenance data, were taken from

the literature and converted from a per kW basis to a per $cm^2$ of active cellular membrane area basis.[13,18–20]

- 100% of the solvents used in the fabrication of the SOFCs—such as, those used for tape casting, drying, and sintering—were reported as being emitted into the atmosphere.[8,12]
- The inventories for the BoP items include the auxiliary components required for a general SOFC-based CHP system (e.g., inverters, piping, heat exchangers, etc.), as well as the energy consumed in assembling the entire system.[8,13]
- It is assumed that the SOFC interconnect and casing, piping, and high-temperature BoP components, such as heat exchangers, are all made of steel.
- It is assumed that the fuel cleaning step (contact with iron oxide) prior to entering the SOFC anode results in more than 90% sulfur removal, so $SO_2$ content in the exhaust is negligible.[13,21,22] See section 2.3.2 for related maintenance.
- The cradle-to-product AC/DC inverter lifecycle inventory data was taken from the Ecoinvent database.[23] It was assumed that there is a 4% loss in power when DC power is converted to AC.
- The BoP components are assumed to have a lifetime of 20 years. The project lifetime is also 20 years. Disposal/decommissioning is not in the scope of the analysis.
- The electricity used in the fabrication of the SOFC and BoP equipment is drawn from the eastern grid in the United States. The electricity in the eastern U.S. grid is generated using a variety of energy sources such as coal, fuel oil, NG, nuclear,

hydropower, and some non-traditional power sources. The electricity data was taken from the U.S. lifecycle inventory (USLCI) database.[24]

### *2.4.2. System maintenance*

- The inventory data for annual system maintenance include replacing the adsorbent material (iron oxide) in the cleaning unit, as well as some of the steel components of the system. It is assumed that 1% of the steel components in the BoP items should be replaced each year due to malfunctioning or incidental damages.

### *2.4.3. NG supply chain*

- The NG supply chain's upstream effects (including extraction, processing, and distribution stages) and the operation of the SOFC using cleaned, processed NG are taken into consideration.
- The NG mixture is assumed to be the average composition of NG consumed in the United States. The characteristics of this NG mixture are provided in Table 4.[25]

  The NG supply chain data used in the current work was taken from Nease and Adams.[12] On average NG mixtures in the U.S. are composed of various onshore and offshore sources. Nease and Adams drew upon data in the literature to identify the various NG sources in the U.S., and to determine their lifecycle environmental effects on the final NG product.[12] For more detail regarding NG sources breakdowns and their associated emissions please refer to the literature.[12] These emissions include the assumption that only 87% of the natural gas extracted from the wells is recovered with the remainder being either flared or emitted to the atmosphere as fugitive emissions.[12]

### 2.4.4. SOFC operation

- The processed NG is cleaned before being supplied to the anode of the SOFC. Therefore, the SOFC's operation stage is presumed to have negligible emissions for the pollutants $SO_x$, $NO_x$, and $N_2O$.[12,13]
- The data for the operation of the SOFC were taken from our prior studies.[14] For more detail, please refer to the Calculation Strategy section.
- It is assumed that the plant has a lifetime of full 20 years, and that the lifetime of the SOFCs is shorter. In this work, we consider two different cases: one in which the SOFCs are replaced every 5 years, and one in which the SOFCs are replaced every 10 years. It should be noted that the replacement cells have the same features and size as the old ones.

Table 1. Inventory data for the construction of 1 $cm^2$ of SOFC active membrane area.

| Resource flows | Amount | Unit |
|---|---|---|
| Nickel oxide (NiO) | 2.40E-04 | kg |
| Yttrium stabilized zirconium (YSZ) | 1.07E-04 | kg |
| Lanthanum strontium manganite (LSM) | 9.92E-07 | kg |
| Ethanol (solvent) | 4.48E-05 | kg |
| Methyl ethyl ketone (solvent) | 8.64E-05 | kg |
| Benzyl alcohol (solvent) | 1.32E-05 | kg |

| | | |
|---|---|---|
| Carbon black | 7.36E-07 | kg |
| Starch (binder) | 1.70E-05 | kg |
| Ethylene glycol (binder) | 1.44E-05 | kg |
| Stainless steel (interconnect) | 4.00E-03 | kg |
| Stainless steel (casing) | 1.60E-03 | kg |
| Electricity (US East grid) | 8.80E-02 | kWh |
| **Emissions to air** | **Amount** | **Unit** |
| Carbon dioxide | 1.73E-04 | kg |
| Ethanol | 4.48E-05 | kg |
| Methyl ethyl ketone | 8.64E-05 | kg |
| Benzyl alcohol | 1.32E-05 | kg |

Table 2. Inventory data for BoP items construction and system assembly per 1 $cm^2$ of SOFC active membrane area.

| **Resource flows** | **Amount** | **Unit** |
|---|---|---|
| Reinforcing steel | 1.95E-02 | kg |
| Stainless steel | 5.76E-03 | kg |
| Sheet rolling, steel | 1.95E-02 | kg |
| Sheet rolling, stainless steel | 5.76E-03 | kg |
| Iron oxide | 4.88E-03 | kg |
| AC/DC inverter | 1.60E-04 | p[2] |
| NG, burned in industrial furnace | 1.95E-04 | kg |
| Electricity (US East grid) | 1.92E-02 | kWh |

---

[2] 1 Piece of 500-KW inverter

Table 3. Inventory data for annual system maintenance per 1 $cm^2$ of SOFC active membrane area.

| Resource flows | Amount | Unit |
|---|---|---|
| Reinforcing steel | 1.95E-04 | kg |
| Stainless steel | 5.76E-05 | kg |
| Iron oxide | 9.76E-03 | kg |

Table 4. Composition of NG.

| Component | %Vol |
|---|---|
| $CH_4$ | 93.1 |
| $C_2H_6$ | 3.2 |
| $C_3H_8$ | 0.7 |
| $C_4H_{10}$ | 0.4 |
| $CO_2$ | 1.0 |
| $N_2$ | 1.6 |
| HHV(MJ/kg) | 52.58 |
| HHV(MJ/scm) | 38.46 |

### 2.5.Impact assessment methodology

LCA is a holistic technique that is commonly used to assess and quantify the overall environmental impact that a product causes over its whole lifecycle. The standard LCA methodology framework is defined in ISO 14040 and 14044.[26,27] For the LCA in this study, we employed ReCiPe 2016 v1.03 midpoint (H) method as well as the Tool for Reduction and Assessment of Chemicals and other environmental Impacts (TRACI 2.1) v1.05 US-Canada 2008 midpoint method using SimaPro v9.0 software. These methodologies analyze lifecycle environmental impacts in relation to several categories, which are selected based on the features of the project. Tables 5 and 6 show the ReCiPe and TRACI impact categories that were selected in this work to represent the environmental effects of power generation using NG-fueled SOFCs at the midpoint level.

Table 5. ReCiPe midpoint impact categories analyzed in this study.

| **Impact Category** | **Abbreviation** | **Unit** |
|---|---|---|
| Global warming | GW | kg $CO_2$-Eq |
| Fine particulate matter formation | PMF | kg PM2.5-Eq* |
| Terrestrial acidification | TA | kg $SO_2$-Eq |
| Fossil resource scarcity | FS | kg oil-Eq |
| Water depletion | WD | $m^3$ |
| Ozone formation, Terrestrial ecosystems | OF | kg NOx Eq |

* Particulate matter with diameters of less than 2.5 micrometers.

Table 6. TRACI midpoint impact categories selected for this study.

| **Impact Category** | **Abbreviation** | **Unit** |
|---|---|---|

| | | |
|---|---|---|
| Global warming | GW | kg $CO_2$-Eq |
| Respiratory effects | RE | kg PM2.5-Eq |
| Acidification potential | AP | kg $SO_2$-Eq |
| Fossil fuel depletion | FFD | MJ surplus |

### 2.6. **Calculation strategy**

In our prior work, we conducted a techno-economic analysis (TEA) considering degradation of SOFCs and we determined the global optimal dynamic trajectories of voltage, current density, and power output over X-year period where SOFC was scheduled to be replaced every X years, where X varied from 1 to 14 years.[14]. It was assumed that no catastrophic failure occurs within X years operation. We examined various replacement times because there is still no consensus on when catastrophic failure will occur in a cell under specific operating conditions. For instance, a recent study has shown that a solid oxide electrolyser cell (SOEC) constructed with the same materials and configuration as a traditional SOFC can be operated for over 14 years at conditions similar to those of fuel cells before catastrophic failure will occur.[28] Given the lack of information on how different operating conditions affect the catastrophic failure time of SOFCs, we solved the economic problem for various replacement times. The results of TEA will allow decision makers to select the proper capacity and operating conditions based on the estimated lifetime of SOFCs as provided by the manufacturer.

In the current work, we reused the economic optimal trajectories for X = 5- and X = 10-year replacement plans as two representative case studies (Fig. 4) to calculate the emissions from the SOFCs' operation phase via stoichiometric reactions. It should be noted that the economic optimal trajectories obtained are independent of size, because none of the components in TEA have costs which scale non-linearly with size. The TEA results are valid for anything above 100 kW, since we used the costs for a 100-kW stack and used a conservative assumption that costs change linearly with size since scale-up involves simple increasing the number of stacks as opposed to increasing the size of the cells themselves. Thus, the costs would be lower in reality due to the economics of scale.

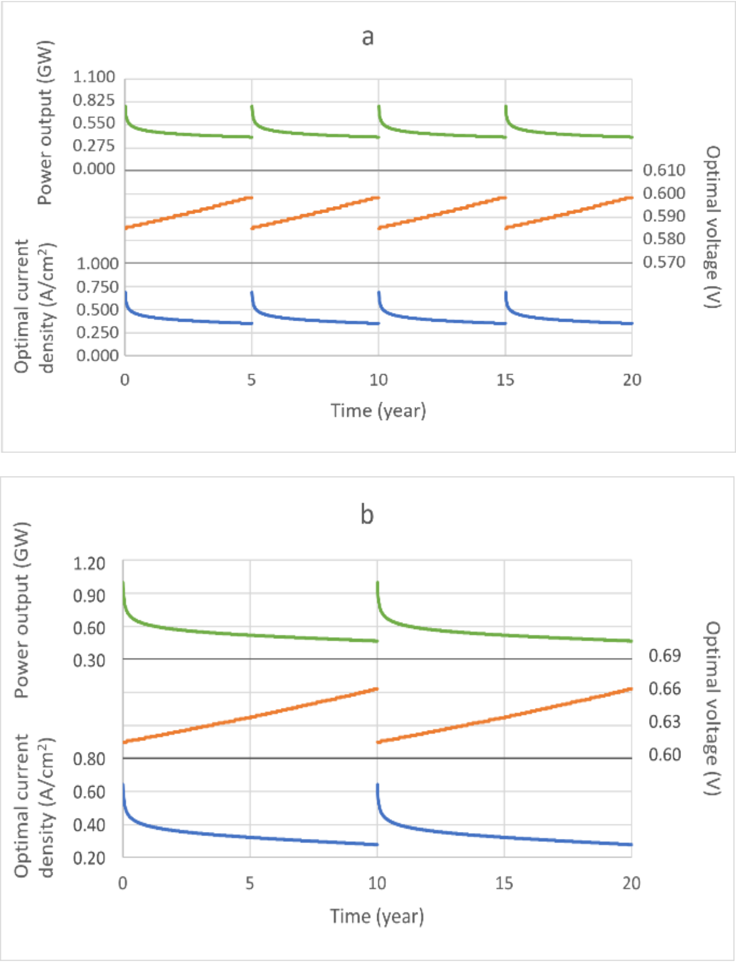

Fig. 4. Optimal trajectories of current density, voltage, and power output for SOFCs with a) 5-year replacement plan and b) 10-year replacement plan.[14]

## 3. Internal combustion engines

Internal combustion engines are a globally commercialized technology with a wide range of applications in transportation, construction, and power generation, among others.[29,30] NG-fueled internal combustion engines have been broadly used for power production or heat and electricity production in CHP systems. In engine-based CHP configurations, recovered heat is usually utilized to heat water or produce low-pressure steam. The capacity of these engines varies from 10 kW to nearly 10 MW for CHP applications, with electrical efficiencies ranging from about 31%$_{HHV}$ for small engines to 41.9%$_{HHV}$ for the large ones.[29–31] However, untreated exhaust from NG-fueled combustion engines contains significant amounts of air pollutants, including $NO_x$, CO, and VOC (amounts can reach as high as 99.8 g of $NO_x$ and CO, and 68 g of VOC per kWh of delivered electricity). Since these gases can be very harmful to the environment and human health, they should therefore be considered in the environmental analysis. Notably, engines can emit different amounts of harmful pollutants depending on their model, capacity, operating conditions, and even their manufacturer.[30] Fortunately, engine exhaust can be treated with selective catalytic reduction (SCR) to reduce $NO_x$ emissions, and with oxidation catalysts to reduce CO and VOC.[30] Table 7 shows the pollutants emitted by NG-fueled internal combustion engines with capacities of 633, 1141, and 9341 kW, that are used in this LCA for comparison purposes, before and after exhaust treatment with SCR and oxidation catalyst. These figures are largely estimates based on manufacturer guarantees, and were acquired from a report published by the United States Department of Energy (U.S. DOE).[30]

Table 7. Natural gas internal combustion engine pollutant emissions before and after exhaust treatment.[30]

| Electrical capacity (kW) | 633 | 1141 | 9341 |
|---|---|---|---|
| Electrical efficiency (%$_{HHV}$) | 34.5 | 37.6 | 41.9 |
| **Untreated exhaust** | | | |
| $NO_x$ (gr/kWh) | <1.34 | <1.34 | <2.01 |
| CO (gr/kWh) | <2.01 | <2.01 | <2.01 |

| | | | |
|---|---|---|---|
| VOC (gr/kWh) | <1.34 | <1.34 | <1.34 |
| **Treated exhaust** | | | |
| $NO_x$ (gr/kWh) | 0.07 | 0.07 | 0.11 |
| CO (gr/kWh) | 0.11 | 0.11 | 0.11 |
| VOC (gr/kWh) | 0.07 | 0.07 | 0.07 |

Marques et al. recently conducted an LCA on a small-scale trigeneration system that uses NG.[31] The internal combustion engine in their micro-trigeneration system had an electrical efficiency of $32\%_{HHV}$, and emitted 0.22, 0.67, and 0.09 g of $NO_x$, CO, and VOC, respectively, per 1 kWh of power produced.

We used the emissions data provided by the U.S. DOE[30] and Marques et al.[30,31] to compare the emissions produced from operating different sized internal combustion engines with SOFCs. To ensure consistency, we used the same upstream NG supply chain data for all of the engines as the SOFCs. Due to the lack of detailed and reliable inventory data related to the manufacturing of internal combustion engines and their associated BoP components for CHP applications, we could not include manufacturing in the LCA of the engines, but for comparative purposes against SOFCs, this makes it a conservative estimate. Even though a number of sources provided manufacturing inventories for this type of engine, the data were usually provided by automobile manufacturers for engines used in specific automobiles, and usually did not specify the electrical output of the engine, or place it in the context of stationary natural gas generation.[23,32] Marques et al. also provided the inventory data for fabrication of a small-scale engine in a micro-trigeneration system, but did not specify the size of the engine.[31]

The data in the U.S. DOE report is for engines that run on U.S. NG mixtures; as such, these engines can be properly compared with the SOFCs in this work. Conversely, the source of the NG used in Marques et al.'s work was not provided. Therefore, we computed the emissions from the same engine (32%$_{HHV}$ electrical efficiency) supplied with an average U.S. NG mixture, assuming that 100% of the gas is combusted in the engine. To this end, we first determined the amount of NG required by this engine to produce 1 kWh of power under the given efficiency. Next, we calculated the emissions from the combustion of the U.S. NG mixture using the stoichiometric combustion reactions. See the Results and Discussion section for a full discussion of the results.

## 4. Gas turbines

Gas turbines are another mature, low-cost technology that has been widely used for power generation and CHP applications. The high-temperature heat recovered from the gas turbines is usually utilized for steam production or, in industrial facilities, for heating or drying.[29,31] Similar to internal combustion engines, the electrical efficiency of gas turbines varies depending on their size, with significantly lower efficiency being observed in partial-load operation compared to full-load operation.[29] The capacities of commercial gas turbines for CHP applications vary from 1 MW to 40 MW, and their electrical efficiencies range from 22%$_{HHV}$ to 37%$_{HHV}$.[29] Different gas turbine models use different combustion systems, and hence emit different amounts of $NO_x$ and CO gases. The emissions from NG-supplied turbines and SOFCs were compared using the emissions data provided by the U.S. DOE for commercial gas turbines of various sizes.[29] In this LCA we used emissions data for 1, 5, 10, 25, and 40 MW gas turbines for comparison purposes. Note that the turbines in the U.S. DOE report ran on a U.S. NG mixture, and used a commercially available combustion system known as dry low $NO_x$ (DLN). Please see [29] for more information.

Table 8. US Natural Gas combustion turbine pollutant emissions.[29]

| Electrical capacity (MW) | 1 | 5 | 10 | 25 | 40 |
|---|---|---|---|---|---|
| Electrical efficiency ($\%_{HHV}$) | 22 | 27 | 29 | 34 | 37 |
| $NO_x$ (gr/kWh) | 1.09 | 0.5 | 0.45 | 0.41 | 0.36 |
| CO (gr/kWh) | 0.32 | 0.27 | 0.23 | 0.18 | 0.18 |

## 5. Results and discussion

All results presented in this section are for the production of 1 kWh of electricity.

### 5.1.SOFCs

Tables 9 and 10 show midpoint characterization results of SOFCs with 5- and 10-year replacement plans obtained by ReCiPe and TRACI methodologies, respectively. The TRACI methodology is an environmental indicator that is commonly used in the United States. Previous studies have primarily used the ReCiPe method to investigate the midpoint impacts of SOFCs; to the best of our knowledge, this is the first TRACI characterization of NG-fueled SOFCs that can be used as a basis of comparison for future LCA studies. To compute these numbers (Tables 9 and 10) with the aid of SimaPro, the life cycle inventories (e.g. mass and energy flows to/from the environment) of each of the cradle-to-product systems considered were taken and their environmental impacts were computed using the ReCiPe and TRACI methods. As mentioned in previous sections, the underlying inventories come from a combination of experimental data and predicted simulation data, depending on what information were available for each step of the process life cycle. It should be noted that the cumulative information over the plant's lifetime was divided by the total electricity produced over the lifetime, and so the tables are normalized to the basis flow of 1 kWh of electricity produced. These tables should be interpreted under normal ISO 14040/14044 Life Cycle Assessment understandings and are presented in standard fashion.

As can be seen, increasing the operational lifetime of the SOFCs and replacing the fuel cells less often led to a reduction in the total environmental impacts of the SOFCs in all of the investigated midpoint categories. Extending the lifetime of the cells by altering the operating conditions not only substantially decreased the impacts of SOFC fabrication and maintenance, but it also improved electrical performance (electrical efficiency increased from $41.3\%_{HHV}$ to $43.7\%_{HHV}$), which in turn reduced fuel consumption, and hence, emissions. It should also be noted that SOFCs with 5- and 10-year replacement plan generate 0.97 and 0.86 kWh heat, respectively per 1 kWh electricity produced. This is the net heat released from the SOFC system (generated from exothermic electrochemical reactions and combustion of unreacted fuel in afterburner) after preheating air and NG and partial reforming of NG in the cells. As it was mentioned above in order to provide reproducible results, we considered heat as a waste product and we did not assign environmental impacts to it. However, using the provided information and lifecycle inventory results of this study, one can quantify lifecycle environmental impacts of different SOFC systems that harvest and utilize waste heat for various purposes. Even though a large amount of steel is used in BoP items, since they have a lifetime of 20 years, the fabrication of BoP items does not have significant impact on the overall lifecycle global warming potential. Fuel cell operation accounts for the highest proportion of this impact category (~97%), which is due to the NG consumption required for power generation. This finding is consistent with Bicer and Khalid's[8] and Nease and Adams'[12] LCAs, wherein the use of NG for SOFC operations was found to be responsible for 94% and 97% of the global warming impact category, respectively.

The release of $SO_2$, $NH_3$, $NO_x$, or primary fine particles (PM2.5) into the atmosphere leads to formation of harmful particulate matters. $SO_2$, $NH_3$, and $NO_x$ react with other gasses in the air and produce secondary aerosols, inhaling which can cause serious health issues and even lead to premature death in people with chronic disease.[8,33] Therefore, even though $SO_x$ and $NO_x$ emissions from SOFCs operation are assumed to be negligible, particulate matter formation indicator is considered as one of the crucial environmental impact indicators that should be investigated in this LCA to show the level of PM2.5 released throughout SOFCs lifecycle.

The results of this study are in good agreement with the literature. For instance, SOFCs with 5- and 10-year replacement plans in this LCA respectively emit 0.597 and 0.561 kg $CO_2$ Eq. over their entire life cycle per kWh, which are of the same orders of magnitude as Bicer and Khalid's [8] (0.41 kg $CO_2$ Eq.) and Strazza et al.'s results [11,34] (0.47 and 0.48 kg

$CO_2$ Eq.). There are a number of potential reasons for why we found higher global warming impacts. First, previous LCA studies have ignored performance degradation of fuel cells, which may result in the underestimation of fuel consumption, and hence, $CO_2$ Eq. emissions. Second, the NG used in these studies had different origins (average European NG mixture, EU-28 Mix in Bicer and Khalid[8]; average Norwegian NG in Strazza et al. [11]; and average U.S. NG mixture in the current LCA), and therefore different upstream impacts, carbon contents, and associated emissions. In addition, unlike the previous LCA studies that commonly divided environmental impacts between the different products of multifunctional systems, we assign all of the impacts to the delivered electrical energy, which results in more conservative and higher values.

The findings related to the other impact categories are also in alignment with the literature. For instance, 0.179 and 0.159 g PM2.5 Eq. were obtained in the particulate matter formation category for SOFCs with 5- and 10-year replacement plans in this LCA, which is comparable to the values calculated by Bicer and Khalid (0.116 g PM10 Eq.) and Rillo et al. (0.155 g PM10 Eq.).[8,13] Our findings indicated that majority of the fine particles released into the atmosphere during SOFC lifecycle are from BoP manufacturing stage due to the large amount of steel being used in BoP items, followed by upstream of NG supply chain, SOFC manufacturing, and maintenance stages. The terrestrial acidification impacts (0.504 and 0.464 g $SO_2$ Eq.) obtained in this LCA were also comparable to those reported by Rillo et al. (0.498 g $SO_2$ Eq.) and Strazza et al. (0.363 g $SO_2$ Eq.).[13,34] Terrestrial acidification is mainly caused by steel production processes during BoP manufacturing stage, and upstream of NG supply chain is the second contributor to this impact category, followed by SOFC fabrication, and maintenance stages. The slight differences in the results could be due to several differences in these LCA studies, such as differing assumptions, using NG from distinct origins, or running SOFCs in different modes under various operating conditions and for different periods of time.

Additionally, Rillo et al. showed that the fossil resource scarcity impact was 0.179 kg oil Eq. throughout the whole lifecycle per 1 kWh power generation from NG-fueled SOFCs, with 97% being consumed in the operation phase. In this study, calculations indicated that SOFCs with 5- and 10-year replacement plans would respectively consume 0.157 and 0.147 kg oil Eq. over their full lifecycle, and that the operation phase with nearly 97% contribution will be the dominant stage in the fossil resource depletion impact category.

Table 9. ReCiPe midpoint impact characterization results for 1kWh electricity production using SOFCs (5- and 10-year replacement plan) lifecycle.

| Impact category | Unit | BoP manufacture | SOFC manufacture | SOFC maintenance | SOFC operation | **Total** |
|---|---|---|---|---|---|---|
| | | **SOFC-5 year replacement plan** | | | | |
| Global warming | kg CO2 eq | 3.84E-03 | 9.94E-03 | 6.91E-03 | 5.76E-01 | 5.97E-01 |
| Stratospheric ozone depletion | kg CFC11 eq | 1.95E-09 | 1.35E-09 | 2.93E-09 | 8.31E-09 | 1.45E-08 |

| | | | | | | |
|---|---|---|---|---|---|---|
| Ozone formation, Human health | kg NOx eq | 1.21E-05 | 2.90E-05 | 3.17E-05 | 4.20E-04 | 4.93E-04 |
| Fine particulate matter formation | kg PM2.5 eq | 6.16E-05 | 3.50E-05 | 3.03E-05 | 5.25E-05 | 1.79E-04 |
| Ozone formation, Terrestrial ecosystems | kg NOx eq | 1.25E-05 | 3.09E-05 | 3.23E-05 | 4.23E-04 | 4.99E-04 |
| Terrestrial acidification | kg SO2 eq | 1.96E-04 | 1.00E-04 | 3.29E-05 | 1.76E-04 | 5.04E-04 |
| Terrestrial ecotoxicity | kg 1,4-DCB | 7.40E-02 | 2.18E-01 | 5.54E-02 | 1.64E-04 | 3.47E-01 |
| Freshwater ecotoxicity | kg 1,4-DCB | 6.63E-04 | 1.47E-04 | 1.22E-03 | 9.33E-11 | 2.03E-03 |
| Marine ecotoxicity | kg 1,4-DCB | 9.48E-04 | 2.70E-04 | 1.78E-03 | 2.18E-08 | 3.00E-03 |
| Human carcinogenic toxicity | kg 1,4-DCB | 2.12E-03 | 9.28E-04 | 4.96E-02 | 3.29E-08 | 5.27E-02 |

| | | | | | | |
|---|---|---|---|---|---|---|
| Human non-carcinogenic toxicity | kg 1,4-DCB | 2.04E-02 | 3.84E-03 | 8.26E-03 | 3.52E-05 | 3.26E-02 |
| Fossil resource scarcity | kg oil eq | 9.37E-04 | 2.79E-03 | 1.74E-03 | 0.00E+00 | 5.46E-03 |
| Water consumption | m$^3$ | 3.20E-05 | 1.89E-05 | 5.00E-05 | 2.61E-02 | 2.62E-02 |
| **SOFC-10 year replacement plan** | | | | | | |
| Global warming | kg CO2 eq | 4.27E-03 | 5.56E-03 | 4.84E-03 | 5.46E-01 | 5.61E-01 |
| Stratospheric ozone depletion | kg CFC11 eq | 2.16E-09 | 7.55E-10 | 2.03E-09 | 7.86E-09 | 1.28E-08 |
| Ozone formation, Human health | kg NOx eq | 1.35E-05 | 1.62E-05 | 2.19E-05 | 3.98E-04 | 4.49E-04 |
| Fine particulate matter formation | kg PM2.5 eq | 6.88E-05 | 1.96E-05 | 2.09E-05 | 4.97E-05 | 1.59E-04 |
| Ozone formation, Terrestrial ecosystems | kg NOx eq | 1.39E-05 | 1.73E-05 | 2.23E-05 | 4.00E-04 | 4.54E-04 |

| | | | | | | |
|---|---|---|---|---|---|---|
| Terrestrial acidification | kg SO2 eq | 2.19E-04 | 5.60E-05 | 2.28E-05 | 1.66E-04 | 4.64E-04 |
| Terrestrial ecotoxicity | kg 1,4-DCB | 8.15E-02 | 1.22E-01 | 3.90E-02 | 1.55E-04 | 2.42E-01 |
| Freshwater ecotoxicity | kg 1,4-DCB | 7.32E-04 | 8.21E-05 | 8.37E-04 | 8.82E-11 | 1.65E-03 |
| Marine ecotoxicity | kg 1,4-DCB | 1.05E-03 | 1.51E-04 | 1.22E-03 | 2.07E-08 | 2.42E-03 |
| Human carcinogenic toxicity | kg 1,4-DCB | 2.37E-03 | 5.19E-04 | 3.37E-02 | 3.11E-08 | 3.66E-02 |
| Human non-carcinogenic toxicity | kg 1,4-DCB | 2.25E-02 | 2.15E-03 | 5.79E-03 | 3.33E-05 | 3.05E-02 |
| Fossil resource scarcity | kg oil eq | 1.04E-03 | 1.56E-03 | 1.21E-03 | 1.12E+00 | 1.13E+00 |
| Water consumption | $m^3$ | 3.55E-05 | 1.06E-05 | 3.51E-05 | 2.47E-02 | 2.48E-02 |

Table 10. TRACI midpoint impact characterization results for 1kWh electricity production using SOFCs (5- and 10-year replacement plan) lifecycle.

| Impact category | Unit | BoP manufacture | SOFC manufacture | SOFC maintenance | SOFC operation | Total |
|---|---|---|---|---|---|---|
| | | **SOFC-5 year replacement plan** | | | | |

| | | | | | | |
|---|---|---|---|---|---|---|
| Ozone depletion | kg CFC-11 eq | 2.65E-10 | 1.65E-10 | 5.94E-10 | 0.00E+00 | 1.02E-09 |
| Global warming | kg CO2 eq | 3.74E-03 | 9.75E-03 | 6.73E-03 | 5.47E-01 | 5.68E-01 |
| Smog | kg O3 eq | 2.87E-04 | 7.03E-04 | 7.64E-04 | 1.04E-02 | 1.21E-02 |
| Acidification | kg SO2 eq | 2.00E-04 | 1.11E-04 | 4.42E-05 | 3.17E-04 | 6.72E-04 |
| Eutrophication | kg N eq | 3.07E-05 | 9.73E-06 | 3.26E-05 | 1.87E-05 | 9.17E-05 |
| Carcinogenics | CTUh | 3.21E-09 | 1.86E-09 | 7.07E-08 | 5.48E-13 | 7.58E-08 |
| Non carcinogenics | CTUh | 6.17E-09 | 3.40E-09 | 6.66E-09 | 7.42E-11 | 1.63E-08 |
| Respiratory effects | kg PM2.5 eq | 1.77E-05 | 1.02E-05 | 2.49E-05 | 3.19E-06 | 5.60E-05 |
| Ecotoxicity | CTUe | 1.89E-01 | 6.43E-02 | 1.02E+00 | 1.14E-06 | 1.27E+00 |
| Fossil fuel depletion | MJ surplus | 3.52E-03 | 6.17E-03 | 6.19E-03 | 1.23E+00 | 1.25E+00 |
| | | **SOFC-10 year replacement plan** | | | | |
| Ozone depletion | kg CFC-11 eq | 2.91E-10 | 4.12E-10 | 9.25E-11 | 0.00E+00 | 7.96E-10 |
| Global warming | kg CO2 eq | 4.16E-03 | 4.71E-03 | 5.45E-03 | 5.18E-01 | 5.33E-01 |
| Smog | kg O3 eq | 3.20E-04 | 5.27E-04 | 3.93E-04 | 9.80E-03 | 1.10E-02 |

| | | | | | | |
|---|---|---|---|---|---|---|
| Acidification | kg SO2 eq | 2.24E-04 | 3.07E-05 | 6.18E-05 | 3.00E-04 | 6.16E-04 |
| Eutrophication | kg N eq | 3.39E-05 | 2.27E-05 | 5.44E-06 | 1.77E-05 | 7.97E-05 |
| Carcinogenics | CTUh | 3.58E-09 | 4.81E-08 | 1.04E-09 | 5.18E-13 | 5.27E-08 |
| Non carcinogenics | CTUh | 6.80E-09 | 4.62E-09 | 1.90E-09 | 7.02E-11 | 1.34E-08 |
| Respiratory effects | kg PM2.5 eq | 1.97E-05 | 1.72E-05 | 5.73E-06 | 3.02E-06 | 4.57E-05 |
| Ecotoxicity | CTUe | 2.09E-01 | 6.93E-01 | 3.60E-02 | 1.08E-06 | 9.38E-01 |
| Fossil fuel depletion | MJ surplus | 3.90E-03 | 4.30E-03 | 3.45E-03 | 1.16E+00 | 1.17E+00 |

These findings illustrate how it is possible to substantially improve the performance of SOFCs, extend their lifetime, and reduce their environmental burdens by simply altering the operating conditions, leaving the materials and structure of the cells untouched.

Lifecycle inventories can be found in the supplementary documentation.

### 5.2. Comparison of SOFCs, internal combustion engines, and gas turbines

Next, we compared the environmental performance of SOFCs to that of various sizes of commercially available internal combustion engines; from a micro engine to a 9341-kW engine; and that of existing gas turbines with capacities ranging from 1 to 40 MW. Fig. 5 a compares the ReCiPe midpoint impacts of SOFCs operation to those of internal combustion engine exhaust before and after treatment and gas turbine exhaust. Fig. 5b compares the impacts of these technologies at the midpoint level using the TRACI methodology. Categories representing the effects of $CO_2$ emissions, acidifying substances, fine particles released into the air, and fossil fuel depletion were selected for this analysis.

Prior to treating the exhaust, internal combustion engines had substantially higher acidification, particulate matter, ozone formation, and respiratory effects, which was due to the large amounts of $NO_x$, CO, and VOC produced by the existing combustion technologies used in these engines. These emissions and their associated environmental burdens can be markedly reduced by using the exhaust treatment technologies discussed in Section 4. $NO_x$, $SO_x$, CO, and VOC are the main environmental concerns with internal combustion engines. Exhaust treatment technologies such as three-way catalysts (TWC), SCR, and oxidation catalysts that have been widely used in engines reduce these emissions to the atmosphere. These numbers (Table 7) consider the use of SCR and an oxidation catalyst to reduce $NO_x$, CO, and VOC emissions. These catalysts work selectively to lower the mentioned emissions. Therefore, the exhaust treatment does not reduce $CO_2$ emissions, and hence has no effect whatsoever on the global warming potential.

As was explained in Sections 3 and 4, the performance of these engines and turbines changes depending on their capacity, with larger systems offering higher electrical efficiency, and hence, lower emissions and environmental burden. The effect of system capacity on environmental burdens can be clearly seen in Fig. 5. Although the largest commercially available internal combustion engine can provide comparable performance to SOFCs with respect to global warming potential, fossil resource scarcity, and water depletion, the results indicate that their performance is inferior in terms of the impacts caused by $NO_x$, CO, and VOC emissions—even after engine exhaust treatment.

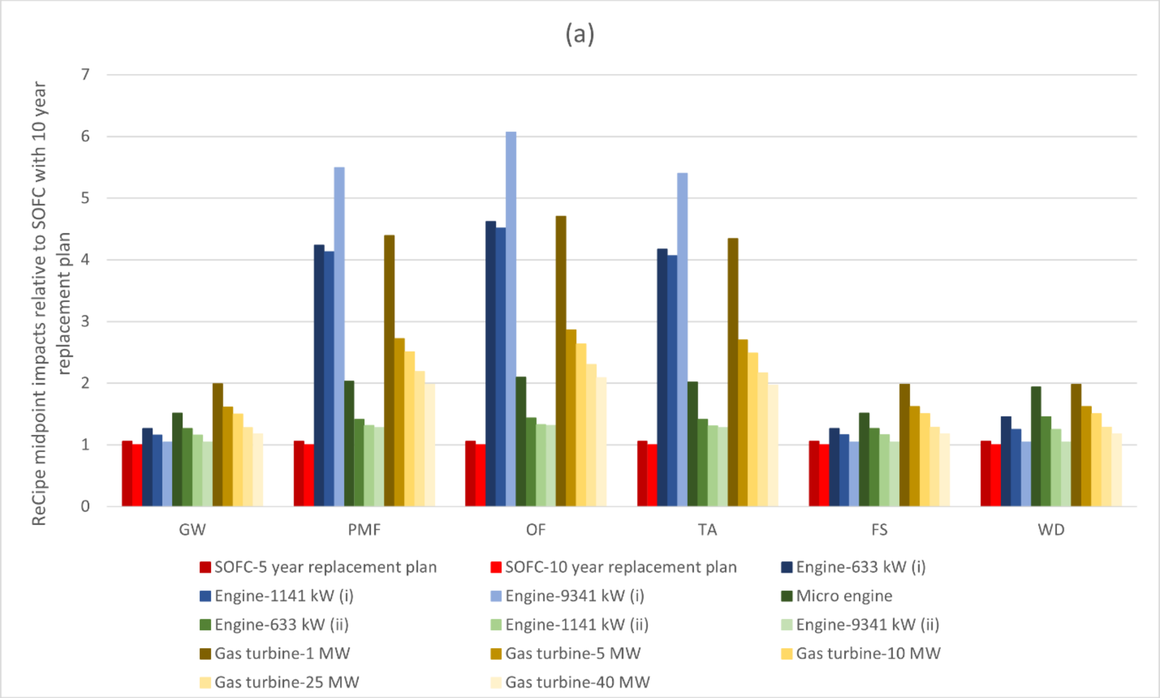

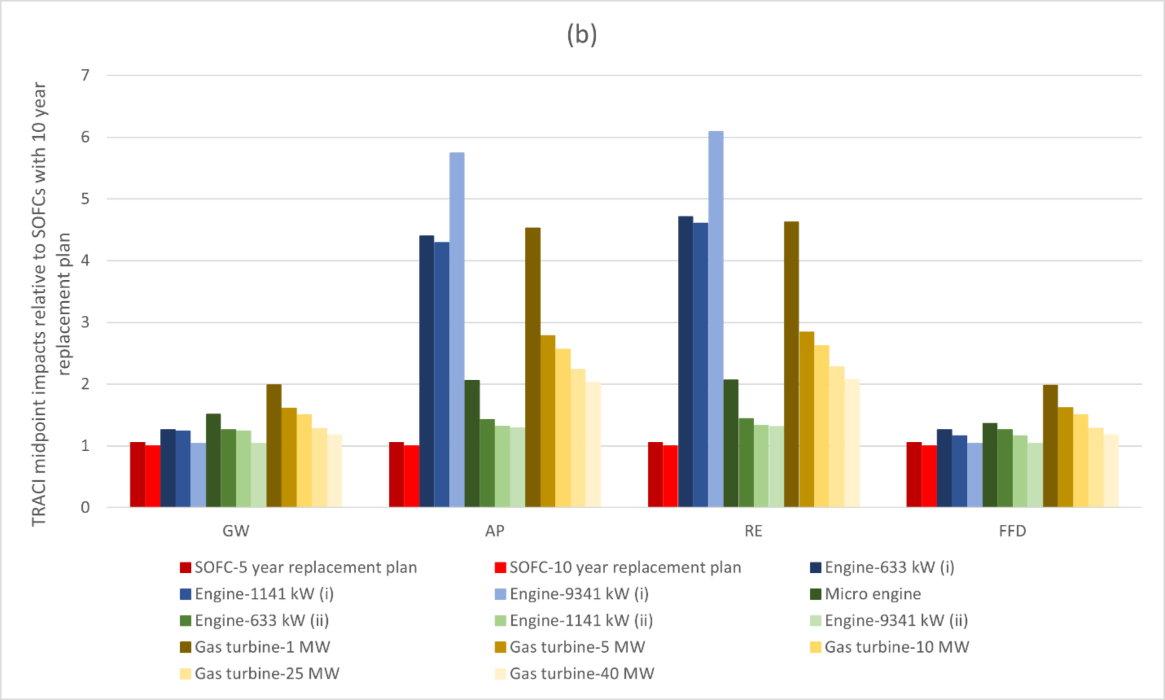

Fig. 5. Selected normalized a) ReCiPe and b) TRACI midpoint impact comparisons for SOFCs, internal combustion engines: i) prior to engine exhaust treatment, and ii) after engine exhaust treatment, and gas turbines (for the list of abbreviations used in this figure please refer to Tables 5 and 6.).

The smallest internal combustion engines reportedly have an electrical efficiency of approximately 32% $_{\text{HHV}}$. As shown in Fig. 5, SOFCs provided superior environmental sustainability compared to this type of engine in all studied environmental categories for small-scale usage.

It should be noted that the engines emissions data are very optimistic as they are based on the estimates for the engines exploiting advanced combustors for proper combustion of the fuel with the best emission reduction technologies. Even though engines do not degrade quickly, misfire or incomplete combustion can occur during their operating lifetime due to several factors. This can influence their environmental burdens in large extent.

Gas turbines have lower electrical efficiency comparing to the other investigated technologies, which results in greater amounts of fuel being consumed for power generation especially in smaller scales, and thus, higher levels of $CO_2$ emissions, and higher impacts on fossil resource scarcity. Additionally, the commercial combustion technologies in existing gas turbines emit high amounts of $NO_x$ and CO into the atmosphere. Combustion systems capable of providing adequate efficiency with low pollutant emission levels for gas turbines are either not technically confirmed, or not commercially available at present.[29] The catalysts for these emissions are usually composed of brittle materials that experience catastrophic failure under the operating conditions of gas turbines. Moreover, it is not yet technically feasible to simultaneously lower $NO_x$ and CO emissions from the gas turbine's combustors, as doing so results in diminished efficiency.[29] The findings of both the ReCiPe and TRACI methodologies revealed that, due to the high concentrations of $NO_x$ and CO emitted from the existing combustors, gas turbines have substantially greater levels of acidification, respiratory effects, fine particles, and ozone formation impacts compared to SOFCs, and the engines with exhaust treatment technologies. Even though gas turbines have been commonly used for CHP applications, considering the environmental factors they are not an attractive technology as our results show that they suffer from poor environmental performance relative to the other options, especially in residential and small-scale applications. Therefore, with increasing concerns about environmental issues and rise in carbon tax using this technology, in spite of its low capital cost, will not be profitable and hence it should be replaced with more environmentally friendly technologies such as SOFCs. Even though SOFCs degrade over time, and thus have limited lifetimes, they generally had smaller environmental burdens in the investigated impact categories at the midpoint level.

As shown above, existing internal combustion engines have maximum capacity of approximately 9 MW for CHP applications, but SOFCs do not have technical limits on the size, and they can scale well to gas turbines size ranges, without the need for technical changes. SOFCs power output can be simply increased by adding more stacks with the same operation and environmental performance.

It should also be noted that in this LCA since we are studying small-scaled CHP systems (less than 40 MW), we do not include carbon capture and sequestration (CCS). However, our past work has shown that incorporating CCS would drastically lower global warming potential for SOFC systems.[12]

In this study, we focused on electricity generation only, and as noted previously, ignored the heat component to be conservative. However, future work should examine and value this heat component more closely (e.g. in a combined heat-and-power system). The results from this work can be directly applied to future studies because the heat is quantified and known, but simply not used for allocations as a part of a larger system. Similarly, many SOFC systems are best hybridized by including a gas turbine that combusts the SOFC off-gases, which can create some interesting long-term system benefits. In our prior work, we have examined SOFC heat recovery (using combined cycles) as well as SOFC/GT hybrids under the consideration of degradation.[35] However, the degradation models used in that work considered degradation in a lumped fashion, and does not have the same degree of nuance as the models used in this work which considers six mechanisms independently. Therefore, we will revisit these systems using the newer degradation model to better understand their impacts.

## 6. Conclusion

While this study produced higher GHG emissions compared to similar studies in the literature, this result was due to the fact that we accounted for SOFC degradation and allocated all lifecycle emissions to the generated electricity rather than splitting them between the electricity and exhaust heat. SOFCs mainly produce GHG emissions during the operation stage as a result of using natural gas to generate power. Our findings illustrated that extending lifetime of SOFCs by varying the operating conditions effectively reduces their environmental impact. In fact, both our prior and present works show that, by adjusting the operating conditions, one can run SOFCs more efficiently, improve their lifetime, and lower their environmental burdens.

In this paper we also compared SOFCs with small- to large-scale existing gas turbines and internal combustion engines to determine which technology is the most environmentally sustainable technology. The results of this comparison showed that SOFCs provided substantially better performance compared to existing commercial gas turbines in all investigated impact categories. The findings also showed that the largest available internal combustion engines can compete with SOFCs in terms of GHG emissions, but have higher acidifying and fine particulate matter impacts, even with exhaust treatment technologies. This is an important finding, as it proves the environmental superiority of SOFCs over traditional CHP systems, even when accounting for fuel cell degradation.

# Acknowledgement

We acknowledge the financial support of the Natural Sciences and Engineering Research Council of Canada [NSERC CRDPJ 509219-2017] and the Ontario Centre of Excellence [OCE 27851-2018].

## 7. Supplementary Information

A Microsoft Excel file containing the cradle-to-product life cycle inventories and the SimaPro files used in this work can be freely downloaded from the Living Archive for Process Systems Engineering at http://PSEcommunity.org/LAPSE:2021.0808.

## 8. References

(1) van Ruijven, B. J.; De Cian, E.; Sue Wing, I. Amplification of Future Energy Demand Growth Due to Climate Change. *Nature Communications* **2019**, *10* (1), 1–12. https://doi.org/10.1038/s41467-019-10399-3.

(2) Liu, L.; Huang, C. Z.; Huang, G.; Baetz, B.; Pittendrigh, S. M. How a Carbon Tax Will Affect an Emission-Intensive Economy: A Case Study of the Province of Saskatchewan, Canada. *Energy* **2018**, *159*, 817–826. https://doi.org/10.1016/j.energy.2018.06.163.

(3) Jackson, R. B.; Friedlingstein, P.; Andrew, R. M.; Canadell, J. G.; Le Quéré, C.; Peters, G. P. Persistent Fossil Fuel Growth Threatens the Paris Agreement and Planetary Health. *Environmental Research Letters* **2019**, *14* (12). https://doi.org/10.1088/1748-9326/ab57b3.

(4) Zaccaria, V.; Tucker, D.; Traverso, A. A Distributed Real-Time Model of Degradation in a Solid Oxide Fuel Cell, Part II: Analysis of Fuel Cell Performance and Potential Failures. *Journal of Power Sources* **2016**, *327*, 736–742. https://doi.org/10.1016/j.jpowsour.2016.01.027.

(5) Jing, R.; Wang, M.; Wang, W.; Brandon, N.; Li, N.; Chen, J.; Zhao, Y. Economic and Environmental Multi-Optimal Design and Dispatch of Solid Oxide Fuel Cell Based CCHP System. *Energy Conversion and Management* **2017**, *154*, 365–379. https://doi.org/10.1016/j.enconman.2017.11.035.

(6) U.S. Department of Energy. *Fuel Cell Handbook*, Seventh Ed.; 2004.

(7) Bharadwaj, S. R.; Varma, S.; Wani, B. N. Electroceramics for Fuel Cells, Batteries and Sensors. In *Functional Materials*; Elsevier Inc., 2012; pp 639–674. https://doi.org/10.1016/B978-0-12-385142-0.00016-7.

(8) Bicer, Y.; Khalid, F. Life Cycle Environmental Impact Comparison of Solid Oxide Fuel Cells Fueled by Natural Gas, Hydrogen, Ammonia and Methanol for Combined Heat and Power Generation. *International Journal of Hydrogen Energy* **2020**, *45* (5), 3670–3685. https://doi.org/10.1016/j.ijhydene.2018.11.122.

(9) Gandiglio, M.; De Sario, F.; Lanzini, A.; Bobba, S.; Santarelli, M.; Blengini, G. A. Life Cycle Assessment of a Biogas-Fed Solid Oxide Fuel Cell (SOFC) Integrated in Awastewater Treatment Plant. *Energies* **2019**, *12* (9). https://doi.org/10.3390/en12091611.

(10) Gandiglio, M.; Lanzini, A.; Santarelli, M.; Acri, M.; Hakala, T.; Rautanen, M. Results from an Industrial Size Biogas-Fed SOFC Plant (the DEMOSOFC Project). *International Journal of Hydrogen Energy* **2020**, *45* (8), 5449–5464. https://doi.org/10.1016/j.ijhydene.2019.08.022.

(11) Strazza, C.; Del Borghi, A.; Costamagna, P.; Traverso, A.; Santin, M. Comparative LCA of Methanol-Fuelled SOFCs as Auxiliary Power Systems on-Board Ships. *Applied Energy* **2010**, *87* (5), 1670–1678. https://doi.org/10.1016/j.apenergy.2009.10.012.

(12) Nease, J.; Adams II, T. A. Life Cycle Analyses of Bulk-Scale Solid Oxide Fuel Cell Power Plants and Comparisons to the Natural Gas Combined Cycle. *Canadian Journal of Chemical Engineering* **2015**, *93* (8), 1349–1363. https://doi.org/10.1002/cjce.22207.

(13) Rillo, E.; Gandiglio, M.; Lanzini, A.; Bobba, S.; Santarelli, M.; Blengini, G. Life

Cycle Assessment (LCA) of Biogas-Fed Solid Oxide Fuel Cell (SOFC) Plant. *Energy* **2017**, *126* (2017), 585–602. https://doi.org/10.1016/j.energy.2017.03.041.

(14) Naeini, M.; Cotton, J. S.; Adams II, T. A. Economically Optimal Sizing and Operation Strategy for Solid Oxide Fuel Cells to Effectively Manage Long-Term Degradation. *Industrial & Engineering Chemistry Research* **2021**, *60*, 17128–17142. https://doi.org/10.1021/acs.iecr.1c03146.

(15) Naeini, M.; Lai, H.; Cotton, J. S.; Adams II, T. A. A Mathematical Model for Prediction of Long-Term Degradation Effects in Solid Oxide Fuel Cells. *Industrial and Engineering Chemistry Research* **2021**, *60* (3), 1326–1340. https://doi.org/10.1021/acs.iecr.0c05302.

(16) Beloin-Saint-Pierre, D.; Albers, A.; Hélias, A.; Tiruta-Barna, L.; Fantke, P.; Levasseur, A.; Benetto, E.; Benoist, A.; Collet, P. Addressing Temporal Considerations in Life Cycle Assessment. *Science of the Total Environment* **2020**, *743*. https://doi.org/10.1016/j.scitotenv.2020.140700.

(17) Sohn, J.; Kalbar, P.; Goldstein, B.; Birkved, M. Defining Temporally Dynamic Life Cycle Assessment: A Review. *Integrated Environmental Assessment and Management* **2020**, *16* (3), 314–323. https://doi.org/10.1002/ieam.4235.

(18) Staffell, I.; Ingram, A.; Kendall, K. Energy and Carbon Payback Times for Solid Oxide Fuel Cell Based Domestic CHP. *International Journal of Hydrogen Energy* **2012**, *37* (3), 2509–2523. https://doi.org/10.1016/j.ijhydene.2011.10.060.

(19) Olausson, P. Life Cycle Assessment of an SOFC/GT Process. **1999**.

(20) Jin, E. Life Cycle Assessment of Two Catalysts Used in the Biofuel Syngas Cleaning Process and Analysis of Variability in Gasification, Oklahoma State University, 2014.

(21) Bahadori, A. Natural Gas Sweetening. *Natural Gas Processing* **2014**, 483–518. https://doi.org/10.1016/B978-0-08-099971-5.00010-6.

(22) Żarczyński, A.; Rosiak, K.; Anielak, P.; Wolf, W. Practical Methods of Cleaning Biogas from Hydrogen Sulphide. Part 1, Application of Solid Sorbents. *Acta Innovations* **2014**, *12*, 20–25.

(23) https://www.ecoinvent.org/database/database.html.

(24) https://www.nrel.gov/lci/.

(25) Fout, T.; Zoelle, A.; Keairns, D.; Turner, M.; Woods, M.; Kuehn, N.; Shah, V.; Chou, V.; Pinkerton, L. Cost and Performance Baseline for Fossil Energy Plants Volume 1a: Bituminous Coal (PC) and Natural Gas to Electricity Revision 3. *National Energy Technology Laboratory (NETL)* **2015**, *1a* (May), 240.

(26) International Organization for Standardization. *Environmental Management: Life Cycle Assessment; Principles and Framework. Vol. 14044. ISO*; 2006.

(27) International Organization for Standardization. *Environmental Management: Life Cycle Assessment; Principles and Framework. Vol. 14040. ISO*; 2006.

(28) Hauch, A.; Küngas, R.; Blennow, P.; Hansen, A. B.; Hansen, J. B.; Mathiesen, B.

V.; Mogensen, M. B. Recent Advances in Solid Oxide Cell Technology for Electrolysis. *Science* **2020**, *370* (6513). https://doi.org/10.1126/science.aba6118.

(29) Goldstein, L.; Hedman, B.; Knowles, D.; Freedman, S. I.; Woods, R. Gas-Fired Distributed Energy Resource Technology Characterizations. *Gas Research Institute and the National Renewable Energy Laboratory (NREL)* **2003**, 226.

(30) U.S. Department of Energy. Combined Heat and Power Technology Fact Sheet Series - Fuel Cells. *Combined Heat and Power Technology Fact Sheet Series* **2016**, DOE/EE-1334.

(31) Marques, A. S.; Carvalho, M.; Ochoa, A. A. V.; Abrahão, R.; Santos, C. A. C. Life Cycle Assessment and Comparative Exergoenvironmental Evaluation of a Micro-Trigeneration System. *Energy* **2021**, *216*. https://doi.org/10.1016/j.energy.2020.119310.

(32) Wolff, S.; Seidenfus, M.; Gordon, K.; Álvarez, S.; Kalt, S.; Lienkamp, M. Scalable Life-Cycle Inventory for Heavy-Duty Vehicle Production. *Sustainability (Switzerland)* **2020**, *12* (13). https://doi.org/10.3390/su12135396.

(33) Pun, B. K.; Seigneur, C. Understanding Particulate Matter Formation in the California San Joaquin Valley: Conceptual Model and Data Needs. *Atmospheric Environment* **1999**, *33* (29), 4865–4875. https://doi.org/10.1016/S1352-2310(99)00266-6.

(34) Strazza, C.; Del Borghi, A.; Costamagna, P.; Gallo, M.; Brignole, E.; Girdinio, P.

Life Cycle Assessment and Life Cycle Costing of a SOFC System for Distributed Power Generation. *Energy Conversion and Management* **2015**, *100*, 64–77. https://doi.org/10.1016/j.enconman.2015.04.068.

(35) Lai, H.; Harun, N. F.; Tucker, D.; Adams II, T. A. Design and Eco-Technoeconomic Analyses of SOFC/GT Hybrid Systems Accounting for Long-Term Degradation Effects. *International Journal of Hydrogen Energy* **2021**, *46* (7), 5612–5629. https://doi.org/10.1016/j.ijhydene.2020.11.032.

# CHAPTER 5: CONSTANT POWER GENERATION BY SCHEDULING INSTALLATION OF SOFC MODULES OPERATING IN VARYING POWER MODE

The content of this chapter is a published reprint of the following non-peer-reviewed publication:

Naeini, M., Adams II, T.A. and Cotton, J.S.. Constant Power Generation by Scheduling Installation of SOFC Modules Operating in Varying Power Mode. *CSChE Systems & Control Transactions* **2021**, LAPSE:2021.0793, 1, pp.30-33.

## Abstract

In this paper, producing constant power load of 550 MW from systems of Solid Oxide Fuel Cells (SOFCs) operating in varying power output mode was investigated. This is useful because previous research has shown that individual cells can have significant lifetime extensions when operated according to certain dynamic trajectories in which power production decreases over time. In this study, we determined that a constant net power output of a system comprised of many individual SOFC modules can be achieved by scheduling the installation and operation of each SOFC module in a particular manner. All the modules were operated under the optimal operating conditions obtained in our previous optimization study where power output of each module declined over time. The dynamic degradation of SOFCs was taken into account by using a detailed mathematical model of long-term performance degradation as a function of operating conditions. The result is a system in which every 5 days, one new SOFC module is brought online, replacing one module near the end of its useable life at the same time. With this staggered approach, the overall power output of the system can be maintained at an almost constant level at all times (550 MW for our example). The new module then gradually reduces its power output over time according to an optimal trajectory. With this approach, the overall system can produce an essentially constant supply of power at lower costs than a traditional approach where all SOFC modules within a large system are each operated at constant power.

**Keywords:** SOFCs, performance degradation, optimal operating conditions, optimal operating mode, constant power output.

## 1. Introduction

Solid Oxide Fuel Cells (SOFCs) are known for their high electrical efficiency and low environmental burdens, but they are yet to be commercialized in large-scale [1]. The degradation of these fuel cells is one main barrier for adoption [1]. SOFCs degrade due to a confluence of multiple phenomena which occur under normal operating conditions [2]. Several research studies focused on overcoming this issue by developing novel materials for different components of SOFC or by changing the structure [3–5]. But none of these new technologies had the required technical or economical feasibility for widespread commercialization. The focus of our research however is to overcome this barrier by understanding the degradation mechanisms through mathematical models and using them to determine operating strategies which reduce the rate of degradation.

In our prior study, we constructed a dynamic mathematical model of degradation by integrating six different models which each represent a different degradation reaction into thermodynamic models of overpotentials [6]. The developed model is capable of accurate prediction of long-term performance decline in SOFCs as a function of operating conditions, most importantly current density. This model allows investigators to extend the lifetime of SOFCs and operate them more economically by avoiding detrimental conditions that accelerate SOFC breakage. This can be easily achieved by adjusting the operating conditions and running SOFCs with an appropriate operating trajectory that involves slow and gradual changes over the course of its lifetime.

The findings of a techno-economic analysis (TEA) performed in our previous study using this model showed that conventional SOFCs can operate as long as 14 years economically if run at optimal operating conditions and with optimal dynamic trajectories [7]. The results also indicated that the optimal strategy for long-term operation of SOFCs is to gradually decrease the current density drawn from the fuel cells and let the power output drop over time. According to those findings, operating an SOFC in constant power mode (i.e. baseload power generation mode) is undesirable, because to achieve constant power one must continually increase the current density to compensate for degradation over time. This increasing current density in turn further accelerates the degradation of the fuel cells and thus should be avoided. Thus, even though constant power mode is often used in practice, the prior work shows that it is significantly more expensive than operating in a mode in which power gradually drops over time.

However, constant power output is nonetheless required for some applications and so gradually decaying power production is not useful or desirable. However, we can overcome this challenge by recognizing that some SOFC systems consist of many individual cells bundled into stacks, which are in turn bundled into modules, and the system itself can contain many modules. Thus, depending on the size of the system, modules, stacks, or even individual cells can be independently operated in varying power mode under optimal conditions, but the modules, stacks, or cells are installed gradually at different points of time such that the overall SOFC system delivers a constant amount of power.

## 2. Demonstration of This Work

For this study, we used the optimal sizes and operating trajectories obtained for SOFCs in varying power mode in our previous TEA study [7]. In other words, we assume that once an SOFC is started, its current density and power should follow a particular declining trajectory that has been predetermined by economic optimization as presented in the previous work (see Figure 1). One key parameter is the desired replacement schedule of the cell modules. The designer can choose the scheduled replacement time of a cell module (between 1 and 10 years in our study), and as long as the cell does not experience unexpected catastrophic failure, there will be some optimal way of operating that cell module within the desired lifetime.

As noted in the previous work, targeting shorter replacement times means it is optimal to use the cell more aggressively, drawing more power out of it but causing significant degradation such that the cell erodes quickly. Longer target replacement times (up to 14 years) are possible but it is optimal to operate much less aggressively and in a fashion which avoids decay. The previous work shows that longer lifetimes are more economical but the target replacement time in practice will depend on factors such as the risk of catastrophic failure, which the model cannot predict and may be unique to each specific manufacturer. Therefore, the target replacement time is taken as a parameter in this work, with two extremes considered for brevity (1 year and 10 year).

In the prior work, the SOFC systems were constrained to produce an average of 550 MW electrical power output during their lifetime, and the optimal size of SOFC active membrane area ($A_m$) for production of this power was found. The optimal cumulative power profile which minimizes levelized cost of electricity (LCOE) for a given target cell lifetime and has this average of 550 MW power produced is shown in Figure 1b. It is assumed that the fuel cells are identical, and each SOFC module contains multiple stacks of identical fuel cells. At the end of lifetime of the SOFCs (which all occur simultaneously), they are all replaced with identical fuel cells of the same size. This procedure is repeated during the 20 years life of the plant.

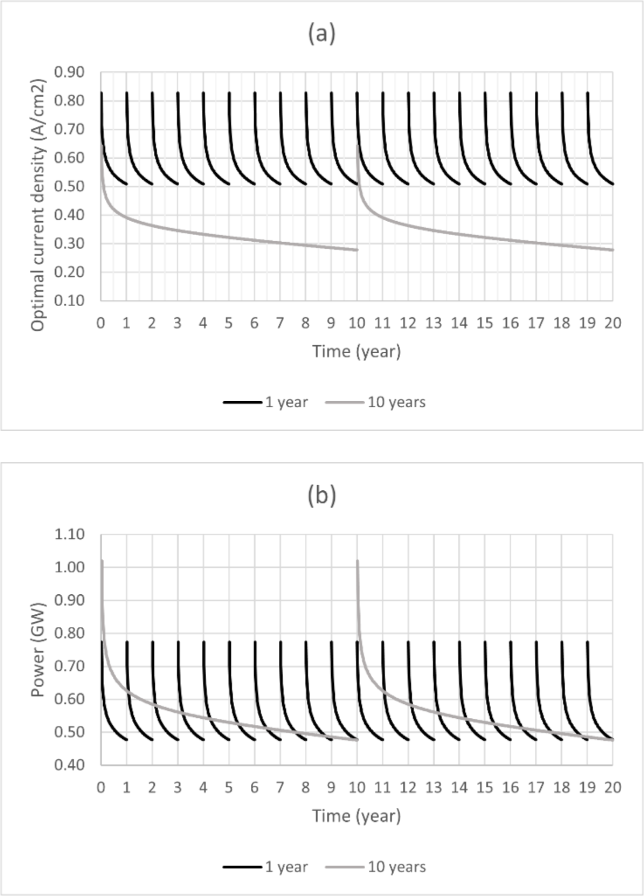

Figure 1. a) Optimal current density and b) power output of SOFCs with 1- and 10-year lifetimes during 20 years life of the plant [7].

In this study, instead of installing all the fuel cells at once, we install one module every 5-days. A module consists of a group of 1 or more stacks. It should be noted that all the modules have the same size and all individual SOFCs follow the same optimal trajectories found in our prior work (Figure 1) [7]. With this approach every 5 days a new module is brought online and at the same time a module that has reached end of its life is replaced. In this scheduled system, even though the SOFC modules in operation degrade and provide less power over time, the brand-new modules, brought online later, provide higher power, and compensate for the performance decline of the older modules. As a result, the system reaches steady state after a while and can provide constant power regardless of the performance drop of individual modules.

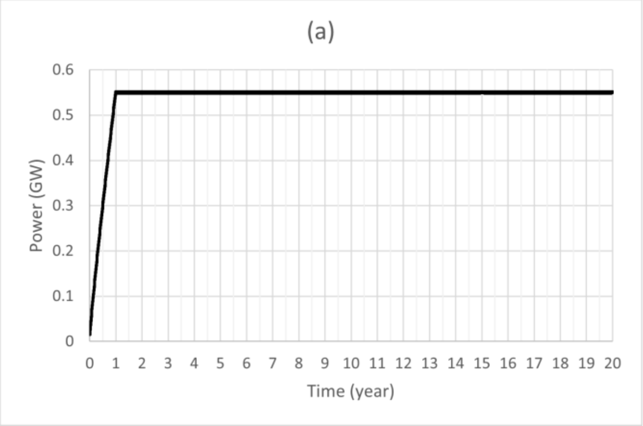

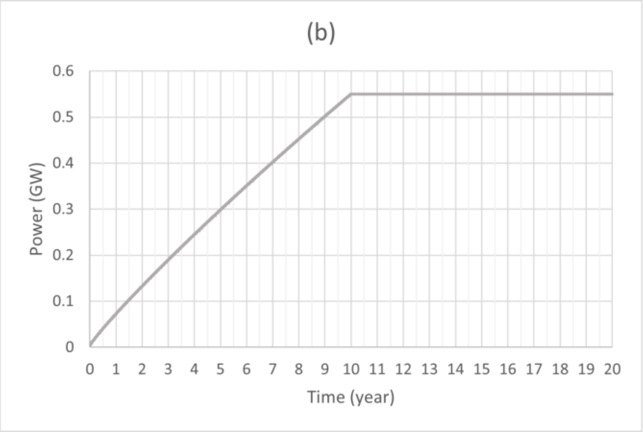

Figure 2 shows the net power output of staggered systems with individual SOFCs in varying power mode with 1- and 10-year lifetimes.

Figure 2. Net power output of systems in which modules are installed every 5 days and individual SOFCs are allowed to have variable power with a) 1- and b) 10-year lifetimes.

With this methodology, the system does not reach steady state instantaneously. Depending on the size of the modules and the optimal trajectories, different systems reach constant net power output at different times. For instance, with the given scheduling plan and optimal trajectories, the system of SOFCs with a 1-year replacement plan reaches almost constant power of 550 MW after 1 year of operation, while the system of SOFCs with a 10-year replacement plan provides nearly constant power of 550 MW after 10 years of operation.

This is a critical finding as it indicates that to get a constant net power from SOFC systems, individual SOFCs in the system should not necessarily be operated in baseload power generation mode. Instead, they can have variable power and constant net system power can be achieved by installing SOFC modules on a scheduled basis. The importance of the current methodology is in enabling constant net power generation with lower costs comparing to traditional baseload power generation mode. The characteristics and economics of systems in current methodology and traditional baseload power generation mode are shown in Table 1.

Table 1: Characteristics and economics of SOFC systems with constant power output. Project lifetime is 20 years.

| | **Individual SOFCs operated in varying power mode. (Modules are staggered every 5 days.)** | | **Individual SOFCs operated in baseload power mode. (All stacks are installed at once.)** | |
|---|---|---|---|---|
| Replacement Schedule: | **1 yr** | **10 yr** | **1 yr** | **10 yr** |
| Area of individual SOFC (cm²) | 414 | 414 | 414 | 414 |
| Average lifetime power produced by one SOFC (W) | 123 | 85 | 106 | 79 |
| SOFCs per stack | 259 | 259 | 259 | 259 |
| Average lifetime power produced by one stack (kW) | 32 | 22 | 27 | 20 |
| Total size needed (m²) | 184,555 | 267,690 | 215,637 | 289,657 |
| Total stacks needed | 17,212 | 24,965 | 220,111 | 120,275 |
| Stacks per module | 236 | 34 | N/A | N/A |
| Total lifetime average power (MW) | 537.9 | 424.3 | 550 | 550 |
| Steady state power (MW) | 550 | 550 | 550 | 550 |
| System power at beginning of replacement cycle (MW) | 789 | 1014 | 550 | 550 |

| | | | | |
|---|---|---|---|---|
| System power at end of replacement cycle (MW) | 477 | 476 | 550 | 550 |
| Time to reach steady state | 1 yr | 10 yr | immediate | immediate |
| LCOE ($/kWh) | 0.357 | 0.131 | 0.409 | 0.143 |

## 3. Future Study

The major drawback of the current approach is that the net system power does not reach a constant load instantaneously. Future work can focus on generation of constant power throughout the entire life of the plant from an SOFC system in which individual SOFCs are allowed to have variable power. This can be achieved using either of the following methods: a) solving a separate problem to find optimal size, installation scheduling, and operation of stacks that should be used before systems shown in Figure 2 reach steady state, such that combination of the system and these additional stacks generate nearly constant load of 550 MW throughout 20 years life of the plant, b) solving a general optimization over 20 years of every individual stack/module to find optimal schedule and operation for each stack/module such that the system produces 550 MW at all times during plant's life. The latter problem may be intractable.

## 4. Conclusion

This research showed that by using stacking capability of SOFCs a net constant power load can be generated from a system of SOFC modules in which individual fuel cells follow an optimal declining trajectory. By bringing a new module online and replacing a module near end of its life every 5 days, the system can reach steady state and produce a constant power output. This is significant because it enables a steady power output while avoiding using fuel cells in traditional baseload power mode in which fuel cells degrade at high rates. As a result, this approach was shown to be more economical than constant load production by running all fuel cells in baseload power mode.

# Acknowledgements

We greatly acknowledge the financial support from Natural Sciences and Engineering Research Council of Canada [NSERC CRDPJ 509219-2017] and the Ontario Centre of Excellence [OCE 27851-2018].

## 5. References

[1] V. Zaccaria, A. Traverso, D. Tucker, A real-time degradation model for hardware in the loop, in: Proc. ASME Turbo Expo 2015 Turbine Tech. Conf. Expo. GT:1-8, (2015).

[2] T. Parhizkar, S. Hafeznezami, Degradation based operational optimization model to improve the productivity of energy systems, case study: Solid oxide fuel cell stacks, Energy Convers. Manag. 158:81-91 (2018).

[3] A. Niemczyk, K. Świerczek, Development of novel air electrode materials for the SOFC and SOEC technologies, E3S Web Conf. 108 (2019).

[4] P.K. Patro, T. Delahaye, E. Bouyer, Development of Pr0.58Sr0.4Fe0.8Co0.2O3 − δ–GDC composite cathode for solid oxide fuel cell (SOFC) application, Solid State Ion. 181:1378-1386 (2010).

[5] F. Tietz, A. Mai, D. Stöver, From powder properties to fuel cell performance – A holistic approach for SOFC cathode development, Solid State Ion. 179:1509-1515 (2008).

[6] M. Naeini, H. Lai, J.S. Cotton, T.A. Adams II, A mathematical model for prediction of long-term degradation effects in solid oxide fuel cells, Ind. Eng. Chem. Res. 60:1326-1340 (2021).

[7] M. Naeini, J.S. Cotton, T.A. Adams II, Economically optimal sizing and operation strategy for solid oxide fuel cells to effectively manage long term degradation, manuscript submitted for publication (2021).

# CHAPTER 6: DATA-DRIVEN MODELING OF LONG-TERM PERFORMANCE DEGRADATION IN SOLID OXIDE ELECTROLYZER CELL SYSTEM

The content of this chapter is a published reprint of the following peer-reviewed publication:

Naeini, M., Cotton, J.S. and Adams II, T.A.. Data-Driven Modeling of Long-Term Performance Degradation in Solid Oxide Electrolyzer Cell System. *Computer Aided Chemical Engineering* **2022**, *49*, 847-852.

## Abstract

One key challenge of Solid Oxide Electrolyzer Cell (SOEC) systems is degradation over long periods of time. Degradation decreases efficiency by increasing the electrical energy required for $H_2$ production. This paper presents the first step in managing long-term degradation in SOEC systems. In this work, the first data-driven dynamic model for the prediction of performance degradation in SOECs as a function of humidity, operating temperature, and current density was developed. The model was trained using experimental data from multiple data sets in the literature under various conditions. The model showed good agreement with validation data over 7000 h operation. One key finding is that the data show there are three distinct time regimes in which degradation behaviour is qualitatively different. This is likely due to different degradation phenomena, although the specific phenomena have not yet been isolated. This is significant for PSE applications because operators can choose to vary the operating conditions over time in order to predict, account for, or minimize the effects of long-term degradation.

**Keywords:** SOEC; Performance Degradation; Data-Driven Model; Operating Condition.

## 1. Background

When baseload power facilities or renewable sources of intermittent power are used for electricity generation, excess electricity may be produced during low demand hours.

Producing surplus electricity can impose additional costs to electricity systems as it should be either curtailed or sold at a low price. Therefore, there is a great need for reliable energy storage systems at low demand hours. SOEC is a promising technology for energy storage that can utilize the excess electricity from the grid to electrolyze steam and generate hydrogen. $H_2$ is a clean, useful source of energy with high energy content per weight unit. The produced $H_2$ can be compressed and stored in cylinders for various purposes, supplied to stationary power generators such as fuel cells to produce electricity, or injected into the existing natural gas network to lower carbon intensity. SOECs are Solid Oxide Fuel Cells (SOFCs) which are operated in reverse. Indeed, the same technology can either generate electricity via some exothermic electrochemical reactions (SOFC mode) when supplied with fuel and air, or it can electrolyze water and produce $H_2$ through endothermic electrochemical reactions (SOEC mode), when supplied with steam and electricity. SOFCs and SOECs feature several advantages over some existing power generation technologies and electrolyzer systems such as high efficiency, low noise, and reduced greenhouse gas (GHG) emissions. However, this technology suffers the drawback of significant long-term degradation under normal operating conditions. This issue has been a barrier for commercialization of SOFCs and SOECs and has limited their application in the industry (Zaccaria et al., 2015). In our prior work, we were able to successfully overcome this problem for SOFCs specifically by constructing a mathematical model for dynamic simulation of the long-term performance drop in SOFC systems (Naeini et al., 2021). Using this model in a techno-economic analysis (TEA) enabled us to determine the optimal capacity and corresponding optimal dynamic operational trajectories of SOFCs that make them more cost-competitive with traditional power generation, by managing their long-term degradation and increasing their useful lifetime (Naeini et al., 2021). This was possible because the individual mechanisms that cause SOFC degradation are known, and thus first principles could be considered directly in the model.

Since the electrochemical reactions and degradation mechanisms in SOFCs are different from those in SOECs, the model developed for degradation in SOFCs cannot be used to predict degradation in SOECs. As such, a dynamic model should be constructed for simulation of long-term performance degradation in SOECs. This is essential for identifying optimal sizing and operating strategies of SOEC systems for a cost-effective energy storage over an extended lifetime, with controlled degradation. Our broad literature survey revealed that a dynamic degradation-based model for SOECs is lacking in the open literature. Also, the mechanisms of degradation phenomena in electrolysis mode are not well known, which prevents us from developing a first-principles model. However, there have been number of experiments investigating impacts of operating conditions on SOEC performance degradation. Hoerlein et al.'s (2018) experiments in particular showed the impacts of current density, humidity, and operating temperature on voltage and ohmic resistance of 20 SOECs over 1000 h of operation. This is a good, representative dataset that contains acceptable ranges of operating parameters as it includes current density ranging from 0 to 1.5 A/cm2, humidity varying from 40 % to 80 %, and temperature from 750 to 850 °C. This dataset is used in the current work to develop a data-driven model for degradation of SOEC.

## 2. Modeling strategy

The following information shows that the time evolution of SOEC's ohmic resistance can be used to calculate SOEC degradation. SOECs produce H2 at a constant rate as long as the current density supplied to the cell is constant (Eq.(1)).

$$r_{H_2} = \frac{i}{nF} \tag{1}$$

Where $r_{H_2}$ is the rate of $H_2$ production, $i$, $n$, and F are the current density, moles of electrons involved in the electrolysis electrochemical reactions, and Faraday constant, respectively. The ohmic resistance of SOECs increases over time due to degradation. According to Ohm's law (Eq.(2)), the voltage of the SOEC and therefore the energy required to produce a constant amount of H2 increase with its degradation (Eq.(3)).

$$V = R\, i \tag{2}$$

$$P = R\, i^2 = V\, i \tag{3}$$

In these equations $R$, $V$, and $P$ represent the SOEC's ohmic resistance, voltage, and power, respectively. The magnitude of resistance increase depends on the operating conditions. Therefore, a model that predicts time evolution of resistance as a function of current density, humidity, and temperature will allow us to quantify performance degradation in the SOEC. Data from Figure 1 is used in the present work to develop a model for SOEC degradation. Given in the y-axis of these plots is $\Delta R_{ohm}$ which shows the ohmic resistance increase with respect to the initial ohmic resistance of the cells.

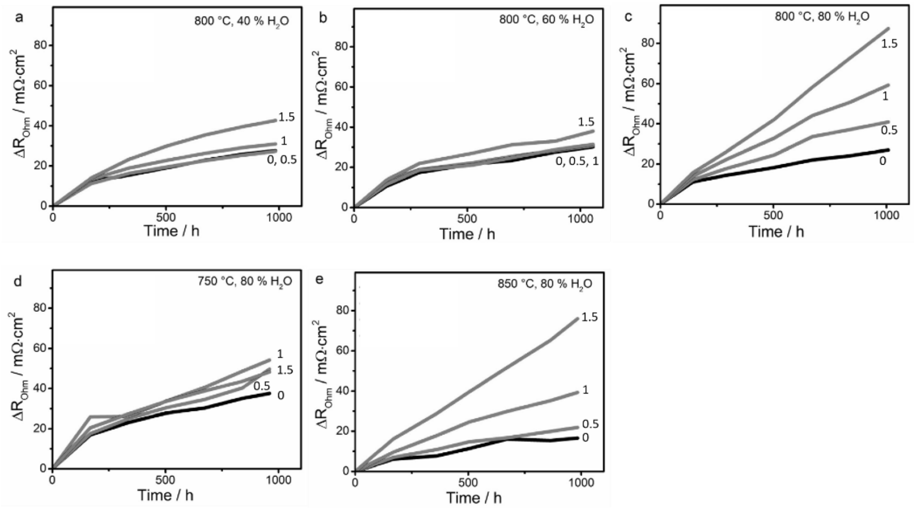

Figure 1. Time evolution of ohmic resistance of SOECs at various current densities from 0 to 1.5 A/cm2 and a) 800°C and 40% humidity, b) 800°C and 60% humidity, c) 800°C and 80% humidity, d) 750°C and 80% humidity, and e) 850°C and 80% humidity. Original data from (Hoerlein et al.).

The data show an unstable behavior in some SOECs during the first 200 h of operation, where the resistance, voltage, and other parameters do not follow a reproducible or consistent trajectory from run to run. This behavior is known as cell conditioning or transition period and cannot be modelled since it does not conform to any known pattern (Sohal; Hubert). However, the data show that the cumulative degradation of the cell at the 200h mark does correlate well with temperature, humidity, and current density, even though the trajectory in getting there does not. We removed the first 200 h from the training data and as a result the developed model applies only beyond 200 h. It should also be noted that even though Hoerlein et al.'s (2018) data includes voltage trajectories of SOECs, voltage is not used for building the SOEC model in this study. The reason is that when there is not any current in the external circuit, i.e. the open circuit voltage condition (OCV), the voltage remains constant and as a result it is not a good state variable for predicting degradation of SOECs.

ALAMO (Automated Learning of Algebraic Models) was used to develop the data-driven model. This software employs a machine learning approach to learn accurate and simple algebraic models from the training dataset (Wilson and Sahinidis). ALAMO models are typically linear combinations of nonlinear transformations of the input variables. The software uses an optimization approach to find not only the best fit of model parameters, but the selection of the basis functions themselves. This avoids overfitting and helps choose basis functions that best characterize the data.

### 2.1.Development of the linear model from 200h to 2500h

First, a partial model was developed based on Hoerlein et al's (2018) dataset (which has data out to 1000h), shown in Eq. (4).

$$R_{t'} = R_0 + \underbrace{0.019\,TH + 7.290\,Hi} + [0.033\,Ht' + 0.017\,it'] \qquad (4)$$

where $t'$ is time since 200h (h), $R_{t'}$ is ohmic resistance at $t'$ (mΩ.cm2), $R_0$ is resistance of virginal SOEC at time 0 h (mΩ.cm2), T is temperature (°C), and H is humidity of the fuel feed expressed as mole fraction of water. Eq.(4) includes two time-independent (underlined) and two time-dependent (enclosed in square brackets) terms. Underlined terms show the change in resistance from $R_0$ within the first 200h. While time-dependent terms show the increase in resistance from 200h and onward. Since the data for the first 200h were removed from training data, the model cannot indicate time evolution of resistance within this period. Instead, it quantifies the total change in resistance from $R_0$ within the first 200h. As can be seen, given a constant molar humidity and current density, ohmic resistance of SOEC increases linearly with time for at least 1000h, and so we refer to this model as the "linear model". This is in agreement with number of other studies that reported linear trend in time for SOEC degradation at fixed operating conditions (Hauch; Hubert; Trofimenko et al.). These studies all consider operation for 2500h or less. Eq.(4) was fit with $R^2$=0.94 across the training datasets considered up to 1000h. Rapid transients may have impacts which are not considered in the model.

### 2.2. Validation of the linear model out to 2500 h

In order to ensure validity of the developed model for predicting performance degradation in SOECs under given operating conditions, Tietz et al.'s (2013) experimental data – which was not considered in building the model – was used to compare with the model. In Tietz et al. (2013) an SOEC was operated at 778±6°C out to 7600h, supplied with current density of 1A/cm2, and 80% humidity. We calculated the SOEC's ohmic resistance trajectory using Eq. (4) and then its voltage trajectory using Eq. (2) under the given condition. The results, given in Figure 2, indicate capability of this linear model to simulate performance deterioration in SOECs for the first 2500 h of operation ($R^2$=0.87). After 2500h, it becomes more apparent that the SOEC degrades sub-linearly and the degradation rate decreases. We note that most studies that conclude that degradation rates are linear, such as Hauch et al. (2006), Hubert et al. (2018), and Trofimenko et al. (2017) do not run the experiments long enough to experience this inflection point around 2500h.

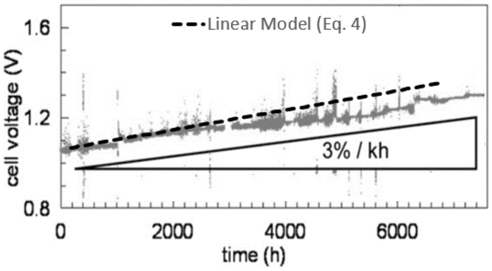

Figure 2. Results of the developed model for SOEC performance degradation compared to experimental data from (Tietz et al.). The dashed line is our model, drawn on top of a modified version of the original figure reproduced from that work.

### 2.3. Sublinear model out to 7000 h

The model was modified to reflect the sublinear nature of the degradation by adding a power term to the time component, and fitting the exponent to Tietz et al.'s data. The basis functions and their parameters were unmodified from Eq. 4. The sublinear model is given in Eq.(5), in which degradation is sublinear to the order of 0.97, and $R^2$=0.95 for Tietz et al.'s data out to 7000h.

$$R_{t'} = R_0 + 0.019\,T + 7.290Hi + (0.033H + 0.017i)(t')^{0.97} \tag{5}$$

A comparison between the linear model, sublinear model, and experimental data is provided in Figure 3. As can be seen, the original and modified models are almost equally good for simulation of short-term operation. But for the long-term operation, sublinear model is significantly better than the linear one.

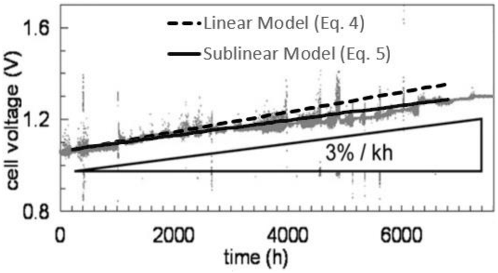

Figure 3. Results of the linear and sublinear models for long-term performance degradation in SOEC compared to experimental data from (Tietz et al.). Figure modified from the original.

## 3. Discussion and Future Work

One key finding is the sublinear nature of the degradation rate, but this is supported only by one data set since most experiments in the open literature are not conducted for long enough in order to see this trend. Additional research is needed to validate this sublinear characteristic. However, sublinear behavior makes sense, as in practice SOECs can be used for many years. If the degradation rate was truly linear such that long-term degradation continued at the same rate as in the first 1000h, the amount of degradation would be much higher than what is actually experienced in practice. For example, comparing extrapolating the sublinear (Eq. (5)) and linear (Eq. (4)) models out to 10 years, the linear model would predict a required voltage of 30% higher than the sublinear model. This will make a significant difference in design and operation of large-scale systems. Using either the linear or sublinear model, as well as Eq.(2) and Eq.(3), one can calculate voltage of SOECs and the required power supply for producing a specific amount of H2 at different points of operating time considering the degradation. This will enable system designers to find the optimal capacity and operation strategy of SOEC system for an economical energy storage with reduced degradation rate. As such, a TEA will be performed on SOEC systems as the future work. The findings will improve cost-effectiveness of this technology and will help its commercialization.

## 4. Conclusions

This paper presented a data-driven model constructed from experimental data derived from the literature for prediction of the performance deterioration in SOEC. To the best of authors' knowledge, this is the first dynamic model for simulation of the SOEC degradation under different operating conditions with high accuracy across a range of cell conditions. This model, developed using ALAMO, is a composition of nonlinear functions of operating parameters namely humidity, temperature, and current density. The model was well-validated using many training and testing sets for the first 2500h of operation, but the extension to 7000h requires additional validation. Both the linear (Eq 4) and sublinear (Eq 5) models work equally well for those first 2500h but the linear model breaks down afterward. The results indicated that the rate of SOEC degradation depends on the humidity and current density, and decays sublinearly in the long-term.

## 5. References

Hauch, Anne. "Performance and Durability of Solid Oxide Electrolysis Cells." *ECS Meeting Abstracts*, vol. 37, no. October, 2006, doi:10.1149/ma2006-01/24/842.

Hoerlein, M. P., et al. "A Parameter Study of Solid Oxide Electrolysis Cell Degradation: Microstructural Changes of the Fuel Electrode." *Electrochimica Acta Journal*, vol. 276, 2018, pp. 162–75, doi:10.1016/j.electacta.2018.04.170.

Hubert, M. “Durability of Solid Oxide Cells: An Experimental and Modelling Investigation Based on Synchrotron X-Ray Nano-Tomography Characterization.” *PhD Thesis*, 2018.

Naeini, Mina, Haoxiang Lai, et al. “A Mathematical Model for Prediction of Long-Term Degradation Effects in Solid Oxide Fuel Cells.” *Industrial and Engineering Chemistry Research*, vol. 60, no. 3, 2021, pp. 1326–40, doi:10.1021/acs.iecr.0c05302.

Naeini, Mina, James S. Cotton, et al. *Economically Optimal Sizing and Operation Strategy for Solid Oxide Fuel Cells to Effectively Manage Long Term Degradation*. 2021.

Sohal, Manohar S. *Degradation in Solid Oxide Cells During High Temperature Electrolysis*. 2009.

Tietz, F., et al. “Degradation Phenomena in a Solid Oxide Electrolysis Cell after 9000 h of Operation.” *Journal of Power Sources*, vol. 223, Elsevier B.V, 2013, pp. 129–35, doi:10.1016/j.jpowsour.2012.09.061.

Trofimenko, Nikolai, et al. “Optimization of ESC Performance for Co-Electrolysis Operation.” *ECS Transactions*, vol. 78, no. 1, 2017, pp. 3025–37, doi:10.1149/07801.3025ecst.

Wilson, Zachary T., and Nikolaos V. Sahinidis. “The ALAMO Approach to Machine Learning.” *Computers & Chemical Engineering*, vol. 106, Pergamon, Nov. 2017, pp. 785–95, doi:10.1016/J.COMPCHEMENG.2017.02.010.

Zaccaria, Valentina, et al. “A Real-Time Degradation Model for Hardware in the Loop.” *Proceedings of ASME Turbo Expo 2015: Turbine Technical Conference and Exposition*

*GT2015*, 2015, pp. 1–8.

# CHAPTER 7: AN ECO-TECHNO-ECONOMIC ANALYSIS OF HYDROGEN PRODUCTION USING SOLID OXIDE ELECTROLYSIS CELLS THAT ACCOUNTS FOR LONG-TERM DEGRADATION

The content of this chapter is a published reprint of the following peer-reviewed publication:

Naeini, M., Cotton, J.S., Adams II, T.A. An Eco-Technoeconomic Analysis of Hydrogen Production Using Solid Oxide Electrolysis Cells that Accounts for Long-Term Degradation. *Frontiers in Energy Research* **2022,** *10:1015465*. doi: 10.3389/fenrg.2022.1015465.

## Abstract

This paper presents an eco-technoeconomic analysis (eTEA) of hydrogen production via solid oxide electrolysis cells (SOECs) aimed at identifying the economically optimal size and operating trajectories for these cells. Notably, degradation effects were accounted by employing a data-driven degradation-based model previously developed by our group for the analysis of SOECs. This model enabled the identification of the optimal trajectories under which SOECs can be economically operated over extended periods of time, with reduced degradation rate. The findings indicated that the levelized cost of hydrogen (LCOH) produced by SOECs (ranging from 2.78 to 11.67 \$/kg $H_2$) is higher compared to gray hydrogen generated via steam methane reforming (SMR) (varying from 1.03 to 2.16 \$ per kg $H_2$), which is currently the dominant commercial process for large-scale hydrogen production. Additionally, SOECs generally had lower life cycle $CO_2$ emissions per kilogram of produced hydrogen (from 1.62 to 3.6 kg $CO_2$ per kg $H_2$) compared to SMR (10.72 to 15.86 kg $CO_2$ per kg $H_2$). However, SOEC life cycle $CO_2$ emissions are highly dependent on the $CO_2$ emissions produced by its power source, as SOECs powered by high-$CO_2$-emission sources can produce as much as 32.22 kg $CO_2$ per kg $H_2$. Finally, the findings of a sensitivity analysis indicated that the price of electricity has a greater influence on the LCOH than the capital cost.

## Keywords

Solid oxide electrolysis cell, Long-term performance degradation, Levelized cost of hydrogen, Operating trajectory, Cost of $CO_2$ avoided.

## 1. Introduction

The widespread implementation of low-carbon electricity generation technologies such as nuclear, solar, and wind is a key step in the transition to a low-carbon future. However, the intermittent nature of solar and wind power limits their application compared to more reliable power sources, such as fossil-fuel-based power generators.[1] On the other hand, nuclear plants can serve as baseload power generators, but this sometimes leads to power output exceeding demand. While this surplus power can be curtailed, doing so usually requires the payment of a penalty charge. Thus, the presence of large amounts of low-carbon power sources on the grid requires the use of storage systems to sequester surplus energy.[2] At present, batteries are the most common commercial energy storage systems in use, but their practical application is still somewhat limited due to their finite lifetime, use of limited rare earth materials, as well as environmental concerns relating to the carbon-intensive process used in their production and the water and air pollution caused by their disposal.[1,3] Electrolysers have shown considerable promise for energy storage, largely due to their higher energy storage density and lower environmental impact compared to lithium-ion batteries.[3] Hydrogen electrolysers are also key elements of the hydrogen economy.[4] Electrolyser cells consume excess electricity from the grid to electrolyze water and produce hydrogen,[2] which is capable of storing high energy content per mass that can then be distributed and utilized for various applications.[5] For example, the produced hydrogen can be supplied to fuel cells during high-demand periods (day/year) to generate electricity to meet energy demands,[2] or it can be added to natural gas (NG) pipelines to lower the carbon intensity of NG.4 Furthermore, injecting hydrogen into the NG network eliminates the need for high-pressure hydrogen compressors, thereby reducing the system's cost and energy consumption.

The ability to produce hydrogen via electrolysis is a major step towards enabling the hydrogen economy. Currently, steam methane reforming (SMR) is the most commonly used method for industrial-scale hydrogen production. The hydrogen generated through SMR, which has a low market price, is known as black or gray hydrogen due to its use of fossil fuels (coal and natural gas, respectively). Significant amounts of carbon dioxide are released during the SMR process. In contrast, electrolysers produce hydrogen without direct $CO_2$ emissions, but the source of the electricity used greatly impacts indirect $CO_2$ emissions. Hydrogen produced through electrolysis can be classified as green hydrogen if the electricity is exclusively derived from solar, wind, or geothermal energy (and biomass in some classifications), and pink hydrogen if it derives from nuclear energy. If mixed energy sources such as municipal power grids are used, life cycle $CO_2$ emissions can vary greatly from location to location and hour to hour. Thus, the carbon intensity of the electricity source plays an important role in the environmental performance of electrolysers.[6]

The suitability of electrolysers for use in the hydrogen economy depends both on their economics and their $CO_2$ emissions per kg of hydrogen generated.6 Alkaline and proton-exchange membrane (PEM) electrolysers are among the most mature types of electrolysers and have been broadly used for hydrogen generation. Conversely, the large-scale commercialization of solid oxide electrolysis cells (SOECs) has yet to be achieved due to the high level of degradation often experienced by these cells. SOECs are efficient, as their high operating temperatures allow them to produce more hydrogen than low-temperature electrolysers per unit of electricity consumed.[7] While hydrogen production via alkaline and PEM electrolysers has been extensively studied,[8–10] there remains a lack of research that examines the economic and environmental performance of SOECs while also considering their degradation. Indeed, a number of studies have investigated the economic optimization of SOECs, but none have employed a degradation-based model in doing so. For example, Seitz et al. performed an economic optimization of a solar-thermal-powered SOEC that had been integrated with thermal energy storage with the objective of minimizing the LCOH.[11] They compared their results with the LCOH of a standalone SOEC and found that the addition of thermal energy storage decreased the LCOH from 0.16 to 0.11 EUR/kWh $H_2$. However, Seitz et al.'s analysis completely ignored the influence of electrolysis cell degradation. Elsewhere, Mastropasqua et al. proposed an SOEC system that was integrated with a parabolic dish solar field to enable the generation of 150 kg $H_2$ per day.[12] Even though Mastropasqua et al.'s models used thermodynamic equations to quantify the inevitable overpotentials of the electrolysis cells, they did not account for the degradation that occurs due to the system reactions. In another study, Lahdemaki used Aspen Plus to develop a black box model for an SOEC system sized to generate enough hydrogen to enable the production of 6000 t of synthetic natural gas (in this paper, t=tonne=1000 kg).

A number of simplifying assumptions were made both in their model and in their optimization problem. For instance, it was assumed that SOECs degrade at a constant rate of 0.3% per 1000 h, and that 16,169 $m^2$ of cells are required. To calculate the degradation rate, it was assumed that the system's power consumption increases by almost 10% after 40000 h of use.

The current paper presents an eco-technoeconomic analysis (eTEA) of SOECs aimed at identifying the optimal operating trajectories for economical hydrogen production. Unlike previous works, we use a data-driven model developed in a prior work [13] for SOEC performance degradation.[14] The developed model, which will be described in the next section, describes how SOEC performance changes over time under specific operating conditions. To the best of the authors' knowledge, this is the first eTEA of SOECs to employ a degradation-based model. This is significant, as the incorporation of a degradation-based model will yield findings that are more accurate and reliable compared to those of other studies in the open literature, which have either ignored or underrated SOEC degradation. The results of this work will allow us to determine whether adjusting the operating parameters can make SOECs economically competitive with mature hydrogen-production technologies, despite their degradation and high capital cost. Since capital costs associated with SOECs can vary significantly with manufacturing volume and electricity rates vary between grids and time (i.e., peak vs. off-peak), a sensitivity analysis is conducted to determine the extent to which these factors influence the cost of hydrogen production. The results of such sensitivity analyses are critical in determining whether SOECs are an economically viable option for a particular region. Furthermore, $CO_2$

emissions per kg of hydrogen generated is another key factor that must be considered when selecting the best technology for use in the hydrogen economy. As such, $CO_2$ emissions associated with SOEC manufacturing and electricity generation from various sources are calculated to determine whether SOECs are suitable for use in the hydrogen economy, and how its suitability is affected by grid emissions. Finally, the cost of $CO_2$ avoided (CCA) is also computed to provide a good metric for comparing SOECs with other hydrogen-production processes, both in terms of economic and environmental performance.

## 2. Background

### 2.1.Data-Driven Model for Long-Term SOEC Performance

SOECs have the same components and structure as solid oxide fuel cells (SOFCs). SOFCs convert the chemical energy from a fuel source to electricity through electrochemical reactions between fuel and oxygen; in contrast, electrical charge moves in the opposite direction in SOECS, electrolyzing steam through endothermic electrochemical reactions.[15] In a previous study, we developed a detailed model that captures how six mechanisms that govern SOFC degradation impact its long-term performance.[16] It is important to note that, since the reactants and electrochemical reactions in SOFCs and SOECs are different, the dominant degradation mechanisms will also be different. Therefore, the SOFC degradation model is unable to describe degradation in SOECs. Due to a lack of adequate openly available information about the various degradation reactions in SOECs, it is not yet possible to construct a first-principles model for SOECs. Consequently, we constructed a data-driven model in our prior work using Hoerlein et al.'s experimental results, which provide data for identical SOECs under various temperatures, current densities, and fuel humidity percentages over 1000 hours of operation.[13,14] The findings of Hoerlein et al.'s studies have shown that temperature, current density, and fuel gas humidity have the highest impacts on SOEC degradation. As such in [14] they only investigated and showed the impacts of these parameters on degradation of the cells. In their work, Hoerlein et al. took increases in a cell's ohmic resistance as a key indicator of the degradation. Changes in the SOEC's ohmic resistance over time can be used to quantify the degradation of SOECs. Several studies have shown that the ohmic overpotential, which can be calculated by Ohm's law, is the main and the most substantial contributor to the SOEC overpotential.[17–20] The rate of hydrogen production by SOECs has a linear correlation with current density (Eq. 1); this means that a constant current density leads to a constant hydrogen production rate in SOEC.

$$\dot{n}_{H_2} = \frac{i}{n_e \mathrm{F}} \tag{1}$$

In this equation $\dot{n}_{H_2}$ is the rate of hydrogen production by SOEC, $i$, $n$, and F are the current density, moles of electrons transferred in the electrolysis reactions, and Faraday constant, respectively. The energy needed for production of a constant amount of hydrogen by the SOEC increases with its ohmic resistance and degradation (Eq. 2).

$$P = R\, i^2 = V\, i \tag{2}$$

Where $P$, $V$, and R are the SOEC's power, voltage, and ohmic resistance, respectively. The amount of resistance increase over time is a function of the SOEC's operating parameters. In our prior work, we used the data from Hoerlein et al.'s experiments (Fig. 1) to build a model that predicts temporal change of resistance with respect to current density, temperature, and the fuel gas molar humidity.[13] This model quantifies degradation of SOEC as a function of the operating conditions.

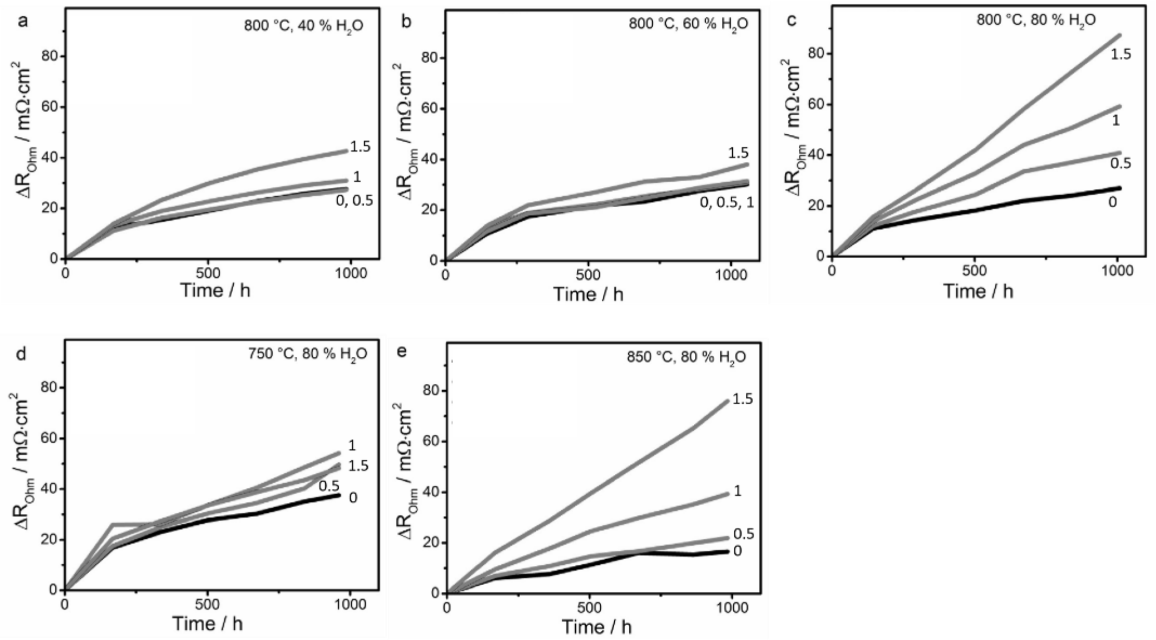

Fig. 1. Temporal change of ohmic resistance of SOECs at different current densities from 0 to 1.5 A/cm$^2$ and a) 800°C and 40% fuel humidity, b) 800°C and 60% fuel humidity, c) 800°C and 80% fuel humidity, d) 750°C and 80% fuel humidity, and e) 850°C and 80% fuel humidity measured by Hoerlein et al.[14] The y-axis, $\Delta R_{ohm}$ is the ohmic resistance increase from the initial ohmic resistance of SOECs. Figure reused with permission from [13].

Hoerlein et al. ensured that a wide range of operating parameters were investigated in their study by varying the temperature from 750 to 850°C, the current density from 0 to 1.5 A/m$^2$, and the fuel gas molar humidity from 40% to 80%.[14] The tested SOECs were in transition period over the first 200 h of use and showed an unstable trend that cannot be modelled. This unstable behavior was also observed previously by other research groups.[21,22] It is worth noting that, even though the degradation trend in the transition period is not reproducible, the value of cumulative degradation at 200 h can be modelled with respect to the operating parameters. As such, we removed the transition period data and used the remaining data to generate the model. In our prior work, we employed Automated Learning of Algebraic Models (ALAMO) to identify an algebraic model from the training dataset.[13]

### 2.1.1. The linear model from 200h to 2500h

Eq. 3 is the linear model generated by ALAMO for the time evolution of SOEC performance degradation.

$$R_{t'} = R_0 + 0.019\,TH + 7.290\,Hi + 0.033\,Ht' + 0.017\,it' \tag{3}$$

In this equation $t'$ represents the time since the 200h transition period has completed (h), $R_{t'}$ and $R_0$ are the SOEC's ohmic resistance (mΩ.cm$^2$) at times $t'$ and 0h (the virginal state), respectively, $T$ is the cell's operating temperature (°C), $H$ is the mole fraction of water in the fuel gas known as fuel gas humidity, and $i$ is the current density (A/cm$^2$). Time-independent terms show the accumulated increase in resistance over the transition period, while time-dependent terms show time variation of ohmic resistance after 200h. When the supplied current density and fuel gas humidity are constant, the model shows linear growth in resistance over time. Even though this linear trend was observed in several experimental studies on SOECs, it should be noted that all of these studies tested SOECs for 2500h or less.[22–24]

### 2.1.2. Validation of the linear model (out to 2500h)

The linear model was compared against Tietz et al.'s experimental data – which was not used in developing the model – for validation purposes (Fig. 2), with the results indicating that the linear model had good ability to predict SOEC degradation over the first 2500h.[25] However, Tietz et al.'s data, which was collected over almost 7600h of SOEC operation, indicated that the degradation rate diminishes after 2500h; thus, the linear model deviated from Tietz et al.'s data after this time. It should be noted that most experiments that show linear degradation rates for SOECs, such as [22–24], are not performed for long enough to encounter the deviation from linear trend at around 2500h.

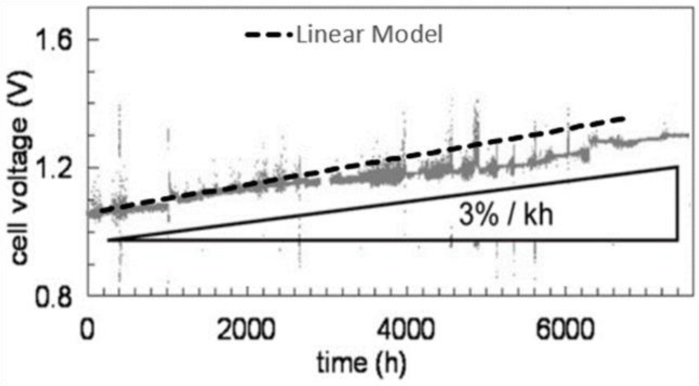

Fig. 2. Results of the simulation of performance degradation in SOEC using our linear model compared to experimental data from [25]. Our linear model is drawn as a dashed line on a modified version of the original figure reproduced from that work. Figure reused with permission from [13].

### 2.1.3. Sublinear model

The model was subsequently modified into a sublinear model by introducing an exponent term to the time component ($t'$). The value of the power term was calculated by fitting it to Tietz et al.'s experimental data. The modified model is expressed as follows:

$$R_{t'} = R_0 + 0.019\,TH + 7.290\,Hi + (0.033H + 0.017i)(t')^{0.97} \qquad 4$$

Comparison of Tietz et al.'s experimental data, the linear model, and sublinear model (Fig. 3) indicates that the linear model is almost as good as the sublinear model for prediction of SOEC's short-term performance. But as can be seen the modified model is substantially better for simulation of the long-term performance of SOECs. Even though this model only accounts for the ohmic overpotential, the model showed a very good agreement with the validation data. Because as it was mentioned above concentration and activation overpotentials have small contributions to the overall overpotential of the cells comparing to the ohmic overpotential.

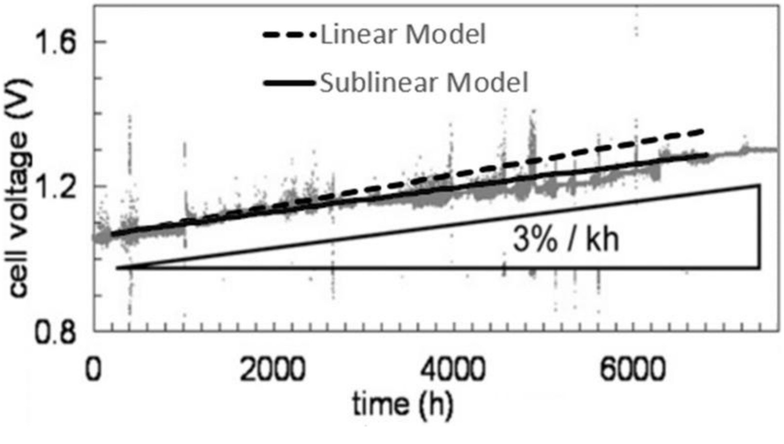

Fig. 3. Results of the simulation of long-term performance degradation in SOEC using the linear and sublinear models compared to experimental data from [25]. Our linear and sublinear models are

drawn as dashed and solid lines, respectively, on a modified version of original figure. Figure reused with permission from [13].

Even though there are not many studies in the open literature that run experiments long enough to observe the sublinear trend of degradation rate, this trend makes sense, since actual SOEC systems are operated for several years. If SOECs were degrading linearly with time at the rates suggested by the linear model, the magnitude of degradation in the long-term would be significantly higher than what actual SOECs undergo, and their lifetimes would be substantially shorter. As such it is important to use the modified model for simulation of long-term operations as it will have considerable impacts on the design and operation of large SOEC systems.

We note that this model can be further modified in the future to be more representative of degradation of SOEC stacks. Currently, there is a lack of sufficient long-term experimental data on stacks of SOEC under different operating conditions which is due to the high cost and long time of these experiments.

## 2.2.Model for Steady-State SOEC Operation

The developed data-driven model projects an increase in SOEC resistance as a result of degradation. As can be seen in Eq. 4, when quantifying the time evolution of resistance under specific operating conditions, it is necessary to know the cells' initial resistance under those conditions. The first-principles model in the literature that is commonly used to describe the steady-state performance of SOECs is applied in this work to calculate the voltage of the SOECs prior to degradation. For a more detailed description of this model, the reader is referred to [26,27]. By combining the first-principles model with Eq. 4 and Ohm's law (Eq. 5), it is possible to quantify the SOEC's performance at each time point.

$$V = i\,R \tag{5}$$

$$V_{t'} = V_0 + i * [\,0.019\,TH + 7.290\,Hi + (0.033H + 0.017i)(t')^{0.97}\,] \tag{6}$$

Where $V_0$ is the voltage of the cells at 0 h, which is obtained via the first-principles model (V). Eq. 6 is applied in the optimization problem to find the operating trajectories best suited for producing hydrogen at the minimum cost. The details of the optimization problem will be discussed in the next section.

## 3. Methodology: Eco-Technoeconomic Analysis of SOECs

The aforementioned model (Eq. 6) was employed in an eco-technoeconomic analysis (eTEA) to determine the optimal trajectories for generating hydrogen via SOECs economically, while accounting for cell degradation. Specifically, this eTEA aimed to minimize the levelized cost of hydrogen (LCOH) generated by SOECs during their operational lifespan. Although LCOH has been computed for SOEC systems in a number of prior studies,[11,12,28] we are unaware of any previous eTEA that accounts for SOEC degradation. This factor is critical, as the rate of SOEC degradation which changes in response to the operating conditions, can substantially impact the lifetime and economic efficiency of SOECs. Thus, the present research makes an important contribution to the literature, as it provides a realistic answer to the long-standing question: "can SOECs, with their existing design and structure, become economically competitive with current hydrogen-production technologies?"

Due to the lack of a definitive definition for the lifetime of SOECs or SOFCs, we include cell lifetime as a parameter in this eTEA's optimization problem, which outlines our planned cell-replacement schedule.[29] The optimization problem contains a number of assumptions. First, it is assumed that the problem is solved over a 20-year project lifetime, and that the SOECs have a lifetime of $L$ years. SOECs are decommissioned after $L$ years of operation and replaced with identical new cells with the same active membrane area and operating conditions. Second, it is assumed that the lifetime parameter ($L$) ranges from 1 to 14 years, and that the problem is solved for each $L$ value separately.[29] SOFCs and SOECs can experience catastrophic failure during long-term operations; the duration of operation prior to catastrophic failure depends on the cell's operating conditions and cannot be predicted by existing degradation models. In a recent experimental study on SOECs, researchers were able to assess the performance of SOECs for 14 years prior to catastrophic failure.[30] To the best of our knowledge, this is the longest time reported for the operation of solid oxide cells before catastrophic failure occurred. As such, we took 14 years as the maximum replacement time, and we solved the problem for replacement periods of 1 to 14 years. These are the same as the assumptions used in our previous TEA of SOFCs.[29]

We implemented and solved the economic hydrogen-production optimization problem in general algebraic modeling system (GAMS). The objective in doing so was to determine the optimal active membrane area for use in SOECs and their optimal operating trajectories for generating hydrogen with a minimal LCOH. We also used CONOPT solver, which is well-suited to solving large non-linear problems (NLP) quickly, and is particularly suitable in situations where a feasible solution cannot be easily achieved.[31] A description of the system and a detailed mathematical explanation of the problem is provided below for SOECs with L years replacement plan.

$$\min_{T_j,H,i_j,A_m,X_j} LCOH \tag{7}$$

A number of equations have been used to calculate $LCOH$ that are slightly different from one another. In this study, we selected Eq. 8 to calculate $LCOH$ because it accounts for the time value of money and it is the equation most commonly used in the literature.[11,32,33]

$$LCOH = \frac{CRF \times CC+OC+EC}{n_{H_2,del,tot} \times HHV_{H_2} \times 0.28 \times 10^{-3} \frac{kWh}{kJ}} \tag{8}$$

In this equation: $LCOH$ is calculated in \$/kWh$_{\mathrm{HHV}}$; $CC$, $OC$, and $EC$ are the total capital costs, non-electricity operating and maintenance costs, and electricity costs (\$), respectively; $n_{H_2,del,tot}$ is the total moles of hydrogen delivered by SOECs over the 20-year life of the plant (mol); $\mathrm{HHV}_{\mathrm{H}_2}$ is the higher heating value of hydrogen (285.8 kJ/mol); and CRF is the capital recovery factor. The CRF is calculated as follows:

$$CRF = \frac{r \times (1+r)^N}{(1+r)^N - 1} \tag{9}$$

Where $r$ is the discount rate, which is set at a value of 10%, and $N$ is the plant's lifetime, which is 20 years in this work.

Subscript $j$ in the decision variables (Eq. 7) is the time-step indicator. Each time step in this optimization problem is 5 days (120 hours), meaning that there are 73 time steps every year. Decision variables such as temperature, current density, and mole gas recycled per mole produced ($X$) are functions of time and are held constant for each time step. In contrast, fuel gas humidity is not time dependent.

Eqs. 10-12 show the lower and upper bounds for temperature, current density, and fuel gas humidity in the optimization problem. These are the acceptable ranges found for the operation of SOECs in the open literature.[1,7,14] The fuel gas should contain some hydrogen to make a reducing environment and prevent fuel electrode oxidation. Usually, a minimum content of 20% hydrogen is required for this purpose.[14,34]

$$923 \leq T_j \leq 1073\ (K) \tag{10}$$

$$100 \leq i_j \leq 18000\ (A/m^2) \tag{11}$$

$$0.4 \leq H \leq 0.8 \tag{12}$$

As can be seen in Eq. 4, the resistance of the cells, and thus their degradation, is highly affected by the current density. Additionally, the hydrogen molar production rate varies in response to changes in the current density. Thus, sudden or large variations in the current density should be avoided to ensure safe and realistic operation. As noted above, current density is held fixed for each time step, and Eq. 13 is then used to ensure that it changes less than ±10% for the next time step.

$$0.9 \times i_{j-1} \leq i_j \leq 1.1 \times i_{j-1} \tag{13}$$

Temperature also significantly impacts the degradation and lifetime of SOECs. Abrupt changes to the cell's temperature or extensive temperature gradients along the cells should be avoided, as they may result in catastrophic failure. Due to a lack of information, the proposed model of SOEC degradation cannot predict when catastrophic failure will happen under different operating conditions. As such, we employ conservative constraints to encourage safe long-term SOEC operation. The temperature of the cells is constant for each time step and constrained to vary less than ±1% for the next time step via Eq. 14.

$$0.99 \times T_{j-1} \leq T_j \leq 1.01 \times T_{j-1} \qquad 14$$

The following constraints are added to limit the temperature gradient between the inlet and outlet of the cells to ±1% of the cells' temperature.

$$0.99 \times T_j \leq T_{in,j} \leq 1.01 \times T_j \qquad 15$$

$$0.99 \times T_j \leq T_{out,j} \leq 1.01 \times T_j \qquad 16$$

The voltage of the cells is calculated via Eq. 6. Normally, SOECs have a voltage of between 0.6 to 1.8 V.[35]

$$0.6 \leq V_j \leq 1.8 \qquad 17$$

The mass balance of the system is provided in the following equations. As it was mentioned in section 2 the hydrogen molar production rate has a linear correlation with the current supplied to the cells and Eq. 1 can be rewritten as:

$$\dot{n}_{H_2\,p,j} = \frac{A_m \times i_j \times 3600\,\frac{s}{h}}{2 \times F} \qquad 18$$

where $\dot{n}_{H_{2,p,j}}$ is the molar production rate of hydrogen in (mol/h) and F is the Faraday constant. The steam molar consumption rate is equal to the production rate of hydrogen, as shown in Eq. 19.

$$\dot{n}_{H_2O_{c,j}} = \dot{n}_{H_{2,p,j}} \qquad 19$$

SOECs do not utilize all of the steam they are supplied with. The molar rate at which steam is fed into the cells can be calculated as follows via Eq. 20.

$$\dot{n}_{H_2O_{in,j}} = \frac{\dot{n}_{H_2O_{c,j}}}{SU} \qquad 20$$

In this equation, $SU$ is steam utilization, which is assumed to be 80% in this study. The inlet stream to SOECs consists of steam and some hydrogen. If the fuel gas humidity and steam supply molar rate are known, then the molar rates of total fuel gas supply and the hydrogen content of the fuel gas can be determined using Eqs. 21 and 22, respectively.

$$\dot{n}_{TOT_{in,j}} = \frac{\dot{n}_{H_2O_{in,j}}}{H} \qquad 21$$

$$\dot{n}_{H_2\,in,j} = (1 - H) \times \dot{n}_{TOT_{in,j}} \qquad 22$$

where $\dot{n}_{TOT_{in,j}}$ and $\dot{n}_{H_2\,in,j}$ are the molar rates of the total inlet fuel gas and its hydrogen content, respectively. The cathode outlet contains hydrogen and some unreacted steam. Next, the molar rates of the gases in the cathode outlet can be determined via Eqs. 23 and 24.

$$\dot{n}_{H_2\,out,j} = \dot{n}_{H_2\,in,j} + \dot{n}_{H_2\,p,j} \qquad 23$$

$$\dot{n}_{H_2O_{out,j}} = \dot{n}_{H_2O_{in,j}} - \dot{n}_{H_2O_{c,j}} \qquad 24$$

Pure oxygen is produced by the electrolysis reaction and leaves the anode at the following rate,

$$\dot{n}_{O_2\,out,j} = 0.5 \times \dot{n}_{H_2\,p,j} \tag{25}$$

A part of the cathode outlet can be recycled and used in the next time periods.

$$\dot{n}_{H_2O_{in,j}} = \dot{n}_{H_2O_{f,j}} + X_j \times \dot{n}_{H_2O_{out,j-1}} \tag{26}$$

$$\dot{n}_{H_2\,in,j} = X_j \times \dot{n}_{H_2\,out,j-1} \tag{27}$$

In Eq. 26, $\dot{n}_{H_2\mathrm{O}_{\mathrm{f},j}}$ is the molar rate of fresh water to be supplied to the cells and $X_j$ is the mole recycled per total mole produced.

Finally, the rate of hydrogen delivered by the SOEC system in the $j$th time step can be determined by,

$$\dot{n}_{H_2\,del,j} = (1 - X_{j+1}) \times \dot{n}_{H_2\,out,j} \tag{28}$$

while the total moles of hydrogen delivered by SOECs over the project's 20-year lifetime is defined as,

$$n_{H_2,del,tot} = \frac{N}{L} \times \sum_{j=1}^{L\times 73} 120\ (h) \times \dot{n}_{H_2\,del,j} \tag{29}$$

where $n_{H_2,del,tot}$ is the moles of hydrogen delivered by SOECs over 20 years and $L$ is the replacement schedule or lifetime of the cells (years). To ensure a good comparison between SOECs with different replacement schedules, we restrict SOEC production to an average of 550 MW of hydrogen (based on $\mathrm{HHV}_{\mathrm{H}_2}$) over their lifetime.

$$\frac{\sum_{j=1}^{L\times 73} \dot{n}_{H_2\,del,j} \times HHV_{H_2}}{L\times 73} \times 0.28 \times 10^{-6}\,\frac{MW}{kJ/h} = 550\ (MW) \tag{30}$$

The energy balance of the system can be described by,

$$P_{DC,j} + E_{in,j} - E_{out,j} = 0 \tag{31}$$

where $P_{\mathrm{DC},j}$ is the DC power supplied to the SOECs in the $j$th time step, and $E_{in,j}$ and $E_{out,j}$ are the inlet and outlet enthalpy flows (MW), respectively. $P_{\mathrm{DC},j}$ is computed via Eq. 32.

$$P_{DC,j} = i_j \times V_j \times A_m \times 10^{-6}\ \frac{MW}{W} \tag{32}$$

To provide $P_{\mathrm{DC},j}$ (MW), AC power is drawn from the grid and converted to DC through an AC/DC inverter, which is assumed to have a 96.5% efficiency.[29] As such, AC power supply in the $j$th time step can be computed as follows:

$$P_{AC,j} = \frac{P_{DC,j}}{96.5\%} \tag{33}$$

$$Q_{in,j} = \Big[\dot{n}_{H_2\,in,j}\, C_{p\ H_2}\left(T_{in,j} - T_1\right) + \dot{n}_{H_2O_{in,j}} C_{p\ H_2O,g}\left(T_{in,j} - T_2\right) + \dot{n}_{H_2O_{in,j}} L_{v\ H_2O} + \dot{n}_{H_2O_{in,j}} C_{p\ H_2O,l}(T_2 - T_1)\Big] \times 2.8 \times 10^{-10}\ \frac{MW}{J/h} \tag{34}$$

$$Q_{out,j} = \Big[\dot{n}_{H_2\,out,j}\, C_{p\ H_2}\left(T_{out,j} - T_1\right) + \dot{n}_{H_2O_{out,j}} C_{p\ H_2O,g}\left(T_{out,j} - T_2\right) + \dot{n}_{H_2O_{out,j}} L_{v\ H_2O} + \dot{n}_{H_2O_{out,j}} C_{p\ H_2O,l}(T_2 - T_1) + \dot{n}_{O_2\,out,j}\, C_{p\ O_2}\left(T_{out,j} - T_1\right)\Big] \times 2.8 \times 10^{-10}\ \frac{MW}{J/h} \tag{35}$$

In the above equations, $C_{p\ k}$ refers to the molar heat capacity of species, $k$ (J/mol·K), which varies with temperature according to the model found in [36]. $T_1$ is the reference temperature (298 K), $T_2$ is the evaporation temperature of water at 4 bar (416 K)—the assumed operation pressure for SOECs—and $L_{v\ H_2O}$ is the latent heat of vaporization of water (J/mol).

All costs in this work are given in 2016 U.S. dollars. Unlike mature technologies, the capital costs of SOECs depend on its commercialization status and production volume. Myrdal et al. consulted number of references and calculated capital costs of SOEC systems for various production volumes at different times.[37] To reduce error, we used the SOEC system costs obtained by Myrdal et al. between 2015 and 2017 through consultations with manufacturers, rather than their predicted costs for after 2017. Myrdal et al. catalogued the costs of SOECs with production volumes ranging from 1,250 to 250,000 $m^2$/year, but we use the costs of SOECs with a production volume of 125,000 $m^2$/year in this eTEA. SOECs produced between 2015 and 2017 at rate of 125,000 $m^2$/year cost 0.24 \$/$cm^2$, which includes the ab factory and turnkey costs. Ab factory costs consists of the costs of the equipment and a 50% mark up. The balance-of-plant (BoP) items in an SOEC system normally include heat exchangers, a compressor, pumps, piping and connections, and electronics. The capital costs of BoP items, excluding the compressor, were 0.596 \$/$cm^2$ of active membrane area installed. This includes costs of heat exchangers, AC/DC inverter, pumps, and separator (flash drum). The present study does not include a detailed model for BoP components. As BoP designs will differ from case to case, it was best to restrict the boundary to the present system in order to have a more generalized result. In this study, the produced hydrogen has a high quality with ~97% purity and is used outside of the system's boundaries. As such, a high-pressure hydrogen compressor and storage are not used in this work. An outline of the system can be seen in Fig. 4.

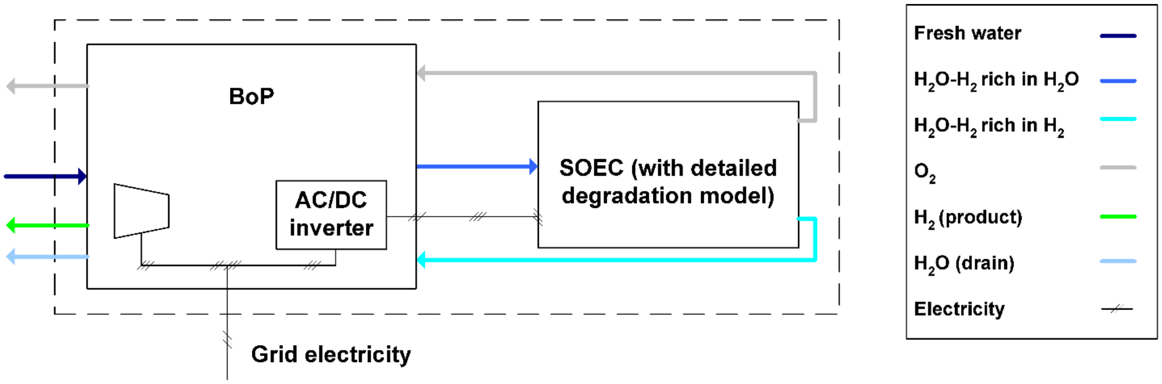

Fig. 4. An outline of the SOEC system.

In a standalone SOEC system, fresh water is evaporated and mixed with hydrogen before being fed into the SOECs. The thermal energy required to pre-heat the fuel gas stream is provided by the anode and cathode outlet streams, which leave the cells at high temperature. Heat transfer takes place through multiple heat exchangers, and the hydrogen for the fuel gas mixture is recycled from the cathode outlet. The cathode outlet pressure slightly drops in the heat exchanger before part of it is recycled and mixed with the fresh water. The recycled stream is passed through a compressor to raise its pressure to 4 bar. The compressor is an expensive component in the BoP, its size depends on the value of $X_j$, and it can substantially increase system costs. Therefore, the capital cost of the compressor is calculated separately as,

$$CC_{comp.} = UC_{comp.} \times \frac{\sum_{j=1}^{L\times73} comp.work_j}{L\times8760} \qquad 36$$

where $CC_{\text{comp.}}$ is the capital cost of the compressor ($), $\text{UC}_{\text{comp.}}$ is the unit cost of the compressor and takes the value of 24.455 $/kW, and $comp.work_j$_j is the compressor work in kWh, which is defined as follows.[37,38]

$$comp.work_j = CW \times (X_j \times \dot{n}_{H_2\,out,j} + X_j \times \dot{n}_{H_2O_{out,j}}) \times 120 \times 10^{-3} \quad 37$$

In the above equation, $CW$ is the compressor work per mole of gas (kWh/kmol), which is computed via Eq. 38, [38]

$$CW = \frac{c_p \times T_{comp.in}}{\eta_{comp.}}(CPR^{\frac{\gamma-1}{\gamma}} - 1) \quad 38$$

where $c_p$ is the specific heat capacity of the gas (kWh/kmol·K); $T_{comp.in}$ is the temperature of the gas at the compressor inlet and is assumed to be 453 K; $\eta_{comp.}$ is the compressor efficiency, which is assumed to be 82%; $CPR$ is the compressor pressure ratio; and $\gamma$ is the specific heat ratio.

$$CPR = \frac{Pr_{comp.out}}{Pr_{comp.in}} \quad 39$$

In Eq. 39, $Pr_{comp.in}$ and $Pr_{comp.out}$ are the pressure of the gas at the inlet and outlet of the compressor, which are 3.9 and 4 bar in this study, respectively.

The capital costs of SOEC and the remaining of BoP components are given in Eqs. 40 and 41.

$$CC_{SOEC} = \frac{N}{L} \times UC_{SOEC} \times A_m \times 10^4 \quad 40$$

$$CC_{BoP} = UC_{BoP} \times A_m \times 10^4 \quad 41$$

In the above equations, $CC_{\mathrm{SOEC}}$ and $CC_{\mathrm{BoP}}$ are the capital costs of the SOEC and BoP items (\$), respectively, and $\mathrm{UC}_{\mathrm{SOEC}}$ and $\mathrm{UC}_{\mathrm{BoP}}$ are the costs of the SOEC and BoP items per active membrane area, which, as noted above, take the values of 0.24 and 0.596 \$/cm$^2$, respectively. The cost of electricity consumed by the compressor and the SOECs can be obtained using the following equation,

$$EC = \frac{N}{L} \times R_{El} \times \left( \sum_{j=1}^{L\times 73} P_{AC,j} \times 120 \times 10^3 + comp.work_j \right) \quad 42$$

where $R_{\mathrm{El}}$ is the electricity rate in \$/kWh. A rate of 0.14 \$/kWh, which is the average price for electricity in Canada, was used in the base-case optimization problem. The operating and maintenance cost is defined via Eq. 43,

$$OC = UC_{oper.} \times n_{H_2,del,tot} \times M_{H_2} \times 10^{-3} \quad 43$$

where $M_{H_2}$ is the molar mass of $H_2$ (2 kg/kmol) and $UC_{oper.}$ is the operating and maintenance cost per kg of hydrogen delivered, which takes a value of 0.452 \$/kg $H_2$. The value used for $UC_{oper.}$ was obtained based on information published by the United States Department of Energy (U.S. DOE).[39]

# 4. Results and Discussion

## 4.1. Base Case Optimization

Fig. 5 shows the minimum LCOHs obtained for SOECs with replacement schedules ranging from 1 to 14 years. As can be seen, SOECs with shorter replacement plans have higher LCOHs, as they need to be replaced with new cells more often over the plant's 20-year lifespan. At this point, it is necessary to note that the obtained results may not be globally optimal, as CONOPT is a local solver. A feasible solution for this optimization problem was difficult to attain. We first tried solving the base-case optimization problem using BARON and ANTIGONE, which are global solvers, but neither were able to arrive at a feasible solution. As such, we employed CONOPT, which is suitable for solving problems where feasibility is difficult to achieve. The optimal solutions determined by CONOPT for SOECs were entered as initial guesses into BARON, which was able to converge upon the same optimal solutions as CONOPT, which guarantees them as a globally optimal solution. A reduction in LCOH can be obtained with longer replacement schedules as can be seen in Fig.5. The differences in LCOH diminish as the lifetime of SOECs increases. Such that the differences are more observable for 1- to 7-year replacement schedules and less distinguishable for longer replacement plans.

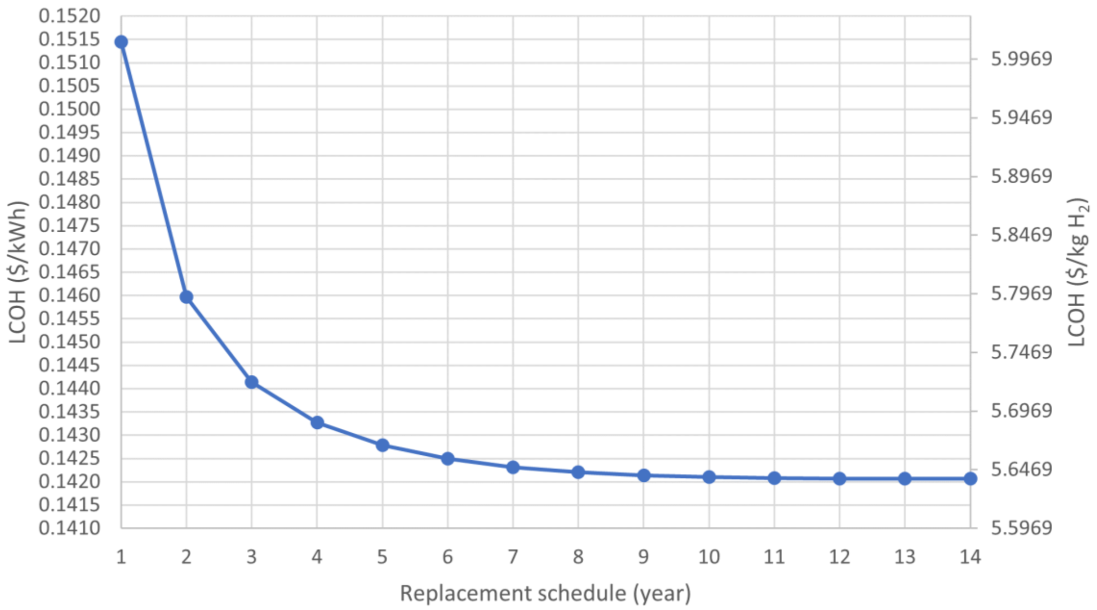

Fig. 5. Minimum LCOHs for SOECs with different replacement schedules.

Fig. 6. illustrates the optimal membrane area sizes, average current densities, and average operating temperatures of SOECs. As shown in Eq. 6, SOECs that are supplied with higher current densities and operated at higher temperatures experience greater degradation over time. While operating cells at lower temperatures and current densities can enable longer lifetimes, the use of lower current densities results in diminished hydrogen production (Eq. 18). As such, when operating cells at lower current densities, it is necessary to use larger active membrane areas to meet the average hydrogen production constraint (Eq. 30). Although the required membrane area size increases alongside the replacement time, the need to replace SOECs less frequently in these cases makes the entire system more cost-effective.

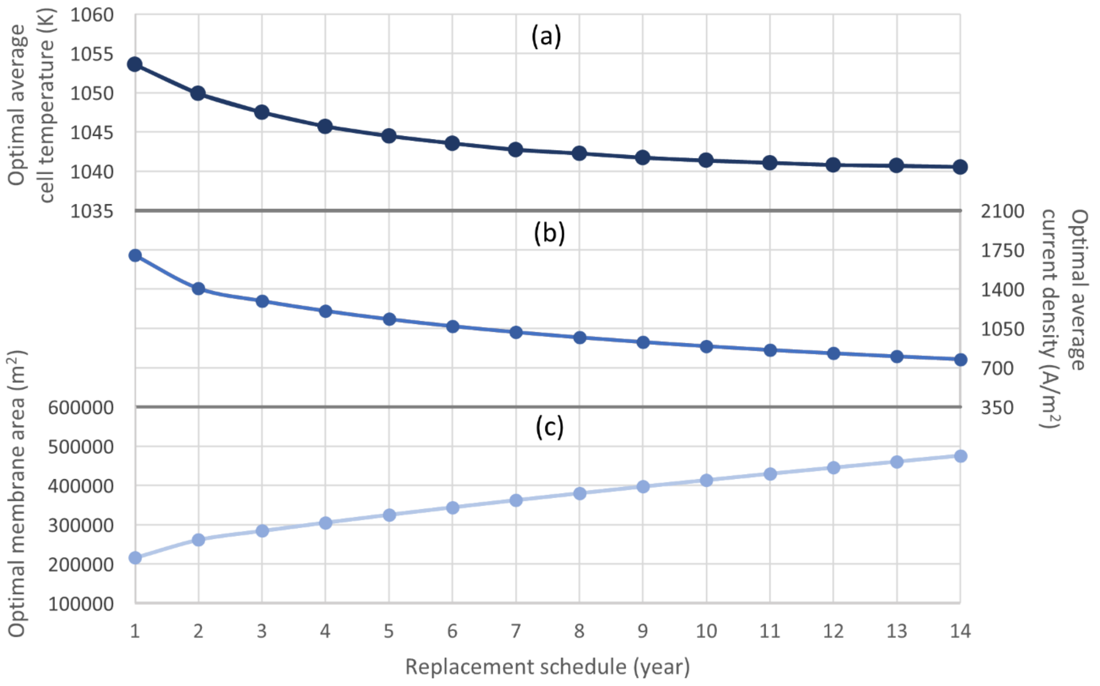

Fig. 6. Optimal (a) average temperature, (b) average current density, and (c) average membrane area of SOECs with replacement schedules from 1 to 14 years.

Hydrogen-delivery yield increases as the fuel gas humidity is increased. As a result, the optimizer found 80% molar humidity for optimal operation of SOECs with any replacement schedule which is the maximum humidity allowed in this problem. The findings revealed that the optimal average mole recycled per mole produced is almost the same for all replacement plans (23.7%). Similarly, the optimal average voltage was also relatively the same for all cases (1.29 V). Moreover, the optimal trajectories revealed that time variations in the optimal mole recycled per mole produced and optimal voltage are insignificant. The optimal trajectories for the operating temperature and current density for the 2-, 5, and 10-

years replacement plans are shown in Fig. 7. For economically optimal operation, current density and temperature should reduce over the lifespan of the SOEC to lower its degradation rate. The optimal trajectories for current density in the first 2 years of operation for SOECs with 5- and 10-year replacement plans are very similar to those of an SOEC with 2-year replacement plan and they can not be discerned in this figure. Also, the optimal current density trajectories in the first 5 years of operation for an SOEC with 10-year replacement plan are very similar to those of an SOEC with 5-year replacement plan and they can not be distinguished in Fig. 7. Even though the upper bound of current density was defined as 18,000 A/m$^2$, the optimal value barely reaches 1780 A/m$^2$ in the beginning of the cell's operation and is reduced over time due to its significant influence on degradation.

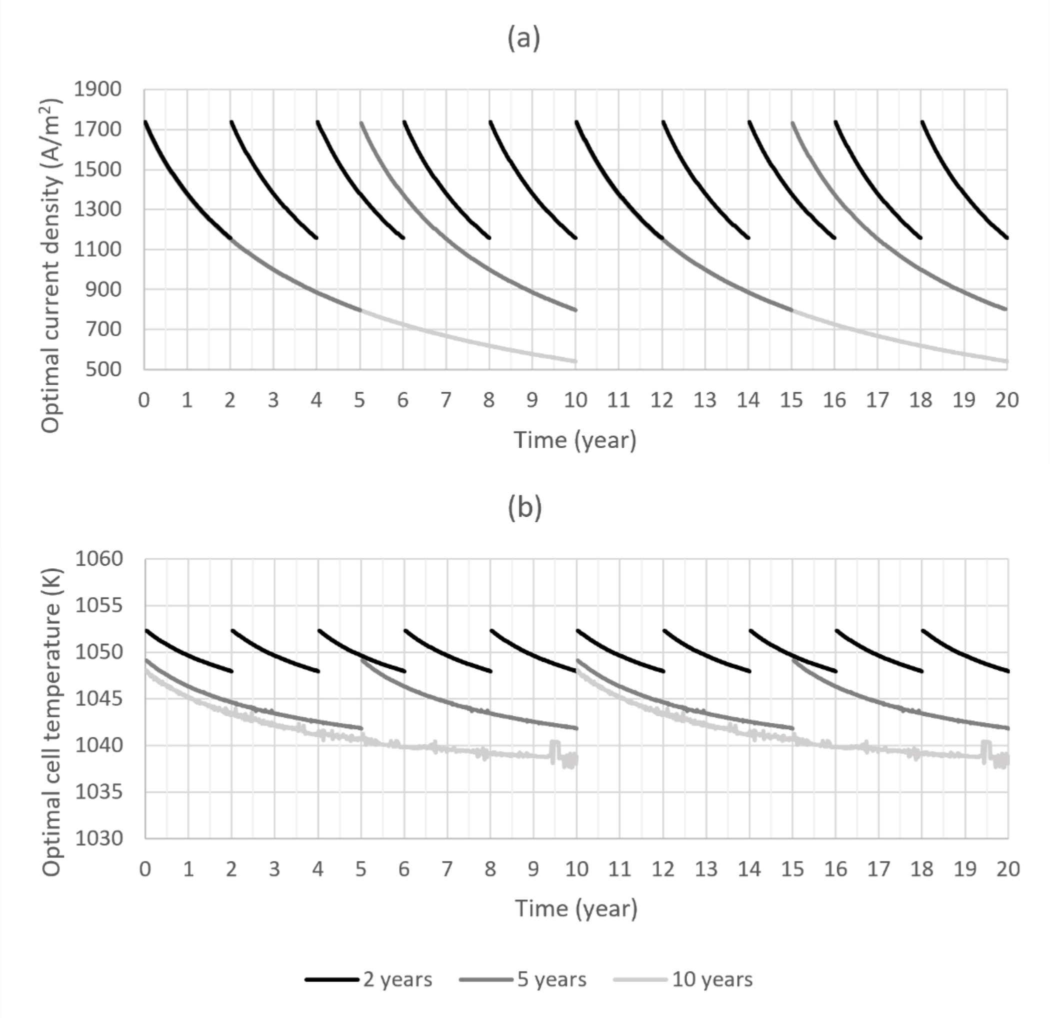

Fig. 7. Trajectories of (a) optimal current density and (b) optimal temperature of SOECs with 2-, 5-, and 10-year replacement schedules over a 20-year project lifespan.

## 4.2.Sensitivity Analysis

As discussed in Section 4, the capital cost of SOECs varies with production volume and the cells' commercialization status. Specifically, the capital costs of SOECs are high for non-commercial, custom-made, small-scale systems, and much lower for large-scale commercial systems. To quantify the sensitivity of the LCOH to the capital cost of SOECs, we repeated the optimization problem for capital costs of 0.12, 0.48, and 0.72 $/cm$^2$, while keeping the remaining conditions, including the other cost parameters, used in the base-case problem described in the previous section. The following trends emerged from this analysis. First, reducing the capital cost from 0.72 to 0.12 $/cm$^2$ resulted in a 21.4% decrease in the LCOH of 1-year SOECs (Fig. 8a). Second, the findings showed that the impact of capital cost on the economics of the system decreases as replacement time increases. For instance, reducing the capital cost from 0.72 to 0.12 $/cm$^2$ resulted in a 6.4% and 3.5% decline in the LCOH of 5- and 14-year SOECs, respectively. Finally, the analysis showed that the tendency for LCOH to decrease as SOEC lifetime increases becomes more observable at higher capital costs. For example, the difference between the LCOHs of SOECs with various lifetimes was more distinct at the relatively high capital cost of 0.72 $/cm$^2$.

The price of electricity varies depending on a grid's location and power generation techniques. To investigate how electricity prices influence the LCOH, we tested prices ranging from 0.06 $/kWh (the lowest rate in Canada, which is for the Quebec grid) to 0.30 $/kWh (the highest electricity rate in Canada, which is for northern grids) at 4-cent increments.[40,41] The optimization problem was solved for the different electricity prices, while all other cost values were kept the same as in the base-case problem. The results showed that the price of electricity significantly influences the LCOH, such that an 80% drop in the price of electricity results in a ~73% decline in the LCOH (Fig. 8b). As such, depending on the grid's electricity rate, SOECs may either be an economical option for hydrogen generation or a very expensive one.

The results of the sensitivity analysis can be of great help to decision makers in selecting the proper technology for energy storage or hydrogen production in specific regions.

Figs. 9a and 9b show the cost breakdowns of SOEC systems supplied with electricity at the lowest (0.06 $/kWh) and highest (0.30 $/kWh) prices considered in this study, respectively. The total electricity consumed at a rate of 0.30 $/kWh costs five times as much as the total electricity consumed at a rate of 0.06 $/kWh. Thus, SOECs supplied with electricity at higher price had higher capital costs than those supplied with cheaper electricity. The reason for this result is that, when electricity was expensive, the optimizer tried to lower electricity consumption by using larger SOECs and lower current densities. Since the cost of BoP also depends on the size of the cells, SOECs with more expensive electricity had higher BoP capital costs. On the other hand, the operation and maintenance costs were calculated based on the mass of hydrogen produced; thus, they were found to be almost the same for all SOECs.

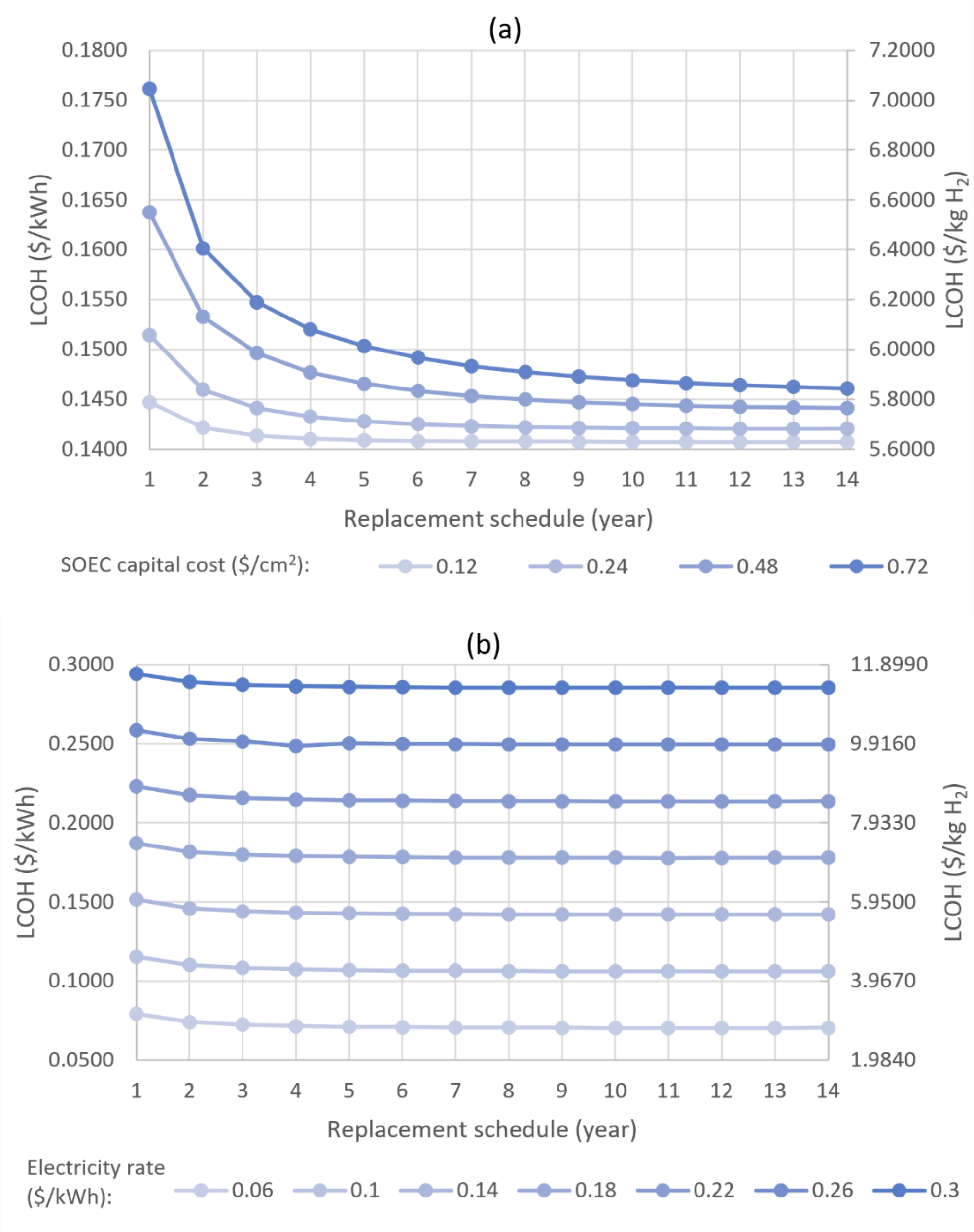

Fig. 8. Impacts of (a) capital costs (b) electricity price on the LCOH of SOECs with various replacement schedules.

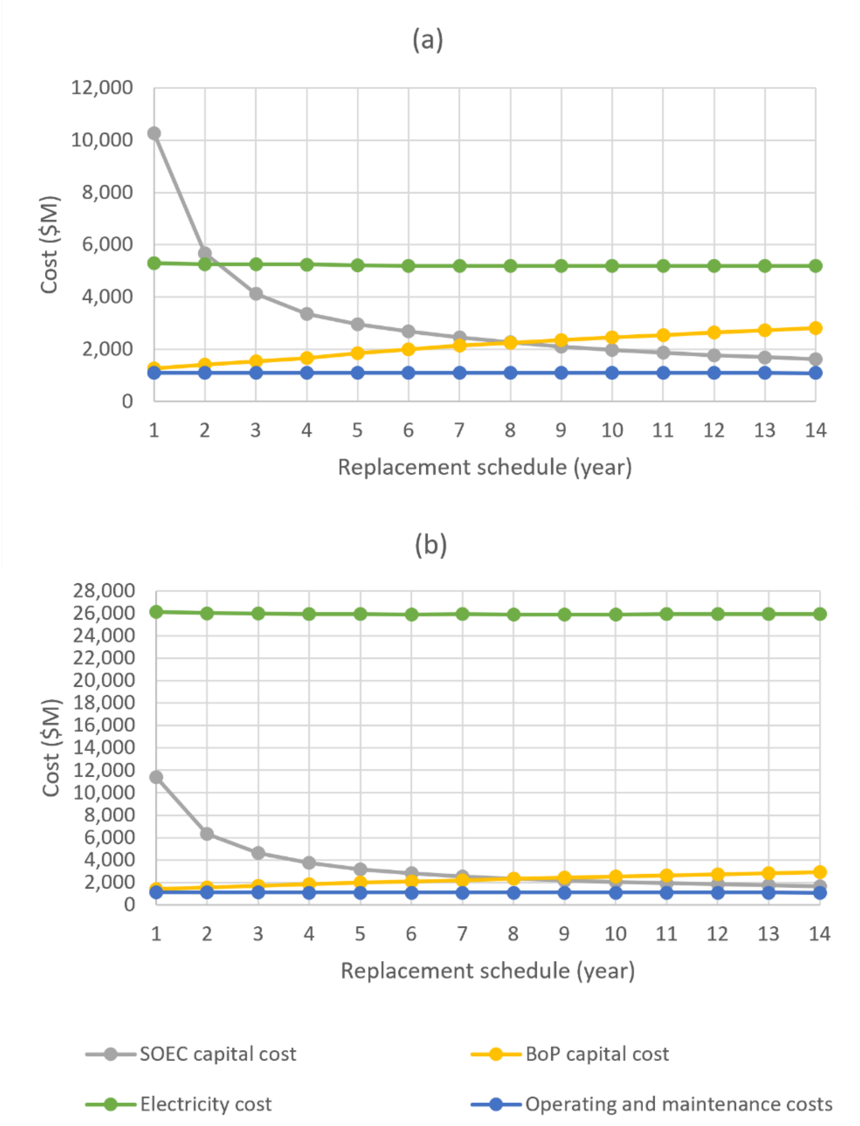

Fig. 9. Cost breakdown of SOEC systems supplied with electricity at (a) 0.06 $/kWh and (b) 0.30 $/kWh.

# 5. Greenhouse Gas (GHG) Emissions from SOEC Manufacturing and Operation

Hydrogen generated through the use of electrolysers has no direct GHG emissions from the water electrolysis process. However, a more detailed environmental assessment is required to quantify the life cycle environmental impact of hydrogen production via SOECs. To this end, we calculated the life cycle GHG emissions created by the SOEC manufacturing process, as well as the life cycle GHG emissions from various electricity generation routes. A number of different grids and various primary energy sources were studied to determine how the electricity generation route impacts the environmental performance of the SOECs. The GHG emissions from the manufacturing of SOFCs was calculated in a prior work where we conducted an environmental analysis based on detailed life cycle inventory data for the manufacturing SOFCs.[42] Since SOECs and SOFCs have the same components, the GHG emissions determined for manufacturing SOFCs in the aforementioned study (1087 kgCO$_2$ eq per m$^2$ of active membrane area) were used for SOECs in the current analysis. The CO$_2$eq emissions from the manufacturing of BoP items are not included in this analysis due to a lack of knowledge regarding the exact size of the equipment and a lack of detailed inventory data. The power sources and power grids considered in this environmental assessment are given in Table 1. Life cycle GHG emissions of Quebec grid are almost identical to those of the hydroelectric power plant as 94% of the Quebec's electricity is generated by hydroelectric resources.[43]

Table 1. Electricity generation routes studied in this work and their CO2eq emissions.

| Electricity generation | GHG emissions (kgCO$_2$ eq/kWh) | ref. |
|---|---|---|

| | | |
|---|---|---|
| Ontario grid | 0.040 [1] | [44] |
| Alberta grid | 0.790 [1] | [44] |
| Quebec grid | 0.001 [1] | [44] |
| Nuclear power | 0.029 [2] | [45] |
| Coal fired power plant | 0.888 [2] | [45] |
| NG power plant | 0.499 [2] | [45] |

[1] The source does not mention whether these are direct emissions from the plants or their life cycle emissions.

[2] These are life cycle GHG emissions. The reference did not specify types of nuclear and NG plants.

The GHG emissions produced from the manufacturing of SOECs and the electricity supply required per kg of hydrogen generated by SOECs under optimal conditions are depicted in Fig. 10. As can be seen, the electricity generation route significantly impacts the GHG emissions per mass of hydrogen produced. Moreover, SOECs with longer replacement times produce lower GHG emissions, as they require a smaller overall membrane area over the 20-year project lifespan. The life cycle GHG emissions per kg of hydrogen produced ranges from 0.34 kg $CO_2$eq (for 14-year SOECs connected to the Quebec grid) to 38.60 kg $CO_2$eq (for 1-year SOECs with coal-fired power generation). These findings demonstrate that hydrogen generated using electrolysers is not necessarily green. Even though electrolysers do not directly produce GHG emissions, they do consume a large amount of electricity; as such, the GHG emissions produced in generating this electricity should be accounted for when evaluating the electrolyser's environmental performance. The GHG emissions of the electricity route and the price of electricity are key factors in determining whether electrolysers are the proper technology for hydrogen production in a specific region. For instance, SOECs are not an environmentally friendly option for hydrogen generation in Alberta, or in areas where electricity is generated by coal power plants. In contrast, running SOECs with electricity from the Quebec grid or nuclear power enables the production of green hydrogen, which has extremely low GHG emissions.

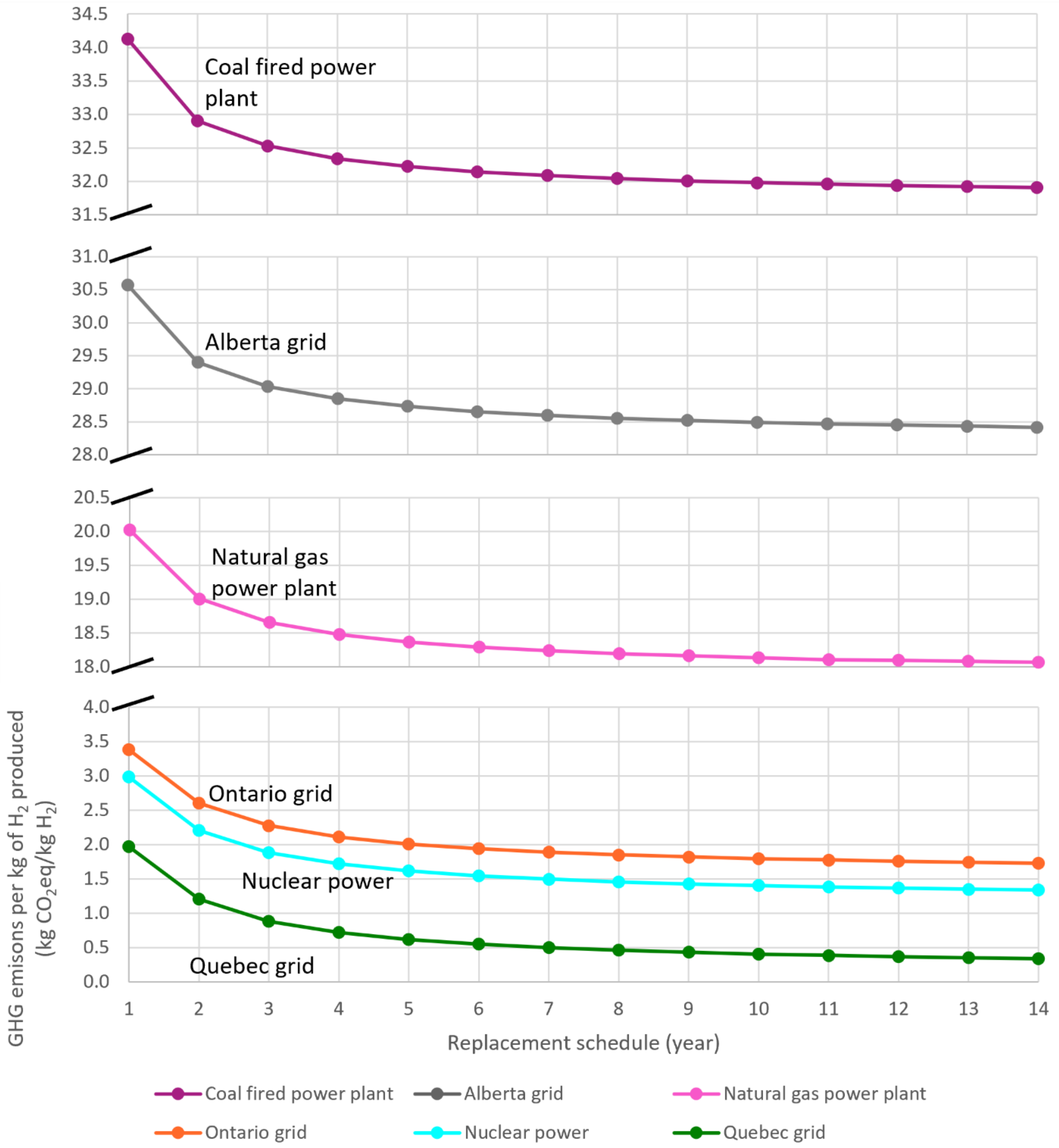

Fig. 10. Life cycle GHG emissions per kg of hydrogen produced by SOECs with various power sources.

Fig 11. shows a comparison of the results in the present work to other hydrogen production systems as reported in the literature. The boxes in Fig. 11 show the range of as-reported life cycle $CO_2$eq emissions of various hydrogen-production technologies versus their LCOH. These ranges were determined by Parkinson et al. through a review of several sources.[46] Notably, the type of electrolysers were not specified in the as-reported data. The scatter points show the results obtained for SOECs in the present study, and the impact of the replacement schedule on both the LCOH and GHG emissions is also illustrated. As can be seen, SOECs with shorter lifetimes have higher a LCOH and GHG emissions given the same power source and price of electricity. SOECs powered by low-carbon electricity have very low life cycle GHG emissions and can be competitive with existing clean technologies such as Cu-Cl cycle and S-I cycle in terms of environmental and economic metrics when the electricity is 0.06 $/kWh. Conversely, the results clearly indicate that SOECs supplied with power from the Alberta grid or coal-fired plants provide inferior environmental performance compared to other technologies. SMR, which is a mature and cost-effective hydrogen-generation route, emits between 10.72 to 15.86 kg $CO_2$eq per 1 kg hydrogen. SMR emissions are comparable to SOECs powered by NG, and are only exceeded by those of SOECs connected to high-carbon grids (Alberta power grid and coal-fired power plants) and coal gasification. SOECs powered by electricity from the Ontario or Quebec grids, and nuclear plant all had lower GHG emissions than SMR. The addition of carbon capture and sequestration (CCS) can reduce the life cycle GHG emissions of SMR and coal gasification by at least 45% and 64%, respectively. In addition, the highest LCOH reported for SMR and coal gasification with CCS are 1.73 and 2.75 times higher than their lowest LCOHs without CCS, respectively.[46]

As shown in Fig. 11, some technologies have large ranges of LCOH or GHG emissions, which may be due to the wide ranges of system capital costs, fuel and electricity prices, and emissions in various regions, or even the use of different assumptions in different studies. As such, this plot would benefit from standardization in which all reported values across the literature were recomputed to instead consider the exact same parameters such as system scale, energy supply chain (cost, energy type, and associated life cycle impacts), same location of construction, same quality of $H_2$ produced, same project and currency year, etc. However, this is beyond the scope of the present study and can be pursued in future research.

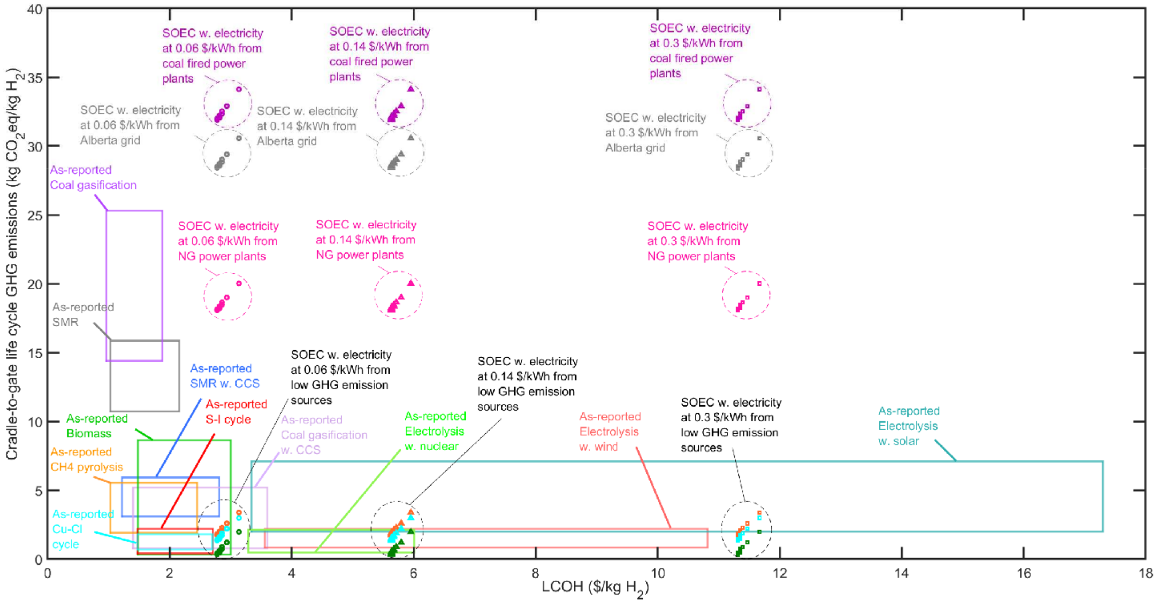

Fig. 11. Life cycle GHG emissions of various hydrogen-production methodologies versus their LCOH. The boxes show as-reported data ranges collected by Parkinson et al.[46] Scatter points have been calculated for SOECs in this study. Marker types indicate the electricity price. Circles, squares, and triangles indicate electricity at 0.06, 0.14, and 0.30 \$/kWh, respectively. Points colors specify the supplied electricity source as follows:

▬ Coal power plant, ▬ Alberta grid, ▬ NG power plant, ▬ Ontario grid, ▬ Nuclear power, ▬ Quebec grid.

## 6. Cost of $CO_2$ Avoided

The cost of $CO_2$ avoided (CCA) is a metric that is used to quantify the excess costs accrued from reducing $CO_2$eq emissions by 1 tonne compared to the base-case technology. Even though assumptions are always made in the definition of the CCAs, this metric enables comparisons of various technologies to determine the most economical and environmentally friendly option. In this study, SMR was used as the status quo system. The CCA was defined as the additional costs a technology must incur to avoid the $CO_2$ emissions of SMR (grey hydrogen, without CCS) over the amount of avoided $CO_2$ emissions (Eq. 44).

$$CCA = \frac{LCOH_{technology} - LCOH_{SMR}}{GHG_{SMR} - GHG_{technology}} \tag{44}$$

where $LCOH_{technology}$ and $GHG_{technology}$ are the $LCOH$ and $GHG$ emissions of the investigated technology in \$/tonne $H_2$ and tonne $CO_2$/tonne $H_2$, respectively, and $LCOH_{\mathrm{SMR}}$ and $GHG_{\mathrm{SMR}}$ are the average of the LCOHs and the GHG emissions reported by Parkinson et al. for SMR (i.e., 1280 \$/tonne $H_2$ and 12.4 tonne $CO_2$/tonne $H_2$). This metric is beneficial for selecting the technology that will incur the lowest costs to reduce GHG emissions. Operating costs such as fuel and electricity prices generally change based on location, as do the life cycle GHG emissions of the fuel and electricity used in these technologies. As such, the same technology can have a range of CCAs depending on where it is implemented. Table 2 presents the CCA values for SOECs on a 5-year replacement schedule operated using electricity from low-GHG-emission power sources obtained at three different prices. The CCAs of SOECs operated with electricity from the Alberta grid, coal-fired, and NG-based power plants are undefined (negative values), as they are more expensive and emit more GHGs compared to SMR.

Parkinson et al. reported CCAs ranging between 97-110 \$/tonne $CO_2$ for SMR systems equipped with CCS (so called "blue hydrogen"). These were calculated for supply chain emissions of 2.97 to 9.16 kg $CO_2$/kg $H_2$. A comparison of the CCAs listed for CCS-equipped SMR and SOECs in Table 2 indicates that, in the current market, SMR with CCS is more efficient at reducing $CO_2$ emissions. Although the use of SOECs to produce hydrogen results in lower GHG emissions (Fig. 11), SMR with CCS remains the preferable option based on the CCA. However, this could change if the capital costs of SOEC can be reduced or if the SOEC can be supplied with less expensive electricity. It is worth noting that the SMR with CCS option requires the existence of CCS infrastructure, such as pipelines and geological sequestration, which may be difficult to achieve, especially in the short term, and so SOECs may still be the practical alternative. It is also worth noting that if the SOEC is operated only during overnight hours when the electricity demand is lower and the electricity is cheaper, the LCOH—and hence, the CCA values—of the SOEC will be significantly lower. Unfortunately, there is a paucity of long-term experiments and adequate data on how cyclic operation affects long-term SOEC degradation. The experimental data used to generate the data-driven degradation-based model in this work were collected from the continuous operation of SOECs. Therefore, the model does not predict performance degradation under cyclic operation. For these reasons, the cyclic operation of SOECs was not studied in this work.

Table 2. CCA values for 5-year SOECs supplied with electricity from various power sources at 0.06, 0.14, and 0.3 $/kWh.

| | CCA ($/tonne $CO_2$) (Electricity 0.06 $/kWh) | CCA ($/tonne $CO_2$) (Electricity 0.14 $/kWh) | CCA ($/tonne $CO_2$) (Electricity 0.3 $/kWh) |
|---|---|---|---|
| SOEC-Ontario grid | 148 | 423 | 969 |
| SOEC-Nuclear | 143 | 408 | 934 |
| SOEC-Quebec grid | 131 | 373 | 855 |

## 7. Conclusion

The findings of this study revealed that it is possible to decelerate the degradation of SOECs, increase their operating lifetime, and lower their LCOH by adjusting the operating conditions. Furthermore, this study identified the optimal operating trajectories under which SOECs can be used for economical hydrogen generation over a particular length of time. This study revealed that the key to expanding the lifetime of SOECs is to gradually decrease the supplied current density and operating temperature.

A sensitivity analysis was conducted to quantify how capital costs and electricity price impact the LCOH of SOECs. The results of this sensitivity analysis can be used to determine whether SOECs are an economical option for hydrogen production in a particular region, depending on their commercial status and the price of electricity.

Lastly, this study evaluated the environmental performance of SOECs by calculating their life cycle GHG emissions per kg of hydrogen delivered. Even though electrolysers do not have direct GHG emissions, this study revealed that their life cycle GHG emissions can vary from very low levels (comparable to those of the cleanest hydrogen-production processes, such as Cu-Cl cycle) to very high amounts (more than those of the SMR process). The findings also revealed that the source of electricity has a significant impact on the environmental performance of SOECs; specifically, it was observed that SOECs may or may not be an environmentally friendly option for hydrogen production depending on how the electricity they use is generated. Finally, the CCA was calculated to help decision makers assess SOECs based on their environmental and economical performance and compare it with other technologies.

## 8. Future work

As mentioned previously, the widespread use of low-carbon power generators such as nuclear, solar, and wind plants is a key step toward a low-carbon future. However, the intermittency of solar and wind power limits their application compared to more consistent power sources. The scope of this study is limited to SOECs that use always-available power sources. Future work will consider wind and solar generators in combination with a variety of energy storage technologies (such as batteries, pumped hydro, or compressed air energy storage) or secondary generators such as natural gas peaking power plants to provide a consistent source of electricity. It would be interesting to determine how this impacts the economics and life cycle greenhouse gas emissions, and whether they might be suitable alternatively to those presented in the present work.

# Acknowledgement

We gratefully acknowledge Natural Sciences and Engineering Research Council of Canada [NSERC CRDPJ 509219-2017] and the Ontario Centre of Excellence [OCE 27851-2018] for financially supporting this research.

**Nomenclature**

| | |
|---|---|
| $t'$ | time since 200 h (h) |
| R | ohmic resistance (mΩ.cm$^2$) |
| $T$ | temperature (°C or K) |
| $H$ | fuel gas humidity as mole fraction of water |
| $i$ | current density (A/cm$^2$ or A/m$^2$) |
| $LCOH$ | levelized cost of hydrogen ($/kWh or $/kg $H_2$) |
| $A_m$ | active membrane area (m$^2$) |

| | |
|---|---|
| $X$ | mole of gas recycled per mole produced |
| CRF | capital recovery factor |
| N | life of the plant (year) |
| $L$ | replacement schedule (year) |
| $r$ | discount interest rate |
| HHV | higher heating value (kJ/mol) |
| $CC$ | capital costs ($) |
| $OC$ | non-electricity operating and maintenance costs ($) |
| $EC$ | electricity costs ($) |
| $V$ | voltage (V) |
| $\dot{n}$ | molar rate (mol/h) |
| F | Faraday constant (C/mol) |
| SU | steam utilization factor |
| $P_{DC}$ | DC power (MW) |
| $P_{AC}$ | AC power (MW) |
| $E$ | heat flow (MW) |
| $C_p$ | molar heat capacity (J/mol.K or kWh/kmol.K) |

| | |
|---|---|
| $L_v$ | latent heat of vaporization (J/mol) |
| $comp.work$ | compressor work (kWh) |
| $CW$ | compressor work per mole of gas (kWh/kmol) |
| $CPR$ | compressor pressure ratio |
| $Pr$ | pressure (bar) |
| $R_{El}$ | electricity rate ($/kWh) |
| $M_{H_2}$ | molar mass of $H_2$ (2 kg/kmol) |
| $CCA$ | cost of $CO_2$ avoided ($/tonne $CO_2$) |

Greek symbols

| | |
|---|---|
| $\eta$ | efficiency |
| $\gamma$ | specific heat ratio |

Subscripts and superscripts

| | |
|---|---|
| $j$ | time step |
| $in$ | inlet |
| $out$ | outlet |
| $del$ | delivered gas |

$p$ produced gas

$comp.$ compressor

$c$ consumed gas

## 9. References

(1) Wang, Z.; Mori, M.; Araki, T. Steam Electrolysis Performance of Intermediate-Temperature Solid Oxide Electrolysis Cell and Efficiency of Hydrogen Production System at 300 Nm3 h-1. *International Journal of Hydrogen Energy* **2010**, *35* (10), 4451–4458. https://doi.org/10.1016/j.ijhydene.2010.02.058.

(2) Sgobbi, A.; Nijs, W.; De Miglio, R.; Chiodi, A.; Gargiulo, M.; Thiel, C. How Far Away Is Hydrogen? Its Role in the Medium and Long-Term Decarbonisation of the European Energy System. *International Journal of Hydrogen Energy* **2016**, *41* (1), 19–35. https://doi.org/10.1016/J.IJHYDENE.2015.09.004.

(3) Garraín, D.; Banacloche, S.; Ferreira-aparicio, P.; Martínez-chaparro, A.; Lechón, Y. Sustainability Indicators for the Manufacturing and Use of a Fuel Cell Prototype and Hydrogen Storage for Portable Uses. *Energies* **2021**, *14* (20). https://doi.org/10.3390/en14206558.

(4) Parra, D.; Valverde, L.; Pino, F. J.; Patel, M. K. A Review on the Role, Cost and Value of Hydrogen Energy Systems for Deep Decarbonisation. *Renewable and Sustainable Energy Reviews* **2019**, *101*, 279–294.

https://doi.org/10.1016/J.RSER.2018.11.010.

(5) Züttel, A.; Remhof, A.; Borgschulte, A.; Friedrichs, O. Hydrogen: The Future Energy Carrier. *Philosophical Transactions of the Royal Society A: Mathematical, Physical and Engineering Sciences* **2010**, *368* (1923), 3329–3342. https://doi.org/10.1098/RSTA.2010.0113.

(6) Mueller-Langer, F.; Tzimas, E.; Kaltschmitt, M.; Peteves, S. Techno-Economic Assessment of Hydrogen Production Processes for the Hydrogen Economy for the Short and Medium Term. *International Journal of Hydrogen Energy* **2007**, *32* (16), 3797–3810. https://doi.org/10.1016/J.IJHYDENE.2007.05.027.

(7) Sanz-Bermejo, J.; Muñoz-Antón, J.; Gonzalez-Aguilar, J.; Romero, M. Part Load Operation of a Solid Oxide Electrolysis System for Integration with Renewable Energy Sources. *International Journal of Hydrogen Energy* **2015**, *40* (26), 8291–8303. https://doi.org/10.1016/j.ijhydene.2015.04.059.

(8) Yates, J.; Daiyan, R.; Patterson, R.; Egan, R.; Amal, R.; Ho-Baille, A.; Chang, N. L. Techno-Economic Analysis of Hydrogen Electrolysis from Off-Grid Stand-Alone Photovoltaics Incorporating Uncertainty Analysis. *Cell Reports Physical Science* **2020**, *1* (10), 100209. https://doi.org/10.1016/J.XCRP.2020.100209.

(9) Gallardo, F. I.; Monforti Ferrario, A.; Lamagna, M.; Bocci, E.; Astiaso Garcia, D.; Baeza-Jeria, T. E. A Techno-Economic Analysis of Solar Hydrogen Production by Electrolysis in the North of Chile and the Case of Exportation from Atacama Desert to Japan. *International Journal of Hydrogen Energy* **2021**, *46* (26), 13709–

13728. https://doi.org/10.1016/J.IJHYDENE.2020.07.050.

(10) Bhandari, R.; Shah, R. R. Hydrogen as Energy Carrier: Techno-Economic Assessment of Decentralized Hydrogen Production in Germany. *Renewable Energy* **2021**, *177*, 915–931. https://doi.org/10.1016/J.RENENE.2021.05.149.

(11) Seitz, M.; von Storch, H.; Nechache, A.; Bauer, D. Techno Economic Design of a Solid Oxide Electrolysis System with Solar Thermal Steam Supply and Thermal Energy Storage for the Generation of Renewable Hydrogen. *International Journal of Hydrogen Energy* **2017**, *42* (42), 26192–26202. https://doi.org/10.1016/j.ijhydene.2017.08.192.

(12) Mastropasqua, L.; Pecenati, I.; Giostri, A.; Campanari, S. Solar Hydrogen Production: Techno-Economic Analysis of a Parabolic Dish-Supported High-Temperature Electrolysis System. *Applied Energy* **2020**, *261* (September 2019), 114392. https://doi.org/10.1016/j.apenergy.2019.114392.

(13) Naeini, M.; Cotton, J. S.; Adams II, T. A. Data-Driven Modeling of Long-Term Performance Degradation in Solid Oxide Electrolyzer Cell System. *Computer Aided Chemical Engineering* **2022**, *49*, 847–852. https://doi.org/10.1016/B978-0-323-85159-6.50141-X.

(14) Hoerlein, M. P.; Riegraf, M.; Costa, R.; Schiller, G. A Parameter Study of Solid Oxide Electrolysis Cell Degradation: Microstructural Changes of the Fuel Electrode. *Electrochimica Acta journal* **2018**, *276*, 162–175. https://doi.org/10.1016/j.electacta.2018.04.170.

(15) Klotz, D.; Leonide, A.; Weber, A.; Ivers-Tiffée, E. Electrochemical Model for SOFC and SOEC Mode Predicting Performance and Efficiency. *International Journal of Hydrogen Energy* **2014**, *39* (35), 20844–20849. https://doi.org/10.1016/j.ijhydene.2014.08.139.

(16) Naeini, M.; Lai, H.; Cotton, J. S.; Adams II, T. A. A Mathematical Model for Prediction of Long-Term Degradation Effects in Solid Oxide Fuel Cells. *Industrial and Engineering Chemistry Research* **2021**, *60* (3), 1326–1340. https://doi.org/10.1021/acs.iecr.0c05302.

(17) Mendoza, R. M.; Mora, J. M.; Cervera, R. B.; Chuang, P. Y. A. Experimental and Analytical Study of an Anode-Supported Solid Oxide Electrolysis Cell. *Chemical Engineering and Technology* **2020**, *43* (12), 2350–2358. https://doi.org/10.1002/ceat.202000204.

(18) Ni, M. Modeling of a Solid Oxide Electrolysis Cell for Carbon Dioxide Electrolysis. *Chemical Engineering Journal* **2010**, *164* (1), 246–254. https://doi.org/10.1016/j.cej.2010.08.032.

(19) Zhang, H.; Wang, J.; Su, S.; Chen, J. Electrochemical Performance Characteristics and Optimum Design Strategies of a Solid Oxide Electrolysis Cell System for Carbon Dioxide Reduction. *International Journal of Hydrogen Energy* **2013**, *38* (23), 9609–9618. https://doi.org/10.1016/J.IJHYDENE.2013.05.155.

(20) Guan, X.; Pal, U. B.; Powell, A. C. Energy-Efficient and Environmentally Friendly Solid Oxide Membrane Electrolysis Process for Magnesium Oxide Reduction:

Experiment and Modeling. *Metallurgical and Materials Transactions E* **2014**, *1* (2), 132–144. https://doi.org/10.1007/s40553-014-0013-x.

(21) Sohal, M. S. Sohal M. Degradation in Solid Oxide Cells during High Temperature Electrolysis. Idaho National Lab.(INL), Idaho Falls, ID (United States); 2009 May 1. **2009**.

(22) Hubert, M. Durability of Solid Oxide Cells: An Experimental and Modelling Investigation Based on Synchrotron X-Ray Nano-Tomography Characterization. *PhD Thesis* **2018**.

(23) Hauch, A. *Performance and Durability of Solid Oxide Electrolysis Cells*; 2006; Vol. 37. https://doi.org/10.1149/ma2006-01/24/842.

(24) Trofimenko, N.; Kusnezoff, M.; Michaelis, A. Optimization of ESC Performance for Co-Electrolysis Operation. *ECS Transactions* **2017**, *78* (1), 3025–3037. https://doi.org/10.1149/07801.3025ecst.

(25) Tietz, F.; Sebold, D.; Brisse, A.; Schefold, J. Degradation Phenomena in a Solid Oxide Electrolysis Cell after 9000 h of Operation. *Journal of Power Sources* **2013**, *223*, 129–135. https://doi.org/10.1016/j.jpowsour.2012.09.061.

(26) Habibollahzade, A.; Gholamian, E.; Behzadi, A. Multi-Objective Optimization and Comparative Performance Analysis of Hybrid Biomass-Based Solid Oxide Fuel Cell/Solid Oxide Electrolyzer Cell/Gas Turbine Using Different Gasification Agents. *Applied Energy* **2019**, *233–234* (September 2018), 985–1002.

https://doi.org/10.1016/j.apenergy.2018.10.075.

(27) Ni, M.; Leung, M. K. H.; Leung, D. Y. C. Parametric Study of Solid Oxide Steam Electrolyzer for Hydrogen Production. *International Journal of Hydrogen Energy* **2007**, *32* (13), 2305–2313. https://doi.org/10.1016/j.ijhydene.2007.03.001.

(28) Hauth, M.; Becker, D.; Rechberger, J. Solid Oxide Fuel Cell - A Key Technology for a Highly Efficient Energy System. *MTZ worldwide* **2021**, *82* (5–6), 58–63. https://doi.org/10.1007/s38313-021-0644-0.

(29) Naeini, M.; Cotton, J. S.; Adams II, T. A. Economically Optimal Sizing and Operation Strategy for Solid Oxide Fuel Cells to Effectively Manage Long-Term Degradation. *Industrial & Engineering Chemistry Research* **2021**, *60*, 17128–17142. https://doi.org/10.1021/acs.iecr.1c03146.

(30) Hauch, A.; Küngas, R.; Blennow, P.; Hansen, A. B.; Hansen, J. B.; Mathiesen, B. V.; Mogensen, M. B. Recent Advances in Solid Oxide Cell Technology for Electrolysis. *Science* **2020**, *370* (6513). https://doi.org/10.1126/science.aba6118.

(31) http://www.conopt.com/Algorithm.htm.

(32) Mohammadi, A.; Mehrpooya, M. Techno-Economic Analysis of Hydrogen Production by Solid Oxide Electrolyzer Coupled with Dish Collector. *Energy Conversion and Management* **2018**, *173*, 167–178. https://doi.org/10.1016/J.ENCONMAN.2018.07.073.

(33) Yadav, D.; Banerjee, R. Economic Assessment of Hydrogen Production from Solar

Driven High-Temperature Steam Electrolysis Process. *Journal of Cleaner Production* **2018**, *183*, 1131–1155. https://doi.org/10.1016/J.JCLEPRO.2018.01.074.

(34) Kim, S. J.; Kim, K. J.; Choi, G. M. A Novel Solid Oxide Electrolysis Cell (SOEC) to Separate Anodic from Cathodic Polarization under High Electrolysis Current. *International Journal of Hydrogen Energy* **2015**, *40* (30), 9032–9038. https://doi.org/10.1016/J.IJHYDENE.2015.05.143.

(35) Mogensen, M. B.; Chen, M.; Frandsen, H. L.; Graves, C.; Hansen, J. B.; Hansen, K. V.; Hauch, A.; Jacobsen, T.; Jensen, S. H.; Skafte, T. L.; Sun, X. Reversible Solid-Oxide Cells for Clean and Sustainable Energy. *Clean Energy* **2019**, *3* (3), 175–201. https://doi.org/10.1093/ce/zkz023.

(36) Petipas, F.; Brisse, A.; Bouallou, C. Model-Based Behaviour of a High Temperature Electrolyser System Operated at Various Loads. *Journal of Power Sources* **2013**, *239*, 584–595. https://doi.org/10.1016/J.JPOWSOUR.2013.03.027.

(37) Mýrdal, J. S. G.; Hendriksen , Peter Vang; Graves, C.; Jensen, Søren Højgaard; Nielsen, E. R. Predicting the Price of Solid Oxide Electrolysers (SOECs). **2016**, No. October, 1–7.

(38) https://www.grc.nasa.gov/www/k-12/airplane/compth.html.

(39) Marcinkoski, J.; Spendelow, J.; Wilson, A.; Papageorgopoulos, D.; Reviewed, P.; Ahluwalia, R.; James, B.; Houchins, C.; Moton, J. DOE Hydrogen and Fuel Cells

Program Record. *DOE Hydrogen and Fuel Cells Program Record Record* **2015**, 15015.

(40) https://www.energyhub.org/electricity-prices/.

(41) https://www.cer-rec.gc.ca/en/data-analysis/energy-commodities/electricity/report/2017-canadian-renewable-power/canadas-renewable-power-landscape-2017-energy-market-analysis-ghg-emission.html.

(42) Naeini, M.; Cotton, J. S.; Adams II, T. A. Dynamic Lifecycle Assessment of Solid Oxide Fuel Cell System Considering Long-Term Degradation Effects. **2022**.

(43) https://www.quebec.ca/en/agriculture-environment-and-natural-resources/energy/energy-production-supply-distribution/sources-energy.

(44) https://www.cer-rec.gc.ca/.

(45) http://www.world-nuclear.org/uploadedFiles/org/WNA/Publications/Working_Group_Reports/comparison_of_lifecycle.pdf.

(46) Parkinson, B.; Balcombe, P.; Speirs, J. F.; Hawkes, A. D.; Hellgardt, K. Levelized Cost of CO 2 Mitigation from Hydrogen Production Routes. *Energy and Environmental Science* **2019**, *12* (1), 19–40. https://doi.org/10.1039/c8ee02079e.

# CHAPTER 8: CONCLUSIONS AND RECOMMENDATIONS

## 8.1. Conclusions

The focus of this thesis project has been on strengthening the commercialization capabilities of SOFC and SOEC without modifying the technology. For this purpose, this thesis first takes strides in understating degradation of conventional SOFC and SOEC and provides models for prediction of long-term performance degradation of SOFC and SOEC. This is followed by studying impacts of degradation on economic and environmental feasibility of SOFC and SOEC for power and hydrogen generation.

The first-ever detailed model for SOFC degradation that considers effects of six main degradation phenomena was developed (chapter 2) to enable predicting performance of SOFC under degradation at each point of time. A technoeconomic analysis of natural gas fueled-SOFC was performed and effects of SOFC degradation on its economic feasibility were investigated (chapter 3). To reflect the current commercial stage of SOFC, high prices were considered for SOFC system. The findings illustrate that even with the current high capital cost of the SOFC system and relatively high price of natural gas as fuel, if destructive operating conditions are avoided and SOFC is operated in optimal mode and under optimal trajectories economics of large-scale natural gas fueled-SOFC system can be comparable to that of commercially mature technologies. This can be achieved by slight decrease in the current density and hence the power output to mange long-term degradation of SOFC and increase its lifetime. Sensitivity study on this plant showed that its economics greatly depends on its capital costs and price of the fuel, and less on $CO_2$ tax. This study also showed that when SOFC stacks are forced to produce constant power the current density should increase over time which results in increasing degradation rate and hence is not economically optimal.

This was followed by cradle-to-product life cycle environmental assessment of 1 kWh power produced by natural gas fueled-SOFC operated under economically optimal conditions, and it was compared with environmental performance of two other technologies fueled by natural gas (i.e. internal combustion engine and gas turbine) using ReCiPe 2016 and TRACI 2.1 US-Canada 2008 methodologies (chapter 4). Comparing the results of this LCA with previous environmental studies that ignored SOFC degradation showed that ignoring the degradation results in underestimating environmental impacts; particularly GHG emissions. The findings also illustrated that the most efficient internal combustion engine could be as good as SOFC in terms of GHG emissions. However, when all aspects of environmental impacts are considered, SOFC is the superior technology for power production with the lowest life cycle environmental burdens.

The motivation of the next parts of the thesis (chapters 5) was the need for constant power load for certain applications and the importance of avoiding using SOFC stacks in constant power mode for long-term economic power production. This work used a staggering approach to examine the possibility of delivering constant power by SOFC system while power output of each SOFC module declines over time. The results demonstrated that by scheduling start-up order of SOFC modules operated in optimal mode, the SOFC system as a whole can deliver constant power.

The first-ever model for predicting long-term performance degradation of SOEC with good level of accuracy without going into details of degradation reactions was developed (chapter 6). This model was used in an eco-technoeconomic analysis of large-scale SOEC system to test economic and environmental feasibility of hydrogen generation using conventional SOEC considering the impacts of its degradation (chapter 7). The results showed that small decrease in the current density and temperature are required to manage the degradation of SOEC for a long-term cost-effective operation. Sensitivity analysis indicated that economics of SOEC system greatly relies on the price of electricity such that based on the price of electricity SOEC might or might not be an economically attractive option. Moreover, it was shown that whether or not SOEC produces green hydrogen highly depends on the level of GHG emitted from its electricity source. Such that SOECs with low GHG emission electricity sources (such as wind and nuclear power) are very environmentally responsible (with 1.62 to 3.6 kg $CO_2$ per kg $H_2$) while SOECs with high GHG emission electricity sources (such as coal and natural gas-based power) have higher life cycle GHG emissions compared to steam methane reforming process (32.22 kg $CO_2$ per kg $H_2$ from SOEC with coal based-power vs. 10.72 to 15.86 kg $CO_2$ per kg $H_2$ from SMR process).

## 8.2. Future Work

The models developed in this thesis project for prediction of SOFC and SOEC degradation do not predict how performance of these cells change in cyclic operations. Particular integrated community energy systems need CHP and energy storage systems to be operated in cyclic manner in order to meet the community’s demands without the need for power curtailment. The effects of cyclic changes of operating conditions on long-term performance degradation of SOFC and SOEC are not well examined. As such, future work can focus on understanding cyclic operation of SOFC and SOEC and how it affects their lifetime. This will require careful monitoring of performance of several identical cells during long-term cyclic operation under different conditions. Post-mortem analyses such as scanning electron microscopy and X-ray diffraction on cells' components will help understanding degradation mechanisms and causes of failure. Such study can benefit from design of experiments (DOE) to reduce the cost and time of the experiments. The findings of these tests can be used to modify the SOFC and SOEC degradation models developed during this thesis project.

The above discussed experiments examine the performance degradation of SOFC and SOEC in cyclic operation at cell level. However, thermal and gas concentration gradients caused as a result of cyclic operation can lead to degradation of interconnects and sealants too. Therefore, a better understanding of the SOFC and SOEC degradation under cyclic operation requires experiments on several stacks at different conditions. Experiments on the SOFC and SOEC stacks however will be much more expensive than testing the cells. A potential alternative approach to obtain the information without the need for testing several stacks is discussed in the following. N sets of cyclic experiments are performed on one stack. In each experiment periodic operation of the stack at two different operating conditions is tested. As such, the stack is operated under condition A for 120 h, then the operating condition is switched to B and the stack is operated under this new condition for 12 h. The cycle is repeated five times and the entire periodic test takes 27.5 days. The longer operation interval (120 h) allows easier and better control of the condition and monitoring the stack performance, while the shorter operation interval (12 h) resembles the stack cyclic operation on daily basis. The degradation rate under a specific condition is expected to diminish over time. These experiments help to determine whether or not cyclic operation affects this trend. These tests can be performed at Hydrogen Laboratory at McMaster University. Hydrogen laboratory has a 1-kW SOFC, a 1-kW SOEC, a testing unit that controls the operating conditions and monitor performance of SOFC and SOEC. If the experiments show that cyclic operation does not have significant negative impact on the long-term performance of SOFC and SOEC, it would make a solid case for widespread use of these technologies in various places for different applications.